

Genomic instability of non-small cell lung cancer circulating tumor cells as a driving force for their metastatic potential

Tala Tayoun

▶ **To cite this version:**

Tala Tayoun. Genomic instability of non-small cell lung cancer circulating tumor cells as a driving force for their metastatic potential. Cancer. Université Paris-Saclay, 2022. English. ⟨NNT : 2022UPASL057⟩. ⟨tel-03855219⟩

HAL Id: tel-03855219

https://theses.hal.science/tel-03855219v1

Submitted on 16 Nov 2022

HAL is a multi-disciplinary open access archive for the deposit and dissemination of scientific research documents, whether they are published or not. The documents may come from teaching and research institutions in France or abroad, or from public or private research centers.

L'archive ouverte pluridisciplinaire **HAL**, est destinée au dépôt et à la diffusion de documents scientifiques de niveau recherche, publiés ou non, émanant des établissements d'enseignement et de recherche français ou étrangers, des laboratoires publics ou privés.



HAL Authorization

THÈSE DE DOCTORAT

NNT : 2022UPASL057

université PARIS-SACLAY

Genomic instability of non-small cell lung cancer circulating tumor cells as a driving force for their metastatic potential

Rôle de l'instabilité génomique dans le potentiel métastatique des cellules tumorales circulantes dans le cancer bronchique non à petites cellules

Thèse de doctorat de l'Université Paris-Saclay

École doctorale n°582 Cancérologie : biologie – médecine - santé
Spécialité de doctorat : Aspects moléculaires et cellulaires de la biologie
Graduate School : Sciences de la vie et santé. Référent : Faculté de médecine

Thèse préparée au sein du groupe « Cellules Tumorales Circulantes », INSERM U981 « Prédicteurs moléculaires et nouvelles cibles en oncologie » - CNRS UAR3655, INSERM US23 AMMICA « Analyse Moléculaire, Imagerie et Modélisation de la maladie cancéreuse » (Gustave Roussy, 94800, Villejuif, France).
Sous la direction du **Docteure Françoise FARACE, Directrice d'équipe**

Thèse soutenue à Villejuif, le 19 octobre 2022, par

Tala TAYOUN

Composition du Jury

Docteure Françoise DANTZER Directrice de Recherche, IREBS, Strasbourg	Présidente
Professeur Guilhem BOUSQUET PU – PH, Hôpital Avicenne, Bobigny	Rapporteur et examinateur
Professeur Jean-Yves PIERGA PU – PH, Institut Curie, Paris	Rapporteur et examinateur
Docteure Sophie POSTEL-VINAY PH, Directrice d'Équipe, Gustave Roussy, Villejuif	Examinatrice
Docteur Sergio ROMAN ROMAN Directeur de la recherche translationelle, Institut Curie, Paris	Examinateur
Docteure Françoise FARACE Directrice d'Équipe, Ingénieure de Recherche, Gustave Roussy, Villejuif	Directrice de thèse

Acknowledgements

Je tiens premièrement à remercier ma directrice de thèse, Docteure Françoise Farace, de m'avoir accueillie au sein de son équipe dès mon stage de M2 et de m'avoir donné la chance de réaliser une thèse de doctorat. Merci pour votre disponibilité au quotidien, vos conseils et la confiance que vous m'avez accordée tout au long de la thèse. Vous m'avez appris la recherche dans toutes ses dimensions, incluant l'opportunité de participer à des congrès internationaux. J'ai beaucoup mûri au sein de votre laboratoire et je vous en suis extrêmement reconnaissante.

Je souhaite aussi remercier le Professeur Fabrice André et le Professeur Jean-Yves Scoazec de m'avoir accueilli au sein de leur structure respective.

Je remercie La Ligue Contre le Cancer de m'avoir accordé ma bourse doctorale, ainsi que la Fondation pour la Recherche Médicale qui a financé ma quatrième année de thèse. J'exprime mes sincères remerciements aux membres du jury qui me font l'honneur d'évaluer mes travaux : Docteure Françoise Dantzer qui a accepté d'être présidente du jury, Professeur Guilhem Bousquet et Professeur Jean-Yves Pierga qui ont accepté la tâche d'être rapporteurs et de prendre le temps de considérer mon manuscrit de thèse, Docteure Sophie Postel-Vinay et Docteur Sergio Roman Roman d'avoir accepté d'être examinateurs. Je souhaite aussi remercier la Docteure Patricia Kannouche pour nos discussions scientifiques très enrichissantes dans le domaine de la réparation de l'ADN, qui ont été d'une grande aide dans ce projet. Merci aussi à la Docteure Valeria Naim et les membres de son équipe, notamment Philippe et Maha pour leur aide dans certains protocoles expérimentaux.

Ce travail n'aurait pas été possible sans un environnement chaleureux et épanouissant de collègues et d'amis. Premièrement, un grand merci à Widad, Catherine, Nathalie, Amélie et Safia pour votre aide au quotidien et votre super gestion qui ont rendu la vie au labo bien meilleure ! Merci à l'ensemble des membres de l'U981 d'hier et d'aujourd'hui ! Bojana, Ingrid et Jonathan, merci pour tous nos beaux moments passés ensemble. Vous avez rendu cette expérience inoubliable. Bien sûr avec Ibra ; merci pour

le divertissement dans les couloirs, mais aussi d'avoir toujours fini par accepter que je m'incruste dans votre duo avec Loïc. Tu sais combien tu comptes pour moi ! Hadia, Ludo, Lucette, Virginie Q, Véro, Olivia, Chloé, Matthieu, Cynthia, Sofia et Clémence A ; un grand merci à toutes et tous pour tous nos moments de fun au labo et à la Butte ! Clémence H, on se retrouvera à la ligne d'arrivée comme promis. Merci à la team « midnight runners » du mardi soir et à son capitaine Francesco. Merci pour nos temps de partage cinéphile et ton aide précieuse pour tout le volet clinique du projet. Boston is lucky to have you ! Merci à la plateforme AMMICa, notamment Nico et surtout à toi Virginie pour ton travail qui a été indispensable à la réussite de ce projet dès son début, mais aussi pour ton sourire qui ne quitte jamais ton visage, malgré mes demandes parfois interminables.

Merci du fond du cœur à notre équipe « PCCCCR » ex-BCC. Patrycja, je te remercie pour ta patience, ton aide au quotidien et ton input scientifique, qui ont été primordiaux pour la publication du papier et l'aboutissement de cette thèse. Vincent, je n'oublierai jamais le jour où tu m'avais annoncé que tu partais de l'IGR : « TT, je pars » et moi : « ah tu vas courir ce soir ? » « *éclats de rire* non non, j'ai trouvé un nouveau job ! ». Contrairement à tous les autres jours au bureau, je n'ai pas beaucoup ri ce jour-là. Merci pour la confiance que tu m'as accordée pour la suite de ton projet. Sans toi et ton travail, cette thèse aurait été très différente. Marianne, merci pour ta positivité, ta disponibilité et surtout d'avoir pris beaucoup de ton temps pour m'aider dans ce projet. Nos discussions sur la vie – qui, j'avoue, peuvent être parfois un peu sombres, en fonction du mood de la journée – vont beaucoup me manquer. Agathe, ma voisine de bureau, merci pour toute ton aide au labo, incluant tes préparations culinaires et les kg en plus. Les éclats de rire dans le bureau 167 ont sûrement rendu ces quatre dernières années exceptionnelles. Je souhaite aussi remercier les anciens membres : Céline, maintenant devenue Dr Hervieu. On s'est connues en tant que « petites M2 », principalement en galère dès que Vincent partait faire son running du soir. Emma, nos parcours se sont croisés rapidement mais je tenais à te remercier pour ta contribution

et ton aide dans ce projet. Anne, tu es arrivée à la dernière ligne droite de ma thèse (et au bout de ma vie…), merci pour ta gentillesse et ton soutien moral !

Et bien sûr, les amis aux quatre coins du monde, sans lesquels survivre les hauts et les bas d'une thèse n'aurait pas été possible. Rayya, Maria R, Maria S et Carine S : merci d'avoir été là depuis le tout début (la maternelle !). On va enfin bientôt vivre sur le même continent et j'ai tellement hâte. Merci à mes amis d'enfance Carine K, Mark et Antoine. Merci aux amis d'AUB devenus maintenant médecins aux US pour leur soutien, surtout Alex, Carine A et Firas ; un remerciement en français pour que Firas n'y comprenne rien. Merci à la belle équipe des Libanais à Paris ; Nour, Carla, Farid, Emile et Léa. Ça fait du bien de faire ressortir ses origines « zghortiotes » avec vous. Petite mention spéciale pour Nour et Carla, mes premières copines « parisiennes », qui ont rendu beaucoup plus sympa un début relativement rude à Paris en 2017. Hâte de fêter cette fin de thèse avec vous ! Enfin, merci de tout mon cœur aux copines et copains Amandine, Mathilde, Margaux, Victor, Anthony, Gustavo et Hugo que j'ai eu la chance de rencontrer il y a quatre ans. Nos sorties et weekends loin de Paris (plus ou moins organisés) sont autant de beaux souvenirs qui m'ont permis d'apprécier ces dernières années et ma vie à Paris ! Sans oublier le dernier venu dans le groupe mais aussi le membre le plus important : notre Titi (Leo) d'amour.

Maintenant, la famille !

Merci à mes parents d'avoir toujours été là et soutenu mes projets. Merci pour tout ce que vous avez fait et tout ce que vous faites encore pour nous aujourd'hui, malgré les difficultés du quotidien libanais ces derniers temps. Vous êtes les meilleurs ! Merci à ma sœur Yara, mon frère Jad et ma belle-sœur Latifa. C'est une vraie chance d'avoir une partie de sa famille à proximité ! Même si l'organisation des brunchs a parfois été farfelue, on s'en est toujours sorti. Sans oublier Yara F et Reem, la famille de cœur. Loïc, merci pour tout, surtout d'avoir toujours été « la voix de la raison » dans les moments difficiles. Nous avons débuté nos thèses respectives ensemble et maintenant que ça se termine, je réalise que ça n'aurait pas été pareil sans toi ! Merci à l'ensemble de ma grande famille au Liban et à l'étranger : les Tayoun, Bou-Haroun et Doueihy. Ça fait du

bien de rentrer vous voir et se ressourcer au pays, même si j'aurais aimé pouvoir le faire plus souvent. Deuxième mention spéciale à Manal et Lea, mes deux cousines devenues sœurs avec lesquelles j'ai partagé et je partage toujours tous les moments importants de la vie. Merci à ma deuxième famille à Paris ! Merci Isabelle de nous avoir toujours réuni autour d'un festin le weekend que ce soit à Paris ou à Noirmout', avec Cléa, Loïc, Thomas, Paul, Lou et Claire. Je souhaite aussi remercier des personnes chères qui ont été là au début de ma thèse mais ne sont plus parmi nous aujourd'hui. Dodo Joseph, tes leçons de vie resteront toujours avec moi pour me guider. Nicole, j'ai eu la chance de te connaître ces quatre dernières années ; merci pour ta bonne humeur, ta générosité et tes conseils, j'en garde les plus beaux souvenirs.

Enfin, merci aux patients, à leurs familles et aux médecins, qui luttent tous au quotidien contre cette maladie et qui donnent un vrai sens à nos travaux de recherche.

Ça va être dur de tourner cette page, mais il est temps maintenant de débuter une nouvelle aventure !

Table of Contents

Publications and Communications 11

List of Figures 13

List of Tables 14

List of Abbreviations 15

List of Genes and Proteins 16

Part A. Introduction 17

I. Lung cancer 17

1) Global epidemiology 17

2) NSCLC classifications 17

a. Histological subtypes 17

b. Molecular subtypes 18

3) Clinical management of non-oncogene addicted NSCLC 24

II. The metastatic process 27

1) Metastatic inefficiency 27

2) Stages of the metastatic cascade 28

a. Proliferation and local invasion 28

b. Intravasation into tumor vasculature and circulation 29

c. Extravasation and colonization of target organs 30

3) EMT during cancer progression 31

4) The pre-metastatic niche and tumor dormancy 34

5) Cancer stem cells 36

III. Circulating tumor cells 38

1) CTC enrichment and detection methods 39

a. Enrichment strategies 39

i. Positive selection approaches 39

ii. Negative selection approaches 40

b. Detection strategies 41

2) Clinical interest of CTCs 42

a. Liquid biopsy applications 42

b. CTC prognostic value 43

c. CTC molecular profiling 45
i. Enriched CTC populations 45
ii. Single CTCs 47
3) CTC functional characterization 49
a. CTC-derived xenografts 50
b. CTC-derived *ex vivo* models 53
REVIEW ARTICLE 1. CTC-derived models: A window into the seeding capacity of Circulating Tumor Cells (CTCs). *Cells* 2019, *8*(10), 1145 57
IV. Genomic instability and the DNA damage response in cancer 74
1) DNA repair pathways 74
a. Classical non-homologous end joining 75
b. Homologous recombination 75
c. Fanconi anemia pathway 77
2) DNA repair alterations in cancer 78
V. Targeting the DDR in cancer 82
1) PARP inhibitors: a synthetic lethal therapy 83
a. PARP1 function in DNA repair 83
b. Targeting PARP1 in the clinic 84
2) Other DDR inhibitors 86
3) DDR-based therapeutic strategies in NSCLC 87
4) Predictive biomarkers of response to DDR-based therapies 88
a. Beyond *BRCA* 88
b. Assessment of DDR-based biomarkers in CTCs 91
REVIEW ARTICLE 2. Tumor evolution and therapeutic choice seen through a prism of circulating tumor cell genomic instability. *Cells* 2021; 10(2):337 93
Aims and Approaches 108
Part B. Additional Materials and Methods 112
1) Western blot analysis 112
a. Whole-cell protein extraction 112
b. Protein separation by gel electropheresis 112
2) Metaphase chromosome spreads 113
3) *In vitro* pharmacological assays 113

Part C. Results **116**

RESEARCH ARTICLE 1. Exploitation of the chick embryo chorioallantoic membrane (CAM) as a platform for anti-metastatic drug testing. *Scientific Reports* 2020; 10:16876 ..... **117**

RESEARCH ARTICLE 2. Targeting genome integrity dysfunctions impedes metastatic potency in non-small cell lung cancer circulating tumor cell-derived explants. *JCI Insight* 2022; 7(11):155804 ..... **139**

Part D. Discussion and Perspectives **197**

Part E. Reference List **204**

Synthèse en français **241**

Publications and Communications

Publications included in this PhD thesis

Review articles

Tayoun T, Faugeroux V, Oulhen M, Aberlenc A, Pawlikowska P, Farace F. *CTC-Derived Models: A Window into the Seeding Capacity of Circulating Tumor Cells (CTCs).* **Cells**. 2019 Sep 25;8(10):1145.

Tayoun T, Oulhen M, Aberlenc A, Farace F, Pawlikowska P. *Tumor Evolution and Therapeutic Choice Seen through a Prism of Circulating Tumor Cell Genomic Instability.* **Cells**. 2021 Feb 5;10(2):337.

Research articles

Pawlikowska P, **Tayoun T**, Oulhen M, Faugeroux V, Rouffiac V, Aberlenc A, Pommier AL, Honoré A, Marty V, Bawa O, Lacroix L, Scoazec JY, Chauchereau A, Laplace-Builhe C, Farace F. *Exploitation of the chick embryo chorioallantoic membrane (CAM) as a platform for anti-metastatic drug testing.* **Scientific Reports**. 2020 Oct 9;10(1):16876.

Tayoun T*, Faugeroux V*, Oulhen M, Déas O, Michels J, Brulle-Soumare L, Cairo S, Scoazec JY, Marty V, Aberlenc A, Planchard D, Remon J, Ponce S, Besse B, Kannouche P, Judde JG, Pawlikowska P[$], Farace F[$]. *Targeting genome integrity dysfunctions impedes metastatic potency in non–small cell lung cancer circulating tumor cell–derived explants.* **JCI Insight**. 2022;7(11): 155804.

Contributions to other publications

Review article

Pawlikowska P, Faugeroux V, Oulhen M, Aberlenc A, **Tayoun T**, Pailler E, Farace F. *Circulating tumor cells (CTCs) for the noninvasive monitoring and personalization of non-small cell lung cancer (NSCLC) therapies.* **Journal of Thoracic Disease**. 2019 Jan;11(Suppl 1):S45-S56.

Research article

Oulhen M*, Pawlikowska P*, **Tayoun T**, Garonzi M, Buson G, Forcato C, Manaresi N, Aberlenc A, Mezquita L, Lecluse Y, Lavaud P, Naltet C, Planchard D, Besse B, Farace F. *Circulating tumor cell copy-number heterogeneity in ALK-rearranged non-small-cell lung cancer resistant to ALK inhibitors.* **NPJ Precision Oncology**. 2021 Jul 16;5(1):67.

Communications

4th ACTC (Advances in Circulating Tumor Cells) meeting 2019 – Corfu, Greece

Oral presentation. Travel Award. Tayoun T[*], Faugeroux V[*], Pailler E, Oulhen M, Deas O, Mezquita L, Brulle-Soumare L, Cairo S, Scoazec JY, Marty V, NgoCamus M, Nicotra C, Planchard D, Kannouche P, Besse B, Judde JG, Pawlikowska P, Farace F.

3R Meeting (Replication, Recombination, Repair) 2019 – Presqu'île de Giens, France

Poster. Tayoun T, Faugeroux V, Deas O, Judde JG, Besse B, Kannouche P, Farace F, Pawlikowska P.

Journée Jeunes & Chercheurs (La Ligue Contre le Cancer) 2020 – Paris, France

Oral presentation. Best Presentation Award. Tayoun T, Faugeroux V, Pailler E, Oulhen M, Deas O, Mezquita L, Brulle-Soumare L, Cairo S, Scoazec JY, Marty V, NgoCamus M, Nicotra C, Kannouche P, Besse B, Judde JG, Pawlikowska P, Farace F.

AACR (American Association for Cancer Research) Annual meeting 2021 – virtual

Poster. Tayoun T[*], Faugeroux V[*], Oulhen M, Deas O, Mezquita L, Brulle-Soumare L, Cairo S, Scoazec JY, Marty V, Aberlenc A, NgoCamus M, Nicotra C, Planchard D, Kannouche P, Besse B, Judde JG, Pawlikowska P, Farace F.

AACR Annual meeting 2022 – New Orleans, USA

Poster. Tayoun T[*], Faugeroux V[*], Oulhen M, Deas O, Michels J, Brulle-Soumare L, Cairo S, Scoazec JY, Marty V, Aberlenc A, Pailler E, Planchard D, Remon J, Ponce S, Besse B, Kannouche P, Judde JG, Pawlikowska P[$], Farace F[$].

EACR (European Association for Cancer Research) 2022 – Sevilla, Spain

Oral presentation. Tayoun T[*], Pawlikowska P[*], Faugeroux V, Oulhen M, Deas O, Brulle-Soumare L, Besse B, Kannouche P, Judde JG, Farace F.

4th Sunrise Meeting Stem Cells and Cancer 2022 – Paris, France

Poster. Tayoun T[*], Faugeroux V[*], Oulhen M, Deas O, Michels J, Brulle-Soumare L, Cairo S, Scoazec JY, Marty V, Aberlenc A, Pailler E, Planchard D, Remon J, Ponce S, Besse B, Kannouche P, Judde JG, Pawlikowska P[$], Farace F[$].

3rd EurOPDX workshop 2022 – Egmond Aan Zee, Netherlands

Keynote speech. Tayoun T. *"CTC-derived models: Insight into the biology of metastatic progression and its therapeutic targeting".*

*[$]both authors contributed equally to the study.

List of Figures

Parts A & B

Figure 1. Lung cancer classifications. 19

Figure 2. Mechanisms of acquired resistance to osimertinib and lorlatinib in *EGFR*-mutant and *ALK*-rearranged NSCLC, respectively. 22

Figure 3. Immunotherapy treatment approaches in NSCLC. 24

Figure 4. Key steps of the metastatic cascade. 31

Figure 5. Role of epithelial-mesenchymal transition (EMT) during cancer progression. 33

Figure 6. Induction and formation of the pre-metastatic niche. 35

Figure 7. Historical medical journal article by Thomas Ashworth in 1869 describing circulating tumor cells for the first time. 38

Figure 8. Circulating tumor cell enrichment technologies. 41

Figure 9. Functional studies on circulating tumor cells. 49

Figure 10. Double-strand break repair pathways in mammalian cells. 76

Figure 11. Cooperation of Fanconi anemia, nucleotide excision repair, translesion synthesis and homologous recombination proteins in a common interstrand crosslink repair pathway. 78

Figure 12. DNA damage response gene somatic alterations across 9,125 PanCanAtlas samples. 80

Figure 13. Synthetic lethality. 82

Figure 14. A schematic model of the PARP1 catalytic cycle. 83

Figure 15. Clinical PARP inhibitors. 85

Figure 16. Multiple paths to PARP inhibitor vulnerability. 91

Figure 17. Example of a 384-well microplate layout for *in vitro* pharmacological assays. 114

List of Tables

Parts A & B

Table 1. Phase III clinical trials and results of immunotherapy-based therapeutic strategies in NSCLC 26

Table 2. Pros and cons of CDX models as compared to PDX models in their use as a preclinical research tool 50

Table 3. Main DDR inhibitors currently in the clinical pipelines 87

Table 4. Drug concentrations *in vitro* 115

List of Abbreviations

BER	base-excision repair
CAF	cancer-associated fibroblasts
CAM	chick embryo chorioallantoic membrane
CDX	CTC-derived xenograft
CIN	chromosomal instability
c-NHEJ	classical non-homologous end joining
CNA	copy number alteration
CNS	central nervous system
CRPC	castration-resistant prostate cancer
CSC	cancer stem cell
CTC	circulating tumor cell
ctDNA	circulating cell-free tumor DNA
CTM	circulating tumor microemboli
DAPI	4',6-diamidino-2-phenylindole
DDR	DNA damage response
DNA	deoxyribonucleic acid
DSB	double-strand break
DTCs	disseminated tumor cells
ECM	extracellular matrix
EFS	event-free survival
ELF	ETS-related transcription factor
EMT	epithelial-mesenchymal transition
MET	mesenchymal-epithelial transition
E/M	epithelial/mesenchymal
ETS	erythroblast transformation specific
FA	fanconi anemia
FACS	fluorescence-activated cell sorting
FDA	food and drug administration
FISH	fluorescence *in situ* hybridization
GFP	green fluorescent protein
HR	homologous recombination
HRD	homologous recombination deficiency
ICI	immune checkpoint inhibitor
IC_{50}	half maximal inhibitory concentration
ICL	interstrand crosslink
IF	immunofluorescence
IHC	immunohistochemistry
KO	knock-out
MMP	matrix metalloproteinase
NER	nucleotide excision repair
miR	microRNA
MMR	mismatch repair
mRNA	messenger ribonucleic acid
NER	nucleotide excision repair
NGS	next-generation sequencing
NK	natural killer
NSCLC	non-small cell lung cancer
NSG	Nod/Scid-IL2R$\gamma^{-/-}$
ORR	objective response rate
OS	overall survival
pH	potential of hydrogen
PARPi	PARP inhibitor
PBS	phosphate buffer saline
PDX	patient-derived xenograft
PFS	progression-free survival
PMN	pre-metastatic niche
RNA	ribonucleic acid
RNA-seq	RNA sequencing
SCLC	small cell lung cancer
SSB	single-strand break
ssDNA	single-strand DNA
TAM	tumor-associated macrophages
TB	tumor biopsy
TFs	transcription factors
TKI	tyrosine kinase inhibitor
UV	ultraviolet
vs	versus
WES	whole-exome sequencing
WGA	whole-genome amplification
WGS	whole-genome sequencing
WHO	world health organization
2D/3D	two-dimensional/three-dimensional

List of Genes and Proteins

AKT1	AKT serine/threonine kinase 1
ALK	anaplastic lymphoma kinase
AR	androgen receptor
ARID1A/B	AT-rich interaction domain 1A/1B
ATM	ataxia telangiectasia mutated
ATR	ataxia telangiectasia and Rad3 related
BRCA1/2	breast cancer susceptibility gene (1/2)
BMP4/7	bone morphogenetic protein (4/7)
BRAF	b-raf proto-oncogene
CCL2	CC-chemokine ligand 2
CD24	cluster of differentitation 24
CD44	homing function and indian blood group system
CD45	protein tyrosine phosphatase receptor type C
CD47	Rh-related antigen, integrin-associated signal transducer
cGAS	cyclic GMP–AMP synthase
CHK(1/2)	checkpoint kinase (1/2)
CK	cytokeratin
CLIP1	CAP-Gly domain-containing linker protein 1
CTLA-4	cytotoxic T-lymphocyte-associated antigen 4
DNA-PKcs	DNA-dependent protein kinase, catalytic subunit
EGFR	epithelial growth factor receptor
EML4	echinoderm microtubule-associated protein-like 4
EpCAM	epithelial cell adhesion molecule
ERCC1	excision repair cross-complementing group 1
ERG	proto-oncogene ETS-related gene
FANCA	fanconi anemia complementation group A
FGF	fibroblast growth factor
HER2/HER3	human epidermal growth factor receptor 2/3
HPSE	heparanase
Ki-67	marker of proliferation Ki-67
KIFC1	kinesin family member C1
KRAS	RAS proto-oncogene, GTPase
LTK	leukocyte receptor tyrosine kinase
MDM2/4	murine double minute 2/4
MEK	mitogen-activated protein kinase kinase
MET	MET proto-oncogene, receptor tyrosine kinase
MLH3	MutL Homolog 3
MSH2/3/6	MutS Homolog 2/3/6
NF-κB	nuclear factor-κappa B
NRG1	neuregulin 1
PALB2	partner and localizer of BRCA2
PARP1/2	poly(ADP-ribose) polymerase 1/2
PD-1	programmed cell death 1
PDGF	platelet-derived growth factor
PD-L1	programmed cell death ligand 1
PI3Kα	phosphatidylinositol-3-kinase alpha
POLQ	DNA polymerase theta
PTEN	phosphatase and tensin homolog
RAD51	RAD51 recombinase
RB1	retinoblastoma 1
ROS1	c-ros proto-oncogene 1
RPA	replication protein A
SLFN11	schlafen family member 11
SNAI1/2	snail family transcriptional repressor 1/2
SOX2	sex determining region Y-box 2
STING	stimulator of interferon genes
TGFβ	tumor growth factor beta
TMPRSS2	transmembrane protease serine 2
TP53/63	tumor protein 53/63
TTF1	thyroid transcription factor 1
VEGF	vascular endothelial growth factor
WEE1	WEE1 G2 Checkpoint kinase
XLF	XRCC4-like factor
XRCC1/4	x-ray repair cross complementing 1/4
ZEB1/2	zinc finger E-box binding homeobox 1/2
γH2AX	gamma histone 2AX
53BP1	tumor protein p53 binding protein

Part A. Introduction

I. Lung cancer

Lung cancer remains the leading cause of cancer-related mortality worldwide (Sung et al., 2021). It is a heterogeneous disease with distinct histological and clinico-pathological characteristics. The two major histological subtypes are non-small cell lung cancer (NSCLC) and small-cell lung cancer (SCLC), accounting for 85% and 15% of lung cancers respectively (**Figure 1**). This doctoral thesis will focus exclusively on NSCLC.

1) Global epidemiology

The most recent GLOBOCAN (Global Cancer Observatory: cancer today) report ranked lung cancer as the second most commonly diagnosed malignancy after female breast cancer and the leading cause of cancer death, with an estimated 1.8 million deaths (18%) in 2020, with two-thirds attributable to tobacco smoking (Sung et al., 2021). Lung cancer trends reflect trends of smoking prevalence: owing to smoking cessation efforts, incidence rates have witnessed a decline in the past decade, which has been slower among women as they have taken up cigarette smoking later than men (Siegel et al., 2022; Sung et al., 2021).

2) NSCLC classifications

a. Histological subtypes

NSCLC tumors are further subdivided according to WHO criteria into adenocarcinoma, squamous cell carcinoma, large cell carcinoma, adenosquamous carcinoma, sarcomatoid carcinoma and carcinomas of salivary gland type (Davidson et al., 2013). Adenocarcinoma is the predominant pathological phenotype (50%) followed by squamous cell carcinoma (40%). Adenocarcinoma tumors are mainly issued from distal airways (alveolar, bronchial or bronchiolar epithelial cells), present glandular differentiation and express thyroid transcription factor 1 (TTF1) and cytokeratin (CK) 7.

On the other hand, squamous cell carcinomas are derived from proximal airways (bronchial cells) and are associated with smoking history. They express CK 5, CK 6 and/or the transcription factors p63 and SRY-box 2 (SOX2), but are TTF1-negative (Z. Chen et al., 2014; Davidson et al., 2013; Langer et al., 2010).

b. Molecular subtypes

A molecular-based classification of NSCLC tumors, based on genetic abnormalities detected at the time of diagnosis or at tumor progression in response to treatment, is also frequently performed. With the advent of high-throughput sequencing technologies, large-scale sequencing of tumor biopsies (TBs) in different cancer types led to the identification of a plethora of molecular alterations implicated in disease progression (*e.g.* chromosomal rearrangements, insertions or deletions, mutations). NSCLC management has witnessed unprecedented improvements over the past two decades owing to the identification of multiple new oncogenic drivers (**Figure 1**), paving the way towards the development of novel targeted therapies. Of note, specific tyrosine kinase inhibitors (TKIs) have been developed and approved in the clinic. These include TKIs targeting mutations in *epidermal growth factor receptor* (*EGFR*) or *b-raf proto-oncogene* (*BRAF*) genes and gene rearrangements of *anaplastic lymphoma kinase* (*ALK)* or c-*ros proto-oncogene 1* (*ROS1*) (Thai et al., 2021). Tumor molecular testing has thus become the standard of care for patients diagnosed with advanced lung adenocarcinoma, as per current guidelines (Kalemkerian et al., 2018).

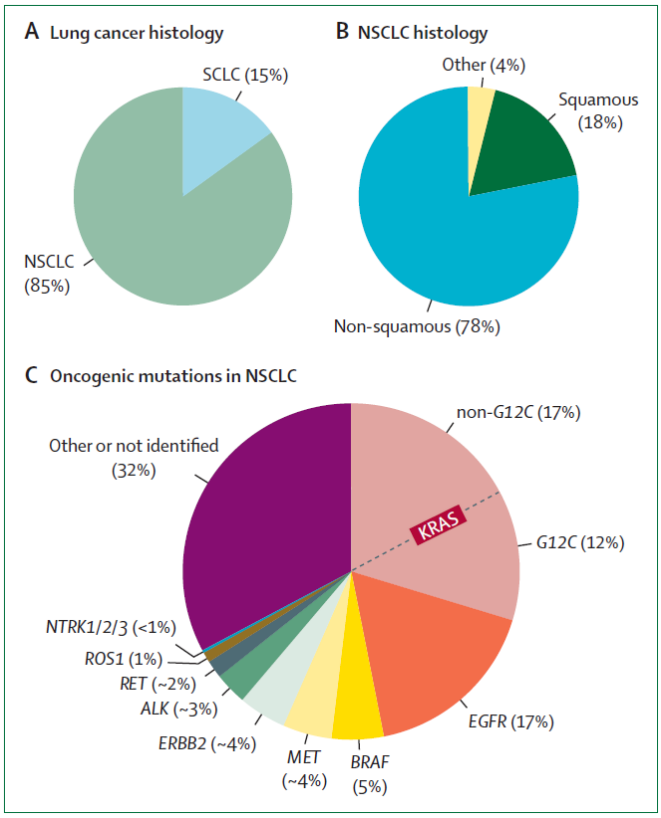


Figure 1. Lung cancer classifications. Lung cancers are classified into SCLC or NSCLC (**A**) and NSCLC is further subdivided into squamous and non-squamous histology (**B**). (**C**) Distribution of oncogenic driver mutation frequencies in NSCLC, based on a cohort of 4064 patients with metastatic NSCLC by Singal and colleagues (Singal et al., 2019). NSCLC = non-small cell lung cancer. SCLC=small-cell lung cancer. ***Figure and legend adapted from Thai et al., The Lancet, 2021.***

EGFR mutations

The discovery of somatic activating mutations in the *EGFR* gene in 2004 has launched the field of TKI-based targeted therapy in NSCLC. *EGFR* exon 19 deletions or exon 21 L858R point mutations are the most common in lung adenocarcinoma, found in ~ 17% of NSCLC patients (**Figure 1**) (Singal et al., 2019; Thai et al., 2021).

Studies with first-generation, reversible TKIs erlotinib and gefinitib and second-generation, irreversible TKIs afatinib and dacomitinib have shown significantly improved progression-free survival (PFS) in patients with *EGFR*-mutated NSCLC compared to standard chemotherapy (Lynch et al., 2004; Mok et al., 2009; Rosell et al., 2012; Sequist et al., 2013; Y.-L. Wu et al., 2017). Nonetheless, resistance to first- and second-generation EGFR inhibitors inevitably develops, with the T790M mutation in

EGFR exon 20 being the most common mechanism of acquired resistance (~ 60%) (Sequist et al., 2011; H. A. Yu et al., 2013).

Osimertinib, a third-generation irreversible TKI selective for both canonical *EGFR*-activating and mutations, was approved for the treatment of *EGFR*^{T790M}-mutated NSCLC patients who had progressed on first- or second-generation TKI (Novello et al., 2016). It has shown increased PFS compared to platinum plus permetrexed therapy (median 10.1 months *vs* 4.4 months respectively) in patients progressing after a first line treatment with earlier-generation TKIs and harboring an *EGFR*^{T790M} mutation (Mok et al., 2017). Importantly, findings from the FLAURA trial (NCT02296125) have shown that osimertinib significantly prolonged overall survival (OS) in treatment-naive *EGFR*-positive NSCLC compared to erlotinib or gefitinib (median 38.6 months *vs* 31.8 months). Osimertinib has now become the preferred first-line treatment for advanced-stage *EGFR*-mutant NSCLC patients (Ramalingam et al., 2020; Soria et al., 2018). Despite success both in the first line setting and after failure of early-generation TKIs, acquired resistance to osimertinib remains a major clinical challenge as important heterogeneity has been identified among resistance mechanisms, which encompass both *EGFR*-dependent (*e.g. EGFR*^{C797S}, *EGFR*^{C797X}) and *EGFR*-independent bypass mechanisms (*e.g. MET* amplification, *KRAS* amplification) (**Figure 2**) (Cooper et al., 2022; Leonetti et al., 2019; Ramalingam et al., 2018).

ALK and *ROS1* gene rearrangements

ALK chromosomal rearrangements define another NSCLC molecular subset found most frequently as fusion oncogenes such as e*chinoderm microtubule associated protein like 4 (EML4)-ALK* fusion, which leads to an aberrant activation of the ALK protein (Soda et al., 2007). Similarly, *ROS1* rearrangements create fusion proteins that constitutively activate ROS1 kinase and cell proliferation (Davies & Doebele, 2013). *ALK* and *ROS1* rearrangements account for 3-5% and 1-2% of patients with NSCLC respectively (**Figure 1**), most commonly presenting adenocarcinoma histological features and minimal or no smoking history. First-generation ALK TKI crizotinib was shown to

improve PFS compared to standard chemotherapy (median 7.7 months *vs* 3 months) in previously treated NSCLC patients with *ALK* rearrangement (Shaw et al., 2013). Similar outcome was obtained when comparing crizotinib to a combination treatment of permetrexed and platinum salts in previously untreated patients (median PFS 10.9 months *vs* 7 months) (Solomon et al., 2014). These studies led to crizotinib becoming the standard treatment in the first-line setting, benefiting both *ALK*- and *ROS1*-rearranged NSCLC patients (Shaw et al., 2013; Shaw, Ou, et al., 2014). Nevertheless, as with early-generation EGFR TKIs, resistance typically develops within one year of treatment. Briefly, mechanisms of acquired resistance to crizotinib implicate either on-target secondary *ALK* gene mutations (*e.g.* L1196M, G1269A), or more frequently off-target mechanisms such as the activation of bypass tracks (*e.g.* EGFR) or epigenetic modifications (*e.g.* epithelial-mesenchymal transition) (Gainor et al., 2016).

Potent second-generation ALK TKIs were then developed against crizotinib resistance mutations, including ceritinib, alectinib, brigatinib and ensartinib. Ceritinib showed clinical activity with 56% objective response rate (ORR) and a median PFS of 7 months in patients with advanced *ALK*-rearranged NSCLC previously treated with crizotinib, with or without detectable resistance mutations (Friboulet et al., 2014; Shaw, Kim, et al., 2014). Similarly, a study comparing second-generation alectinib to crizotinib showed that the former had a higher PFS rate (68.4%) compared to the latter (48.7%). Moreover, alectinib was more active in the central nervous system (CNS), with 12% of patients presenting a CNS progression event in the alectinib group, compared to 45% in the crizotinib-treated group (Peters et al., 2017). Two subsequent interim analyses (99 *vs* 150 events) of the phase III ALTA-1L trial (NCT0273501) evaluating brigatinib in ALK TKI-naive *ALK*-positive patients showed a significantly longer PFS and superior efficacy for brigatinib compared to crizotinib. Importantly, in both analyses, brigatinib significantly improved intracranial ORR in patients with baseline brain metastases compared to crizotinib (78% *vs* 29% and 78% *vs* 26%) and delayed CNS progression (Camidge et al., 2018, 2020). More recently, ensartinib has also proven efficacy in the first-line setting with a longer PFS (median 25.8 *vs* 12.7 months) and superior

intracranial efficacy in patients presenting brain metastases at baseline in comparison to crizotinib (Horn et al., 2021).

Lorlatinib is a third-generation ALK/ROS1 TKI with proven efficacy in treatment-naive patients as well as in overcoming a broad spectrum of resistance mutations acquired to first- or second-generation ALK TKIs, including *ALK*^{G1202R} ceritinib resistance mutation (Solomon et al., 2018; Zou et al., 2015). Moreover, results from the phase III CROWN trial (NCT03052608) showed the superior efficacy of first-line lorlatinib in the treatment of *ALK*-positive patients, as well as its improved CNS penetration compared to crizotinib, supporting its use as first-line treatment in patients with advanced *ALK*-rearranged NSCLC (Shaw et al., 2020; Solomon et al., 2022). Nevertheless, as with third-generation EGFR TKI, resistance to lorlatinib remains an unresolved clinical issue (**Figure 2**) (Cooper et al., 2022; Recondo et al., 2020).

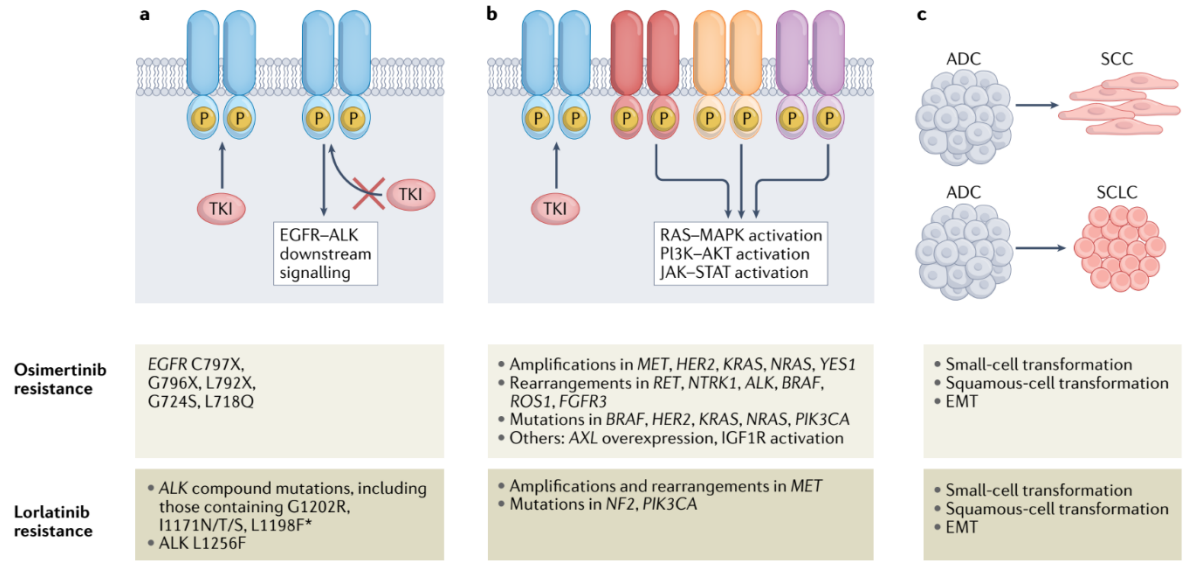


Figure 2. Mechanisms of acquired resistance to osimertinib and lorlatinib in *EGFR*-mutant and *ALK*-rearranged NSCLC, respectively. Mechanisms of resistance to these agents can be divided into several main categories, including alterations that prevent inhibition of the target receptor tyrosine kinase by the tyrosine kinase inhibitor (TKI) (**a**), activation of bypass and/or downstream signaling pathways that promote cell survival and proliferation despite adequate TKI binding (**b**), and changes in tumor cell lineage such as transformation from adenocarcinoma (ADC) to squamous cell carcinoma (SCC) or small-cell lung cancer (SCLC) phenotype and epithelial–mesenchymal transition (EMT) (**c**). Specific selected examples of these mechanisms are also provided. ***Figure and legend adapted from Cooper et al., Nature Reviews Clinical Oncology, 2022.***

BRAF mutations

Somatic *BRAF* mutations have been reported in 1% to 5% of lung adenocarcinoma cases (**Figure 1**), with V600E being the most prevalent (50%). The dual inhibition of BRAF and MEK by association of dabrafenib with MEK inhibitor trametinib has shown improved survival when compared to monotherapy in patients with $BRAF^{V600E}$-mutant NSCLC, having progressed after at least one line of treatment with chemotherapy (Planchard, Besse, et al., 2016; Planchard et al., 2021; Planchard, Kim, et al., 2016). These findings led to the Food and Drug Administration (FDA) approval of dabrafenib-trametinib combination therapy for the treatment of $BRAF^{V600E}$-mutant NSCLC regardless of previous treatment.

Other oncogenic drivers

The notion of oncogene-addicted subgroups of NSCLC is expanding. The most prevalent oncogenic driver is the *KRAS* mutation, which is found in 20-30% of lung adenocarcinomas (**Figure 1**). There has been stalling progress in targeting KRAS for many decades until a recent major breakthrough has been made with the direct targeting of mutant G12C protein. Two potent molecules, sotorasib (AMG510) and adagrasib (MRTX849), have shown clinical efficacy in $KRAS^{G12C}$-mutant NSCLC and subsequently received accelerated FDA approval (Jänne et al., 2022; Skoulidis et al., 2021). More recently, a novel *CLIP1–LTK* fusion has been identified in 0.4% of cases, sensitive to targeted therapy using ALK TKI lorlatinib (Izumi et al., 2021). Additionally, *neuregulin 1* (*NRG1*) fusions issued from chromosomal rearrangements are rare oncogenic drivers that may occur at high frequencies in NSCLC. Exciting findings reported at the American Society of Clinical Oncology (ASCO) 2022 meeting showed that zenocutuzumab – a HER2/HER3 bispecific antibody – has robust clinical activity in patients with $NRG1^{+}$ solid tumors, showing 34% ORR, including 35% ORR in NSCLC (NCT02912949) (Schram et al., 2022).

3) Current clinical management of non-oncogene addicted NSCLC

Clinical management of NSCLC patients without actionable oncogenic driver mutations depends on the clinical staging of the disease as well as its histological classification. The advent of immune checkpoint inhibitors (ICIs) targeting either programmed cell death 1 (PD-1) receptor, its ligand PD-L1 or cytotoxic T-lymphocyte-associated antigen 4 (CTLA-4) has revolutionized the therapeutic landscape of advanced NSCLC over the last few years (**Figure 3**).

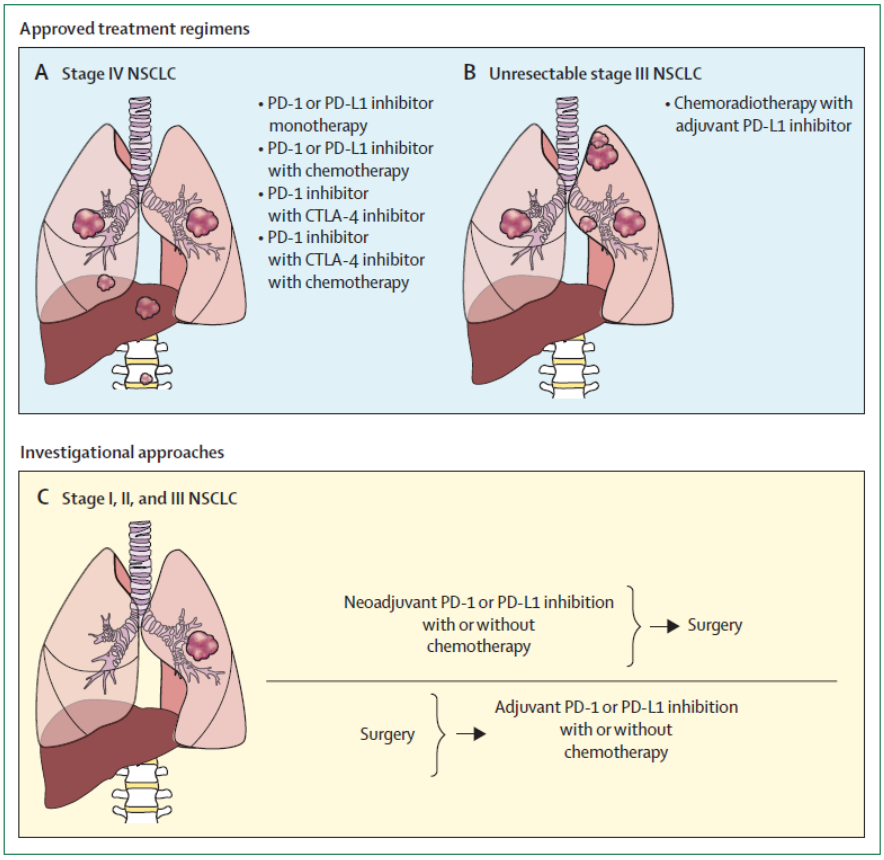


Figure 3. Immunotherapy treatment approaches in NSCLC. (**A**) Multiple regimens are approved for patients with stage IV NSCLC, based on tumor histology and PD-L1 expression. (**B**) For patients with unresectable stage III NSCLC, standard treatment consists of curative intent chemoradiotherapy and then 12 months of adjuvant PD-L1 inhibition. (**C**) It is hoped that benefit of immune checkpoint inhibitors in stage IV and stage III NSCLC can be shifted to earlier stage disease. ***Figure and legend adapted from Thai et al., The Lancet, 2021.***

Indeed, immunotherapy-based treatments of advanced NSCLC in the first-line setting have significantly improved OS compared to chemotherapy alone, according to findings from multiple clinical trials (**Table 1**). The current cornerstone treatment

regimen for stage IV NSCLC – irrespective of PD-L1 status – is either PD-1 inhibitor pembrolizumab plus permetrexed and chemotherapy in non-squamous histology (KEYNOTE-189), or dual PD-1 and CTLA-4 inhibition by nivolumab and ipilimumab (CheckMate-227) (Gadgeel et al., 2020; Gandhi et al., 2018; Hellmann et al., 2019; L. G. Paz-Ares et al., 2022). Pembrolizumab alone is indicated for the treatment of advanced NSCLC patients presenting a PD-L1 tumor score of 50% or greater (Reck et al., 2016) (**Figure 3**). In 2021, CheckMate-9LA study findings revealed that the addition of two cycles of chemotherapy to nivolumab plus ipilimumab combination further improved clinical benefit, thus adding an option for first-line treatment of stage IV NSCLC regardless of PD-L1 expression and histology (L. Paz-Ares et al., 2021). In patients with previously untreated, PD-L1$^{+/-}$ metastatic squamous NSCLC, combination of pembrolizumab and chemotherapy (carboplatin+paclitaxel or nab-paclitaxel) has proven efficacy in the first-line setting (L. Paz-Ares et al., 2018, 2020).

On the other hand, more therapeutic approaches are needed in early-stage resectable disease (stage IB-IIA NSCLC), as surgery with curative intent remains the standard of care but 30-55% of patients still experience disease recurrence (Thai et al., 2021). Administration of neoadjuvant (before main surgical treatment) or adjuvant (after surgery) chemotherapy has shown modest benefit over surgery alone but generated important toxicity. Benefit from ICIs observed in advanced stages led to ICI-based investigational approaches in stage I-III NSCLC. Recent findings reported from phase III CheckMate-816 study in resectable NSCLC showed that nivolumab plus chemotherapy neoadjuvant therapy had significantly improved clinical efficacy over chemotherapy alone (Forde et al., 2022). While for most patients with stage IIB-IIIC inoperable NSCLC, chemoradiotherapy followed by adjuvant anti-PD-L1 durvalumab is the standard of care since 2018 (**Figure 3**) (Antonia et al., 2017, 2018).

Table 1. Phase III clinical trials and results of immunotherapy-based therapeutic strategies in NSCLC.

Study / agent	Clinical setting	Experimental arms	Primary endpoint	References
KEYNOTE-024 Pembrolizumab	Advanced PD-L1≥50% NSCLC - 1st line	Pembro *vs platinum-doublet*	PFS 10.3 months *vs PFS 6.0 months*	(Reck et al., 2016)
KEYNOTE-189 Pembrolizumab	Advanced nonsquamous NSCLC - 1st line	Pembro+permetrexed-platinum *vs placebo+ permetrexed-platinum*	2-year OS rate 46% *vs 2-year OS rate 30%*	(Gadgeel et al., 2020; Gandhi et al., 2018)
CheckMate-227 Nivolumab	Advanced or recurrent NSCLC - 1st line	Nivo+ipilimumab *vs platinum-doublet*	4-year OS rate 29% months *vs OS rate 18 months (PD-L1≥1%)*	(Hellmann et al., 2019; L. G. Paz-Ares et al., 2022)
CheckMate-9LA Nivolumab	Advanced or recurrent NSCLC - 1st line	Nivo+ipilimumab+platinum doublet *vs chemotherapy*	OS rate 15.6 months *vs OS rate 10.9 months*	(L. Paz-Ares et al., 2021)
CheckMate-816 Nivolumab	Stage IB-IIIA resectable NSCLC	Neoadjuvant Nivo+chemotherapy *vs chemotherapy*	EFS 31.6 months *vs EFS 20.8 months*	(Forde et al., 2022)
PACIFIC Durvalumab	Stage III unresectable, previously treated NSCLC	Durvalumab *vs placebo*	2-year OS rate 66.3% *vs OS rate 55.6%*	(Antonia et al., 2018)
KEYNOTE-407 Pembrolizumab	Advanced squamous NSCLC - 1st line	Pembro+carbo-pacli or [nab]pacli *vs placebo+* carbo-pacli or [nab]pacli	OS rate 15.9 months *vs OS rate 11.3 months*	(L. Paz-Ares et al., 2018, 2020)

Abbreviations: CTC, circulating tumor cell; CDX, CTC-derived xenograft; PDX, patient-derived xenograft. Pembro, pembrolizumab; PFS, progression-free survival; OS, overall survival; nivo, nivolumab; EFS, event-free survival; carbo, carboplatin; nab, nanoparticle albumin-bound; pacli, paclitaxel.

II. The metastatic process

Despite significant therapeutic advances in cancer treatment, more than 90% of cancer deaths are due to severe metastatic dissemination and acquired resistance to treatment. Research on the metastatic cascade has been long hampered by its enormous complexity and the lack of adequate experimental models of metastasis. Nevertheless, recent progress using patient-derived mouse models and circulating tumor cell (CTC) characterization has provided significant insight into this complex multi-step process and further improved our understanding of its basic biological principles.

1) Metastatic inefficiency

The main route to metastatic spread is cancer cell dissemination from the primary tumor and/or distinct metastatic foci by invasion of blood and lymphatic capillaries. Nevertheless, metastatic colonization is a highly inefficient process, consisting of several rate-limiting steps in which "survival of the fittest" is applied. Indeed, a key critical aspect of blood-borne metastasis is the half-life of CTCs in circulation, which is likely in the order of a few hours, based on an estimation of CTC count decline following primary tumor surgical resection (Meng et al., 2004; Stott, Lee, et al., 2010). These clinical observations are in line with experimental findings in the mouse model. This was evaluated for the first time in 1975 in a study by Fidler *et al*, which demonstrated that B16 melanoma tumor cell survival and metastatic fate is directly related to tumor cell characteristics, including the degree of initial capillary arrest (Fidler, 1975). Following this study, Luzzi and colleagues aimed to determine the portion of B16F1 melanoma cells injected in the mouse portal vein which would successfully form distant lesions. The authors have shown that, while 82 % of injected cells had extravasated into the liver parenchyma, only 2% formed micrometastases and only 1 in 100 of these micrometastases (0.02% of injected cells) grew as tumors (Chambers et al., 2002; Luzzi et al., 1998). Another study has highlighted the early role of apoptosis in impeding metastatic growth in the lungs (Wong et al., 2001). Such observations *in vivo* imply that

the factors regulating survival and tumor-initiating capacity of tumor cells in secondary sites are crucial determinants of metastatic outcome.

2) Stages of the metastatic cascade

a. Proliferation and local invasion

The initial steps of the metastatic process requiring primary tumor cell proliferation and invasion of the parenchyma have been extensively studied (**Figure 4**) (Massagué & Obenauf, 2016). Tumor growth begins with the disruption of the basement membrane and is thought to be enabled by the activation of epithelial-mesenchymal (EMT) transition in tumor cells – loss of cell–cell junctions and cell polarity as well as dynamic reorganization of cytoskeletal elements, enabling cell migration (described in **Introduction section II. 3)** below) (Lambert et al., 2017; Shibue & Weinberg, 2017). These physiological and morphological changes are enabled *via* the secretion of extracellular matrix (ECM)-degrading matrix metalloproteinases (MMPs) as well as dynamic changes in cell-cell (*e.g.* cadherins) and cell-matrix adhesion molecules (*e.g.* integrins). After basement membrane rupture, cancer cells come into contact with stromal cells such as cancer-associated fibroblasts (CAFs) and tumor-associated macrophages (TAMs) that help sustain cancer cell proliferation and survival, thus constituting the tumor microenvironment (Massagué & Ganesh, 2021; Quail & Joyce, 2013). While normal fibroblasts are predominant in connective tissue, promote an epithelial phenotype and suppress metastasis, CAFs are present in substantial amounts in the tumor microenvironment and carry distinct pro-tumorigenic functions (Dumont et al., 2013). They are activated *via* growth factors and cytokines secreted by neighboring cells in the stroma (*e.g.* transforming growth factor beta - TGFβ, fibroblast growth factor - FGF, platelet-derived growth factor - PDGF) (Y. Chen et al., 2021; Öhlund et al., 2014; Quail & Joyce, 2013). Moreover, they promote cancer cell proliferative and invasive properties by stimulating inflammation and angiogenesis, mainly through vascular endothelial growth factor (VEGF) secretion (Erez et al., 2010). On the other hand, TAMs regulate tumorigenesis by several aspects including the mediation of

immune defense, as well as the secretion of large amounts of proteases that support cancer cell invasion and resistance to therapy (Gocheva et al., 2010; Shree et al., 2011). Importantly, a co-operation between multiple components of the tumor microenvironment is required to favor angiogenesis, a key hallmark of cancer promoting tumor vascularization (Folkman, 1971). This will in turn enable intravasation of tumor cells in newly formed vasculature and subsequent dissemination (**Figure 4**).

b. Intravasation into tumor vasculature and circulation

In response to all microenvironmental cues from the stroma, tumor cells undergo EMT to enter the circulatory system (Thiery et al., 2009). In circulation, CTCs are subject to several physical and biological constraints such as shear stresses, pH and immune surveillance, from which only very few are able to evade (~ 0.01%). Hence, cancer cells must rapidly adapt to overcome these threats. CTCs may circulate as single cells or less frequently as clusters or "circulating tumor microemboli" (CTM) of 2 to 50 CTCs with significantly enhanced tumor-initiating capacity (Aceto et al., 2014; Krebs et al., 2014). The survival advantage they hold over single CTCs stems from their capacity to resist physical constraints and apoptosis events such as anoikis – a physiological elimination induced by the disruption of cell-matrix and cell-cell interactions. CTC clusters may also consist of other cell types such as platelets, neutrophils or fibroblasts, which in turn provide CTCs with immune protection as well as an improved capacity to disseminate (Haemmerle et al., 2018; Hurtado et al., 2020; Labelle & Hynes, 2012; Massagué & Ganesh, 2021; Szczerba et al., 2019). Notably, cooperative platelet-coating of CTCs protects them against natural killer (NK) cell attacks *via* platelet-mediated secretion of immunosuppressive factors such as TGFβ and PDGF, or through fibrinogen, a physical barrier which impedes NK cell-mediated clearance (Labelle & Hynes, 2012; Palumbo et al., 2005). Neutrophils may serve immunosuppressive functions as well as promote metastasis through MMP secretion by favoring CTC extravasation (Spiegel et al., 2016).

c. Extravasation and colonization of target organs

During transit, CTCs become trapped in small capillary beds by adhering to the endothelium using organ-specific endothelial molecules, before extravasation into the organ parenchyma by crossing endothelial barriers and establishment of overt metastasis (Massagué & Ganesh, 2021). While a vast majority perishes in circulation, successful CTC extravasation may be primed by platelet-CTC interactions**,** which have been shown to synergistically activate TGFβ and NF-κB signaling pathways, leading to a pro-metastatic EMT-like phenotype (Labelle et al., 2011). Alternatively, in response to chemokine secretion (*i.e.* CC-chemokine ligand 2 - CCL2) by tumor cells, myeloid cells such as monocytes may be recruited to stimulate extravasation by producing endothelial permeability factors such as VEGF (Qian et al., 2011; Reymond et al., 2013; Wolf et al., 2012). Tumor cells also express specific integrins that mediate their interactions with capillaries as well as their adhesion to the new ECM.

Organ colonization is the most biologically complex step of the metastatic process. Disseminated tumor cells (DTCs) may undergo phenotypic transformation to adapt to and proliferate in distant sites, with some tumor types preferentially relapsing in specific organs (*i.e.* organ tropism) (Lambert et al., 2017; Massagué & Ganesh, 2021). Moreover, similarly to EMT during invasion, mesenchymal-epithelial transition (MET) seems to be necessary for extravasation and tissue colonization (Craene & Berx, 2013; Thiery et al., 2009). MET is controlled by the overexpression of epithelium-specific transcription factors (TFs) such as grainyhead-like protein 2 homologue (GRHL2) or ETS-TFs ELF3/ELF4 in mesenchymal cells, as well as microRNAs (miRs) (Craene & Berx, 2013). After their infiltration into target organs, cancer cells are challenged by host-tissue defences against which they must develop barriers to be able to from micro- and macrometastases. However, as mentioned above, only very few cells possess intrinsic or acquired ability to overcome these barriers and the lack of appropriate microenvironmental cues in the distant organ may lead to the elimination of cancer cells after extravasation (**Figure 4**). Conversely, cells may settle in supportive niches

and subsequently enter into protective quiescence, a state which will be further described in **Introduction section II. 4)**.

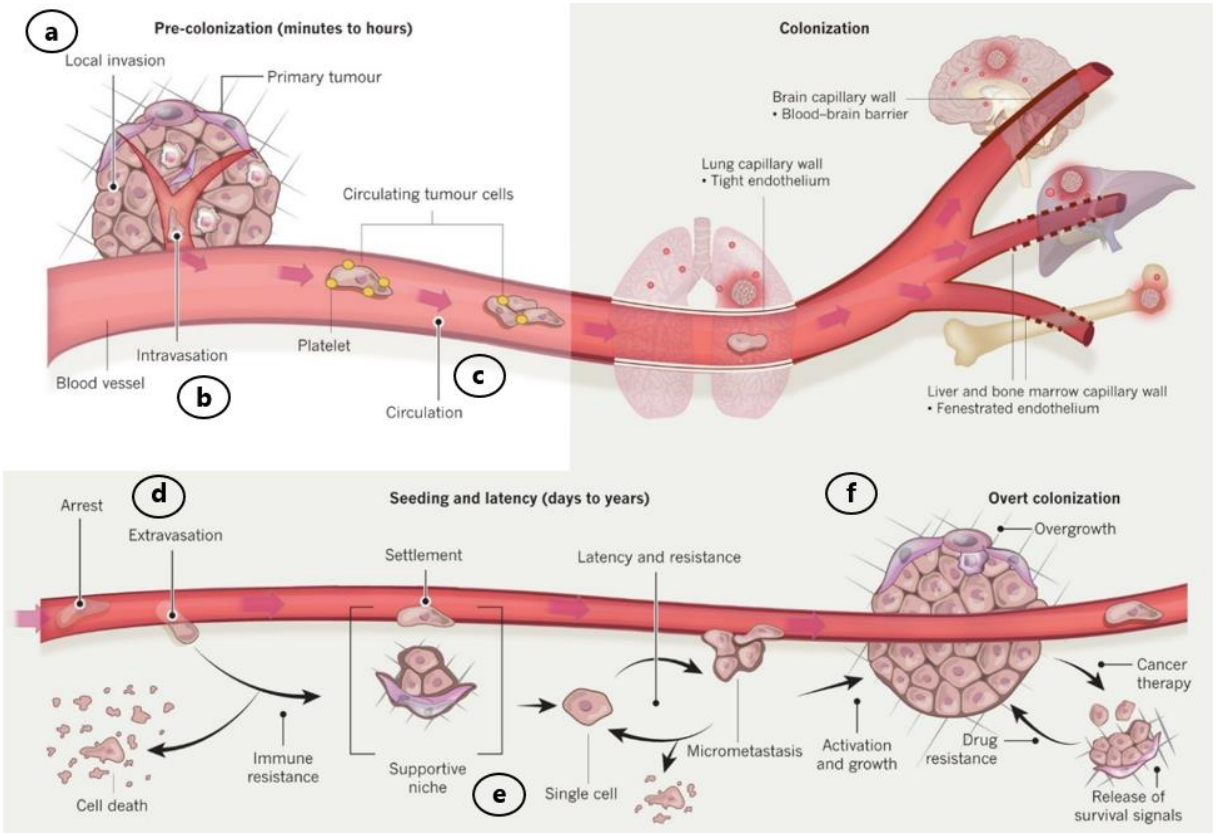


Figure 4. Key steps of the metastatic cascade. Metastasis proceeds through multiple steps and restrictive bottlenecks. The pre-colonization phase of metastasis comprises a series of events that occur on a timescale of minutes to hours. Local invasion of the primary tumor by cancer cells **(a)** is followed by intravasation into tumor vasculature **(b)**. Cancer cells then enter the circulatory system as single cells or as a cluster **(c)**. CTCs may be coated with platelets, which protects them from oxidative stress during transit. Circulatory patterns and the differing structure of the capillary walls in each organ influence the dissemination of CTCs. On their arrest in capillaries at distant sites, the cancer cells extravasate into the parenchyma of target organs **(d)** to commence colonization, which proceeds in several steps on a timescale of years. After extravasation, colonizing cancer cells settle in supportive niches that enable them to survive and retain stem cell-like tumor-initiating capacity **(e)**. Tumor cells then enter a latency phase, which can last from months to decades, during which they must achieve long-term survival. Cells then break out of latency and overtake the local tissue microenvironment **(f)**. ***Figure and legend adapted from Massagué & Obenauf, Nature, 2016.***

3) EMT during cancer progression

Metastatic progression involves several key biological processes, including EMT, an essential phenomenon in embryonic development. During EMT, epithelial cells lose their polarity and cell-cell adhesion, detach from the basement membrane and acquire mesenchymal features before migrating and invading nearby tissue (Kalluri &

Weinberg, 2009). A plethora of molecular networks are implicated in EMT, including TGFβ, Wnt, Notch, FGF and epidermal growth factor signaling pathways (Thiery et al., 2009). Furthermore, EMT events are dynamically governed by major EMT-inducing TFs (EMT-TFs) including SNAI1/2, ZEB1/2 and TWIST, interacting with epigenetic regulators to transcriptionally repress cell-cell adhesion molecule E-cadherin (Morel et al., 2012; Puisieux et al., 2014; Thiery et al., 2009).

The implication of EMT in the metastatic process has long been a controversial topic. Two main reports have shown that EMT-induced mesenchymal features are not required for metastatic dissemination but EMT rather contributes molecularly and phenotypically to chemoresistance (Fischer et al., 2015; X. Zheng et al., 2015). Indeed, this EMT function may be possible through EMT-TFs-mediated bypass of oncogene-induced safeguard mechanisms, such as premature senescence and apoptosis, by abrogating p53- and RB1-dependent pathways (Ansieau et al., 2008; Morel et al., 2012; Ohashi et al., 2010). Despite long-standing debate, mounting evidence indicates the involvement of EMT in epithelial carcinogenesis, promoting invasion and dissemination (**Figure 5**). This viewpoint has been strengthened by the elucidation of transitional EMT states. Indeed, EMT may not be a dichotomous cell fate but rather a highly dynamic and reversible process, as cells could undergo partial EMT and present a "hybrid" or "intermediate" E/M phenotype, thus reflecting important cellular plasticity in tumor cells (Kalluri & Weinberg, 2009; Nieto et al., 2016). One of the first studies describing EMT in CTCs was done by Hou *et al* in lung cancer. The captured CTCs harbored heterogeneous expression of EMT markers (Hou et al., 2011). Our group and others have subsequently supported these observations in several malignancies including NSCLC, breast and prostate cancer (Armstrong et al., 2011; Kallergi et al., 2011; Lecharpentier et al., 2011; Lindsay et al., 2017; Papadaki et al., 2019; M. Yu et al., 2014). This led to the current hypothesis that CTC subclones displaying intermediate E/M features may generate more aggressive populations with a high seeding ability. The reverse MET process is believed to be critical in triggering tumor cell migration arrest

and colonization at distant organ sites, as mentioned previously in **Introduction section II. 2)c.** (**Figure 5**) (Craene & Berx, 2013).

These dynamic processes are tightly regulated by the tumor microenvironment (Shibue & Weinberg, 2017). Multiple miRs have emerged as potent regulators of EMT and MET programs by targeting EMT-TFs or other relevant actors (Lamouille et al., 2013). Moreover, miR-induced regulatory mechanisms have been described, such as the double-negative feedback ZEB1/2-miR200 loop which regulates EMT through the maintenance of stemness properties (Bracken et al., 2008). Other regulatory pathways include alternative splicing events and post-translational modifications at the protein level (Nieto et al., 2016).

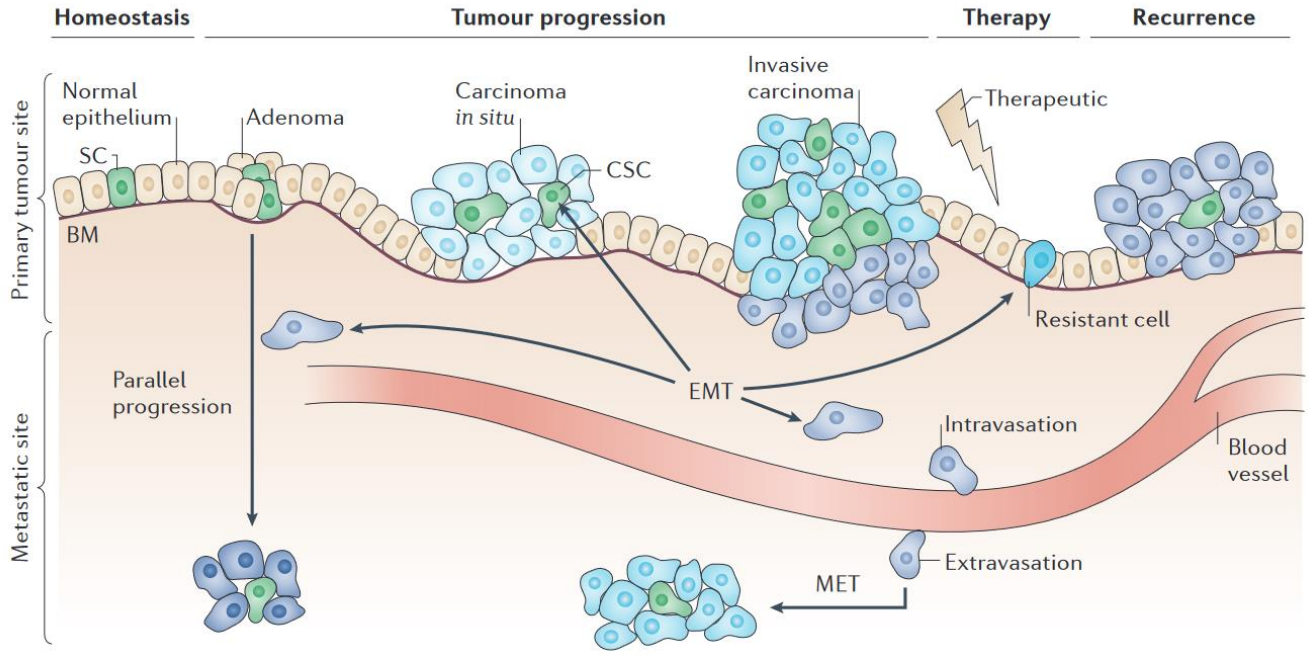


Figure 5. Role of epithelial-mesenchymal transition (EMT) during cancer progression. In tumor cells, EMT-inducing transcription factors may primarily redefine the epithelial status of the cell, potentially — but not necessarily — assigning stem cell (SC) characteristics to dedifferentiated tumor cells, or they may redefine resident genetically altered stem cells to be cancer stem cells (CSCs). Tumor cell dissemination from primary tumor and subsequent migration after breakdown of the basement membrane can only be achieved if the cancer cell has acquired the necessary genetic aberrations and received the appropriate signals at the tumor–host interface. At this point, the active contribution of the EMT-associated program is probably to give survival signals and to maintain the mesenchymal status of the metastasizing cell. It is likely that EMT also has a role in parallel progression, in which tumor cells escape early and metastasis progresses in parallel to the primary tumor. EMT features may further promote resistance to therapy, leading to recurrence and a poor prognosis. The degree of EMT during

the different steps in cancer progression probably depends on the imbalance of several associated regulatory networks with activated oncogenic pathways. MET, mesenchymal to epithelial transition. ***Figure and legend adapted from De Craene B & Berx, Nature Reviews Cancer, 2013.***

4) The pre-metastatic niche and tumor dormancy

According to the "seed and soil" theory postulated by Stephen Paget in 1889, the homing of tumor cells – termed "seed" – at specific sites depends on interactions with the organ-specific extrinsic/supportive microenvironment, termed "soil" (Paget, 1889). This discovery was challenged a few decades later by James Ewing, who proposed that metastatic dissemination occurs solely *via* the dynamics of the lymphatic or haematogenous flow (Ewing, 1928). Ewing's perspective prevailed until Fidler and colleagues demonstrated the selective nature of metastasis (Fidler & Nicolson, 1976; Hart & Fidler, 1980). A pioneer study in 2005 highlighted that cues from primary tumor-secreted factors maintain a pre-metastatic niche (PMN), which dictates site-specific tumor dissemination and is indispensable for tumor cell survival (Kaplan et al., 2005). Following its discovery, dissecting the role of the PMN in metastasis and the cellular and molecular aspects that define it has attracted significant attention over the years. It is now acknowledged that the complex interplay between tumor-specific humoral factors implicated in the PMN is crucial in defining organ-specific metastatic tropisms (**Figure 6**) (Y. Liu & Cao, 2016; Peinado et al., 2017; Psaila & Lyden, 2009). For example, chemo-attractants S100A8 and S100A9 have been shown to promote pre-metastasis in lung tissues through inflammation *via* the activation of NF-κB signaling (Hiratsuka et al., 2008). In breast cancer, exosomal integrins $\alpha_6\beta_4$ and $\alpha_v\beta_5$ dictated metastasis in the liver and the lung respectively (Hoshino et al., 2015). More recently, lung stromal fibroblasts have been shown to confer an immunosuppressive phenotype in myeloid cells *via* prostaglandin E2 production and support lung metastasis in breast cancer models (Z. Gong et al., 2022).

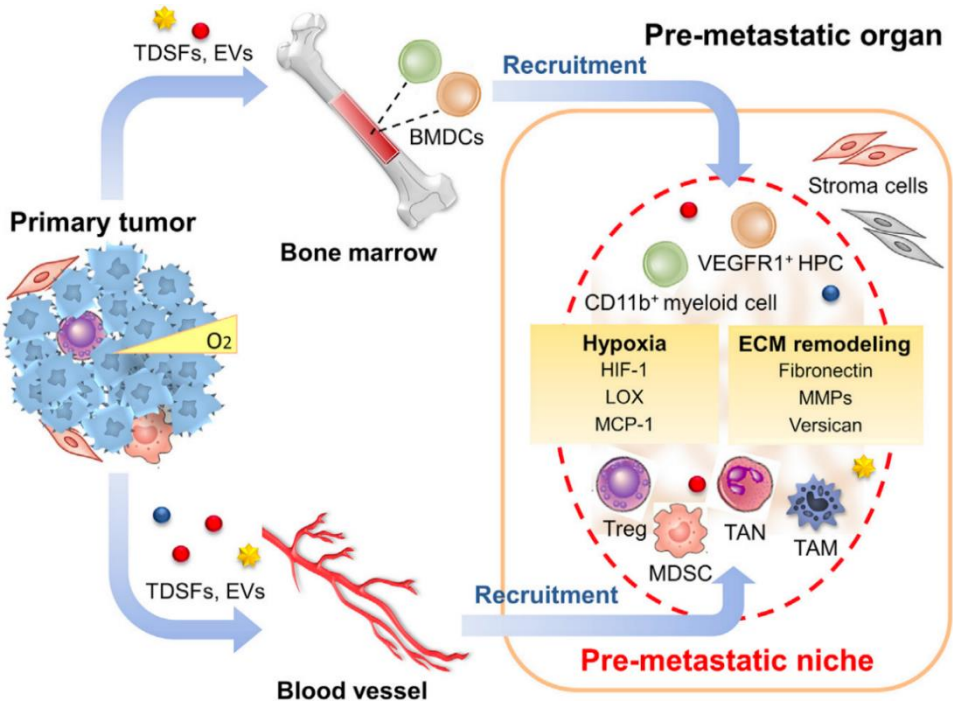


Figure 6. Induction and formation of the pre-metastatic niche. Tumor-derived secreted factors (TDSFs) and extracellular vesicles (EVs) induce the mobilization and recruitment of several cell populations to secondary organ sites, including bone marrow-derived cells (BMDCs) such as VEGFR1$^+$ hematopoietic progenitor cells (HPCs) and CD11b$^+$ myeloid cells as well as regulatory/suppressive immune cells, including myeloid-derived suppressive cells (MDSCs), Treg cells, TAMs, and tumor-associated neutrophils (TANs). The interaction among these TDSFs, tumor-recruited cells, and local stroma may create a suitable niche microenvironment for metastatic tumor cell colonization. Hypoxia and ECM remodeling also promote the formation of pre-metastatic niche. ***Figure and legend adapted from Liu & Cao, Cancer Cell, 2016.***

Alternatively, other tumors may create a "silent" PMN, in which tumor cells could survive in a dormant state. Dormant metastasis is a phenomenon of major importance in the clinic, as it may be in part responsible for cancer recurrence decades after the end of treatment (Massagué & Ganesh, 2021). Although much remains to be unraveled to establish a direct causal link between cancer cell dormancy and relapse, the detection of minimal residual disease in breast cancer patients correlated with a higher risk of relapse and poor prognosis (Braun et al., 2005). Another study showed that patients with surgically-removed early-stage estrogen receptor-positive breast cancer may still experience metastatic recurrence up to 20 years after initial diagnosis (Pan et al., 2017). More recently, Baldominos and colleagues reported that quiescent cancer cells may form hypoxic clusters that evade immune infiltration and resist to

immunotherapy in triple-negative breast cancer (Baldominos et al., 2022). Several growth-inhibitory cues present in the perivascular microenvironment that induce and maintain dormancy of DTCs have been elucidated, notably TGFβ2 in the bone marrow (Bragado et al., 2013; Risson et al., 2020). In addition, bone morphogenetic protein 4 (BMP4) has been shown to induce dormancy of breast cancer cells exclusively in the lung (Gao et al., 2012), while BMP7 mediated reversible senescence of prostate cancer stem cell-like cells in bone (Kobayashi et al., 2011). Conversely, to escape dormancy, DTCs may activate the canonical TGFβ2 pathway (Bragado et al., 2013) or express BMP inhibitors such as Coco (H. Gao et al., 2012). Furthermore, fibronectin and type I collagen-enriched microenvironments have been shown to generate proliferation-permissive signals (Aguirre-Ghiso et al., 2001; Barkan et al., 2010; Risson et al., 2020).

5) Cancer stem cells

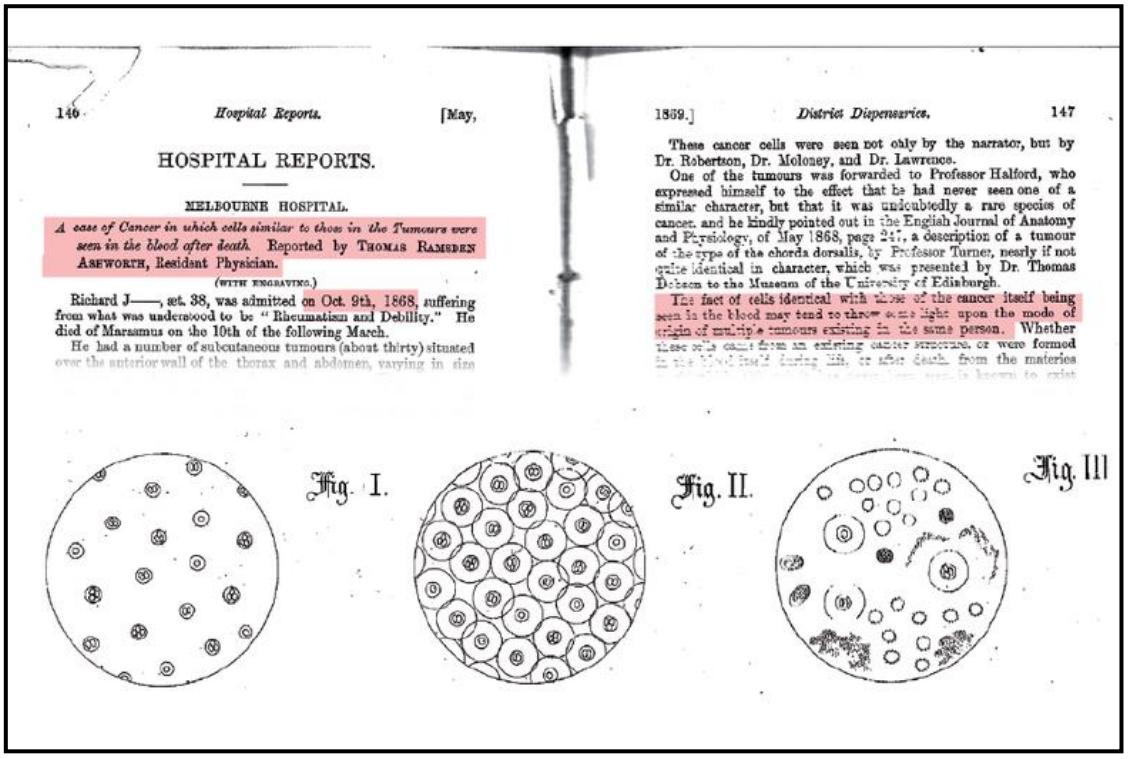
It is now widely accepted that stem cell features are rooted in the biology of several types of human malignancies. The cancer stem cell (CSC) concept posits that cancer initiation and propagation, similarly to healthy tissue homeostasis, is fueled by a minor subset of tumor cells harboring adult stem cell properties, *i.e.* self-renewal, pluripotency, as well as the capacity to proliferate indefinitely (Jordan et al., 2006). There are two distinct hypotheses depicting the origin of CSCs: one postulates that CSCs arise from the malignant transformation of adult stem cells, the other suggests that CSCs may originate from the re-gain of self-renewal properties in differentiated stem cells, through the accumulation of multiple genetic mutations (Huntly & Gilliland, 2005; Krivtsov et al., 2006). Regardless of their origin, it is widely accepted that cancer stemness is a collective product of genetic alterations, epigenetic modifications and microenvironmental factors (Kreso & Dick, 2014).

In an effort to characterize CSCs, several groups have shown that EMT confers stem cell-like properties (Mani et al., 2008; Morel et al., 2008). Phenotypic plasticity acquired through EMT allows CSCs to initiate malignancy when transplanted in immunodeficient mice (Al-Hajj et al., 2003; H. Liu et al., 2010; Mani et al., 2008; Ricci-Vitiani et al., 2007).

The Weinberg laboratory has demonstrated that EMT induction *via* ectopic expression of TWIST and SNAIL in immortalized mammary epithelial cells generated cells with mammosphere-forming abilities (Mani et al., 2008). These cells exhibited a $CD44^{high}/CD24^{low}$ antigen phenotype – an expression pattern that has been shown to be enriched in tumor-initiating breast cancer cells (Al-Hajj et al., 2003). Hence, among DTCs, CSCs constitute the cell population with tumor initiation features and xenograft assays are therefore central for their characterization (Kreso & Dick, 2014). CSCs are also required for organ colonization at distant sites, which necessitates cues from specialized microenvironmental niches that help maintain self-renewal and tumor-initiating potential (Malanchi et al., 2012; Oskarsson et al., 2014). Several signaling pathways are key players in supporting CSC survival and fitness, including Wnt, Notch and Sonic hedgehog cascades (Reya et al., 2001). Indeed, breast cancer xenotransplantation studies have shown that *in vivo* activation of CSC Wnt and Notch pathways is necessary for metastatic cell outgrowth in the lungs (Oskarsson et al., 2011). CSC populations are present in multiple malignancies but their analysis in CTCs has been hindered by complex CTC heterogeneity and paucity in blood. Nevertheless, phenotypic, genetic and functional characterization of patient CTCs and CTC-derived models may provide further insight into the CSC properties of CTC subsets.

III. Circulating tumor cells

The existence of circulating tumor cells (CTCs) was first documented by Thomas Ashworth in 1869 (**Figure 7**). During an autopsy study of a patient with metastatic cancer, he discovered non-hematopoietic cells in the blood with features resembling tumor cells found in the patient's secondary tumor sites. He hypothesized that if these cells are indeed issued from existing tumors, they must have disseminated through the circulatory system, thus contributing to secondary lesions present in this patient (T. Ashworth, 1869).



146 *Hospital Reports.* [May,

HOSPITAL REPORTS.

MELBOURNE HOSPITAL.

A case of Cancer in which cells similar to those in the Tumours were seen in the blood after death. Reported by THOMAS RAMSDEN ASEWORTH, Resident Physician.

(WITH ENGRAVING.)

Richard J——, æt. 38, was admitted on Oct. 9th, 1868, suffering from what was understood to be "Rheumatism and Debility." He died of Marasmus on the 10th of the following March.

He had a number of subcutaneous tumours (about thirty) situated over the anterior wall of the thorax and abdomen, varying in size

1869.] *District Dispensaries.* 147

These cancer cells were seen not only by the narrator, but by Dr. Robertson, Dr. Moloney, and Dr. Lawrence.

One of the tumours was forwarded to Professor Halford, who expressed himself to the effect that he had never seen one of a similar character, but that it was undoubtedly a rare species of cancer, and he kindly pointed out in the English Journal of Anatomy and Physiology, of May 1868, page 247, a description of a tumour of the type of the chorda dorsalis, by Professor Turner, nearly if not quite identical in character, which was presented by Dr. Thomas Dobson to the Museum of the University of Edinburgh.

The fact of cells identical with those of the cancer itself being seen in the blood may tend to throw some light upon the mode of origin of multiple tumours existing in the same person. Whether these cells came from an existing cancer structure, or were formed

Fig. I. Fig. II. Fig. III

Figure 7. Historical medical journal article by Thomas Ashworth in 1869 describing circulating tumor cells for the first time (T. Ashworth, 1869). *Figure adapted from Nieva & Kuhn, Future Oncology, 2012.*

CTC scarcity in peripheral blood, which is estimated at as few as one CTC per ~ 10^7 white blood cells per mL of blood, is still a key technical challenge for their detection and characterization (Krebs et al., 2014; van de Stolpe et al., 2011). Nonetheless, the tremendous technological advances of the past two decades have prompted the investigation of CTC biology and their role in metastatic dissemination. To date, CTC research has focused on two main aspects: evaluating the role of CTCs as predictive

biomarkers of patient response in the clinic and investigating the underlying biology of their metastatic potential.

1) CTC enrichment and detection methods

The field of research on CTCs remains an enormous technological challenge despite significant progress over the years. Indeed, owing to CTC heterogeneity, a multitude of diverse assays have been developed and most of them include two key steps: enrichment followed by detection. CTCs are either positively- or negatively-enriched based on their protein marker expression or physico-biological properties such as size, density and electric charge that distinguish them from a pool of blood cells, or the combination of the two (*e.g.* protein expression and cell size) (**Figure 8**) (Alix-Panabières & Pantel, 2014; Ross et al., 2015).

a. Enrichment strategies

i. Positive selection approaches

Positive CTC selection captures tumor cells using bead-conjugated antibodies directed against cell-surface antigens. Epithelial cell adhesion molecule (EpCAM) tumor cell surface marker is the most commonly used marker for positive enrichment of epithelial CTCs using the CellSearch® System (Menarini-Silicon Biosystem, Bologna, Italy). In 2004, the CellSearch was the first semi-automated platform validated for the detection and enumeration of CTCs in a blood sample. It is the only technology cleared by the FDA to aid in predicting prognosis for patients with metastatic breast, prostate or colorectal cancer (Allard et al., 2004). The CellSearch platform uses ferromagnetic beads coupled to EpCAM, followed by fluorescent detection of CK 8, 18 and/or 19, CD45 and the nucleus (4',6-diamidino-2-phenylindole – DAPI). The detected CTCs must present a $DAPI^+/CD45^-/CK^+$ profile. This system is adapted solely for the capture of CTCs expressing moderate or high EpCAM expression and excludes non-epithelial cells, thereby missing CTCs that may have undergone EMT. Although limited by substantial CTC heterogeneity, the CellSearch system is a highly robust, standardized, reproducible

technology which remains the gold standard reference of CTC technologies today. The development of a number of techniques based on EpCAM enrichment has followed, notably microfluidic devices such as the CTC-chip (Nagrath et al., 2007) and the herringbone chip (Stott, Hsu, et al., 2010), as well as the immunomagnetic MagSweeper device, which isolates viable EpCAM$^+$ CTCs (Talasaz et al., 2009). The novel GILUPI CellCollector® allows a wire-based *in vivo* capture and isolation of EpCAM$^+$ CTCs directly from the patient's arm vein (Gorges et al., 2016).

To broaden the scope of CTC capture beyond EpCAM expression, multiple label-free enrichment approaches based on physical properties were developed, notably methods that use a filtration system, which enriches CTCs according to their large size compared to leukocytes and/or deformability, without phenotypic *a priori*. These include the ISET® (isolation by size of tumor cells) technique (Vona et al., 2000), the ScreenCell® system (Desitter et al., 2011), the CellSieve™ microfiltration system (Adams et al., 2015) and the VyCap microsieves (Wit et al., 2015). The major differences among these techniques are filter material, pore size, the need for a pre-filtration red blood cell lysis step, as well as the possibility to control the pressure against the filter. More recently, the microfluidic Parsortix® (Angle plc, Guildford, UK) technology has been developed and allows the capture of viable CTCs by reversing flow (Hvichia et al., 2016). Another widely used method is CTC enrichment by centrifugation based on a Ficoll-PAQUE™ (GE healthcare) density gradient.

ii. Negative selection approaches

Negative selection approaches aim to discard non-cancer cells (*e.g.* leukocytes), using for example a bead-conjugated antibody directed against the common hematopoietic antigen CD45. An example of enrichment approach which combines protein expression features and density of CTCs is the one combining RosetteSep™ (Stem Cell) and Ficoll density gradient: the RosetteSep contains bi-specific antibodies against hematopoietic cells and erythrocytes, which allows the formation of rosettes that will be subsequently eliminated through a Ficoll density gradient.

Overall, although tremendous effort has been put into developing capture strategies adapted for further CTC characterization, none of the technologies discussed above fully respond to the phenotypic heterogeneity of CTCs. Indeed, each presents a set of advantages and limitations.

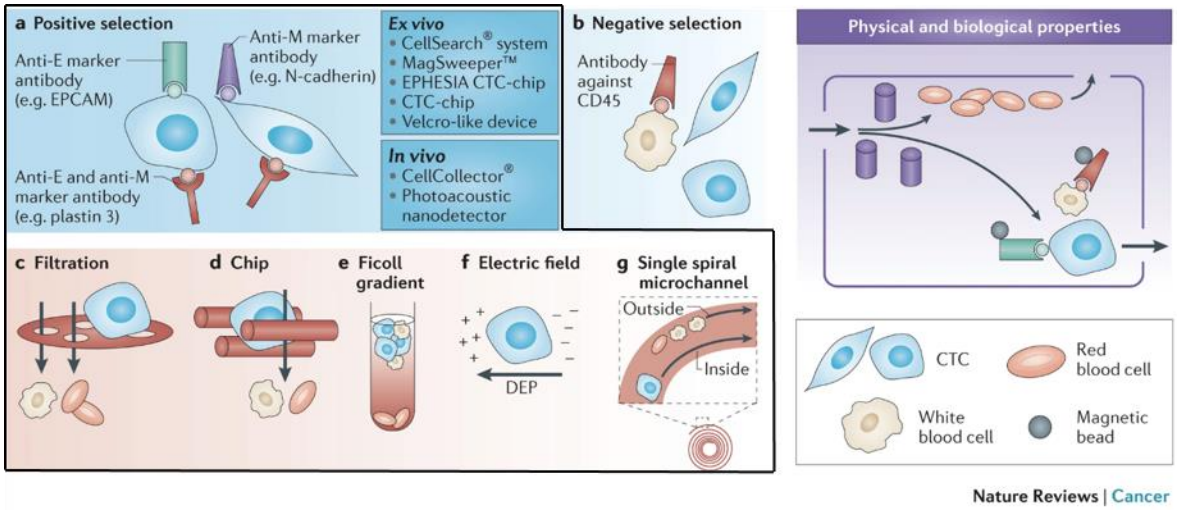


Figure 8. Circulating tumor cell enrichment technologies. CTCs can be positively (**a**) or negatively (**b**) enriched based on expression of protein markers: (**a**) using an anti-epithelial (E) antibody, an anti-mesenchymal (M) antibody or an anti-E and anti-M antibody, or (**b**) using antibodies against CD45 to deplete the unwanted leukocytes. CTCs can also be positively or negatively enriched based on properties such as size, density, deformability or electric charges through a membrane and filtration-based system based on CTC size (**c**); through posts in a microchip based on CTC size plus deformability (large and stiff CTCs are trapped on a basket of three posts) (**d**); through a centrifugation on a Ficoll density gradient based on CTC density (**e**), through dielectrophoresis (DEP) based on CTC electric charges (**f**); through a spiral CTC chip based on CTC size (**g**). Positive or negative enrichment of CTCs can also be achieved based on both physical and biological properties (CTC-iChip). ***Figure and legend adapted from Panabières & Pantel, Nature Reviews Cancer, 2014.***

b. Detection strategies

Following enrichment, individual CTCs are mostly detected by immunocytological or immunofluorescent assays using epithelial, mesenchymal, tissue- or tumor-specific markers, for subsequent visualization by microscopy or flow cytometry. Molecular DNA- or RNA-based assays on whole-blood are performed to detect and characterize CTCs and will be described in **Introduction section III.2)c.** below. Functional assays are also adapted for the detection and characterization of viable CTCs both *in vitro* (*e.g.* EPISPOT assay) and *in vivo* in xenograft models, which will be introduced in

Introduction section II.3) (Alix-Panabières & Pantel, 2014; Krebs et al., 2014; Pantel & Alix-Panabières, 2019).

To overcome technical hurdles and bias related to CTC enrichment, Epic Sciences Inc. (San Diego, CA, USA) developed the EPIC CTC platform which detects and characterizes CTCs without enrichment and with the added capacity of sample storage (Werner et al., 2015).

2) Clinical interest of CTCs

Many studies have focused on determining the clinical significance of CTCs and evaluating their use as a liquid biopsy as well as a prognostic, predictive and pharmacodynamic biomarker.

a. Liquid biopsy applications

Intratumoral heterogeneity is a major mediator of poor patient outcomes and thus constitutes a pivotal limiting factor for personalized medicine (McGranahan & Swanton, 2017). Large-scale collaborative human cancer omics studies of primary and metastatic tumor samples, such as The Cancer Genome Atlas (TCGA) and the Pan-Cancer Analysis of Whole Genomes Consortium of the International Cancer Genome Consortium (ICGC), have elucidated extensive intra- and intertumoral heterogeneity across multiple cancer types (P. J. Campbell et al., 2020; Hoadley et al., 2018). This has been further evidenced with the advent of single-cell sequencing analyses (Gawad et al., 2016).

Over the past few years, technological developments in the detection and analyses of liquid biopsy specimens from blood samples have enabled real-time monitoring of the evolving tumor landscape and resistance (Alix-Panabières & Pantel, 2021). Indeed, these assays constitute a minimally invasive alternative to tissue biopsy, feasible throughout the course of the disease. Liquid biopsy analytes in peripheral blood include CTCs, circulating tumor-derived factors such as circulating cell-free tumor DNA (ctDNA), extracellular vesicles (*e.g.* exosomes), tumor-educated platelets and metabolites (Alix-Panabières & Pantel, 2021; Ignatiadis et al., 2021). Integration of

liquid biopsy assays into the routine clinical workflow is still slow, mainly due to challenges in the standardization of preanalytical and analytical procedures. Nonetheless, we have recently been witnessing rapid progress in liquid biopsy assays. The use of ctDNA has proven to be a powerful tool for guiding treatment decisions and the new European Society for Medical Oncology (ESMO) recommendations on ctDNA use for advanced cancers genotyping and to guide targeted therapy for selected patients were just published (Chaudhuri et al., 2017; Pascual et al., 2022; Tie et al., 2022). Overall, integrating information from several circulating biomarkers is essential to define a tumor profile, stratify patients to therapeutic strategies and monitor response. CTCs represent a particularly interesting analyte as their phenotypic and molecular characterization may offer unique insight into metastatic subclones that are omitted from tissue biopsies (single-site) and other liquid biopsy assays.

b. CTC prognostic value

Clinical interest of CTCs posits on the assessment of their enumeration as a prognostic, predictive and pharmacodynamic biomarker. Numerous studies have explored CTC detection and enumeration using CellSearch and underlined the clinical significance of CTC levels in a 7.5 mL blood sample in informing PFS and OS in metastatic disease.

In metastatic breast cancer, Cristofanilli *et al* demonstrated that patients presenting at least five CTCs before the start of a new systemic therapy had worse prognosis, with significantly shorter PFS and OS than patients with fewer than five CTCs. CTC count measured at baseline is thus an independent predictive biomarker of PFS and OS in this malignancy (Cristofanilli et al., 2004). Similar results were reported in newly-diagnosed patients and further confirmed in a pooled analysis a decade later (Bidard et al., 2014; Cristofanilli et al., 2005). The prognostic value of CTCs was also reported in lung cancer, with a cut-off of five CTCs per 7.5 mL blood in NSCLC and 50 CTCs per 7.5 mL blood in SCLC (Hou et al., 2012; Krebs et al., 2011; Lindsay et al., 2017). A more recent multicenter study by Lindsay *et al* confirmed the prognostic value of an additional threshold of ≥2 CTCs in NSCLC (Lindsay et al., 2019). In castration-resistant prostate cancer (CRPC), CTC counts at baseline and after treatment predicted OS and

thus also present an independent prognostic factor (de Bono et al., 2008; Olmos et al., 2009). Furthermore, our group showed that the detection of vimentin- and Ki-67-expressing CTCs was associated with poorer outcomes in metastatic CRPC (Lindsay et al., 2016). In colorectal cancer, patients presenting at least three CTCs per 7.5 mL blood had worse PFS and OS compared to patients with less than three CTCs (Cohen et al., 2008). Pierga *et al* showed that CTC detection before/after neoadjuvant chemotherapy is associated with a higher risk of early relapse at the low cut-off level of one CTC per 7.5 mL (Pierga et al., 2008). More recently, prognostic significance of flow cytometry-detected CTCs was depicted in multiple myeloma for the first time (Garcés et al., 2022). The role of CTC count as a pharmacodynamic biomarker has also been demonstrated. In metastatic breast cancer, a longitudinal study has shown that a decrease in CTC level below the five CTC/7.5 mL cut-off was associated with better prognosis (Hayes et al., 2006). A large multicenter study reported that dynamic changes in CTC counts in response to treatment correlated with clinical benefit and thus PFS and OS in this malignancy (Bidard et al., 2014). Furthermore, in SCLC, a decrease in CTC levels after one cycle of chemotherapy was favorably associated with a significant increase in PFS and OS (Hou et al., 2012). On the other hand, without using CellSearch CTC enumeration, Scher *et al* showed the clinical relevance of the quantification of CTC phenotypic heterogeneity in informing treatment decision for CRPC and metastatic prostate cancer patients (Scher et al., 2017). More recently, transcriptomic profiling of CTCs by multiplex gene expression revealed key molecular changes related to *de novo* resistance mechanisms in metastatic prostate cancer, which could potentially help guide treatment decisions if detected early (Sperger et al., 2021).

Importantly, exciting findings were recently reported from the STIC CTC randomized open-label phase III trial conducted in patients diagnosed with hormone receptor-positive *HER2*-negative metastatic breast cancer, which suggested CTC count as a reliable biomarker in guiding first-line treatment choice for these patients (chemotherapy if count is ≥5 CTCs/7.5 ml; endocrine therapy if <5 CTCs/7.5 ml) (Bidard et al., 2021).

c. CTC molecular profiling

i. Enriched CTC populations

A wide range of molecular profiling assays can be applied to CTCs. At first, most studies were performed on DNA or RNA extracted from a CTC-enriched fraction or whole-blood. However, these methods present limited sensitivity and are not representative of the true tumor profile, mainly due to contamination of the sample by DNA from leukocytes (Krebs et al., 2014). One example is a study by Punnoose *et al* which explored the possibility to analyze the expression of *EGFR* mutation among others in CellSearch-enriched NSCLC patient CTC populations. Only one out of eight *EGFR* mutations identified in matched patient TBs was detected in enriched fractions, which highlights the limitations of this method (Punnoose et al., 2012).

Fluorescence *in situ* hybridization (FISH) has been adopted for the detection of gene amplifications and alterations in tumor specimens (McGranahan et al., 2012). Chromosome copy number variations may be assessed using centromere-binding fluorescence-labelled DNA probes. FISH method has been subsequently optimized for use in CTCs for the detection of aneuploidy, gene rearrangements and/or amplifications, which has revealed unforeseen chromosomal heterogeneity across CTCs in different malignancies. One of the first successful applications of the FISH assay was done in prostate cancer and allowed the detection of *ERG* rearrangement, *AR* copy number gain and/or *PTEN* loss in CRPC patient CTCs (Attard et al., 2009; Leversha et al., 2009). In the multicentric PETRUS study of biomarker assessment, we reported high concordance between biopsies from metastatic CRPC tumors and corresponding patient CTCs for *ERG*-rearrangement, with additional alteration patterns in CTCs highlighting their heterogeneity (Massard et al., 2016). FISH detection of *ALK*-rearrangement in NSCLC patient CTCs and corresponding tumor tissue biopsies was also performed (Ilie et al., 2012; Pailler et al., 2013; Tan et al., 2016). In 2013, our group reported using filter-adapted (FA)-FISH technique the presence of a unique split *ALK*-rearrangement pattern in patient CTCs, which also harbored a mesenchymal

phenotype (detection of vimentin expression) (Pailler et al., 2013). We also provide the first proof-of-concept for the detection of *ROS1* chromosomal rearrangements in CTCs from *ROS1*-rearranged NSCLC patients treated with crizotinib. Interestingly, CTCs harbored high aneuploidy and numerical CIN, highlighting a potential therapy escape mechanism (Pailler et al., 2015). Similarly, assessment of *HER2* amplification in CTCs using FISH has been reported by several groups and may be useful for stratification of patients eligible to *HER2*-targeted therapy (Frithiof et al., 2016; Mayer et al., 2011; Munzone et al., 2010). In a longitudinal study of a cohort of *ALK*-rearranged NSCLC patients monitored at early stage of crizotinib treatment, our group reported significant association between a decrease in the number of CTCs presenting *ALK*-copy number gain and longer PFS. This study suggests that monitoring the dynamic change in CTC count may serve as a predictive biomarker of treatment efficacy in *ALK*-rearranged NSCLC patients (Pailler et al., 2017).

To overcome the particularly laborious task of manual FISH analysis of CTC samples due to the retainment of a substantial number of hematopoietic cells in the filters, technological advancements in the field led to the development of a semi-automated microscopy method. CTCs from NSCLC and CRPC patients were analyzed using a combined assay of phenotypic analysis by immunofluorescence (DAPI/CD45) followed by the detection of molecular biomarkers (*e.g.* *ALK*, *ROS1* and *ERG* gains and rearrangements) by FA-FISH on selected $CD45^-$ cells (Pailler et al., 2016). Another group has reported the use of integrated subtraction enrichment and immunostaining FISH for enumeration and karyotyping of CTCs of patients with malignancies such as nasopharyngeal carcinoma or esophageal cancer. Notably, CTC karyotyping revealed chromosome 8 aneuploidy, which strongly associated with chemotherapy-related efficacy and prognosis (Y. Chen et al., 2019; J. Zhang et al., 2018).

Overall, aforementioned studies mainly evaluated the clinical interest of CTCs as a predictive biomarker and the FISH technique in CTCs as a valuable tool for the detection of tumor biomarkers. However, as mentioned above, analyses of enriched

CTC fractions do not account for true heterogeneity as their sensitivity is very limited due to wild-type DNA contaminations.

ii. Single CTCs

Single-cell studies are thus required to overcome this contamination bias and assess tumor heterogeneity though CTC characterization. Molecular profiling of CTCs at the single-cell level requires an additional isolation step after enrichment and detection (as described previously in **Introduction section III. 1)**). Multiple CTC isolation techniques exist including physical micromanipulation, laser microdissection of filters, fluorescence-activated cell sorting (FACS), the CellCelector™ (Automated Lab Solutions GmbH, Jena, Germany) and the automated DEPArray (Silicon Biosystems, Bologna, Italy) technology (Fabbri et al., 2013; Neumann et al., 2017; Ross et al., 2015). Next, as a single cell contains very small amounts of DNA (~ 6.6 picograms), a single-cell DNA whole-genome amplification (WGA) step is essential before molecular analysis, but is prone to amplification bias, polymerase errors and allelic dropout (Adalsteinsson & Love, 2014; Gasch et al., 2013). The first studies aimed to assess technical feasibility by comparing single CTC mutational profiles to corresponding primary tumors (Gasch et al., 2013; Heitzer et al., 2013; Maheswaran et al., 2008). In brief, after performing WGA from isolated colorectal cancer patient single CTCs, hotspot mutations in *PIK3CA*, *KRAS* and *BRAF* genes were identified using Sanger sequencing, which may be predictive of resistance to EGFR inhibition. Importantly, two distinct *PIK3CA* mutations were identified in two different CTCs, underlining the benefit of using single-cell profiling to decipher tumor mutational heterogeneity (Gasch et al., 2013). Another study in colorectal cancer reported the first comprehensive genotyping of single CTCs using array-comparative genomic hybridization and next-generation sequencing (NGS), in comparison to matched patient primary tumor and metastases. Multiple copy number changes were detected in CTCs, as well as private CTC mutations that were also found at the subclonal level in the primary tumor (Heitzer et al., 2013). Significant progress in sequencing technologies followed, notably whole-genome sequencing (WGS) (Gulbahce et al., 2017; Gupta et al., 2017; Jiang et al., 2015) and whole-exome

sequencing (WES) (Faugeroux, Lefebvre, et al., 2020; Faugeroux, Pailler, et al., 2020; Lohr et al., 2014; Ni et al., 2013; Su et al., 2019). Our group reported the first WES analysis of both epithelial and non-epithelial single CTCs isolated from metastatic CRPC patients. This study revealed significant mutational profile similarities between a small number of CTCs or pools and matched metastasis biopsy, as well as CTC-exclusive mutations recapitulating metastasis-seeding clones (Faugeroux, Lefebvre, et al., 2020).

Low-pass WGS studies were also adopted to investigate chromosomal instability (CIN) in CTCs from different malignancies such as lung, breast and prostate cancer through copy number alteration (CNA) analysis (Carter et al., 2017; Hodara et al., 2019; Malihi et al., 2020; Ni et al., 2013; Oulhen et al., 2021; Pailler et al., 2019). Carter *et al* identified distinct chemoresistance CNA profiles in CTCs from relapsed SCLC patients (Carter et al., 2017). Similarly, the predictive value of CTC CNA scores for SCLC patient outcomes in response to first-line chemotherapy was also demonstrated (Su et al., 2019). To optimize the method of genome-wide copy number profiling for clinical applications, Ferrarini *et al* established a single-tube single-step *Ampli*1™ WGA-based low-pass workflow for CNA detection in single CTCs from prostate and lung cancer patients (Ferrarini et al., 2018; Hodara et al., 2019; Oulhen et al., 2021; Pailler et al., 2019). In NSCLC, our group investigated resistance mutations in CTCs from crizotinib- and lorlatinib-resistant *ALK*-rearranged patients. Using combined workflow of *Ampli*1™ WGA-based low-pass followed by targeted NGS of single CTCs, our study elucidated an array of CNAs and mutations in different bypass resistance mechanisms (Pailler et al., 2019). More recently, a complementary CTC comprehensive CNA analysis was performed, which revealed significant intra- and interpatient heterogeneity of CNA profiles in several pathways including TKI resistance bypass mechanisms (Oulhen et al., 2021). Linking genetic and epigenetic modifications to phenotypic differences through transcriptomic analysis of single CTCs is also of importance but remains challenging, as preserving RNA quality is difficult. Nonetheless, several studies have explored this, including the development of the single-cell mRNA sequencing protocol Smart Seq (Ramsköld et al., 2012), as well as single-cell RNA sequencing (RNA-seq) of CTCs

(Franses et al., 2020; Hong et al., 2021; Miyamoto et al., 2015; Stewart et al., 2020; Sun et al., 2021; G. X. Y. Zheng et al., 2017).

Together, these studies highlight how CTC profiling at the single-cell resolution allows a comprehensive capture of tumor heterogeneity as well as a monitoring of disease evolution through minimally invasive longitudinal CTC sampling in tumors harboring oncogenic driver mutations (~20 % of patients).

3) CTC functional characterization

Functional characterization of CTCs provides a unique insight into the biology of cells that fuel metastasis through the analysis of their tumor-initiating properties. To this end, considerable efforts have been put into the establishment of clinically relevant CTC-derived systems to study CTC biology in different malignancies and identify new therapeutic targets. Nonetheless, the establishment of such models remains challenging mainly due to low CTC prevalence (**Figure 9**). We have recently reported a comprehensive review of existing CTC-derived models (Tayoun et al., 2019). We provide below an updated overview of established models and the main study findings.

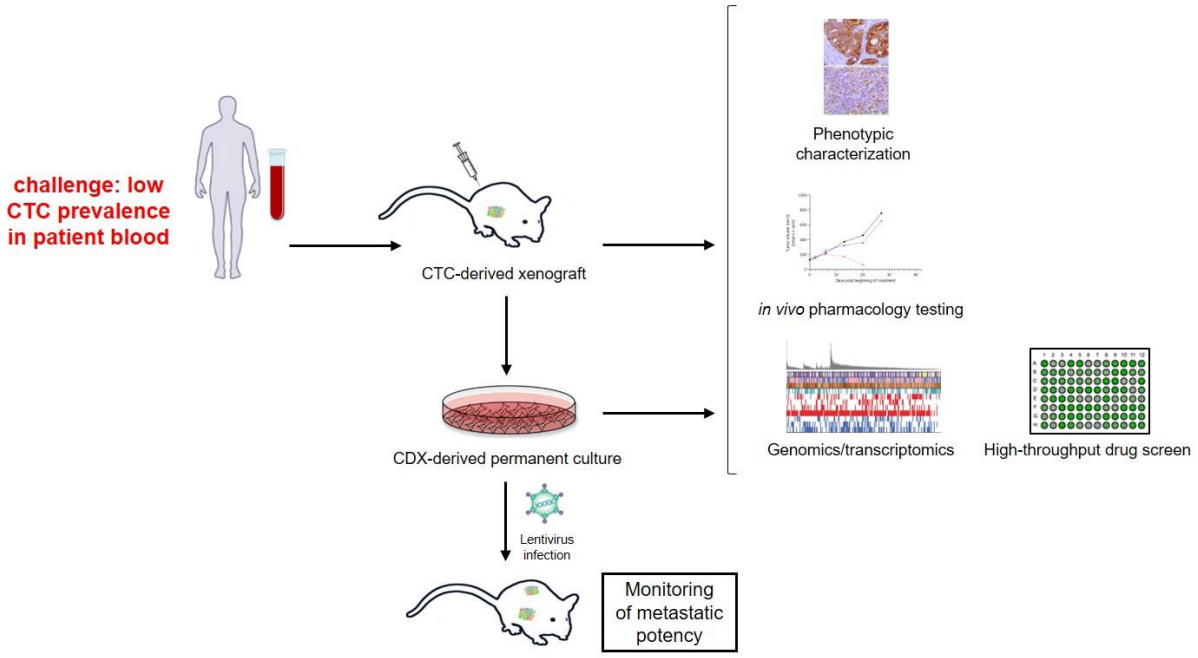


Figure 9. Functional studies on circulating tumor cells. CTCs enriched and isolated from advanced-stage cancer patients may be used to generate tractable CTC-derived xenografts (CDX) or may be expanded *in vitro* to explore biological properties of tumor-initiating cells and perform pharmacological

testings. CDX tumors can be dissociated into *ex vivo* cultures for drug screening and genome-wide analyses. These CDX-derived cultures are amenable to genetic modification such as lentiviral infection and can be re-injected into mice to be used as tools to track tumor dissemination.

a. CTC-derived xenografts

Patient-derived xenograft (PDX) models have rapidly become a core component of translational research, as they improve our biological understanding of cancer and provide a drug screening platform to test novel treatment approaches (Bousquet & Janin, 2016; Hidalgo et al., 2014). PDX are generated by implantation of surgically removed primary or metastatic tumor tissue into immunodeficient mice. Although they are considered robust preclinical tools for cancer research, PDX feasibility remains challenged by limited tumor tissue availability, as biopsy sampling may be detrimental or even impossible in some patient cases (Byrne et al., 2017). CDX models established from a readily accessible CTC-enriched blood sample have emerged as an attractive, minimally-invasive alternative to PDX models, albeit with significantly lower take rates (**Table 2**) (Blackhall et al., 2018; Lallo et al., 2017; Pantel & Alix-Panabières, 2015; Tayoun et al., 2019).

Table 2. Pros and cons of CDX models as compared to PDX models in their use as a preclinical research tool.

	CDX	PDX
Tumor origin	issued from enriched patient CTCs	issued from patient tissue biopsy
Relevance	representative of distinct metastatic clones and aggressive disease	single-site, may underestimate heterogeneity
Feasibility	readily accessible, repetitive blood draw	biopsy sampling may be unavailable/invasive
Success rate	extremely low CTC prevalence in blood	millions of tumor cells available in tissue biopsy
	low take rate, limited number of models available	relatively high take rate, PDX biobanks

Abbreviations: CTC, circulating tumor cell; CDX, CTC-derived xenograft; PDX, patient-derived xenograft.

To date, CDX have been generated in breast, melanoma, lung and prostate cancers and are discussed in this section.

- **Breast cancer**

The first experimental proof that primary human luminal breast cancer CTC populations had metastasis-initiating capacities in a xenograft assay was reported in 2013 (Baccelli et al., 2013). Six recipient mice injected with at least 1100 CTCs from three patients developed bone, lung and liver metastases within six to 12 months after CTC transplant. FACS analysis of the CTC population depicted a common $EpCAM^{+}CD44^{+}CD47^{+}MET^{+/-}$ phenotype, highlighting a CSC profile. Furthermore, the authors showed that a higher frequency of $CD44^{+}CD47^{+}MET^{+}$ CTCs strongly correlated with decreased OS in metastatic breast cancer patients (Baccelli et al., 2013). A second group derived one CDX model from one metastatic triple-negative breast cancer patient that presented with high CellSearch CTC counts (969 CTCs and 74 CTC clusters/7.5 mL). Serial blood sampling allowed the tracking of molecular changes among primary and metastatic tumors, as well as CTCs. The authors also performed RNA-seq analysis of the CDX tumor, which disclosed key mechanisms relevant in triple-negative breast cancer biology, such as the upregulation of the Wnt pathway (Pereira-Veiga et al., 2019). An additional CDX model was established in the same malignancy, which recapitulated liver metastasis in four sequential CDX generations. Notably, the authors deciphered a novel 597-gene CTC signature related to liver metastasis in triple-negative breast cancer (Vishnoi et al., 2019).

- **Melanoma**

Feasibility of CDX in advanced-stage melanoma was first shown by Girotti *et al*. The authors reported a success rate of 13% with six CDX established and 26 additional models monitored at the time of publication. The CDX recapitulated patient tumors and response to therapy. This proof-of-concept study simultaneously involved the development of PDX technology and ctDNA analysis, as part of a precision medicine platform for optimized melanoma patient care. Biological characterization of tumorigenic melanoma CTCs was not performed (Girotti et al., 2016).

- **SCLC**

Hodgkinson *et al* showed that CTCs from chemosensitive or chemorefractory SCLC patients are tumorigenic in immunodeficient mice. Patients having more than 400 $EpCAM^{+}CK^{+}$ CTCs gave rise to CDX tumors detected at approximately two months post-implantation. The CDX recapitulated the genomic profile of isolated CTCs and donor patients' response to standard of care chemotherapy, which validated the clinical relevance of these models (Hodgkinson et al., 2014). CDX tumors were subsequently dissociated and expanded into faithful short-term *in vitro* CDX cultures. CDX-derived cells were then infected *in vitro* with the GFP lentivirus and successfully implanted into mice for tracking tumor dissemination *in vivo* (Lallo et al., 2019). Drapkin *et al* reported 38% efficiency in the establishment of 16 SCLC CDX models. WES analysis revealed similar mutational landscapes between patient tumors and the CDX. Furthermore, serial CDX models from one patient were developed at two different time points: prior to olaparib plus temozolomide treatment and at relapse. The CDX showed accurate concordance with the evolving drug sensitivity profiles of the patient tumor, highlighting the utility of serial CDX characterization to monitor treatment resistance in SCLC (Drapkin et al., 2018). The Dive laboratory currently has a biobank of 38 SCLC CDX models, including six CDX pairs established at baseline and at disease progression, amenable to in-depth molecular and functional characterization (Hodgkinson et al., 2014; Lallo et al., 2018; Simpson et al., 2020).

- **NSCLC**

In NSCLC, the first CDX model described was established from mesenchymal vimentin-expressing CTCs collected post-brain radiotherapy. Importantly, the authors reported that no $EpCAM^{+}/CK^{+}$ CTCs were detected by CellSearch analysis at disease progression, underlining the fact that the tumor-initiating potential of NSCLC CTCs cannot be solely attributed to $EpCAM^{+}$ phenotype (Morrow et al., 2016). More recently, our group has established and extensively characterized four epithelial CDX models from advanced-

stage NSCLC patient CTCs and three *in vitro* CDX-derived cell lines that will be extensively described in this manuscript (Tayoun et al., 2022).

- **Prostate cancer**

Our group reported the establishment of the first CDX model of CRPC and its permanent *in vitro* cell line from CDX-derived cells (Faugeroux, Pailler, et al., 2020). Initial trials from blood samples were not successful. On the other hand, diagnostic leukapheresis products (part of a European FP7 prospective multicenter study CTCTrap (Andree et al., 2018)) significantly increased CTC yields and injection of a high number of CTCs (~ 20000 CTCs) obtained from one patient out of seven gave rise to a palpable tumor within five months. Immunohistochemistry (IHC) showed that the patient TBs, the CDX and the cell line presented an epithelial phenotype. Moreover, the CDX and the cell line expressed *AR*-null, neuroendocrine marker-positive features. Genomic analysis by WES showed that both models faithfully recapitulated patient tumor characteristics as well as patient response to CRPC standard of care (*i.e.* enzalutamide and docetaxel). Interestingly, phylogenetic reconstruction revealed that the loss of 17p12-*tel* region (carrying *TP53*) in one tumor biopsy (TB) was conserved in all CTC samples, the CDX and the cell line, which suggests that tumorigenic CTCs are issued from a primary tumor subclone harboring *TP53* loss. *PTEN* and *RB1 losses* were subsequently acquired in CTCs over the course of the disease. Our study therefore elucidated the order of acquisition of key genetic drivers governing the transformation of CRPC into a CRPC-neuroendocrine malignancy in CTCs, highlighting the role of tumorigenic CTCs in this transdifferentiation mechanism (Faugeroux, Pailler, et al., 2020).

b. CTC-derived *ex vivo* models

CDX feasibility is tumor type-dependent and the process could take several months, a time frame that would not provide proper aid for the clinical guidance of donor patients. Expansion of viable CTCs *ex vivo* may be possible, sometimes in a relatively shorter time, but CTC low prevalence in patient blood remains an important hurdle

causing extremely low CTC culture success rate. *Ex vivo* CTC cultures – mostly short-term – were reported in colon, breast, melanoma, prostate and lung cancers and are discussed in this section.

- **Colon cancer**

Cayrefourcq *et al* derived the first permanent colon cancer CTC cell line from $EpCAM^+$ metastatic colon cancer patient CTCs. Genomic, transcriptomic, proteomic and secretome studies were performed on the cell line, which resembled donor patient tumor features and was tumorigenic *in vivo* (Cayrefourcq et al., 2015). In a follow-up study, eight additional cell lines were established from the same patient with CTCs collected at different time points during the treatment course. Transcriptomics analyses in the nine cell lines revealed stem cell-like properties, as well as an intermediate E/M phenotype. CTC-derived cultures also promoted angiogenesis *in vitro* and tumorigenesis *in vivo*, through the secretion of potent angiogenesis inducers (Cayrefourcq et al., 2015; Soler et al., 2018).

- **Breast cancer**

Zhang *et al* reported the culture and characterization of three cell lines from $EpCAM^-$ CTCs isolated from brain metastatic breast cancer patients. The study revealed a brain metastasis protein signature $HER2^+/EGFR^+/HPSE^+/Notch1^+$ in CTC lines, which is suggestive of breast cancer CTC metastatic competency to the brain (L. Zhang et al., 2013). Another report demonstrated the establishment of non-adherent CTC cultures (over six months) under hypoxic conditions from patients with estrogen receptor-positive breast cancer. Three out of five were tumorigenic *in vivo*, with tumors recapitulating primary patient tumor features. Furthermore, this study identified targetable mutations acquired *de novo* in CTC cell lines, which were explored *via* pharmacological assays (M. Yu et al., 2014). A follow-up characterization study was recently performed and revealed a CTM-specific DNA hypomethylation status at binding sites for stemness- and proliferation-associated TFs, which correlated with poor prognosis in patients (Gkountela et al., 2019). More recently, a novel permanent

estrogen receptor-positive breast cancer CTC line was established from a patient presenting 1547 CellSearch CTCs. High concordance of CNA profiles was detected between the CTC cell line and isolated CTCs collected at the time of the blood draw, which suggests that the cell line may have derived from CTCs shed from metastasis (Koch et al., 2020).

- **Melanoma**

More recently, in an effort to investigate resistance mechanisms in melanoma, *Hong et al* established a culture from melanoma CTCs and performed RNA-seq single-cell analysis in primary and cultured CTCs (Hong et al., 2021). Another CTC-derived cell line was established from metastatic melanoma patient CTCs detected by the DEPArray system. The cells presented an intermediate E/M phenotype and stem cell features as well as metastatic potency *in vivo* (Felici et al., 2022).

Despite some successful attempts at *in vitro* expansion of patient CTCs in several cancer types, important limitations in two-dimensional (2D) cultures should be taken into account, including: (a) cell morphology alterations due to adherence to plastic and (b) lack of tumor microenvironment and spatial interactions *in vitro*, which are available *in vivo* (Tayoun et al., 2019; Tellez-Gabriel et al., 2018). These constraints may interfere with tumor cell physiology and biological response, making the model less relevant. To overcome this challenge, the establishment of 3D organoids and co-culture systems was reported in prostate and lung cancer respectively (D. Gao et al., 2014; Z. Zhang et al., 2014). In prostate cancer, Gao *et al* generated seven 3D organoid lines from CRPC patient tumor samples, including one from patient CTCs. The models harbored prostate cancer-specific genetic alterations including *PTEN* loss and *TMPRSS2-ERG* fusion and were tumorigenic *in vivo* (D. Gao et al., 2014). In early-stage lung cancer, a novel short-term *ex vivo* CTC-derived model was developed using a microenvironment-simulating 3D co-culture system. NGS detected several matching mutations (*e.g. TP53*) found in cultured CTCs and patient primary tumors (Z. Zhang et al., 2014). More recently, organoids were derived from pancreatic ductal carcinoma CTCs: the authors reported

a high success rate (87.8%) and showed, for the first time, that organoids drug sensitivity profiles correlated with corresponding patient clinical response (Y.-H. Wu et al., 2022).

Overall, the establishment of tractable CTC-derived models such a CDX and their genomic and functional characterization may help explore CTC biology and elucidate key features of their metastatic potency. Moreover, these models provide a robust pre-clinical tool for pharmacological drug testing of biology-driven therapeutic strategies targeting tumorigenic CTC vulnerabilities.

REVIEW ARTICLE 1. CTC-derived models: A window into the seeding capacity of Circulating Tumor Cells (CTCs). *Cells* 2019, *8*(10), 1145
Open access publication.

cells

MDPI

Review

CTC-Derived Models: A Window into the Seeding Capacity of Circulating Tumor Cells (CTCs)

Tala Tayoun [1,2,3], Vincent Faugeroux [1,2], Marianne Oulhen [1,2], Agathe Aberlenc [1,2], Patrycja Pawlikowska [2] and Françoise Farace [1,2,*]

1 "Circulating Tumor Cells" Translational Platform, CNRS UMS3655 – INSERM US23AMMICA, Gustave Roussy, Université Paris-Saclay, F-94805 Villejuif, France; tala.tayoun@gustaveroussy.fr (T.T.); vincent.faugeroux@laposte.net (V.F.); marianne.oulhen@gustaveroussy.fr (M.O.); agathe.aberlenc@gustaveroussy.fr (A.A.)

2 INSERM, U981 "Identification of Molecular Predictors and new Targets for Cancer Treatment", F-94805 Villejuif, France; patrycjamarta.pawlikowska@gustaveroussy.fr

3 Faculty of Medicine, Université Paris Sud, Université Paris-Saclay, F-94270 Le Kremlin-Bicetre, France

* Correspondence: francoise.farace@gustaveroussy.fr; Tel.: +33-1-42-11-51-98

Received: 11 July 2019; Accepted: 24 September 2019; Published: 25 September 2019



Abstract: Metastasis is the main cause of cancer-related death owing to the blood-borne dissemination of circulating tumor cells (CTCs) early in the process. A rare fraction of CTCs harboring a stem cell profile and tumor initiation capacities is thought to possess the clonogenic potential to seed new lesions. The highest plasticity has been generally attributed to CTCs with a partial epithelial-to-mesenchymal transition (EMT) phenotype, demonstrating a large heterogeneity among these cells. Therefore, detection and functional characterization of these subclones may offer insight into mechanisms underlying CTC tumorigenicity and inform on the complex biology behind metastatic spread. Although an in-depth mechanistic investigation is limited by the extremely low CTC count in circulation, significant progress has been made over the past few years to establish relevant systems from patient CTCs. CTC-derived xenograft (CDX) models and CTC-derived ex vivo cultures have emerged as tractable systems to explore tumor-initiating cells (TICs) and uncover new therapeutic targets. Here, we introduce basic knowledge of CTC biology, including CTC clusters and evidence for EMT/cancer stem cell (CSC) hybrid phenotypes. We report and evaluate the CTC-derived models generated to date in different types of cancer and shed a light on challenges and key findings associated with these novel assays.

Keywords: metastasis; tumor-initiating cells (TICs); circulating tumor cells (CTCs); CTC-derived xenografts; CTC-derived ex vivo models

1. Introduction

Metastatic spread and its resistance to treatment remain the leading cause of death in cancer patients. This process is fueled by malignant cells that dissociate from the primary tumor and travel through the bloodstream to colonize distant organs. These cells are referred to as "circulating tumor cells" (CTCs) and are able to enter vasculature during the early course of disease. Nonetheless, the majority of the tumor cell population dies during transit as a result of biological and physical constraints such as shear stress and immune surveillance, and only a minor subset of the surviving CTCs (0.01%) acquires the capacity of tumor-initiating cells (TICs) [1–4]. The outcome of tumor dissemination is dependent on a selection process that favors the survival of a small proportion of cancer cells holding the self-renewal ability of stem cells along with TIC properties, which enables them to seed tumors and reconstitute tumor heterogeneity [5–7]. These cells are termed "cancer stem cells"

(CSCs), and CTCs holding a CSC phenotype have been detected and associated with high invasiveness and tumorigenicity in many cancers including breast cancer (BC), colorectal cancer, and glioma [8–11].

An important aspect of CTC research is to study the mechanistic basis behind their TIC properties and explore new CTC-based biomarkers and targeting strategies. The generation of CTC-derived xenografts (CDXs) or CTC-derived cell lines at relevant time points during disease progression is therefore crucial to achieve a longitudinal and functional characterization of these cells, along with in vivo and in vitro pharmacological testing. Although this task remains challenging owing to CTCs scarcity in peripheral blood and technical hurdles related to their enrichment strategies, significant efforts have been made in the establishment of clinically relevant systems to study CTC biology in different cancer types. In this review, we briefly cover basic knowledge of TIC-related properties in CTCs and evaluate the existing CTC-derived models, including both in vivo CDXs and in vitro functional culture assays in different cancers. We also highlight the important findings which have helped unveil new insights into CTC biology and novel therapeutic strategies.

2. Brief Glimpse into TIC-Related Properties of CTCs

CTC profile evolves as the initial events of the metastatic cascade take place. Indeed, CTCs undergo reversible phenotypic alterations to achieve intravasation, survival in vasculature and extravasation, known as epithelial-to-mesenchymal transition (EMT). During EMT—a key phenomenon in embryonic development—cancer cells undergo cytoskeletal changes and typically lose their cell–cell adhesion proteins as well as their polarity to become motile cells and intravasate [12,13]. EMT signatures were detectable in CTCs of BC patients [14–17]. Increasing experimental evidence draws a potential link between EMT and acquisition of stemness [12,13,18,19]. In fact, several EMT-inducing transcription factors have been shown to confer malignancy in neoplastic cells, leading to the emergence of highly aggressive clones with combined EMT/CSC traits [20–23]. Nevertheless, this association is not universal. Indeed, it has been suggested that the loss of the EMT-inducing factor *Prxx1* is required for cancer cells to colonize organs in vivo, which revert to the epithelial state and acquire CSC traits, thus uncoupling EMT and stemness [19,24,25]. Moreover, the requirement of EMT for CTC dissemination has long been subject to debate. Several studies have shown that mesenchymal features in tumor cells may indeed be dispensable for their migratory activity but could contribute molecularly and phenotypically to chemoresistance [26–28]. It is currently hypothesized that CTC subclones displaying an intermediate phenotype between epithelial and mesenchymal have the highest plasticity to adapt to the microenvironment and generate a more aggressive CTC population resistant to conventional chemotherapy and capable of metastatic outgrowth. Our group showed the existence of a hybrid epithelial/mesenchymal (E/M) phenotype in CTCs from patients with non-small cell lung cancer (NSCLC) [29]. Heterogeneous expression of EMT markers within SCLC and NSCLC patient cohorts was described by Hou et al., while Hofman et al. reported the presence of proportions of NSCLC CTCs which expressed the mesenchymal marker vimentin and correlated with shorter disease-free survival [30,31]. Recent data in metastatic BC patients showed the enrichment of CTC subpopulations with a CSC^{+}/partial EMT^{+} signature in patients post-treatment, which correlated with worse clinical outcome [32]. Indeed, the CTC population is described as a highly heterogeneous pool of tumor cells with low numbers of metastasis-initiating cells (MICs) that are sometimes prone to apoptosis [33]. The different factors influencing MIC properties of CTCs and their survival underlie the complexity and inefficiency of organ invasion and macro-metastases formation, relevant both clinically and in experimental mouse models [4,34,35]. Recent advances in single-cell technologies have unraveled CTC-specific genetic mutations and profiling of the CTC population thus points out the emergence of subclones with dynamic phenotypes that contribute to the evolution of the tumor genome during disease progression and treatment [36–39]. CTCs are less frequently found in clusters, also termed "circulating tumor microemboli" (CTM), which travel as 2–50 cells in vasculature and present extremely enhanced metastatic competency [40]. This can be explained by the survival advantage they hold over single CTCs, as CTM were shown to escape anoikis as well as stresses in

circulation [30,41]. A recent report showed that these characteristics are due to CSC properties of CTM, notably a CD44-directed cell aggregation mechanism that forms these clusters, promotes their survival and favors polyclonal metastasis [42]. Another group also investigated the factors behind CTM metastatic potential: Gkountela et al. reported that CTC clusters from BC patients and CTC cell lines exhibit a DNA methylation pattern distinct from that of single CTCs and which represents targetable vulnerabilities [43]. Moreover, CTC-neutrophils clusters are occasionally formed in the bloodstream and in vivo evidence shows that this association triggers cell cycle progression and thus drives metastasis formation in BC [44].

3. Brief Introduction to CTC Enrichment and Detection Strategies

A plethora of technologies have been developed over the last decade to respond to specific CTC applications. CTC identification remains a technically challenging task due to the extreme phenotypic heterogeneity and rarity of these cells in the bloodstream and therefore requires methods with high sensitivity and specificity. Enrichment strategies can be based on either biological properties (i.e., cell-surface markers) or physical characteristics (i.e., size, density, electric charge) and are usually combined with detection techniques (e.g., immunofluorescence, immunohistochemistry, FISH) to identify CTCs. CTC capture relies on a positive selection among normal blood cells or a negative selection by leukocyte depletion. Among biologically-based technologies is the CellSearch system (Menarini-Silicon Biosystem, Bologna, Italy). It is the most commonly applied assay for CTC enumeration in which CTCs are captured in whole blood by EpCAM (epithelial cell adhesion molecule)-coated immunomagnetic beads followed by fluorescent detection using anti-cytokeratins (CK 8, CK 18, CK 19), anti-CD45 (leukocyte marker), and a nuclear stain (DAPI). It is the only technology cleared by the US Food and Drug Administration to aid in prognosis for patients with metastatic breast, prostate, and colorectal cancer [45–49]. Although standardized and reproducible, this method has a limited sensitivity most likely due to failure in recognizing cells undergoing EMT and thus inevitably misses an aggressive and clinically relevant CTC subpopulation. Platforms relying on the depletion of leukocytes (negative selection) are being investigated and used to overcome this bias. One example is the widely used RosetteSep technique which enriches CTCs without phenotypic a priori by excluding $CD45^+$ and $CD36^+$ cells in rosettes and eliminating them in a Ficoll-Paque PLUS density-gradient centrifugation. Physical property-based methods including filtration systems have been developed to capture CTCs based on their large size compared to leukocytes, notably the ISET® (*Isolation by Size of Tumor Cells*) (RareCells Diagnostics, Paris, France) and the ScreenCell® (Paris, France) methods, which are able to detect CTCs as well as CTM using microporous polycarbonate filters [50,51]. In line with this notion, we and others have reported an overall higher recovery rate using ISET compared to CellSearch for CTC enumeration in NSCLC and prostate cancer patients [31,52]. Our lab developed a novel CTC detection approach combining ISET filtration with a FISH assay, optimized for the detection of *ALK*- or *ROS1*-rearranged pattern of NSCLC CTCs on filters [53,54]. To ensure a wider coverage of CTC heterogeneity, new devices are being developed (and some commercially) such as the CTC-iChip which relies on both biological and physical properties of CTCs: it applies size-based filtration using microfluidics processing, followed by positive selection of CTCs with EpCAM-conjugated beads or negative selection with $CD45^-$-coated beads to deplete hematopoietic cells [55]. Different technologies have been implemented to isolate live CTCs (without a fixation step) and perform subsequent functional studies. Some strategies have integrated isolation protocols for molecular analysis of single CTCs. One example is the DEPArray™ (Silicon Biosystems S.p.A., Bologna, Italy), a microfluidic system which sorts live single CTCs based on image selection followed by entrapment of CTCs inside dielectrophoretic cages [56–58]. FACS has also been adapted for molecular characterization of CTCs as well as their isolation in the aim of xenograft establishment [59].

At this point, none of the technologies fully respond to the phenotypic heterogeneity of CTCs. Indeed, each method has its own advantages and limitations and researchers have based the development of capture strategies on the specific aim of further CTC characterization studies. New

insights in CTC biology should be integrated into current enrichment, detection, and isolation techniques to optimize the process and improve their reliability. As shown in Table 1, RosetteSep and FACS have been used for CDX establishment. Enrichment using RosetteSep may be advantageous owing to the lack of phenotypic a priori on tumorigenic CTCs and a higher recovery rate.

4. CTC-Derived Xenografts

Patient-derived xenograft (PDX) technology has rapidly emerged as a standard translational research platform to improve understanding of cancer biology and test novel therapeutic strategies [60]. PDXs are generated by implantation of surgically-removed tumor tissue (primary or metastasis) into immunodeficient mice. Although these models have proven utility as a preclinical tool in many cancers, their feasibility remains challenged by limited tumor tissue availability, as single-site biopsies may be impossible or detrimental in some malignancies [61]. This limitation can be overcome by the generation of CDX models after enrichment of CTCs collected from a readily accessible blood draw and subsequent injection into immunodeficient mice [62–64]. Nevertheless, it is noteworthy that CDX development still presents an enormous challenge due to low CTC prevalence in several cancers. Until now, CDXs have been established in breast, melanoma, lung and prostate cancer and are discussed in this section (Table 1).

In 2013, Baccelli et al. reported the first experimental proof that primary human luminal BC CTC populations contain MICs in a xenograft assay. Injection of CTCs from 110 patients was performed. Six recipient mice developed bone, lung, and liver metastases within 6–12 months after CTC transplant (~1000 CTCs) from three patients with advanced metastatic BC. Cell sorting analysis of the MIC-containing population shared a common $EpCAM^{+}CD44^{+}MET^{+}CD47^{+}$ phenotype, highlighting a CSC characteristic of CTCs. The authors also showed that the number of CTCs positive for these markers strongly correlated with decreased progression-free survival of metastatic BC patients. This study has therefore revealed a first phenotypic identification of luminal BC CTCs with MIC properties, making them an attractive tool to track and potentially target metastatic development in BC [59]. A second group derived a CDX model from a metastatic triple-negative BC (TNBC) patient for the first time. The patient selected for CDX establishment had advanced TNBC with a very high CTC count obtained with CellSearch analysis (969 CTCs and 74 CTC clusters/7.5 mL). Enriched cells were injected subcutaneously into nude mice and a palpable tumor was observed five months later. The authors carried out a longitudinal study and samples were collected at two different time points (metastasis and progression) during the course of the disease, which allowed real-time assessment of molecular changes between patient tumor, CTCs, and CDXs samples. The obtained CDX phenocopied the patient tumor. Most importantly, RNA sequencing of the CDX tumor disclosed key mechanisms relevant in TNBC biology such as the WNT pathway, which is necessary for the maintenance of CSCs and was shown to correlate with metastasis and poor clinical outcome in TNBC subtypes. CTC analysis also deciphered a panel of potential tumor biomarkers [65]. An additional TNBC CDX model of liver metastasis was established very recently by Vishnoi et al. Similar genomic profiling of metastatic tissue was obtained in four sequential CDX generations, representing the recapitulation of liver metastasis in all the models. Notably, the authors deciphered a first 597-gene CTC signature related to liver metastasis in TNBC which, despite small sample size bias, can provide insight into the mechanistic basis of TNBC disease progression in the liver [66].

In melanoma, Girotti et al. demonstrated the tumorigenicity of advanced-disease CTCs in immunocompromised mice. The authors resorted to CDX development when tumor material was inaccessible for PDX generation. They reported a success rate of 13% with six CDX established, 15 failed attempts, and 26 additional models followed at the time of publication. CDX tumor growth was detectable as of one month after CTC implantation and was sustainable in secondary hosts. Moreover, the CDXs were representative of patient tumors and mirrored therapy response. This proof-of-principle was developed along with PDX technology and circulating tumor DNA analysis as part of a platform

to optimize precision medicine for melanoma patients. It explored the TIC properties of melanoma CTCs but did not achieve a biological characterization of these cells [67].

In lung cancer, Hodgkinson et al. showed that CTCs in chemosensitive or chemorefractory SCLC are tumorigenic. CTCs were isolated from six late-stage SCLC patients having never received chemotherapy and were subsequently injected into NSG mice. Each patient presented with more than 400 CTCs and four out of six CTC samples gave rise to CDX tumors detected as of 2.4 months post-implantation. CDXs recapitulated the genomic profile of CellSearch-enriched CTCs and mimicked donor patients response to standard of care chemotherapy (platinum and etoposide), proving the clinical relevance of these models [68]. CDX tumors were subsequently dissociated and expanded into short-term in vitro CDX cultures (Table 2). These cells maintained the genomic landscape of donor tumors as well as their drug sensitivity profiles. CDX-derived cells were also labeled in vitro with the GFP lentivirus and successfully implanted into mice, where they can serve as a tracking tool to study tumor dissemination patterns in vivo [69]. Additional 16 SCLC CDX models were recently generated by Drapkin et al. from CTCs collected at initial diagnosis or at progression, with 38% efficiency. Somatic mutations were maintained between patient tumors and CDX as shown by whole-exome sequencing (WES) and the genomic landscape remained stable throughout early CDX passages showing clonal homogeneity. The authors also developed serial CDX models from one patient at baseline of the combination olaparib and temozolomide and at relapse. Interestingly, the models accurately reflected the evolving drug sensitivity profiles of the patient's malignancy, which highlights the potential utility of serial CDXs to study the evolution of resistance to treatment in SCLC [70]. One CDX model was also described in NSCLC. In this study, CTC samples were retrieved at two different time points: Baseline and post-brain radiotherapy. No CDX was developed at baseline. Notably, no $EpCAM^+$ CTCs were detected during CellSearch analysis at disease progression, yet injection of post-radiotherapy CTCs gave rise to a palpable tumor 95 days after engraft. Phenotypic and molecular characterizations showed no epithelial CTCs, but revealed a sizeable population of phenotypically heterogeneous CTCs mostly expressing the mesenchymal marker vimentin. This study suggests that the absence of $EpCAM^+$ CTCs in NSCLC does not preclude the existence of CTCs with TIC potential in patients and underlines the importance of investigating CTCs undergoing EMT in this malignancy [71].

Our group generated the first CDX model of castration-resistant prostate cancer (CRPC) and derived a permanent ex vivo culture from CDX tumor cells. A total of 22 samples from metastatic CRPC patients were collected, among which seven were obtained from diagnostic leukapheresis (DLA). DLA products were generated as part of the European FP7 program CTCTrap which aimed for an increased CTC yield to perform molecular characterization of the tumor [72]. One patient with a very high CTC count (~20,000 CTCs) obtained by DLA gave rise to a palpable tumor within 5.5 months. Acquisition of key genetic drivers (i.e., *TP53, PTEN*, and *RB1*) that govern the trans-differentiation of CRPC into CRPC-neuroendocrine (CRPC-NE) malignancy was detected in CTCs, highlighting the role of tumorigenic CRPC-NE CTCs in this transformation. Moreover, the obtained in vitro CDX-derived cell line faithfully recapitulated the genetic characteristics and tumorigenicity of the CDX and mimicked patient response to standard of care treatments for CRPC (i.e., enzalutamide and docetaxel) (Table 2) [73,74].

Table 1. Overview of in vivo circulating tumor cell (CTC)-derived models established to date.

CTC-Derived Xenografts								
Type of Cancer	**Stage**	**Live CTC Isolation Technique**	**# of CTCs**	**Injection Procedure**	**Take Rate**	**Passaging**	**Main Findings**	**Ref**
Breast cancer	Metastatic luminal	FACS isolation ($PI^-CD45^-EpCAM^+$) or RosetteSep	≥1109 CTCs $EpCAM^+$(CellSearch)	- Dilution in matrigel - Injection in femoral medullar cavity	5%	N/A	- Specific CTC MIC signature $EpCAM^+CD44^+MET^+CD47^+$ - Recapitulation of patient metastases phenotype in CDX metastases - No drug sensitivity study	[59]
	Metastatic triple-negative	Density gradient centrifugation: Histopaque®	969 CTCs $EpCAM^+$ (CellSearch)	- Dilution in matrigel - Subcutaneous injection	3%	Piece of tumor explant or injection of explant culture	- RT-qPCR for genomic profiling of CTC/CDX samples before and after injection - WNT pathway upregulation as a potential therapeutic target in TNBC identified by RNAseq - No drug sensitivity study	[65]
	Metastatic triple-negative	FACS ($CD45^-/CD34^-/CD105^-/CD90^-/CD73^-$)	N/A	Intracardiac injection	33%	Minced metastatic liver tissue	- Identification of a TNBC liver metastasis CTC-specific signature (whole-transcriptome)- Survival analyses for signature transcripts	[66]
Melanoma	Stage IV	RosetteSep	N/A	- Dilution in matrigel - Subcutaneous injection	13%	Tumor fragments	- recapitulation of patient response to dabrafetinib in the CDX - concordance in SNV profiles (WES/RNAseq)	[67]
SCLC	Metastatic	RosetteSep	>400 CTCs $EpCAM^+$ (CellSearch)	Dilution in matrigel/subcutaneous	67%	Tumor fragments	- Recapitulation of CTC genomic profile by CDX tumors - CDX mimicked donor's response to chemotherapy	[68]
	Limited or extensive stage	CTC-iChip + RosetteSep Ficoll	N/A	Dilution in matrigel/subcutaneous	38%	Tumor fragments	- Faithful recapitulation of the tumor genome - Reflection of evolving treatment sensitivities of patient tumor	[70]

Table 1. *Cont.*

CTC-Derived Xenografts								
Type of Cancer	**Stage**	**Live CTC Isolation Technique**	**# of CTCs**	**Injection Procedure**	**Take Rate**	**Passaging**	**Main Findings**	**Ref**
NSCLC	Metastatic	RosetteSep	>150 CTCs by FACS (CD45/CD144/ vimentin/CK)	Dilution in matrigel/subcutaneous	100%	Disaggregation of tumor	- Importance of mesenchymal CTCs with tumorigenic capacity	[71]
CRPC	Metastatic	DLA/RosetteSep	~20,000 CTCs $EpCAM^+$ (CellSearch)	Dilution in matrigel/subcutaneous	14%	Tumor fragments	- Recapitulation of genome characteristics in CTC, patient tumor and CDX (WES) - Tumorigenic CTCs with acquired CRPC-NE features	[73]

* N/A: not available; FACS: Fluorescent-activated cell sorting; CDX: CTC-derived xenograft; MIC: Metastasis-initiating cell; TIC: Tumor-initiating cell; TNBC: Triple-negative breast cancer; SCLC: Small-cell lung cancer; SNV: Single nucleotide variant; NSCLC: Non-small cell lung cancer; CRPC: Castration-resistant prostate cancer; NE: Neuroendocrine; WES: Whole-exome sequencing.

Table 2. Overview of CDX-derived ex vivo cultures established to date.

CDX-Derived* Ex Vivo *Cultures				
Type of Cancer	**Stage**	**Culturing Conditions**	**Main Findings**	**Ref**
SCLC	Metastatic	HITES medium with ROCK inhibitor—non-adherent cell clusters—short-term	Recapitulate genomic landscape and in vivo drug response Tumorigenic in vivo Lentiviral transduction of one cell line	[69]
CRPC	Metastatic	DMEM/F12 medium—adherent conditions—permanent	Recapitulation of genomic characteristics and standard of care drug response	[73]

5. CTC-Derived Ex Vivo Models

Although CDXs represent classical preclinical mouse models that are relatively easy to handle, they cannot be derived from every patient depending on tumor type and the process could take several months, a time frame that would not provide proper aid for the clinical guidance of donor patients. Expansion of viable CTCs ex vivo may offer an attractive alternative allowing both molecular analysis and high-throughput drug screening in a shorter time, but with CTC scarcity remaining, a fortiori, a significant limitation. In vitro CTC cultures were reported in colon, breast, prostate, and lung cancer and are evaluated in this section (Table 3).

The first long-term colon cancer CTC cell line was derived by Cayrefourcq et al. from a metastatic colon cancer patient who had 302 $EpCAM^+$ CTCs detected by the CellSearch platform. Importantly, the characterized CTC-MCC-41 cell line shared the main genomic features of both the donor patient primary tumor and lymph node metastasis [9]. In a second study, the authors established and characterized eight additional cell lines from the same patient with CTCs collected at different time points during his follow-up. Transcriptomics analyses in the nine cell lines revealed an intermediate epithelial/mesenchymal phenotype promoting their metastatic potential, as well as stem cell-like properties that increased in cell lines isolated at later stages of progression. This may highlight the selection mechanism of treatment-resistant clones with specific phenotypes that drive disease progression. Functional experiments showed that these cells favor angiogenesis in vitro, which was concordant with the secretion of potent angiogenesis inducers such as VEGF and FGF2 as well as the tumorigenicity of these cells in vivo [9,10].

In BC, Zhang et al. presented the characterization of $EpCAM^-$ CTCs and revealed a shared protein signature $HER2^+/EGFR^+/HPSE^+/Notch1^+$ in CTCs competent for brain metastasis. Indeed, the three established CTC lines expressing this signature promoted brain and lung localization after xenotransplantation into nude mice. The authors therefore deciphered a preliminary signature which provides insight into metastatic competency of BC CTCs and pushes towards using CTC research to explore new potential biomarkers [75]. Another study reported the establishment of non-adherent CTC lines under hypoxic conditions (4% O_2) with CTCs issued from six patients with metastatic luminal-subtype BC. Three out of five tested cell lines were tumorigenic in vivo, giving rise to tumors with histological and immunohistochemical similarities with the primary patient tumor. This proof-of-concept study also identified targetable mutations acquired de novo in CTC cell lines, elucidating the importance of monitoring the mutational evolution of the tumor throughout the disease. To explore this, the authors performed sensitivity assays on the CTC lines with large panels of single drug and drug combinations targeting the different mutations identified [76]. In vitro phenotypic analysis of these cell lines and patient CTCs was recently performed. A CTM-specific DNA methylation status was revealed in which binding sites for stemness and proliferation transcription factors were hypomethylated, suggesting potential targets. This pattern correlated with poor prognosis in patients and targeting of clusters with Na+/K+ ATPase inhibitors shed them into single cell and enabled DNA methylation remodeling, leading to suppression of metastasis. These data therefore highlight a key connection between phenotypic properties of CTCs and DNA methylation patterns at specific stemness- and proliferation-related sites [43].

add what needs to be on a landscape page

Table 3. Overview of ex vivo CTC-derived models established to date.

CTC-Derived* Ex Vivo *Models						
Type of Cancer	**Stage**	**Live CTC Isolation Technique**	**# of CTCs (CellSearch)**	**Culturing Conditions**	**Success Rate**	**Main Findings**	**Ref**
Colon cancer	Nonresectable metastatic	RosetteSep	≥300	- Hypoxic in medium 1 DMEM/F12 to normoxic conditions in medium 2 RPMI1640 - 2D, sustained for >6months	1%	- Recapitulation of main genomic features - Tumorigenic in vivo - Intermediate EMT + stem cell properties	[9,10]
Breast cancer	Metastatic	FACS	0	- Normoxic stem cell culture medium - 2D	8%	- Tumorigenic in vivo, brain metastasis signature ($EpCAM^{-}HER2^{+}/EGFR^{+}/HPSE^{+}/Notch1^{+}$)	[75]
	Metastatic luminal	CTC-iChip	3–3000	- Hypoxic, nonadherent - 2D, Sustained for >6 months	83%	- Tumorigenic in vivo - Drug sensitivity panels and CTM-specific methylation profile	[43,76]
CRPC	Metastatic	RosetteSep-Ficoll	>100	- Growth factors reduced Matrigel/Advanced DMEM/F12 - 3D, sustained for >6 months	6%	- Tumorigenic in vivo	[77]
NSCLC	Early stage	Microfluidic CTC-capture device	1–11	- Matrigel + collagen - 3D, sustained for ~1 month	73%	- Common mutations between cultured CTCs and primary tumor	[78]

Despite successful in vitro expansion of patient CTCs in several cancer types as reported above, important limitations should be noted when handling 2D cultures, including cell morphology alterations due to adherence to plastic and lack of tumor microenvironment. Moreover, cell-cell and spatial interactions in vitro are not fully representative of the setting in the tumor mass in vivo [79]. These constraints can thus interfere with physiological functions and molecular responses of the tumor cells, making them less representative of the actual malignancy. To circumvent this problem, 3D models were proposed in prostate and lung cancer [77,78]. In prostate cancer, Gao et al. generated the first seven fully characterized organoid lines from a CRPC patient including a CTC-derived 3D organoid system from a patient who had more than 100 CTCs in 8 mL of blood. Success rate for the establishment of the CTC-derived organoid was not provided. Whole-exome sequencing (WES) analysis showed that all the 3D models recapitulated the molecular diversity of prostate cancer subtypes and were amenable to pharmacological assays. Engraftment of the CTC-derived organoid in vivo gave rise to tumors with a histological pattern similar to that of the primary cancer. This research, therefore, contributes a patient-derived model of CRPC which, with further optimization, may respond to the pressing need of in vitro models that faithfully recapitulate CRPC [77]. In lung cancer, Zhang et al. developed a novel ex vivo CTC-derived model using a 3D co-culture system which stimulated a microenvironment to sustain tumor development. CTCs were enriched and expanded for a short period of time from 14 to 19 early lung cancer patients. Next-generation sequencing detected several mutations including *TP53* found in both cultured CTCs and matched patient primary tumors [78].

6. Discussion

During the last decade, tremendous technological progress has been made to reliably detect, quantify and characterize CTCs at phenotypic, genomic, and functional levels. The characterization of CTC-derived models has paved the way toward an improved understanding of tumor dissemination by these cells (Figure 1). As depicted in Table 1, procedures for developing CDXs can vary from one study to another. Subcutaneous (SC) injection of cells in mice is the simplest method for tumor engrafts which has been used for decades and was most recently applied for PDX establishment. It facilitates tumor growth monitoring as it does not require fluorescent labeling or imaging. Most CDX models published to date have been developed through SC injection of CTCs. SC tumors do not usually metastasize probably due to the absence of the human microenvironment and the impact of murine angiogenesis, which influence dissemination of primary human tumors. Moreover, as the time-frame needed for tumor growth extends to several months, ethical regulations may not allow waiting for metastatic spread. To this end, these studies were limited to the characterization of the CDX primary tumor. Injection in mouse bone marrow as done by Baccelli et al. may also be an appropriate way to investigate MICs as this microenvironment has been previously described as a reservoir for disseminating tumor cells [35,59]. Conversely, studies aiming to assess metastatic and not only tumorigenic competency of CTCs have resorted to intracardiac injection [66,75]. This method, similarly to tail vein (TV) injection, allows a more rapid spread of the cells as they directly enter the bloodstream and thus mimics CTCs in their original setting. Propagation of CDX models through intracardiac or TV injection is less common or completely lacking, most likely due to potential dissemination bias. Indeed, organ metastasis could be influenced by the injection site of CTCs and defined by the first capillary bed encountered by cells post-injection. TV has been observed to induce lung metastases, thus generating false-positive results [80].

Another important challenge is ensuring the CDX consistently maintains its clinical relevance and serves as a patient surrogate. To this end, stringent validation is required and several aspects must be addressed. Firstly, it is crucial to verify the human origin of the CDX, as spontaneous tumors could grow in immunocompromised mouse models. Secondly, confirming cancer type and comparing the CDX tumor to the donor patient's biopsy through histopathology, followed by genomic studies to assess CDX genomic fidelity with patient tumor. Moreover, in the context of establishing preclinical

models for precision medicine, functional drug sensitivity assays are needed to evaluate recapitulation of patient response to therapy in the CDX [68].

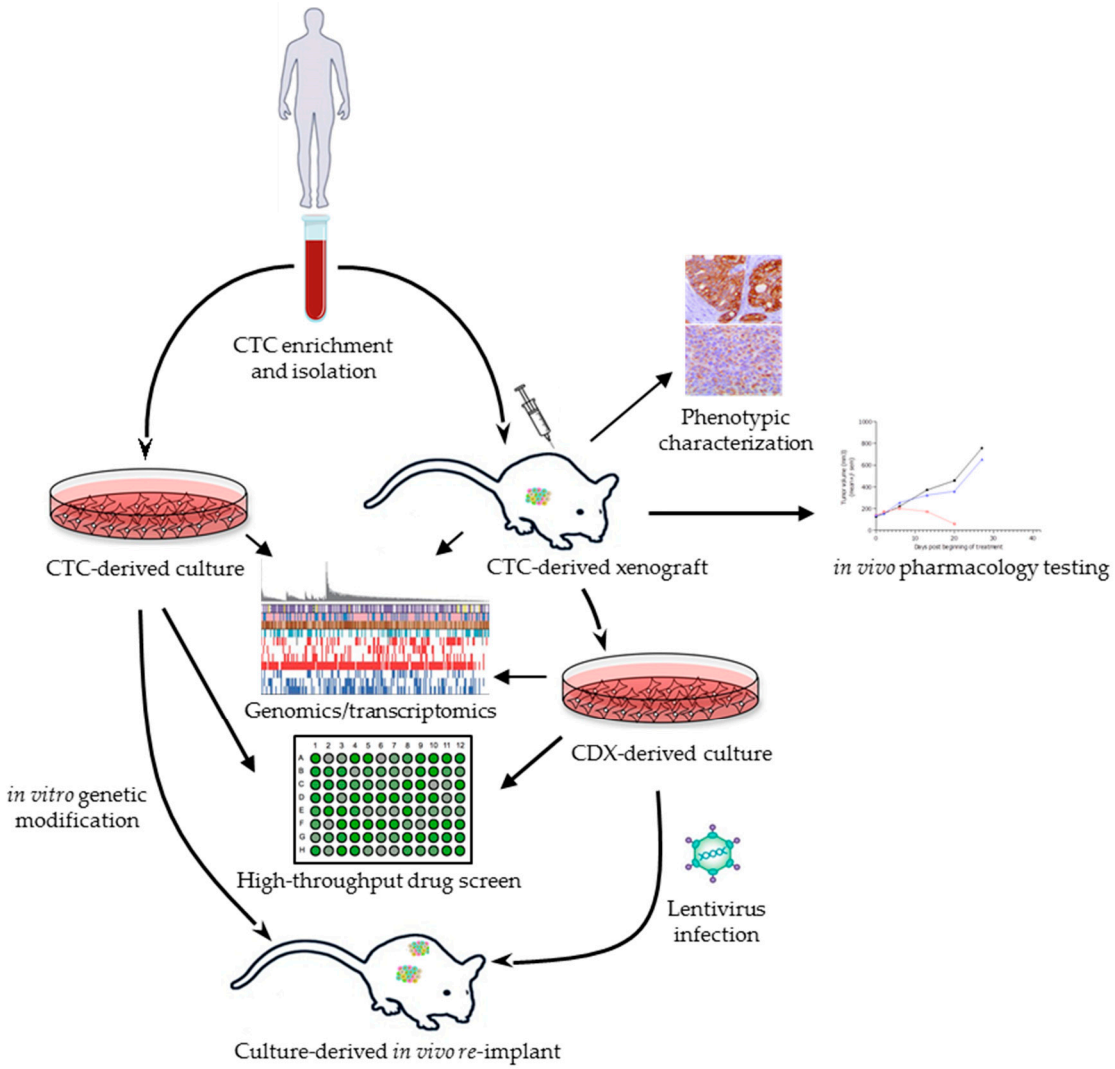


Figure 1. CTC-derived models as tractable systems to explore tumor-initiating cells (TICs) and new therapeutic strategies. CTCs isolated from late-stage cancer patients are used to generate CTC-derived xenografts (CDXs) to perform functional characterizations and pharmacology studies. CDX tumors can be isolated and dissociated into ex vivo cultures for drug screening and genome-wide analyses. CDX-derived cultures are amenable to lentiviral infection and can be re-injected into mice and used as tools to track tumor dissemination. In parallel, CTCs can be expanded in vitro and used as readouts of drug sensitivity. CTC = circulating tumor cell. CDX = CTC-derived xenograft.

Although PDX models serve as reliable tools for tumor modeling, CDXs offer added value for the understanding of tumor biology and metastasis. Detection and characterization of metastasis-competent CTCs using in vivo models offer a more representative molecular snapshot of the disease, as they serve as easily accessible "surrogates" of metastatic tissue, which is otherwise unobtainable in many cancer organs (e.g., bones or lungs) [81]. Indeed, CDX models could help showcase tumor heterogeneity in the metastatic setting in contrast to a localized biopsy in the case of PDX and are attainable at different time points throughout disease progression [63]. Most importantly, CDX models established to date reveal the high tumorigenic capacity of CTCs—even at a low number of cells (as low as 400 CTCs [68]). As reviewed above, CTCs with survival and MIC properties are assumed to be selected for seeding CDX tumors, similar to what has been observed in PDXs [82]. It is expected that the

proportion of tumorigenic CTCs may vary between cancer types and patients as well as under selective pressure of treatment, which highlights a potential selective process for the acquisition of minor metastasis-competent CTC subclones [73]. CTC clusters and hybrid E/M CTCs have been described as the most aggressive cells with a high propensity for tumorigenesis. However, it is currently difficult to evaluate the impact each subpopulation could have on CDX tumor take rate. Indeed, as detailed before, Aceto et al. have shown an increased metastatic competency in CTM vs. single CTCs but this remains limited to murine models and is difficult to translate to human subjects [40]. It is worth noting however that, although in vivo models are sustained by the host tissue microenvironment and can faithfully recapitulate the tumor genome, the absence of immune components constitutes an important bias.

On the other hand, CTC expansion ex vivo is promising but is still very far from routine applications as culturing conditions are still under investigation and need further optimization. Therefore, CDX-derived cultures represent an attractive intermediate model to characterize this aggressive population in vitro. In the event of molecular similarities between the two models, CDX and CDX-derived cell lines offer complementary, tractable systems for CTC functional characterization and therapy testing. Re-injection of the CDX-derived cell line in immunodeficient mice could allow the identification of candidate genes in metastasis and chemoresistance mechanisms [64,69]. Additional model systems such as the chick embryo chorioallantoic membrane have also opened up new promising avenues in the in vivo studies of tumor metastasis, as the highly vascularized setting sustains tumor formation and dissemination rapidly after engraft [83]. Moreover, organoids have recently emerged as novel robust 3D models optimized to propagate in vitro and reminiscent of tumoral heterogeneity, with amenability to genetic modifications and drug screening assays [77,84]. One can hypothesize that the establishment of several CTC-derived organoid lines from the same patient could be useful in modeling metastatic disease and acquired CTC mutational profiles to monitor disease progression. However, these models lack in vivo host complexity and recent efforts have been put into the generation of 3D co-cultures in microfluidic devices to model ex vivo tumor microenvironments by the integration of different cell populations (e.g., immune cells, fibroblasts) [78,85].

7. Concluding Remarks

CDX models have shown unprecedented opportunities to provide insight into the complex biology of the metastatic process. However, at the present time, these functional models serve as proof-of-principle tools as their development is limited to late-stage disease settings and high CTC counts. The main goal of functional CTC studies being the identification and characterization of MICs and candidate target genes among CTCs, it is crucial to expand analyses to earlier stages of cancer [63]. Unfortunately, these rare preclinical models are derived from patients in exceptional clinical situations and we are currently unable to predict if the limitation caused by CTC scarcity could be circumvented. Nevertheless, the establishment of CTC-derived models from only a few CTCs is a major achievement today and an invaluable opportunity to decipher new biomarkers, which are urgently needed for novel therapeutic strategies in advanced cancers.

Funding: Our CDX project was supported by ANR-15-CE17-0006-01, CTCTrap FP7 HEALTH #305341 and the Innovative Medicines Joint Undertaking CANCER ID (IMI-JU-11- 2013, grant no. 115749. TT is supported by La Ligue Nationale Contre le Cancer.

Acknowledgments: We are grateful to the patients and their families.

Conflicts of Interest: The authors declare no conflict of interest.

References

1. Fidler, I.J. Metastasis: Quantitative Analysis of Distribution and Fate of Tumor Emboli Labeled with ^{125}I-5-Iodo-2′ -deoxyuridine23. *JNCI J. Natl. Cancer Inst.* **1970**, *45*, 773–782. [PubMed]
2. Chambers, A.F.; Groom, A.C.; MacDonald, I.C. Dissemination and growth of cancer cells in metastatic sites. *Nat. Rev. Cancer* **2002**, *2*, 563–572. [CrossRef] [PubMed]

3. Luzzi, K.J.; MacDonald, I.C.; Schmidt, E.E.; Kerkvliet, N.; Morris, V.L.; Chambers, A.F.; Groom, A.C. Multistep Nature of Metastatic Inefficiency. *Am. J. Pathol.* **1998**, *153*, 865–873. [CrossRef]
4. Massagué, J.; Obenauf, A.C. Metastatic colonization by circulating tumour cells. *Nature* **2016**, *529*, 298–306. [CrossRef] [PubMed]
5. Fidler, I.J. Tumor heterogeneity and the biology of cancer invasion and metastasis. *Cancer Res.* **1978**, *38*, 2651–2660. [CrossRef]
6. Al-Hajj, M.; Wicha, M.S.; Benito-Hernandez, A.; Morrison, S.J.; Clarke, M.F. Prospective identification of tumorigenic breast cancer cells. *Proc. Natl. Acad. Sci. USA* **2003**, *100*, 3983–3988. [CrossRef] [PubMed]
7. Ricci-Vitiani, L.; Lombardi, D.G.; Pilozzi, E.; Biffoni, M.; Todaro, M.; Peschle, C.; De Maria, R. Identification and expansion of human colon-cancer-initiating cells. *Nature* **2007**, *445*, 111–115. [CrossRef] [PubMed]
8. Agnoletto, C.; Corrà, F.; Minotti, L.; Baldassari, F.; Crudele, F.; Cook, W.; Di Leva, G.; d'Adamo, A.; Gasparini, P.; Volinia, S. Heterogeneity in Circulating Tumor Cells: The Relevance of the Stem-Cell Subset. *Cancers* **2019**, *11*, 483. [CrossRef] [PubMed]
9. Cayrefourcq, L.; Mazard, T.; Joosse, S.; Solassol, J.; Ramos, J.; Assenat, E.; Schumacher, U.; Costes, V.; Maudelonde, T.; Pantel, K.; et al. Establishment and Characterization of a Cell Line from Human Circulating Colon Cancer Cells. *Cancer Res.* **2015**, *75*, 892–901. [CrossRef] [PubMed]
10. Soler, A.; Cayrefourcq, L.; Mazard, T.; Babayan, A.; Lamy, P.-J.; Assou, S.; Assenat, E.; Pantel, K.; Alix-Panabières, C. Autologous cell lines from circulating colon cancer cells captured from sequential liquid biopsies as model to study therapy-driven tumor changes. *Sci. Rep.* **2018**, *8*, 15931. [CrossRef]
11. Liu, T.; Xu, H.; Huang, M.; Ma, W.; Saxena, D.; Lustig, R.A.; Alonso-Basanta, M.; Zhang, Z.; O Rourke, D.M.; Zhang, L.; et al. Circulating glioma cells exhibit stem cell-like properties. *Cancer Res.* **2018**. [CrossRef] [PubMed]
12. Nieto, M.A.; Huang, R.Y.-J.; Jackson, R.A.; Thiery, J.P. EMT: 2016. *Cell* **2016**, *166*, 21–45. [CrossRef] [PubMed]
13. Shibue, T.; Weinberg, R.A. EMT, CSCs, and drug resistance: The mechanistic link and clinical implications. *Nat. Rev. Clin. Oncol.* **2017**, *14*, 611–629. [CrossRef] [PubMed]
14. Kasimir-Bauer, S.; Hoffmann, O.; Wallwiener, D.; Kimmig, R.; Fehm, T. Expression of stem cell and epithelial-mesenchymal transition markers in primary breast cancer patients with circulating tumor cells. *Breast Cancer Res.* **2012**, *14*. [CrossRef] [PubMed]
15. Yu, M.; Bardia, A.; Wittner, B.S.; Stott, S.L.; Smas, M.E.; Ting, D.T.; Isakoff, S.J.; Ciciliano, J.C.; Wells, M.N.; Shah, A.M.; et al. Circulating Breast Tumor Cells Exhibit Dynamic Changes in Epithelial and Mesenchymal Composition. *Science* **2013**, *339*, 580–584. [CrossRef] [PubMed]
16. Kallergi, G.; Papadaki, M.A.; Politaki, E.; Mavroudis, D.; Georgoulias, V.; Agelaki, S. Epithelial to mesenchymal transition markers expressed in circulating tumour cells of early and metastatic breast cancer patients. *Breast Cancer Res.* **2011**, *13*. [CrossRef] [PubMed]
17. Giordano, A.; Gao, H.; Anfossi, S.; Cohen, E.; Mego, M.; Lee, B.-N.; Tin, S.; Laurentiis, M.D.; Parker, C.A.; Alvarez, R.H.; et al. Epithelial–Mesenchymal Transition and Stem Cell Markers in Patients with HER2-Positive Metastatic Breast Cancer. *Mol. Cancer Ther.* **2012**, *11*, 2526–2534. [CrossRef]
18. Tam, W.L.; Weinberg, R.A. The epigenetics of epithelial-mesenchymal plasticity in cancer. *Nat. Med.* **2013**, *19*, 1438–1449. [CrossRef]
19. Puisieux, A.; Brabletz, T.; Caramel, J. Oncogenic roles of EMT-inducing transcription factors. *Nat. Cell Biol.* **2014**, *16*, 488–494. [CrossRef]
20. Mani, S.A.; Guo, W.; Liao, M.-J.; Eaton, E.N.; Ayyanan, A.; Zhou, A.Y.; Brooks, M.; Reinhard, F.; Zhang, C.C.; Shipitsin, M.; et al. The Epithelial-Mesenchymal Transition Generates Cells with Properties of Stem Cells. *Cell* **2008**, *133*, 704–715. [CrossRef]
21. Morel, A.-P.; Lièvre, M.; Thomas, C.; Hinkal, G.; Ansieau, S.; Puisieux, A. Generation of Breast Cancer Stem Cells through Epithelial-Mesenchymal Transition. *PLoS ONE* **2008**, *3*, e2888. [CrossRef] [PubMed]
22. Polyak, K.; Weinberg, R.A. Transitions between epithelial and mesenchymal states: Acquisition of malignant and stem cell traits. *Nat. Rev. Cancer* **2009**, *9*, 265–273. [CrossRef] [PubMed]
23. Creighton, C.J.; Li, X.; Landis, M.; Dixon, J.M.; Neumeister, V.M.; Sjolund, A.; Rimm, D.L.; Wong, H.; Rodriguez, A.; Herschkowitz, J.I.; et al. Residual breast cancers after conventional therapy display mesenchymal as well as tumor-initiating features. *Proc. Natl. Acad. Sci. USA* **2009**, *106*, 13820–13825. [CrossRef] [PubMed]

24. Ocaña, O.H.; Córcoles, R.; Fabra, Á.; Moreno-Bueno, G.; Acloque, H.; Vega, S.; Barrallo-Gimeno, A.; Cano, A.; Nieto, M.A. Metastatic Colonization Requires the Repression of the Epithelial-Mesenchymal Transition Inducer Prrx1. *Cancer Cell* **2012**, *22*, 709–724. [CrossRef] [PubMed]
25. Beerling, E.; Seinstra, D.; de Wit, E.; Kester, L.; van der Velden, D.; Maynard, C.; Schäfer, R.; van Diest, P.; Voest, E.; van Oudenaarden, A.; et al. Plasticity between Epithelial and Mesenchymal States Unlinks EMT from Metastasis-Enhancing Stem Cell Capacity. *Cell Rep.* **2016**, *14*, 2281–2288. [CrossRef] [PubMed]
26. Fischer, K.R.; Durrans, A.; Lee, S.; Sheng, J.; Li, F.; Wong, S.T.C.; Choi, H.; El Rayes, T.; Ryu, S.; Troeger, J.; et al. Epithelial-to-mesenchymal transition is not required for lung metastasis but contributes to chemoresistance. *Nature* **2015**, *527*, 472–476. [CrossRef] [PubMed]
27. Zheng, X.; Carstens, J.L.; Kim, J.; Scheible, M.; Kaye, J.; Sugimoto, H.; Wu, C.-C.; LeBleu, V.S.; Kalluri, R. Epithelial-to-mesenchymal transition is dispensable for metastasis but induces chemoresistance in pancreatic cancer. *Nature* **2015**, *527*, 525–530. [CrossRef]
28. Bailey; Martin Insights on CTC Biology and Clinical Impact Emerging from Advances in Capture Technology. *Cells* **2019**, *8*, 553. [CrossRef]
29. Lecharpentier, A.; Vielh, P.; Perez-Moreno, P.; Planchard, D.; Soria, J.C.; Farace, F. Detection of circulating tumour cells with a hybrid (epithelial/mesenchymal) phenotype in patients with metastatic non-small cell lung cancer. *Br. J. Cancer* **2011**, *105*, 1338–1341. [CrossRef]
30. Hou, J.-M.; Krebs, M.; Ward, T.; Sloane, R.; Priest, L.; Hughes, A.; Clack, G.; Ranson, M.; Blackhall, F.; Dive, C. Circulating tumor cells as a window on metastasis biology in lung cancer. *Am. J. Pathol.* **2011**, *178*, 989–996. [CrossRef]
31. Hofman, V.; Ilie, M.I.; Long, E.; Selva, E.; Bonnetaud, C.; Molina, T.; Vénissac, N.; Mouroux, J.; Vielh, P.; Hofman, P. Detection of circulating tumor cells as a prognostic factor in patients undergoing radical surgery for non-small-cell lung carcinoma: Comparison of the efficacy of the CellSearch Assay^{TM} and the isolation by size of epithelial tumor cell method. *Int. J. Cancer* **2011**, *129*, 1651–1660. [CrossRef] [PubMed]
32. Papadaki, M.A.; Stoupis, G.; Theodoropoulos, P.A.; Mavroudis, D.; Georgoulias, V.; Agelaki, S. Circulating Tumor Cells with Stemness and Epithelial-to-Mesenchymal Transition Features Are Chemoresistant and Predictive of Poor Outcome in Metastatic Breast Cancer. *Mol. Cancer Ther.* **2019**, *18*, 437–447. [CrossRef] [PubMed]
33. Wong, C.W.; Lee, A.; Shientag, L.; Yu, J.; Dong, Y.; Kao, G.; Al-Mehdi, A.B.; Bernhard, E.J.; Muschel, R.J. Apoptosis: An early event in metastatic inefficiency. *Cancer Res.* **2001**, *61*, 333–338. [PubMed]
34. Bednarz-Knoll, N.; Alix-Panabières, C.; Pantel, K. Clinical relevance and biology of circulating tumor cells. *Breast Cancer Res. BCR* **2011**, *13*, 228. [CrossRef] [PubMed]
35. Braun, S.; Vogl, F.D.; Naume, B.; Janni, W.; Osborne, M.P.; Coombes, R.C.; Schlimok, G.; Diel, I.J.; Gerber, B.; Gebauer, G.; et al. A Pooled Analysis of Bone Marrow Micrometastasis in Breast Cancer. *N. Engl. J. Med.* **2005**, *353*, 793–802. [CrossRef]
36. Faugeroux, V.; Lefebvre, C.; Pailler, E.; Pierron, V.; Marcaillou, C.; Tourlet, S.; Billiot, F.; Dogan, S.; Oulhen, M.; Vielh, P.; et al. An Accessible and Unique Insight into Metastasis Mutational Content Through Whole-exome Sequencing of Circulating Tumor Cells in Metastatic Prostate Cancer. *Eur. Urol. Oncol.* **2019**. [CrossRef] [PubMed]
37. Fernandez, S.V.; Bingham, C.; Fittipaldi, P.; Austin, L.; Palazzo, J.; Palmer, G.; Alpaugh, K.; Cristofanilli, M. TP53 mutations detected in circulating tumor cells present in the blood of metastatic triple negative breast cancer patients. *Breast Cancer Res. BCR* **2014**, *16*, 445. [CrossRef]
38. Jordan, N.V.; Bardia, A.; Wittner, B.S.; Benes, C.; Ligorio, M.; Zheng, Y.; Yu, M.; Sundaresan, T.K.; Licausi, J.A.; Desai, R.; et al. HER2 expression identifies dynamic functional states within circulating breast cancer cells. *Nature* **2016**, *537*, 102–106. [CrossRef]
39. Heitzer, E.; Auer, M.; Gasch, C.; Pichler, M.; Ulz, P.; Hoffmann, E.M.; Lax, S.; Waldispuehl-Geigl, J.; Mauermann, O.; Lackner, C.; et al. Complex Tumor Genomes Inferred from Single Circulating Tumor Cells by Array-CGH and Next-Generation Sequencing. *Cancer Res.* **2013**, *73*, 2965–2975. [CrossRef]
40. Aceto, N.; Bardia, A.; Miyamoto, D.T.; Donaldson, M.C.; Wittner, B.S.; Spencer, J.A.; Yu, M.; Pely, A.; Engstrom, A.; Zhu, H.; et al. Circulating Tumor Cell Clusters Are Oligoclonal Precursors of Breast Cancer Metastasis. *Cell* **2014**, *158*, 1110–1122. [CrossRef]
41. Aceto, N.; Toner, M.; Maheswaran, S.; Haber, D.A. En Route to Metastasis: Circulating Tumor Cell Clusters and Epithelial-to-Mesenchymal Transition. *Trends Cancer* **2015**, *1*, 44–52. [CrossRef] [PubMed]

42. Liu, X.; Taftaf, R.; Kawaguchi, M.; Chang, Y.-F.; Chen, W.; Entenberg, D.; Zhang, Y.; Gerratana, L.; Huang, S.; Patel, D.B.; et al. Homophilic CD44 Interactions Mediate Tumor Cell Aggregation and Polyclonal Metastasis in Patient-Derived Breast Cancer Models. *Cancer Discov.* **2019**, *9*, 96–113. [CrossRef] [PubMed]
43. Gkountela, S.; Castro-Giner, F.; Szczerba, B.M.; Vetter, M.; Landin, J.; Scherrer, R.; Krol, I.; Scheidmann, M.C.; Beisel, C.; Stirnimann, C.U.; et al. Circulating Tumor Cell Clustering Shapes DNA Methylation to Enable Metastasis Seeding. *Cell* **2019**, *176*, 98–112.e14. [CrossRef] [PubMed]
44. Szczerba, B.M.; Castro-Giner, F.; Vetter, M.; Krol, I.; Gkountela, S.; Landin, J.; Scheidmann, M.C.; Donato, C.; Scherrer, R.; Singer, J.; et al. Neutrophils escort circulating tumour cells to enable cell cycle progression. *Nature* **2019**, *566*, 553–557. [CrossRef] [PubMed]
45. Allard, W.J.; Matera, J.; Miller, M.C.; Repollet, M.; Connelly, M.C.; Rao, C.; Tibbe, A.G.J.; Uhr, J.W. Tumor Cells Circulate in the Peripheral Blood of All Major Carcinomas but not in Healthy Subjects or Patients with Nonmalignant Diseases. *Clin. Cancer Res* **2004**, *10*, 6897–6904. [CrossRef] [PubMed]
46. Cristofanilli, M.; Budd, G.T.; Ellis, M.J.; Stopeck, A.; Matera, J.; Miller, M.C.; Reuben, J.M.; Doyle, G.V.; Allard, W.J.; Terstappen, L.W.M.M.; et al. Circulating Tumor Cells, Disease Progression, and Survival in Metastatic Breast Cancer. *N. Engl. J. Med.* **2004**, *351*, 781–791. [CrossRef] [PubMed]
47. Cristofanilli, M.; Hayes, D.F.; Budd, G.T.; Ellis, M.J.; Stopeck, A.; Reuben, J.M.; Doyle, G.V.; Matera, J.; Allard, W.J.; Miller, M.C.; et al. Circulating Tumor Cells: A Novel Prognostic Factor for Newly Diagnosed Metastatic Breast Cancer. *J. Clin. Oncol.* **2005**, *23*, 1420–1430. [CrossRef]
48. De Bono, J.S.; Scher, H.I.; Montgomery, R.B.; Parker, C.; Miller, M.C.; Tissing, H.; Doyle, G.V.; Terstappen, L.W.W.M.; Pienta, K.J.; Raghavan, D. Circulating Tumor Cells Predict Survival Benefit from Treatment in Metastatic Castration-Resistant Prostate Cancer. *Clin. Cancer Res.* **2008**, *14*, 6302–6309. [CrossRef]
49. Cohen, S.J.; Punt, C.J.A.; Iannotti, N.; Saidman, B.H.; Sabbath, K.D.; Gabrail, N.Y.; Picus, J.; Morse, M.; Mitchell, E.; Miller, M.C.; et al. Relationship of Circulating Tumor Cells to Tumor Response, Progression-Free Survival, and Overall Survival in Patients With Metastatic Colorectal Cancer. *J. Clin. Oncol.* **2008**, *26*, 3213–3221. [CrossRef]
50. Vona, G.; Sabile, A.; Louha, M.; Sitruk, V.; Romana, S.; Schütze, K.; Capron, F.; Franco, D.; Pazzagli, M.; Vekemans, M.; et al. Isolation by Size of Epithelial Tumor Cells. *Am. J. Pathol.* **2000**, *156*, 57–63. [CrossRef]
51. Desitter, I.; Guerrouahen, B.S.; Benali-Furet, N.; Wechsler, J.; Jänne, P.A.; Kuang, Y.; Yanagita, M.; Wang, L.; Berkowitz, J.A.; Distel, R.J.; et al. A new device for rapid isolation by size and characterization of rare circulating tumor cells. *Anticancer Res.* **2011**, *31*, 427–441. [PubMed]
52. Farace, F.; Massard, C.; Vimond, N.; Drusch, F.; Jacques, N.; Billiot, F.; Laplanche, A.; Chauchereau, A.; Lacroix, L.; Planchard, D.; et al. A direct comparison of CellSearch and ISET for circulating tumour-cell detection in patients with metastatic carcinomas. *Br. J. Cancer* **2011**, *105*, 847–853. [CrossRef] [PubMed]
53. Pailler, E.; Adam, J.; Barthélémy, A.; Oulhen, M.; Auger, N.; Valent, A.; Borget, I.; Planchard, D.; Taylor, M.; André, F.; et al. Detection of Circulating Tumor Cells Harboring a Unique *ALK* Rearrangement in *ALK* -Positive Non–Small-Cell Lung Cancer. *J. Clin. Oncol.* **2013**, *31*, 2273–2281. [CrossRef] [PubMed]
54. Pailler, E.; Oulhen, M.; Borget, I.; Remon, J.; Ross, K.; Auger, N.; Billiot, F.; Ngo Camus, M.; Commo, F.; Lindsay, C.R.; et al. Circulating Tumor Cells with Aberrant *ALK* Copy Number Predict Progression-Free Survival during Crizotinib Treatment in *ALK* -Rearranged Non–Small Cell Lung Cancer Patients. *Cancer Res.* **2017**, *77*, 2222–2230. [CrossRef] [PubMed]
55. Ozkumur, E.; Shah, A.M.; Ciciliano, J.C.; Emmink, B.L.; Miyamoto, D.T.; Brachtel, E.; Yu, M.; Chen, P.-i.; Morgan, B.; Trautwein, J.; et al. Inertial Focusing for Tumor Antigen-Dependent and -Independent Sorting of Rare Circulating Tumor Cells. *Sci. Transl. Med.* **2013**, *5*, 179ra47. [CrossRef] [PubMed]
56. Fabbri, F.; Carloni, S.; Zoli, W.; Ulivi, P.; Gallerani, G.; Fici, P.; Chiadini, E.; Passardi, A.; Frassineti, G.L.; Ragazzini, A.; et al. Detection and recovery of circulating colon cancer cells using a dielectrophoresis-based device: KRAS mutation status in pure CTCs. *Cancer Lett.* **2013**, *335*, 225–231. [CrossRef] [PubMed]
57. Bulfoni, M.; Gerratana, L.; Del Ben, F.; Marzinotto, S.; Sorrentino, M.; Turetta, M.; Scoles, G.; Toffoletto, B.; Isola, M.; Beltrami, C.A.; et al. In patients with metastatic breast cancer the identification of circulating tumor cells in epithelial-to-mesenchymal transition is associated with a poor prognosis. *Breast Cancer Res.* **2016**, *18*. [CrossRef]

58. Ross, K.; Pailler, E.; Faugeroux, V.; Taylor, M.; Oulhen, M.; Auger, N.; Planchard, D.; Soria, J.-C.; Lindsay, C.R.; Besse, B.; et al. The potential diagnostic power of circulating tumor cell analysis for non-small-cell lung cancer. *Expert Rev. Mol. Diagn.* **2015**, *15*, 1605–1629. [CrossRef] [PubMed]
59. Baccelli, I.; Schneeweiss, A.; Riethdorf, S.; Stenzinger, A.; Schillert, A.; Vogel, V.; Klein, C.; Saini, M.; Bäuerle, T.; Wallwiener, M.; et al. Identification of a population of blood circulating tumor cells from breast cancer patients that initiates metastasis in a xenograft assay. *Nat. Biotechnol.* **2013**, *31*, 539–544. [CrossRef]
60. Hidalgo, M.; Amant, F.; Biankin, A.V.; Budinská, E.; Byrne, A.T.; Caldas, C.; Clarke, R.B.; de Jong, S.; Jonkers, J.; Mælandsmo, G.M.; et al. Patient Derived Xenograft Models: An Emerging Platform for Translational Cancer Research. *Cancer Discov.* **2014**, *4*, 998–1013. [CrossRef]
61. Byrne, A.T.; Alférez, D.G.; Amant, F.; Annibali, D.; Arribas, J.; Biankin, A.V.; Bruna, A.; Budinská, E.; Caldas, C.; Chang, D.K.; et al. Interrogating open issues in cancer precision medicine with patient-derived xenografts. *Nat. Rev. Cancer* **2017**, *17*, 254–268. [CrossRef] [PubMed]
62. Blackhall, F.; Frese, K.K.; Simpson, K.; Kilgour, E.; Brady, G.; Dive, C. Will liquid biopsies improve outcomes for patients with small-cell lung cancer? *Lancet Oncol.* **2018**, *19*, e470–e481. [CrossRef]
63. Pantel, K.; Alix-Panabieres, C. Functional Studies on Viable Circulating Tumor Cells. *Clin. Chem.* **2016**, *62*, 328–334. [CrossRef] [PubMed]
64. Lallo, A.; Schenk, M.W.; Frese, K.K.; Blackhall, F.; Dive, C. Circulating tumor cells and CDX models as a tool for preclinical drug development. *Transl. Lung Cancer Res.* **2017**, *6*, 397–408. [CrossRef] [PubMed]
65. Pereira-Veiga, T.; Abreu, M.; Robledo, D.; Matias-Guiu, X.; Santacana, M.; Sánchez, L.; Cueva, J.; Palacios, P.; Abdulkader, I.; López-López, R.; et al. CTCs-derived xenograft development in a triple negative breast cancer case. *Int. J. Cancer* **2018**, *144*, 2254–2265. [CrossRef]
66. Vishnoi, M.; Haowen Liu, N.; Yin, W.; Boral, D.; Scamardo, A.; Hong, D.; Marchetti, D. The identification of a TNBC liver metastasis gene signature by sequential CTC-xenograft modelling. *Mol. Oncol.* **2019**. [CrossRef]
67. Girotti, M.R.; Gremel, G.; Lee, R.; Galvani, E.; Rothwell, D.; Viros, A.; Mandal, A.K.; Lim, K.H.J.; Saturno, G.; Furney, S.J.; et al. Application of Sequencing, Liquid Biopsies, and Patient-Derived Xenografts for Personalized Medicine in Melanoma. *Cancer Discov.* **2016**, *6*, 286–299. [CrossRef]
68. Hodgkinson, C.L.; Morrow, C.J.; Li, Y.; Metcalf, R.L.; Rothwell, D.G.; Trapani, F.; Polanski, R.; Burt, D.J.; Simpson, K.L.; Morris, K.; et al. Tumorigenicity and genetic profiling of circulating tumor cells in small-cell lung cancer. *Nat. Med.* **2014**, *20*, 897–903. [CrossRef]
69. Lallo, A.; Gulati, S.; Schenk, M.W.; Khandelwal, G.; Berglund, U.W.; Pateras, I.S.; Chester, C.P.E.; Pham, T.M.; Kalderen, C.; Frese, K.K.; et al. Ex vivo culture of cells derived from circulating tumour cell xenograft to support small cell lung cancer research and experimental therapeutics. *Br. J. Pharmacol.* **2019**, *176*, 436–450. [CrossRef]
70. Drapkin, B.J.; George, J.; Christensen, C.L.; Mino-Kenudson, M.; Dries, R.; Sundaresan, T.; Phat, S.; Myers, D.T.; Zhong, J.; Igo, P.; et al. Genomic and Functional Fidelity of Small Cell Lung Cancer Patient-Derived Xenografts. *Cancer Discov.* **2018**, *8*, 600–615. [CrossRef]
71. Morrow, C.J.; Trapani, F.; Metcalf, R.L.; Bertolini, G.; Hodgkinson, C.L.; Khandelwal, G.; Kelly, P.; Galvin, M.; Carter, L.; Simpson, K.L.; et al. Tumourigenic non-small-cell lung cancer mesenchymal circulating tumour cells: A clinical case study. *Ann. Oncol.* **2016**, *27*, 1155–1160. [CrossRef] [PubMed]
72. Andree, K.C.; Mentink, A.; Zeune, L.L.; Terstappen, L.W.M.M.; Stoecklein, N.H.; Neves, R.P.; Driemel, C.; Lampignano, R.; Yang, L.; Neubauer, H.; et al. Toward a real liquid biopsy in metastatic breast and prostate cancer: Diagnostic LeukApheresis increases CTC yields in a European prospective multicenter study (CTCTrap). *Int. J. Cancer* **2018**, *143*, 2584–2591. [CrossRef] [PubMed]
73. Faugeroux, V.; Pailler, E.; Deas, O.; Brulle-Soumare, L.; Hervieu, C.; Marty, V.; Alexandrova, K.; Andree, K.C.; Stoecklein, N.H.; Tramalloni, D.; et al. Genetic characterization of a Unique Neuroendocrine Transdifferentiation Prostate Circulating Tumor Cell - Derived eXplant (CDX) Model. *Nat. Commun.* **2019**. under review.
74. Faugeroux, V.; Pailler, E.; Deas, O.; Michels, J.; Mezquita, L.; Brulle-Soumare, L.; Cairo, S.; Scoazec, J.-Y.; Marty, V.; Queffelec, P.; et al. Development and characterization of novel non-small cell lung cancer (NSCLC) Circulating Tumor Cells (CTCs)-derived xenograft (CDX) models. In Proceedings of the AACR Annual Meeting 2018, Chicago, IL, USA, 14–18 April 2018.

75. Zhang, L.; Ridgway, L.D.; Wetzel, M.D.; Ngo, J.; Yin, W.; Kumar, D.; Goodman, J.C.; Groves, M.D.; Marchetti, D. The Identification and Characterization of Breast Cancer CTCs Competent for Brain Metastasis. *Sci. Transl. Med.* **2013**, *5*, 180ra48. [CrossRef] [PubMed]
76. Yu, M.; Bardia, A.; Aceto, N.; Bersani, F.; Madden, M.W.; Donaldson, M.C.; Desai, R.; Zhu, H.; Comaills, V.; Zheng, Z.; et al. Ex vivo culture of circulating breast tumor cells for individualized testing of drug susceptibility. *Science* **2014**, *345*, 216–220. [CrossRef] [PubMed]
77. Gao, D.; Vela, I.; Sboner, A.; Iaquinta, P.J.; Karthaus, W.R.; Gopalan, A.; Dowling, C.; Wanjala, J.N.; Undvall, E.A.; Arora, V.K.; et al. Organoid Cultures Derived from Patients with Advanced Prostate Cancer. *Cell* **2014**, *159*, 176–187. [CrossRef]
78. Zhang, Z.; Shiratsuchi, H.; Lin, J.; Chen, G.; Reddy, R.M.; Azizi, E.; Fouladdel, S.; Chang, A.C.; Lin, L.; Jiang, H.; et al. Expansion of CTCs from early stage lung cancer patients using a microfluidic co-culture model. *Oncotarget* **2014**, *5*, 12383–12397. [CrossRef]
79. Tellez-Gabriel, M.; Cochonneau, D.; Cadé, M.; Jubelin, C.; Heymann, M.-F.; Heymann, D. Circulating Tumor Cell-Derived Pre-Clinical Models for Personalized Medicine. *Cancers* **2018**, *11*, 19. [CrossRef]
80. Khanna, C. Modeling metastasis in vivo. *Carcinogenesis* **2004**, *26*, 513–523. [CrossRef]
81. Alix-Panabières, C.; Pantel, K. Challenges in circulating tumour cell research. *Nat. Rev. Cancer* **2014**, *14*, 623–631. [CrossRef]
82. Eirew, P.; Steif, A.; Khattra, J.; Ha, G.; Yap, D.; Farahani, H.; Gelmon, K.; Chia, S.; Mar, C.; Wan, A.; et al. Dynamics of genomic clones in breast cancer patient xenografts at single-cell resolution. *Nature* **2015**, *518*, 422–426. [CrossRef] [PubMed]
83. Stoletov, K.; Willetts, L.; Paproski, R.J.; Bond, D.J.; Raha, S.; Jovel, J.; Adam, B.; Robertson, A.E.; Wong, F.; Woolner, E.; et al. Quantitative in vivo whole genome motility screen reveals novel therapeutic targets to block cancer metastasis. *Nat. Commun.* **2018**, *9*. [CrossRef] [PubMed]
84. Praharaj, P.P.; Bhutia, S.K.; Nagrath, S.; Bitting, R.L.; Deep, G. Circulating tumor cell-derived organoids: Current challenges and promises in medical research and precision medicine. *Biochim. Biophys. Acta BBA - Rev. Cancer* **2018**, *1869*, 117–127. [CrossRef] [PubMed]
85. Nguyen, M.; De Ninno, A.; Mencattini, A.; Mermet-Meillon, F.; Fornabaio, G.; Evans, S.S.; Cossutta, M.; Khira, Y.; Han, W.; Sirven, P.; et al. Dissecting Effects of Anti-cancer Drugs and Cancer-Associated Fibroblasts by On-Chip Reconstitution of Immunocompetent Tumor Microenvironments. *Cell Rep.* **2018**, *25*, 3884–3893.e3. [CrossRef] [PubMed]



© 2019 by the authors. Licensee MDPI, Basel, Switzerland. This article is an open access article distributed under the terms and conditions of the Creative Commons Attribution (CC BY) license (http://creativecommons.org/licenses/by/4.0/).

IV. Genomic instability and the DNA damage response in cancer

Genome instability is an important hallmark of cancer development, fueling tumor evolution throughout disease progression (Hanahan, 2022; Hanahan & Weinberg, 2011). It is determined by accumulated DNA damage, which may be caused by tumor exposure to exogenous insults such as ionizing- or ultraviolet (UV) radiation-inducing DNA damage, as well as endogenous stress resulting from tumor-specific DNA repair dysfunctions. To counteract threats to genome integrity, cells have evolved a complex network of cellular mechanisms collectively called the DNA damage response (DDR), which recognizes DNA damage through "damage sensors" such as ataxia telangiectasia mutated (ATM), ataxia telangiectasia and Rad3-related (ATR), checkpoint kinase 1 and 2 (CHK1 and CHK2) or p53 and halts the cell cycle to promote repair (Abraham, 2001; Maréchal & Zou, 2013).

1) DNA repair pathways

Different types of DNA damage (modified bases, abasic sites, DNA single-strand breaks – SSBs, DNA double-strand breaks – DSBs) may elicit response from a variety of DNA repair mechanisms, including mismatch repair (MMR), base-excision repair (BER), nucleotide excision repair (NER), classical non-homologous end joining (c-NHEJ) and homologous recombination (HR). DSBs are considered the most cytotoxic form of DNA lesions and their repair is dominated by c-NHEJ and HR pathways in healthy somatic mammalian cells. DSB mode of repair is determined by several factors such as DSB complexity, chromatin state and cell cycle phase. Indeed, a critical determinant in the c-NHEJ/HR interplay is DNA 5'-end resection, which is promoted by cyclin-dependent kinase phosphorylation (Ceccaldi, Rondinelli, et al., 2016; Symington & Gautier, 2011). While chromatin recruitment of 53BP1 suppresses end resection and favors c-NHEJ, breast cancer susceptibility gene 1 *(*BRCA1) antagonizes 53BP1, promoting DSB repair by HR (Bunting et al., 2010; Ceccaldi, Rondinelli, et al., 2016). Herein, we discuss the major DSB repair pathways (**Figure 10**).

a. Classical non-homologous end joining

c-NHEJ is a major DSB repair mechanism active throughout the cell cycle. However, it does not use a complementary template, making it an error-prone process. Ku70-Ku80 first recognizes DSB ends, engaging the recruitment of additional NHEJ factors, including the DNA-dependent protein kinase catalytic subunit (DNA-PKcs), DNA nucleases and the DNA ligase complex composed of ligase IV, XRCC4, XRCC4-like factor (XLF) and XRCC4 and XLF paralogue PAXX. Ku70-Ku80 and DNA-PKcs form the DNA-PKcs holoenzyme, implicated in DNA broken end synapsis. This in turn activates additional repair proteins (*e.g.* Artemis exonuclease) implicated in end-processing, before the final rejoining step by the DNA ligase IV (LigIV)-XRCC4-XLF-PAXX complex. DNA end resection intereferes with c-NHEJ engagement by removing Ku from DNA ends; a crucial step for HR initiation (Burma et al., 2006; Scully et al., 2019; Trenner & Sartori, 2019).

b. Homologous recombination

HR is highly relevant in cancer risk as it involves the two breast cancer susceptibility genes 1 (*BRCA1*) and 2 (*BRCA2*). HR requires the presence of an intact sister chromatid and is thus restricted to the S and G2 phases of the cell cycle, promoting error-free repair (Scully et al., 2019). When DNA end resection occurs, c-NHEJ repair pathway is blocked and three homology-based mechanisms, *i.e.* single-strand annealing (SSA), alternative end joining (alt-EJ) or HR compete for the repair. For the purpose of this study, this subsection will be focused exclusively on the HR repair mechanism.

HR repairs DSBs through homologous DNA sequence alignment. DSBs are first sensed by the MRE11-RAD50-NBS1 (MRN) complex, which enables a short-range resection of the 5′ strand with the help of BRCA1 and CtBP-interacting protein (CtIP), thus displacing Ku70-80 from the DNA end. Exonuclease 1 (EXO1) or DNA2-Bloom's syndrome helicase (BLM) heterodimer then perform further 5′-3′ resection, generating long 3′ single-stranded DNA (ssDNA) overhangs. The resulting ssDNA becomes subsequently coated with the heterotrimeric replication protein A (RPA) complex. During canonical HR,

tumor suppressor BRCA2 BRC domains form a complex along with PALB2 and RAD51 paralogs, which positively mediates RAD51 loading onto RPA-coated ssDNA through RPA displacement, promoting RAD51 nucleofilament formation. The RAD51-ssDNA nucleoprotein filament in turn stimulates homology search and strand invasion of a homologous DNA template (collectively called synapsis), generating the D-loop intermediate. The 3′-invading strand template-dependent extension is followed by its re-annealing to the complementary strand of the second-end tail, which is known as "synthesis-dependent strand annealing" and results in a non-crossover gene conversion. Alternatively, a double Holliday junction may be formed, which can be resolved either as a non-crossover or as a crossover (Li & Heyer, 2008; Scully et al., 2019; Trenner & Sartori, 2019).

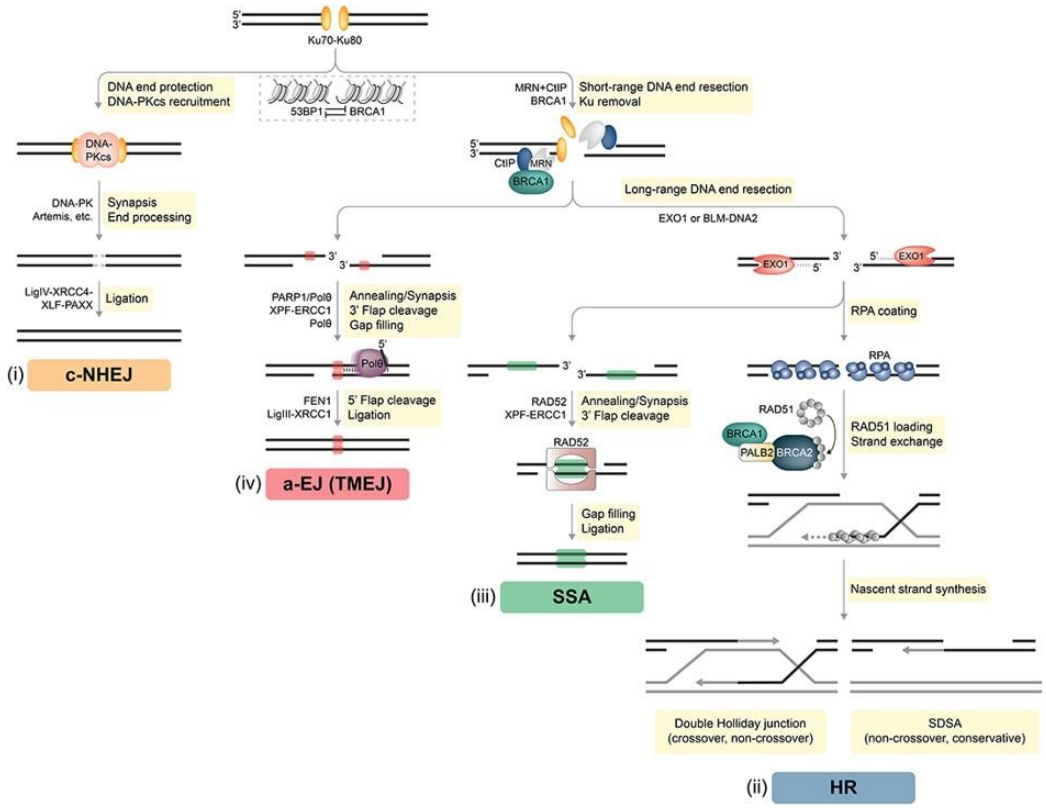


Figure 10. Double-strand break repair pathways in mammalian cells. Two major competing pathways repair two-ended DSBs: classical non-homologous end joining (c-NHEJ) (**i**) and homologous recombination (HR) (**ii**) (described in detail in **Introduction section IV.1)a. and b.)**. DSBs can also be subjected to single-strand annealing (SSA) (**iii**) or alternative end joining (a-EJ) (**iv**). (**iii**) SSA requires at least 20–25 base pairs (bp) of DNA sequence homology, typically found between repetitive elements (green boxes) in the genome. Subsequently, RAD52 promotes annealing of complementary ssDNA and leftover non-homologous flaps of the 3′ overhangs are cleaved by XPF-ERCC1. The factors that promote gap filling and ligation during SSA remain largely elusive. (**iv**) a-EJ (or TMEJ) utilizes short

microhomologies (MHs) of 2–20 bp (red boxes) to join the two DNA strands. PARP1 has been implicated in promoting DNA end synapsis and recruiting the specialized DNA polymerase θ (Polθ) to DSBs. Polθ stabilizes MH-mediated joints between the two DNA ends serving as primers for fill-in synthesis. 3′ flaps extending from the joints are removed by XPF/ERCC1. Flap endonuclease 1 (FEN1) has recently been implicated in the removal of 5′ flaps generated by Polθ-mediated strand displacement, while the DNA Ligase III (LigIII)-XRCC1 complex is essential for the final ligation step. ***Figure and legend adapted from Trenner & Sartori, Frontiers in Oncology, 2019.***

c. Fanconi anemia pathway

DNA interstrand crosslinks (ICLs) are highly deleterious lesions for the cell as they inhibit essential processes such as replication fork progression and transcription. Their toxicity is exploited in the clinic and ICL-inducing agents are widely used in chemotherapeutic treatments of cancer patients. These include nitrogen mustards (cyclophosphamide, melphalan), mitomycin C and platinum compounds (cisplatin, carboplatin, etc.). DNA repair of ICLs is initiated by the Fanconi anemia (FA) pathway (also known as Fanconi anemia/BRCA pathway) (**Figure 11**).

FA pathway-mediated ICL repair occurs in several coordinated steps, starting with the unloading of the CMG helicase from the stalled forks by BRCA1. ICL recognition by FANCM and associated proteins triggers the assembly and recruitment of the nuclear E3 ubiquitin ligase (FA core complex) consisting of FA protein subunits A, B, C, E, F, G, L and M. The FA core complex subsequently catalyzes the monoubiquitylation (Ub) and phosphorylation of FANCD2-FANCI – a critical event of the FA repair pathway – leading to its recruitment to chromatin. Activated FANCD2-FANCI then interacts with several downstream effector proteins at the ICL site including endonucleases and polymerases, to orchestrate ICL nucleolytic incision and subsequently release the ICL *via* "unhooking". Next, lesion bypass is carried out by translesion synthesis polymerases such as REV1 or DNA polymerase ζ. The intact ligated strand generated by translesion synthesis then acts as a template to complete repair *via* HR and re-establish the replication fork. Upon completion of ICL repair, FANCD2 is deubiquitylated by USP1-UAF1, promoting its release from chromatin (Ceccaldi, Sarangi, et al., 2016; Deans & West, 2011).

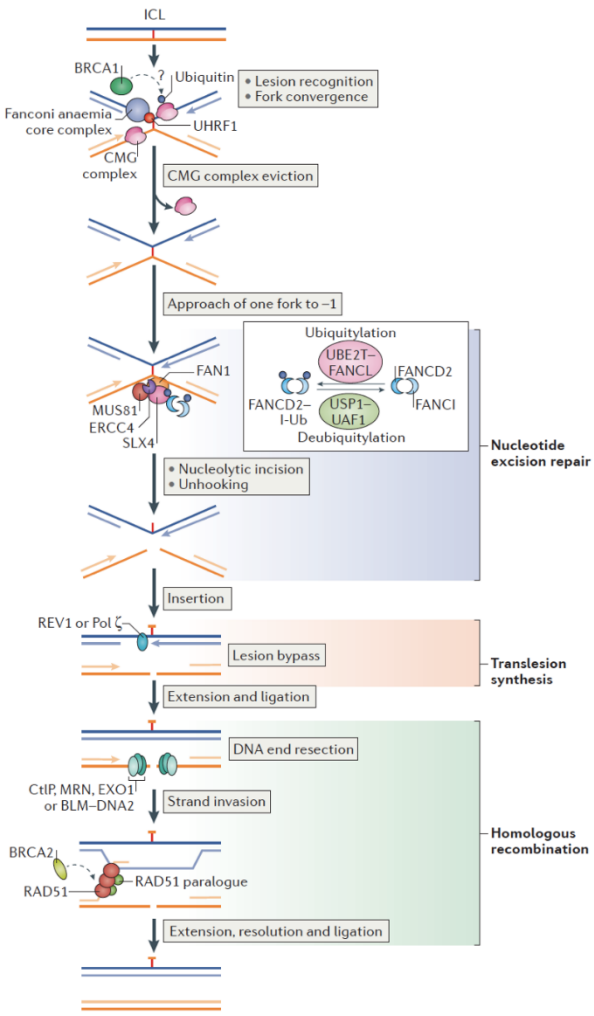


Figure 11. Cooperation of Fanconi anemia, nucleotide excision repair, translesion synthesis and homologous recombination proteins in a common interstrand crosslink repair pathway. UHRF1, ubiquitin-like with PHD and RING finger domains; ATR, ataxia telangiectasia and RAD3-related; UBE2T, ubiquitin-conjugating enzyme E2 T; BRCA1, breast cancer type 1 susceptibility protein; FAN1, Fanconi-associated nuclease 1; DNA polymerase ζ, REV3–REV7; CtIP, CtBP-interacting protein; MRN, MRE11–RAD50–NBS1; EXO1, exonuclease 1; BLM–DNA2, Bloom syndrome protein–DNA replication ATP-dependent helicase/nuclease 2; ssDNA, single-stranded DNA; RPA, replication protein A; USP1–UAF1, ubiquitin carboxyl-terminal hydrolase 1– USP1-associated factor 1. ***Figure and legend adapted from Ceccaldi et al., Nature Reviews Molecular Cell Biology, 2016.***

2) DNA repair alterations in cancer

DDR pathway dysfunctions are a common feature of human cancers and are thought to modulate tumor development, progression and therapeutic response (Lord & Ashworth, 2012). Importantly, they are believed to act at early stages of neoplastic development, as DDR activation markers such as phosphorylated nuclear histone H2AX (Ser139) foci (γH2AX at DSBs and arrested replication forks) have been previously

detected in precancerous lesions, resulting from replication stress-induced oncogene activation (Bartkova et al., 2005; Gorgoulis et al., 2005). Progression of precancerous lesions into tumors is thought to occur *via* the inactivation of major DNA damage signal transducers such as ATM, ATR and TP53, which renders the DDR dysfunctional and allows collapsed forks to proceed without repair and accumulate mutations. The role of DDR deficiency in the acquisition of a neoplastic phenotype was also evident in the association between loss-of-function mutations in DDR genes and a number of rare syndromes. These conditions include Fanconi anemia, a rare genetic disorder caused by germline inactivation of FA genes, as well as Ataxia Telangiectasia, which results from *ATM* mutations (Lord & Ashworth, 2012).

A plethora of deleterious DDR gene alterations can be found across human cancer types. For example, MMR (pathway implicated in the repair of DNA replication errors) deficiency, along with microsatellite instability, occur in around 15% of colorectal cancer cases, where MMR genes *MSH3/6* and *MLH3* are frequently mutated (Hewish et al., 2010; Muzny et al., 2012). Similarly, a mutational signature associated with HR defects may be harbored by a subset of both sporadic and inherited cancers. These defects are mostly fueled by loss-of-function somatic/germline mutations in *BRCA1*, *BRCA2* and FA genes including *RAD51C* and *PALB2* and are found in half of ovarian carcinomas, in triple-negative breast cancer and at a low prevalence in familial cases of pancreatic cancer (~ 2%) (Koboldt et al., 2012; J. Lee et al., 2014; Rahman et al., 2007; The Cancer Genome Atlas Research Network, 2011; Walsh et al., 2011). A recent comprehensive analysis of DDR deficiency across 33 cancer types deciphered HR to be the most frequently altered DNA repair pathway (in ~ 40% of cancers), especially in ovarian cancer. HR-deficient mutational profiles included alterations in *BRCA1*, *BRCA2* and *RAD51* paralogs (*RAD51B*, *RAD51C*) (**Figure 12**) (Knijnenburg et al., 2018).

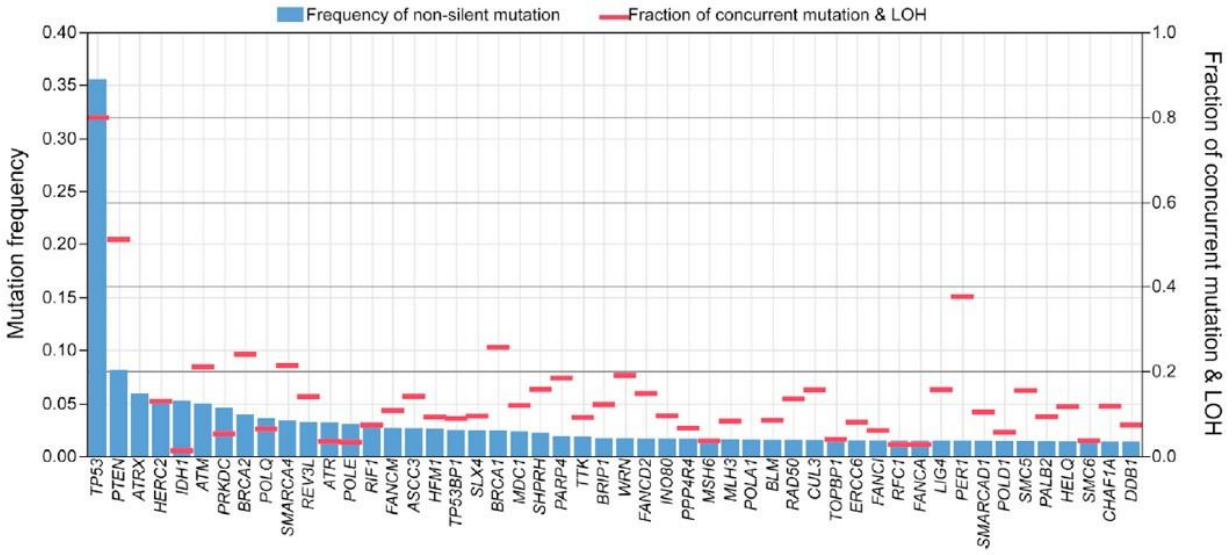


Figure 12. DNA damage response gene somatic alterations across 9,125 PanCanAtlas samples. The top 50 most frequently mutated genes among 276 DDR genes are listed in order of frequency of non-synonymous mutations (y axis left, blue rectangles), together with the fraction of concurrent mutations and LOH events (y axis right, red bars). ***Figure and legend adapted from Knijnenburg et al., Cell Reports, 2018.***

A focus on NSCLC

DDR defects are important contributors to NSCLC etiology and progression, with mutations or reduced expression in DNA repair genes such as *BRCA1*, *ATM*, *MSH2* and *excision repair cross-complementing protein 1* (*ERCC1*) being frequent in NSCLC (Heeke et al., 2018). Loss of ERCC1 is the most common DDR abnormality, found in ~ 30-50% of NSCLC tumors (Postel-Vinay et al., 2012). ERCC1 plays a key rate-limiting role in NER mechanism, which detects and mediates the removal of platinum-DNA bulky adducts, thus linking its expression to platinum response (Shuck et al., 2008). A genome-wide association study has previously identified rare germline variants in *BRCA2* and *CHK2* genes associated with lung cancer risk (Y. Wang et al., 2014). In a large-scale WES analysis of 1,144 lung tumors (adenocarcinoma and squamous cell carcinoma), seven tumors exhibited an MMR deficiency mutational signature, which is commonly observed in colorectal cancers with microsatellite instability (J. D. Campbell et al., 2016). More recently, using targeted genome sequencing of 266 NSCLC patient tumors, Ricciuti *et al* have reported that a proportion of ~ 50% presented a DDR-mutated profile involved in DNA damage sensing, as well as several DNA repair pathways

including MMR, HR, FA and NER. Among DDR-mutated NSCLC tumors, the most common mutations were found in *ATM* (9.4%), *ATR* (4.8%), *BRCA2* (4.1%), *POLQ* (3.7%) and *RAD50* (3.0%) DDR genes (Ricciuti et al., 2020).

Altogether, these studies demonstrate that DDR defects foster tumorigenesis and constitute critical determinants of the tumor mutational landscape in several malignancies. Importantly, they also represent exploitable cancer cell vulnerabilities.

V. Targeting the DDR in cancer

Loss of activity in high-fidelity DDR processes during tumorigenesis, such as HR-mediated DSB repair, significantly increases genome instability, leading to a greater reliance on compensatory mechanisms. Tumor cell DDR dependencies thus present an exploitable anticancer therapeutic opportunity, which has laid the groundwork for the use of DNA-damaging agents (*e.g.* radiation, chemotherapy), as well as the development of selective DDR-targeted therapies (O'Connor, 2015; Pilié, Tang, et al., 2019). For example, platinum chemotherapy is efficient in part by inducing DNA ICLs that are unresolvable in cancers with HR defects such as ovarian and breast cancers, or in NER-deficient lung cancers (Dann et al., 2012; Olaussen et al., 2006; Tutt et al., 2018). More recently, selective DDR enzyme inhibitors have been developed to target a specific DDR defect through synthetic lethal mechanisms (**Figure 13**) (A. Ashworth & Lord, 2018; De Vos et al., 2012).

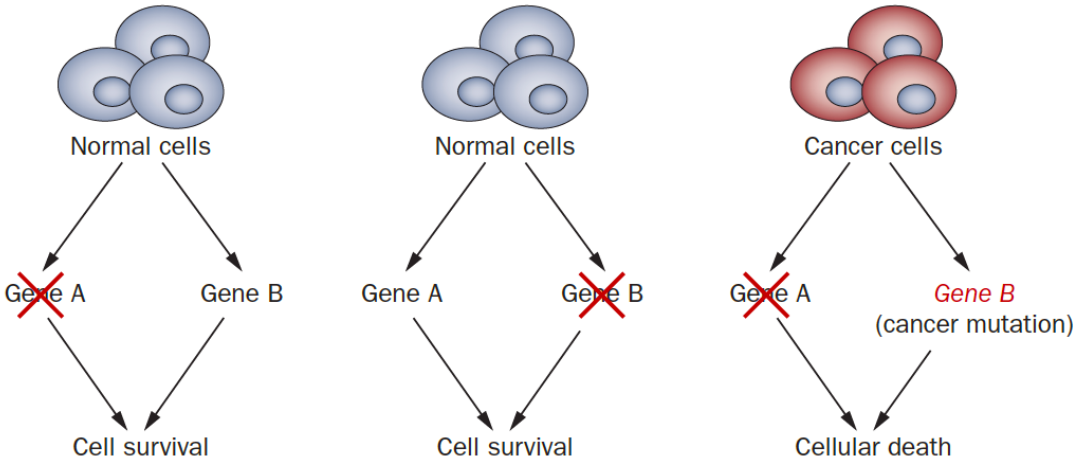


Figure 13. Synthetic lethality. Loss of either gene A or gene B in normal cells is compensated by the action of the remaining gene. In tumor cells, however, a mutation in one of these genes leaves the cell vulnerable to loss of the other gene by drug inhibition. This approach is the basis of drugs that target synthetic lethal relationships but spare normal cells. ***Figure and legend adapted from Rehman et al., Nature Reviews Clinical Oncology, 2010.***

1) PARP inhibitors: a synthetic lethal therapy

a. PARP1 function in DNA repair

The poly(ADP-ribose) polymerases 1 and 2 (PARP1 and PARP2) enzymes operate early in the DDR as key DNA damage sensors and signal transducers through the synthesis of negatively charged, branched PAR chains – an event known as PARylation – on a range of target proteins as a post-translational modification (Ray Chaudhuri & Nussenzweig, 2017; Satoh & Lindahl, 1992). PARylation reactions are implicated in several crucial cellular functions including the DDR, through the repair of SSBs and DSBs, DNA replication fork stabilization and chromatin remodeling. PARP1 primarily binds DNA at SSB sites, which stimulates its catalytic activity through a series of allosteric changes in its structure (**Figure 14**). This in turn promotes PARylation and the rapid recruitment of several DNA repair effectors to the damage site, such as X-Ray Repair Cross Complementing 1 (XRCC1), which acts a scaffold of SSB repair proteins. At the end of its catalytic cycle, PARP1 undergoes auto-PARylation eventually releasing it from repaired DNA. PARP1 is also an important mediator of NER for the removal of UV-induced DNA lesions *via* the regulation of chromatin remodeling, while it has also been shown to function in BER. Its role in DSB repair through HR and NHEJ has also been documented (Beck et al., 2014; Dantzer et al., 2000; Ray Chaudhuri & Nussenzweig, 2017).

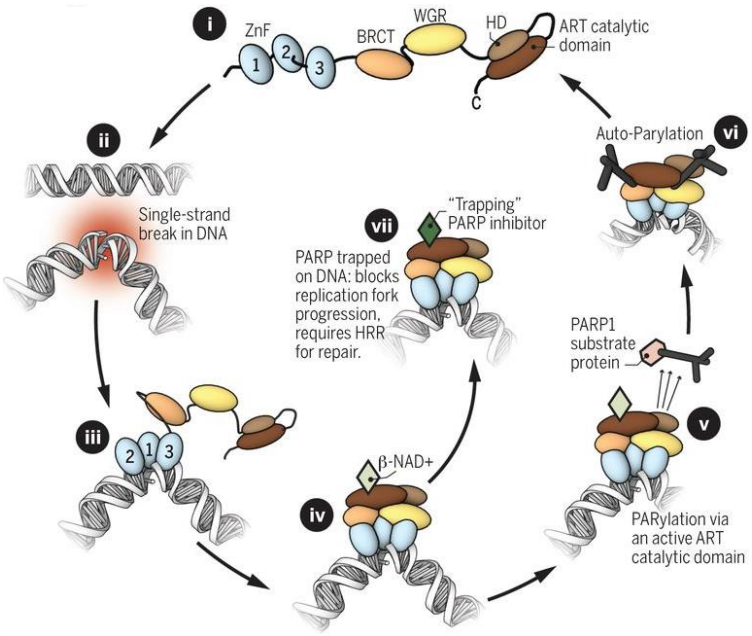


Figure 14. A schematic model of the PARP1 catalytic cycle. (**i**) In its non-DNA bound state, PARP1 exists in a relatively disordered conformation. The domain structure of PARP1 includes three zinc finger-related domains (ZnF 1, 2, and 3): the BRCA1 C-terminus domain (BRCT); the tryptophan-, glycine-, arginine-rich domain (WGR); and the catalytic domain, which encompasses two subdomains; a helical domain (HD) and an ADP-ribosyltransferase (ART) catalytic domain. In this non-DNA bound state, HD acts as an autoinhibitory domain preventing binding of the PARP-superfamily cofactor, β-NAD^+, to its ART binding site. (**ii**) Damage of the DNA double helix often causes the formation of SSBs, inducing a change in the normal orientation of the double helix, which, in turn, (**iii**) provides a binding site for DNA-binding PARP1 ZnF domains. (**iv**) Interaction of ZnF 1, 2, and 3 with DNA initiates a stepwise assembly of the remaining PARP1 protein domains onto the PARP1/DNA nucleoprotein structure, leading to a change in HD conformation, and the resulting loss of its autoinhibitory function, thus an allosteric activation of PARP1 catalytic activity. (**v**) ART catalytic activity drives the PARylation of PARP1 substrate proteins, mediating the recruitment of DNA repair effectors, chromatin remodeling, and eventually DNA repair. (**vi**) PARP1 autoPARylation finally causes the release of PARP1 from DNA and the restoration of a catalytically inactive state (as shown in **i**). (**vii**) Clinical PARPi bind the catalytic site and prevent the release of PARP1 from DNA. This PARP1 "trapping" at the site of damage removes PARP1 from its normal catalytic cycle. ***Figure and legend adapted from Lord & Ashworth, Science, 2017.***

b. Targeting PARP1 in the clinic

In-depth understanding of the predominant role of PARP1 in the DDR sparked interest in the development of small-molecule inhibitors of PARP1 and its paralogs (Zaremba & Curtin, 2007). Initially, the rationale behind it was that PARP inhibitors (PARPis) could potentiate DNA-damaging therapies, including chemotherapy or radiotherapy, by inhibiting PARP1-mediated repair of lesions created by these regimens. More than four decades ago, it was demonstrated that small molecule nicotinamide analogs inhibited PARylation (Purnell & Whish, 1980). In 2005, two pioneer studies have demonstrated for the first time the clinical potential of synthetic lethal interactions between PARP inhibition and the complete loss of function of *BRCA1* or *BRCA2*, suggesting a novel therapeutic approach in treatment of patients with deleterious *BRCA1/2* mutations (Bryant et al., 2005; Farmer et al., 2005).

Subsequent drug discovery efforts led to the development of several PARPis, including first-generation inhibitors veliparib (ABT-888, Abbvie), rucaparib (Rubraca®, Clovis), olaparib (Lynparza®, AstraZeneca) and niraparib (Zejula®, Tesaro), and the second-generation PARPi talazoparib (Talzenna®, Pfizer) (**Figure 15**). More recently, a next-generation highly selective PARPi, AZD5305, has shown a favorable safety profile and promising clinical activity compared to first-generation inhibitors in patients with

breast, ovarian, prostate, or pancreatic cancer presenting mutations in *BRCA1/2*, *PALB2,* or *RAD51C/D*, according to preliminary findings from the ongoing PETRA clinical trial presented at the AACR Meeting 2022 in New Orleans (NCT04644068) (Illuzzi et al., 2022; Yap et al., 2022).

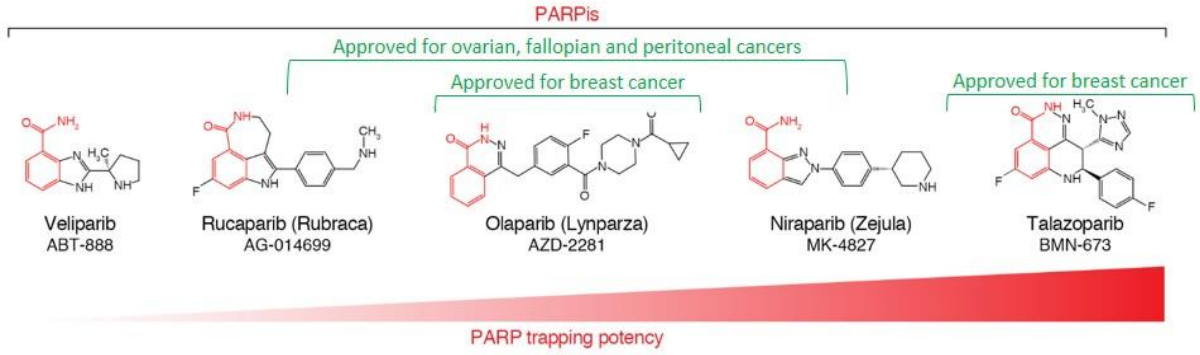


Figure 15. Clinical PARP inhibitors (PARPis). Four PARPis are FDA-approved for ovarian and/or breast cancers. All present a nicotinamide moiety (shown in red) which competes with the β-NAD^+ site of PARP-1 and PARP-2. The ability of each inhibitor to trap PARP1 on DNA varies, with talazoparib being the most potent PARPi and veliparib being the least potent. ***Figure and legend adapted from Thomas A et al., Journal of Clinical Investigation, 2018.***

The initial mode of action proposed was that SSBs resulting from PARP inhibition would remain unrepaired and are converted into cytotoxic DSBs at the encounter of the replication fork. This in turn leads to low-fidelity repair of DSBs in cancer cells presenting HR deficiency (HRD) (such as *BRCA1/2*-mutant cells), thus accumulating genome instability and ultimately resulting in cancer cell death (A. Ashworth, 2008). This view was completed later on with the concept of PARPi-induced PARP1 "trapping" on DNA, which prevents auto-PARylation and subsequent PARP1 release from damage sites, leading to cytotoxicity and cell death (Murai et al., 2012; Pommier et al., 2016). Although PARPis present similar catalytic inhibition capacities, they differ greatly in their trapping potency, with talazoparib being the most potent (**Figure 15**). Nevertheless, inherent or acquired resistance to PARPi monotherapy is common. A number of resistance mechanisms have been elucidated and most of them involve restoration of HR repair. This may occur through reversion mutation in *BRCA* genes or *via* indirect mechanisms involving alterations in other DNA repair proteins

such as 53BP1 or REV7, that restore HR (Baxter et al., 2022; Noordermeer et al., 2018; Pilié, Tang, et al., 2019; Xu et al., 2015).

2) Other DDR inhibitors

The success of PARPis and the underlying synthetic lethal therapeutic strategy led to the entry into preclinical and clinical development of multiple other agents targeting key DDR components. For example, ATM and ATR play a critical role in orchestrating the DDR and thus present prime targets for DDR inhibition, with highly selective ATR inhibitors currently being tested in a variety of tumor types (Durinikova et al., 2022; Roulston et al., 2022; Yap et al., 2021). Other DDR inhibitors include CHK1/2, DNA-PKcs and WEE1 inhibitors, as well as the POLQ inhibitor (Cleary et al., 2020; Zhou et al., 2021). A recent study reported synthetic lethality upon dual inhibition of NHEJ (using DNA-PK inhibitor peposertib) and microhomology-mediated end joining (using POLQ inhibitor) in *TP53*-deficient tumor cells, suggesting a novel DDR-based approach for the treatment of *TP53*-mutant cancers (Patterson-Fortin et al., 2022). Several DDR kinase inhibitors are currently under investigation (as monotherapy or in combination), although, unlike PARPis, they are currently limited to early phase trials, while some of them have been discontinued mainly due to toxicity (Baxter et al., 2022; Brown et al., 2017; Cleary et al., 2020; Pilié, Gay, et al., 2019). The main DDR inhibitors currently found in the clinical pipelines are outlined in **Table 3** below, while many others have been discovered and integrated preclinical studies (Cheng et al., 2022). Furthermore, DDR inhibitors may act as sensitizers to other agents such as radiotherapy, alkylating agents or targeted therapies such as PARPis. Another DDR inhibitor currently in the clinical pipielines is the first-in-class short dsDNA molecule AsiDNA™, which mimics DSBs thereby triggering false DDR signaling (decoy mechanism) (Berthault et al., 2022; Quanz et al., 2009). It is currently being evaluated in ovarian cancer in association with PARPis (REVOCAN clinical trial - NCT04826198). Several drug combinations of DDR inhibitors are currently being evaluated, with the main aim of overcoming acquired

resistance mechanisms (Banerjee et al., 2021; Dillon et al., 2018; Serra et al., 2022; Yap et al., 2020).

Table 3. Main DDR inhibitors currently in the clinical pipelines.

CHK1 inhibitors	ATR inhibitors	DNA-PK inhibitors	WEE1 inhibitors	ATM inhibitors
SRA-737 (Sierra oncology)	Ceralasertib (AstraZeneca)	AZD7648 (AstraZeneca)	Adavosertib (AstraZeneca)	AZD0156 (AstraZeneca)
	Elimusertib (Bayer)	CC-115 (Celgene)		
	Berzosertib (Merck)	M9831 (Merck)		
	M4344 (Merck)	Peposertib (Merck)		
	RP-3500 (Repare)			

3) DDR-based therapeutic strategies in NSCLC

Although there is clear evidence that DDR defects are commonly found in NSCLC and induce higher tumor mutational burden, their therapeutic exploitation has shown limited efficacy so far (Passiglia et al., 2021; Postel-Vinay et al., 2012). A phase III study evaluating PARPi veliparib in combination with a platinum-doublet in previously untreated advanced squamous NSCLC failed to show OS benefit to veliparib addition. Nonetheless, an exploratory biomarker analysis in the study (LP52 histological subtype signature) highlighted the importance of using predictive biomarkers of response to guide therapeutic choice (Ramalingam et al., 2021). In line with this notion, the presence of deleterious DDR mutations in NSCLC tumors was linked with improved clinical response to immunotherapy (Ricciuti et al., 2020). Based on the premise that tumors sensitive to DNA-damaging therapies may harbor DDR deficiencies, two phase II trials PIN and PIPSeN evaluated olaparib maintenance compared to placebo in chemosensitive NSCLC. Unfortunately, no statistically significant trend towards longer

PFS was detected (Fennell et al., 2020; Postel-Vinay et al., 2021). The phase II HUDSON study (NCT03334617) is currently investigating durvalumab-based combinations in biomarker-selected NSCLC patients having progressed on anti-PD-1/PD-L1. Tested therapies include the combination of ATR inhibitor ceralasertib plus durvalumab, which has shown promising preliminary results including efficacy signals in *ATM*-deficient patients and an upcoming phase III trial has recently been announced (Besse et al., 2021). Multiple other trials evaluating PARPi (mostly as combination treatment) in NSCLC are ongoing, notably the ARIANES phase II trial assessing the efficacy and safety of rucaparib and atezolizumab combination in DNA repair-deficient (*i.e.* harboring loss-of-function alerations in HR-related genes) or platinum-sensitive patients (NCT04276376).

4) Predictive biomarkers of response to DDR-based therapies

The therapeutic landscape of drugs targeting DDR signaling pathways has become an exciting and promising advancement in the field of cancer therapy in several malignancies. However, expanding and optimizing its use beyond *BRCA*-mutant cancers of treatment remains limited due to the lack of accurate, validated biomarkers predictive of response to DDR-based strategies. The development and validation of DDR predictive biomarkers is therefore critical for better patient stratification and implementation of DDR-based precision medicine strategies to a wider population (Cleary et al., 2020; Pilié, Gay, et al., 2019).

a. Beyond *BRCA*

In the absence of germline *BRCA1* or *BRCA2* mutations, some cancers may display a "BRCAness" phenotype, *i.e.* an HR defect phenocopying a *BRCA*-mutant (Lord & Ashworth, 2016). Indeed, since the initial reports describing the PARP/BRCA synthetic lethality, other synthetic lethal relationships involving PARP inhibition have been unraveled in tumors harboring alterations in DDR genes such as *RAD51, ATM*, *ATR*, *PALB2* and *FANCA*, which may confer tumor sensitivity to PARPi activity (McCabe et al., 2006). The identification of BRCAness phenotypes across human cancers has now been

rendered possible owing to recent advances in tumor sequencing technologies, a development which further extends the cancer population that may benefit from PARPi therapy (Lord & Ashworth, 2016). Importantly, the clinical validity of HRD testing through HR gene level tests (*BRCA* and non-*BRCA* genes) genomic scars or functional assays (*e.g.* RAD51) is now well-established in ovarian cancer and helps predict PARPi benefit (Miller et al., 2020). Additionally, a pattern of single-base substitution mutations labeled "signature 3" is strongly concordant with defective HR repair of DSBs through the pathogenic loss of *BRCA1* or *BRCA2* (Alexandrov et al., 2013; Nik-Zainal et al., 2012). In lung cancer, ERCC1 expression has been identified as a potent predictive biomarker of response to platinum-based regimens, with low levels of ERCC1 being associated with better response to chemotherapy in multiple reports (Olaussen et al., 2006; Postel-Vinay et al., 2012). Nevertheless, ERCC1 status assessment in the clinic in a phase III biomarker trial was not prognostic in NSCLC (S. M. Lee et al., 2017).

A top biomarker candidate of therapeutic response which has emerged recently and is under extensive investigation in several malignancies is *schlafen family member 11* (*SLFN11*). Findings from *in vitro* analyses and patient-derived models have highlighted this DNA/RNA helicase as a strong determinant of sensitivity to alkylating agents (*e.g.* cisplatin), topoisomerase I and II and DNA synthesis inhibitors (Barretina et al., 2012; Conteduca et al., 2020; Coussy et al., 2020; Murai et al., 2019; Zoppoli et al., 2012). SLFN11 overexpression has also been associated with sensitivity to PARPis, while its inactivation dictated resistance (Lok et al., 2017; Murai et al., 2016; Stewart et al., 2017). For example, in SCLC, Lok et *al* demonstrated that *SLFN11* expression strongly correlated with sensitivity to talazoparib *in vitro*, while its loss conferred PARPi resistance. Furthermore, its immunohistochemical expression was associated with PDX tumor response to talazoparib, thus suggesting *SLFN11* as a potential predictor of PARPi monotherapy efficacy in SCLC (Lok et al., 2017). In parallel, mechanistic studies have elucidated SLFN11 mode of action. When expressed, SLFN11 is recruited at replication forks in an RPA-dependent manner in response to induced replication stress, opens chromatin and irreversibly blocks replication fork progression leading to

cell death (**Figure 16**) (Mu et al., 2016; Murai et al., 2016, 2018; Pilié, Gay, et al., 2019). Conversely, in *SLFN11*-negative cells, ATR orchestrates response to replication stress and preclinical models have shown that targeting these cells with a combination of ATR inhibitor plus PARPi or another DNA-targeting agent may be beneficial (Murai et al., 2016, 2018; Winkler et al., 2021). Additional data showed that SLFN11 inhibits checkpoint maintenance and HR *via* RPA removal from ssDNA (Mu et al., 2016). Moreover, SLFN11 expression is dynamic and has been shown to be regulated epigenetically, transcriptionally and *via* viral infection (Murai et al., 2019). Interestingly, epigenetic silencing of *SLFN11* gene expression through hypermethylation was associated with poor response to platinum treatment and shorter PFS in both NSCLC and ovarian cancer (Nogales et al., 2015). The evaluation of SLFN11 role as an exploratory predictive biomarker has also integrated clinical trials, where its expression is assessed *via* tumor immunohistochemical screening. Most recently, in a study assessing the addition of veliparib to temozolomide treatment in patients with relapsed SCLC, SLFN11 expression was found to be associated with improved PFS and OS in patients treated with the combination (Pietanza et al., 2018). Another phase II trial is currently investigating the efficacy of atezolizumab in combination with talazoparib compared to atezolizumab alone, as maintenance therapy in *SLFN11*-positive advanced SCLC (NCT04334941). SLFN11 is therefore a very promising predictive biomarker of response to PARPi independently of *BRCA1/2*-related HRD, but its implementation in the clinic warrants further investigation in large cohorts.

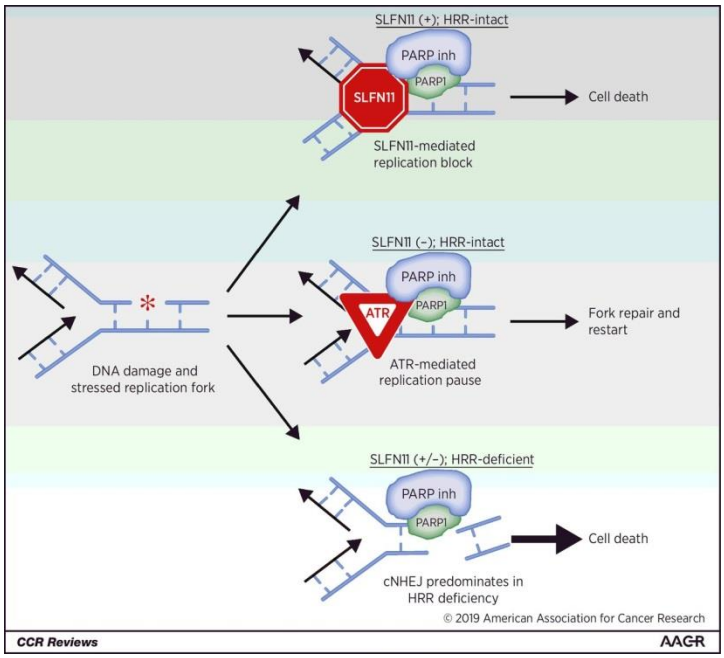


Figure 16. Multiple paths to PARP inhibitor vulnerability. HRR-intact tumors that express high levels of SLFN11 experience irreversible replication block and cell death in response to unrepaired SSBs and PARP entrapment after PARP inhibitor addition (top right). HRR-intact tumors lacking SLFN11 instead undergo only temporary replication pause, mediated by ATR, in response to same DNA damage, which allows for eventual fork repair and replication restart (middle right). In HRR-deficient tumors, regardless of SLFN11 status, PARP trapping leads to DSBs that cannot be resolved accurately due to absence of HRR and result in genome instability and cell death (bottom right). HRR, homologous recombination repair; PARP inh, PARP inhibitor. ***Figure and legend adapted from Pilié et al., Clinical Cancer Research, 2019.***

b. Assessment of DDR-based biomarkers in CTCs

Functional assessment of DDR protein expression has also been reported in CTCs, with the purpose of their evaluation as a pharmacodynamic biomarker (Tayoun et al., 2021). Nuclear γH2AX expression in CTCs has been assessed as a dynamic indicator of therapy-induced DNA damage in several malignancies including NSCLC, where γH2AX$^+$ CTC levels increased in response to chemotherapy, radiation and a combination of radiotherapy plus PARPi (Martin et al., 2014; Reiss et al., 2015; L. H. Wang et al., 2010). Nuclear RAD50 foci tracking – a marker of HR activity – has also been performed in lung cancer patient CTCs to detect irradiated cells (Adams et al., 2017). Lack of ERCC1 expression in CTCs was found to correlate with improved PFS in metastatic NSCLC patients undergoing platinum-based chemotherapy, while the detection of *ERCC1*-positive CTCs post-treatment in breast cancer indicated worse

patient outcome (Das et al., 2012; Kasimir-Bauer et al., 2016). The predictive role of ERCC1 expression in CTCs was also confirmed in ovarian cancer (Chebouti et al., 2016; Kuhlmann et al., 2014). Interestingly, SLFN11 protein expression was evaluated in CTCs along with metastatic tumors of CRPC patients treated with platinum chemotherapy: patients presenting *SLFN11*-positive CTCs had longer PFS compared to patients with *SLFN11*-negative CTCs (Conteduca et al., 2020). More recently, Zhang *et al* reported the feasibility and the predictive utility of monitoring SLFN11 expression in SCLC CTCs in response to chemotherapy (B. Zhang et al., 2022).

Despite accumulating evidence, the clinical validation of pharmacodynamic biomarkers in CTCs remains complex due to the lack of standardization in CTC technology and most importantly, their scarcity in peripheral blood. Functional characterization through the establishment of CDX models is crucial to study the biology of CTCs that fuel blood-borne metastasis and understand mechanisms of resistance. Importantly, such studies provide an invaluable opportunity to identify CTC biomarkers and test novel therapeutic strategies in aggressive malignancies.

REVIEW ARTICLE 2. Tumor evolution and therapeutic choice seen through a prism of circulating tumor cell genomic instability. *Cells* 2021; 10(2):337
Open access publication.

cells

MDPI

Review

Tumor Evolution and Therapeutic Choice Seen through a Prism of Circulating Tumor Cell Genomic Instability

Tala Tayoun [1,2,3], Marianne Oulhen [1,2], Agathe Aberlenc [1,2], Françoise Farace [1,2,*] and Patrycja Pawlikowska [2]

[1] Gustave Roussy, Université Paris-Saclay, "Circulating Tumor Cells" Translational Platform, CNRS UMS3655–INSERM US23AMMICA, F-94805 Villejuif, France; tala.tayoun@gustaveroussy.fr (T.T.); marianne.oulhen@gustaveroussy.fr (M.O.); agathe.aberlenc@gustaveroussy.fr (A.A.)
[2] Gustave Roussy, INSERM, U981 "Molecular Predictors and New Targets in Oncology", F-94805 Villejuif, France; patrycjamarta.pawlikowska@gustaveroussy.fr
[3] Faculty of Medicine, Université Paris-Saclay, F-94270 Le Kremlin-Bicetre, France
* Correspondence: francoise.farace@gustaveroussy.fr; Tel.: +33-(14)-2115198

Abstract: Circulating tumor cells (CTCs) provide an accessible tool for investigating tumor heterogeneity and cell populations with metastatic potential. Although an in-depth molecular investigation is limited by the extremely low CTC count in circulation, significant progress has been made recently in single-cell analytical processes. Indeed, CTC monitoring through molecular and functional characterization may provide an understanding of genomic instability (GI) molecular mechanisms, which contribute to tumor evolution and emergence of resistant clones. In this review, we discuss the sources and consequences of GI seen through single-cell analysis of CTCs in different types of tumors. We present a detailed overview of chromosomal instability (CIN) in CTCs assessed by fluorescence in situ hybridization (FISH), and we reveal utility of CTC single-cell sequencing in identifying copy number alterations (CNA) oncogenic drivers. We highlight the role of CIN in CTC-driven metastatic progression and acquired resistance, and we comment on the technical obstacles and challenges encountered during single CTC analysis. We focus on the DNA damage response and depict DNA-repair-related dynamic biomarkers reported to date in CTCs and their role in predicting response to genotoxic treatment. In summary, the suggested relationship between genomic aberrations in CTCs and prognosis strongly supports the potential utility of GI monitoring in CTCs in clinical risk assessment and therapeutic choice.

Keywords: circulating tumor cells; genomic instability; chromosomal instability; DNA-repair; tumor genetic heterogeneity

check for updates

Citation: Tayoun, T.; Oulhen, M.; Aberlenc, A.; Farace, F.; Pawlikowska, P. Tumor Evolution and Therapeutic Choice Seen through a Prism of Circulating Tumor Cell Genomic Instability. *Cells* **2021**, *10*, 337. https://doi.org/10.3390/cells10020337

Academic Editor: Catherine Alix-Panabieres
Received: 13 January 2021
Accepted: 2 February 2021
Published: 5 February 2021

Publisher's Note: MDPI stays neutral with regard to jurisdictional claims in published maps and institutional affiliations.

Copyright: © 2021 by the authors. Licensee MDPI, Basel, Switzerland. This article is an open access article distributed under the terms and conditions of the Creative Commons Attribution (CC BY) license (https://creativecommons.org/licenses/by/4.0/).

1. Introduction

Circulating tumor cells (CTC), present in peripheral blood of patients with cancers, are released from spatially distinct metastatic sites and primary tumor and thus may provide a comprehensive genomic picture of tumor content. The number of CTCs consists an independent prognostic factor and can be used to monitor treatment efficacy [1,2]. Alongside technological advances, CTCs have attracted clinical interest as a liquid biopsy to detect predictive biomarkers of sensitivity and resistance for therapy selection. Moreover, recent data on single CTC genomic analysis revealed the wide heterogeneity of CTCs, emphasizing the potential clinical utility of single CTC sequencing in identifying resistant clones that are arguably an important subset of cancer cells to target and eradicate. Indeed, growing evidence shows that CTCs may represent tumor phenotypic, genomic and transcriptomic heterogeneity and hence constitute a valuable sample to investigate tumor vulnerabilities. The phenotypes associated with tumor resistance and metastases require a complex pattern of cooperating processes among which genomic instability (GI) is a major actor. Oncogenic mutations as well as large-scale genomic alterations, copy number changes, DNA damage repair deficiencies or cell cycle perturbations may serve as an origin

of GI and subsequent tumor heterogeneity. By offering real-time monitoring of a constantly evolving disease and by examining tumor GI through simple blood draws, CTCs may be of great utility to monitor patient response to treatment and precision medicine. Moreover, CTC-derived models have recently emerged as tractable platforms to explore functional capacities of CTCs.

In this review, we discuss different sources of GI and their impact on potential therapeutic solutions. We explore CTC genomic heterogeneity through fluorescence in situ hybridization (FISH) and single-cell sequencing and discuss how profiling of CTCs can be used to trace GI of tumors. We emphasize the importance of GI characterization in the context of tumor evolution and therapeutic choice. We outline the availability and utility of CDX models in functional characterization of tumor-adapted GI mechanisms. Finally, we highlight the dynamic changes of DNA-repair-related protein expression as functional biomarkers of GI and/or response to genotoxic treatment.

2. Genomic Instability, More Than a Hallmark of Cancer

Over the past few years, genomic studies have demonstrated the complex and heterogeneous landscape of cancer and its potential impact on treatment resistance and metastasis development. GI is a driving force promoting continuous modification of tumor genomes and leading to clonal evolution and tumor genomic heterogeneity. Alterations in the DNA damage response (DDR), endogenous and oncogene-induced replication stress or cell division deregulation promote GI in cancer (Figure 1).

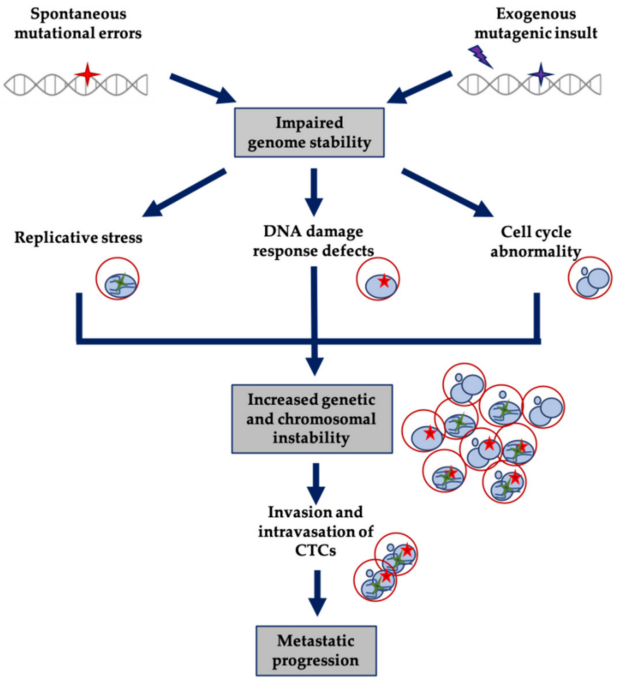


Figure 1. Concept diagram representing mechanisms of genome instability implicated in tumor evolution, including CTC contribution and their potential exploitation as biomarkers.

2.1. DNA Damage Defects

The DNA damage response (DDR) is a dynamic process based on the successive recruitments of different actors to DNA lesions. DNA damage occurs as a result of exogenous events such as ionizing irradiation or intercross-link agents, or as a part of perturbed physiological processes (see "Replicative stress" below). Resulting DNA double-strand breaks (DSBs) are the most cytotoxic lesions. Typically, two main repair mechanisms intervene to repair DSBs: homologous recombination (HR) and classical nonhomologous end joining. Histone H2AX (γH2AX), Nijmegen breakage syndrome 1 (nibrin/NBS1) and mediator of DNA damage checkpoint protein 1 (MDC1) create a signal amplifica-

tion loop adjacent to DSBs, which engages the recruitment of DDR proteins, including the MRN (MRE11-RAD50-NBS1) complex and breast cancer 1 (BRCA1) [3,4]. In-depth investigation of functional, "real time" biomarkers of DDR is crucial for monitoring this process under therapy. Phosphorylated γH2AX has emerged as a biomarker of DSBs, allowing the monitoring of genotoxic events [5]. Its expression also correlated with sensitivity to chemotherapy, radiotherapy, treatment with poly(ADP-ribose) polymerase (PARP) inhibitors (PARPi) and chemical genotoxicity [6,7].

Tumors deficient in one DNA repair pathway often rely on a compensatory mechanism to resolve the damage, i.e., fit their DNA-repair machinery, giving concomitantly potential opportunities for targeted therapeutic approaches. PARPi have demonstrated synthetic lethality in HR deficient BRCA1/BRCA2 mutant tumors, which led to their approval in platinum-sensitive (with/without BRCA1/2 mutation) ovarian cancer and in germline BRCA1/2 (gBRCA)-mutated metastatic breast cancer [8–10]. Germline g*BRCA* mutations remain the most common clinical biomarker for PARPi therapy response because BRCA-mutant cells show clear evidence of HR deficiency. The prevalence and clinical relevance of somatic mutations in Fanconi anemia (FA) genes (23 FANC genes identified up to now) have been recently reported as "BRCAness", traits of sensitivity to PARPi treatment first identified in breast cancer and later acknowledged in other types of cancers [11]. Indeed, FA genes are commonly altered in several cancers. According to The Cancer Genome Atlas, alterations in FA genes (mutations, deletions, and amplifications) were detected in 40% of tumors [12]. The canonical function of FA proteins is to eliminate chromosome-breaking effect of intercross-linking agents and preserve genomic integrity by stabilizing replication forks, moderating RS and regulating mitotic division. Thus "BRCAness"-positive tumors are also frequently sensitive to platinum salts. However, amplifications of FA genes may be advantageous to cancer cells and contribute to resistance to chemotherapy. Deep deletions and loss-of-function mutations in DNA-repair-related genes may confer tumor sensitivity to DNA-repair-related targeted therapy. Recently, the potential utility of RAD51 protein, a surrogate marker of HR functionality, has been reported [13,14]. RAD51 assay performed in clinical practice on tumor tissue samples may improve patient selection for PARPi therapy in non-BRCA1/2-related cancers, which likewise present HR deficiency.

2.2. Replicative Stress

Any possible obstacle that disturbs DNA replication and prevents cells from finalizing their genome duplication before mitosis causes replicative stress (RS). It is a frequent phenomenon among cancer cells and is usually associated with structural chromosomal instability (CIN), which arises from prone to damage under-replicated DNA. Many cancers harbor persistent RS due to oncogene activation or compromised DNA-repair machinery in the absence or loss-of-function of essential that ensure protection or repair of stressed replication forks. Indeed, constitutive activation of oncogenes such as c-MYC, HRAS and KRAS has been shown to disturb the accurate DNA replication and has been associated with increased GI [15–17]. Recently, Wilhelm et al. proposed a mechanism through which RS contributed to numerical aneuploidy in both healthy and CIN^+ cancer cells, by driving chromosome mis-segregation via premature centriole disengagement [18]. This study was concordant with previously published observations where RS increased incidence of lagging chromosomes during cellular division [19,20]. Nonetheless, cancer cells cope with RS through different mechanisms, such as overexpression of checkpoint mediators Claspin and Timeless (members of ATR/CHK1 pathway), which may increase RS tolerance by protecting replication forks [21]. Therefore, similarly to DNA-repair-deficient tumors, RS response may also be exploited for cancer treatment.

2.3. Cell Division Abnormality

Mitotic CIN is defined as inability to faithfully segregate equal chromosome contents to two daughter cells during mitosis. Indeed, abnormal chromosome numbers or numerical aneuploidy is a common alteration in human cancer. It may be promoted by

mitotic checkpoint deregulation and may lead to the loss of tumor suppressors or gain of oncogenic signals. However, the loss of key mitotic checkpoint genes is rare in clinical samples. Whole-genome doubling (WGD) induced through cytokinesis failure is a one-off event which may promote aneuploidy. Its prognostic utility has been first shown in early-stage colorectal cancer and was later proposed in other cancer types [22,23]. Tumor cells experiencing WGD have developed centrosome clustering as a mechanism to prevent lethal mitotic spindle multipolarity, by merging multiple centrosomes into two functional spindle poles. Interestingly, centrosome amplification stimulates cytoskeleton alterations, which might in turn be responsible for tumor cell invasions and thus metastatic development [24]. Inhibition of centrosome clustering may represent an anti-tumor specific strategy based on the formation of multipolar spindles and subsequent tumor cell death [25]. GI has also been associated with epithelial-mesenchymal transition (EMT) through the activation of the cytosolic DNA response pathway [26]. Indeed, altered chromosome segregation arising from GI promotes micronuclei formation whose rupture spills DNA into the cytosol. Presence of DNA in the cytosol induces the cGAS-STING (cyclic GMP-AMP synthase-stimulator of interferon genes) cytosolic DNA-sensing pathway and downstream noncanonical NF-κB signaling, thus inducing a proinflammatory response, which factors were recognized as EMT stimulators [27]. Identification of cGAS/STING activators is an area of active research, with several ongoing clinical trials evaluating such molecules [28,29].

Sequencing studies and mechanistic investigations have revealed alterations in GI-related genes and events (e.g., *TP53*, *BRCA1/2*, *RB1* loss, *CDKN2A* loss) relevant in cancer progression [12,30]. These have important clinical implications as they may give the possibility to better stratify the patients and help clinicians in therapy selection.

3. GI-Related Biomarkers in CTCs and Their Utility for Clinical Decision Making

In-depth assessment of GI in bulk biopsy sample is frequently incomplete due to limited sample availability, surrounding normal tissue contamination and tumor heterogeneity. Additionally, serial tumor tissue biopsies are not feasible in clinical practice and metastasis biopsies are limited to accessible sites. Blood-based liquid biopsies containing CTCs have emerged as a noninvasive and accessible alternative enabling serial sampling. CTC analysis is technically challenging due to their low prevalence in the bloodstream and their phenotypic heterogeneity. Nevertheless, several groups have recently illustrated the feasibility of single-cell profiling in CTCs, providing a spectrum of genomic alterations that may potentially represent tumor heterogeneity and unravel aggressive subclones. CTCs acquiring genomic alterations can initiate and drive selection of resistant clones responsible for tumor evolution and metastatic progression [31].

3.1. CIN Analysis in CTCs by FISH

FISH technique has been adopted as one of the main methods for the assessment of CIN status in tumors (reviewed by McGranahan et al. [32]). Variations in chromosome copy number across the cell population can be quantified using fluorescently labeled DNA probes that bind to the centromeres of specific chromosomes. In CTCs, FISH has been developed and optimized to detect biomarkers of sensitivity to selected treatments and better stratify the patients. However, research revealed an unforeseen aspect of chromosomal heterogeneity across CTCs. Indeed, one of the first successful applications of the FISH assay showed important CIN in prostate cancer (PCa) CTCs through the detection of heterogeneous chromosomal abnormalities among patients [33]. A study in castration-resistance prostate cancer (CRPC) showed that *ERG* oncogene status was maintained in CTCs, while significant genetic heterogeneity was observed in *AR* copy number gain and *PTEN* loss. This suggested that *ERG* rearrangements might constitute an early event in prostate tumorigenesis [34]. In the multicentric PETRUS study of biomarker assessment, we reported phenotypic and FISH genetic heterogeneity of metastatic tumor tissue and CTCs in patients with CRPC [35]. High concordance between metastatic biopsies and CTCs for *ERG*-rearrangement was observed in spite of higher heterogeneity in CTCs. Other groups have also performed FISH analysis in metastatic

CRPC CTCs revealing amplification of the *AR* locus and *MYC* [36] as well as the presence of PCa-specific TMPRSS2-ERG fusion [37]. The comparative detection of *ALK*-rearranged CTCs in NSCLC patients and corresponding tumor tissue biopsies was also performed. In a cohort of 87 patients with lung adenocarcinoma, positive ALK immunostaining was reported in CTCs isolated from five patients, corresponding to the same patients presenting *ALK*-rearranged tumors [38]. Our group reported the detection of unique *ALK* rearrangement patterns in CTCs in patients with metastatic NSCLC. Notably, we noted a high concordance in *ALK* rearrangement patterns between CTCs and tumor biopsies in 18 *ALK*-positive and 14 *ALK*-negative patients. Additionally, the presence of a unique *ALK* rearrangement pattern and EMT features was observed in CTCs [39]. Utility of *ALK* FISH testing in CTCs in the longitudinal follow-up of crizotinib resistance profiling was also demonstrated [40]. We showed that patients monitored at the early stage of crizotinib treatment presented significant correlation between dynamic evolution of the amount of *ALK* copy number gained in CTCs and PFS, suggesting that increased CIN in CTCs may be associated with a worse outcome in *ALK*-rearranged NSCLC [41]. These reports consistently demonstrate that monitoring tumor genomic characteristics via CTCs FISH analysis may serve as a predictive biomarker of treatment efficacy in NSCLC patients.

In 2015, we reported the detection of rearrangement in the ROS1-tyrosine kinase gene (present in 1% of NSCLC) in CTCs from *ROS1*-rearranged NSCLC patients. High levels of aneuploidy and numerical CIN have been proposed as a mechanism of genetic diversity in CTCs of *ROS1*-rearranged patients. DNA content quantifications and chromosome enumeration underscored increased CIN in CTCs [42]. Further studies based on FISH analysis emphasized CTC genomic heterogeneity through assessment of their numerical CIN. Another report demonstrated the assessment of *MET* amplification by FISH in CTCs from *EGFR*-mutated NSCLC patients at progression on erlotinib. *MET* amplification was detected in 3 of 39 samples but interestingly all *MET*-amplified CTCs were identified at disease progression [43]. Similarly, *MET* amplification was detected using FISH technique in CTCs of patients with gastric, colorectal and renal cancers following a capture of c-MET-expressing cells [44]. This particular aberration may have prognostic importance if confirmed, as c-MET protein overexpression increases distinctly in metastasis [45].

In breast cancer, assessment of *HER2* status is considered as standard practice for therapy selection [46]. Interestingly, assessment of *HER2* amplification using FISH in CTCs has been reported by several groups and may be used to stratify patients eligible to HER2-targeted therapy [47–49]. *PTEN* gene loss may drive tumor progression through activation of PI3K/AKT pathway and occurs frequently in CRPC. *PTEN* gene status was assessed in CTCs using the Epic Sciences platform, which identifies CTCs through an algorithm-based image analysis followed by FISH [50,51]. *PTEN* losses determined by FISH in CTCs correlated with PTEN expression loss measured by IHC in corresponding tumors biopsies. They were also associated with worse prognosis in CRPC patients [50]. These FISH studies highlight the importance of serial CTC genomic analysis for the identification of biomarkers predictive of therapeutic efficacy in different cancer types. The data also emphasize heterogeneous CIN as a characteristic feature of CTCs from different tumor types and show the importance of single-cell analysis to evaluate CNA changes as possible mechanisms of resistance and/or tumor evolution. FISH analysis of tumor samples is in most cases still manually performed and is particularly laborious given the important number of hematopoietic cells still retained in enriched CTC fractions. Nevertheless, technological advancements in the field led to the development of semi-automated microscopy method that allows the identification of filtration-enriched CTCs from NSCLC and PCa patients and the detection of *ALK*, *ROS1* and *ERG* gains and rearrangements in these cells, as we reported (Figure 2) [52]. Moreover, integrated subtraction enrichment and immunostaining FISH (SE-iFISH) was used to characterize CTCs of patients with malignancies such as nasopharyngeal carcinoma or esophageal cancer. Notably, CTC karyotyping allowed the assessment of chromosome 8 aneuploidy, which strongly associated with chemotherapy efficacy and prognosis [53,54]. Aforementioned studies show that although FISH has been

developed to detect biomarkers of sensitivity to different selected treatments, it constitutes a valuable tool for the assessment of CIN across CTCs.

3.2. Copy Number Alterations (CNA) Landscape to Describe CIN in CTCs

The rarity and biological heterogeneity of CTCs have imposed technical challenges for their isolation and analyses at the single-cell level and impacted the success of robust processing of complex and costly downstream methodologies. The single-nucleus next-generation sequencing relies on successful whole genome amplification (WGA) of an individual cell to generate good-quality DNA for subsequent sequencing. All WGA systems generate nonlinear amplification bias, which may decrease genome coverage and thus needs to be taken into consideration during sequence analysis [55]. Reproducible CNA patterns among single CTCs and corresponding metastatic biopsy were obtained after multiple annealing and looping-based amplification cycles of WGA of single CTCs from lung cancer patients [56]. Indeed, each CTC from an individual patient exhibited reproducible CNA patterns similar to the metastatic tumor but not the primary tumor. This report also showed that different patients with adenocarcinoma shared similar CNA patterns, whereas patients with small-cell lung cancer (SCLC) had distinctly different CNA patterns. CNA profiling studies in the context of GI suggested that certain genomic loci may confer a selective advantage for metastasis through their action on different signaling pathways. To tackle the issue of protocol speed for clinical applications, Ferrarini et al. developed a single-tube method consisting of a single step, with ligation-mediated PCR (LM-PCR) WGA for low-pass whole genome sequencing and CNA calling from single cells [57]. This was adapted to analyze CTCs from patients with lung adenocarcinoma and PCa. The *Ampli*1™ WGA-based low-pass workflow (Menarini Silicon Biosystems) successfully captured substantial heterogeneity across CTCs, highlighting the utility of single-cell profiling application for genome-informed therapeutic strategies [57]. Another group assessed GI through genome-wide copy number profiling of CTCs from seven metastatic CRPC patients [58]. CTCs were identified and characterized using the Epic Sciences CTC platform and subclonal tumor suppressor loss, oncogene amplification and GI were measured by the distribution of large-scale state transitions (LST) genome-wide (frequency of CNV breakpoints > 10 Mb). A broad range of copy number changes in *AR* and *PTEN* were detected in most CRPC patients accompanied by high heterogeneity in LST distribution, highlighting important GI in CTCs at the single-cell resolution [58]. Additional CNA profiling studies in CRPC highlight high levels of genomic heterogeneity among CTCs [59,60]. The compound losses of three tumor suppressors (*PTEN*, *RB1* and *TP53*) in PCa CTCs and the corresponding circulating tumor DNA analysis were recently reported and linked to the aggressive trait of the tumor [61]. Moreover, gains in *PTK2* and *MYC* together with *TP53* loss were also detected in CTCs and were strongly associated with poor prognosis in PCa patients. Despite frequent copy number traces that highly resembled corresponding biopsies, unique gains in *MYC* were revealed in CNA profiles of CTCs captured from apheresis of PCa patients [62]. Previously, *MYCN* gain and simultaneous *AR* loss was proposed as a possible mechanism of neuroendocrine differentiation in PCa tumor samples [63] and was later confirmed in CTCs as part of highly complex profile containing additional aberrations in *ERG*, *c-MET* and *PI3K* genes during CRPC progression [59]. Evaluation of CNA profiles in CTCs from metastatic breast cancer patients suggested potentially targetable alterations in *PTCH1* and *NOTCH1* that were absent in baseline biopsies, indicating subclonal tumor evolution [64]. The predictive value of CNA profiles of CTCs has also been recently evidenced in SCLC patients. Characteristic CNA signature of subsequent chemosensitivity was reported with an 83.3% accuracy to classify SCLC CTCs as chemosensitive or chemorefractory [65]. Similarly, predictive single CTC-based CNA score in the response to first-line chemotherapy was demonstrated in SCLC patients by Su et al. CNA profiles across CTCs of individual SCLC patients were highly concordant with copy number losses in two frequently inactivated genes, *TP53* and *RB1*, found in 64.6% and 81.3% of patients respectively [66].

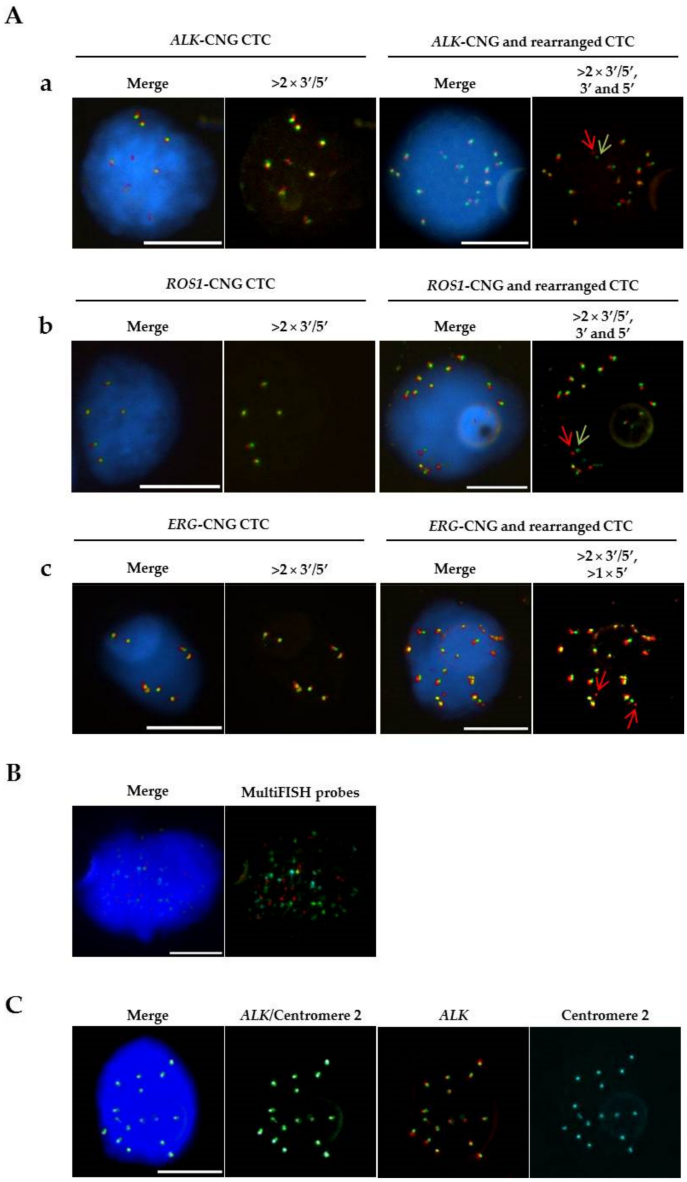


Figure 2. Detection of CTCs harboring *ALK* and *ROS-1* gene aberrations in NSCLC patients and *ERG* gene alterations in metastatic CRPC patients by combined immunofluorescent staining and filter-adapted FISH (FA-FISH). (**A**). (**a**) Example of FISH patterns in NSCLC CTCs with *ALK*-copy number gain (*ALK*-CNG) and *ALK*-rearrangement. Red and green arrows correspond to *ALK* 3′ and *ALK* 5′ probes (Vysis *ALK* Break Apart rearrangement Probe Kit from Abbott Molecular Inc., Chicago, IL, USA) respectively. (**b**) Example of FISH patterns in NSCLC CTCs bearing *ROS1*-CNG and *ROS1*-rearrangement. Green and red arrows correspond to 3′ and 5′ *ROS1*-rearrangement extremities (Vysis 6q22 *ROS1* Break Apart FISH probe RUO Kit from Abbott Molecular Inc.) respectively. (**c**) Example of FISH patterns in CRPC CTCs with *ERG*-CNG and *ERG*-rearrangement. Green and red arrows correspond to 3′ and 5′ *ERG* gene ends (Kreatech *ERG* Break Apart Rearrangement Probes kit) respectively. (**B**). Example of hybridized CTC using the AneuVysion Multicolor DNA Probe Kit (Abbott Molecular Inc.). Green spots indicate hybridization of locus-specific identification (LSI) 13 probe and centromere-specific enumeration probe (CEP) X. Red spots indicate hybridization of LSI 21 probe and CEP Y. Blue spots indicate hybridization of CEP 18. (**C**). Example of FISH patterns in CTCs with *ALK*-CNG detected by combined immunofluorescent staining and three-color FA-FISH for *ALK* gene and chromosome 2 centromere detection (XCyting Centromere Enumeration Probe XCE2 from MetaSystems GmbH), showing the existence of true gains of *ALK* gene in CTCs. Scale: white bars = 10μm.

Overall, single-cell heterogeneity revealed by CNA analysis clearly represents a challenge for CTC molecular biomarker studies. Nevertheless, in-depth analysis of a sufficient number of CTCs may allow the profiling of characteristic CNA burden, which may be informative for future treatment strategies.

3.3. Using CTC-Derived Models to Investigate GI Mechanisms

Over the past decade, CTC-derived models have emerged as tractable tools to explore metastatic disease by studying the tumorigenic capacity of CTCs in several malignancies [67]. Despite technical challenges due to CTC rarity in the bloodstream, significant efforts were provided in the establishment of CTC-derived xenografts (CDX). The first one was generated in 2013 from breast cancer patient CTCs [68], while other groups reported successful models in lung, melanoma and prostate cancers [69–72]. We recently reported sequential acquisition of key genetic events promoting an aggressive neuroendocrine transformation in CRPC CDX. *PTEN* and *RB1* losses were acquired in CTCs, while *TP53* loss harbored in a subclone of the primary tumor was suggested as the driver of the metastatic event leading to CDX development. Interestingly, co-occurring losses of tumor suppressor genes *PTEN*, *RB1* and *TP53* were found in single CTCs characterized by extremely high CIN. Neuroendocrine transformation was promoted by the high number of CNAs and WGD, highlighting GI acquired during metastatic development [72]. In SCLC, single-cell analysis of CDX revealed the existence of co-existing heterogeneous cell subpopulations that are contributing to multiple concurrent resistance mechanism to chemotherapy [73]. Ex vivo expansion of viable CTCs has also been described [74–78]. Transcriptomic analysis of a CTC cell line derived from a metastatic colon cancer patient indicated altered expression of DNA-repair-related genes compared to a primary colon cancer cell line [77,79]. Another CTC-derived breast cancer cell line was recently established from a patient with metastatic estrogen receptor-positive breast cancer. Its CNA profile was highly concordant with that of patient CTCs and WES analysis deciphered alterations in common DNA damage-related genes (e.g., *ATM, CDKN1A*) [78].

The current time frame required for developing CTC-derived models does not allow for real-time monitoring of cancer patients and thus may not inform clinical decisions. However, their genomic analysis may help decipher molecular events involved in CTC-mediated tumor progression and reveal potential CTC biomarkers relevant for clinical management.

3.4. DNA Repair-Related Protein Biomarkers in CTCs

Functional analysis of DNA-repair-related protein expression in CTCs has been used as a pharmacodynamic biomarker for monitoring response to chemotherapy or targeted therapy (Table 1). Expression of DSB marker γH2AX has been evaluated as a dynamic indicator of DNA damage in CTCs from patients with advanced cancers after topotecan treatment using immunofluorescent staining followed by FACS analysis [80]. Data showed feasibility of monitoring dynamic changes in CTC nuclear biomarkers at response to treatment. γH2AX foci were also evaluated in CTCs after CellSearch analysis performed during radiation therapy as well as during combination treatment of low-dose of radiotherapy combined with PARPi [81,82]. Another DSB protein, RAD50, has been sequentially monitored in CTCs and its expression was estimated after radiotherapy of single side lesions in advanced lung cancer patients. CTCs were additionally screened for the immunotherapeutic target PD-L1 after enrichment with CellSieve Microfiltration Assay [83]. Results showed that RAD50 nuclear foci formation in CTCs may serve as a noninvasive tracer in cancer patients receiving side-directed radiotherapy independently of PD-L1 screening. ERCC excision repair 1 (*ERCC1*) is required for the repair of cisplatin-induced DNA lesions and may play the role of a biomarker for predicting response to platinum therapy. Indeed, it has been suggested that tumor cells overexpressing ERCC1 may be characterized with an enhanced capacity to resolve DNA platinum-adducts and consequently bypassing platinum cytotoxicity [84]. ERCC1 expression in CTCs was found to negatively correlate with PFS in metastatic NSCLC patients under platinum-based chemotherapy [85] and presence of CTCs

expressing ERCC1 after therapy indicated a worse outcome for breast cancer patients [86]. Another group showed that ERCC1 transcript expression in CTCs was more predictive of response to platinum-based chemotherapy than standard ERCC1 protein expression detected on primary tumor biopsy samples [87]. Additionally, ERCC1 transcript-positive CTCs were used for monitoring platinum-based chemotherapy and to assess the post-therapeutic outcome of ovarian cancer [88]. These studies suggested that CTCs may represent dynamic intra-cellular changes in response to DNA-repair-related treatments more accurately than tumor biopsy. Furthermore, overexpression of the DNA/RNA helicase Schlafen family member 11 (SLFN11) has been described as an emerging biomarker of tumor cell sensitivity to DNA-damaging agents, including platinum chemotherapy [89] and to PARPi in several cancers [90,91]. SLFN11 protein expression was evaluated by immunofluorescent staining in CTCs from CRPC patients treated with platinum chemotherapy. SLFN11 overexpression in CTCs was associated with longer PFS compared to patients with *SLFN11*-negative CTCs [92]. Despite accumulating data, identification of CTC subpopulations expressing DNA-repair-related markers remains complex due to the existing variations among the technologies used to this end, as well as their low prevalence in patient blood. Therefore, further research is required to determine the clinical relevance of such biomarkers, notably in patients with advanced malignancies presenting significant levels of CTCs.

Table 1. DNA damage repair-related biomarkers in CTCs.

DNA Repair-Related Protein Markers in CTCs	Tumor Type	Treatment	Key Findings	Ref.
YH2AX (phosphorylated Ser 139 H2AX variant histone)	Various advanced cancers	Topotecan	- A dose-dependent increase of YH2AX-positive patient CTCs with topotecan - Monitoring of pharmacodynamics effects of chemotherapy via nuclear YH2AX levels	[80]
	NSCLC	Radiotherapy	Elevated YH2AX signal in CTCs post-radiotherapy	[81]
	Peritoneal cancers and advanced solid malignancies	Radiotherapy and PARPi (veliparib)	- Exploratory study showing the use of YH2AX in CTCs - Increase in $YH2AX^{+}$ CTC levels after treatment in few patients while one patient presented a decrease, suggestive of treatment failure	[82]
RAD50 (double strand break repair protein)	NSCLC	Radiotherapy	- RAD50 foci formation used to label and track CTCs subjected to radiation at primary site - Monitoring of tumor dynamics	[83]
ERCC1 (Excision repair cross-complementation group 1)	NSCLC	Platinum chemotherapy	Correlation between low ERCC1 expression in CTCs and progression-free survival after platinum-based therapies	[85]
	Breast cancer	Neoadjuvant chemotherapy	- 72% of *ERCC1*-positive CTCs after therapy - No significant correlation between CTCs and clinical parameters	[86]
	Ovarian cancer	Platinum chemotherapy	*ERCC1*-positive CTC at diagnosis predictive of resistance to platinum-based therapy	[87]
SLFN11 (DNA/RNA helicase Schlafen family member 11)	CRPC	Platinum chemotherapy	Potential use of SLFN11 expression in CTCs for selection of patients with better response to platinum therapy	[92]
RAD23B (RAD23 homolog B)	Rectal cancer	Radiation and 5-FU Or radiation and capecitabine	Expression of thymidylate synthase (TYMS) and RAD23B has predictive value of nonresponse to neoadjuvant chemoradiation	[93]

4. Conclusions

The study of GI-related biomarkers in CTCs is an emerging field, and their real-time monitoring may be useful in clinical decision making. The technical advances and robust CTC isolation methods may now allow us to capture phenotypic and genetic heterogeneity and, subsequently, to reconstitute tumor characteristics. The relationship between GI, prognosis and acquired resistance to treatment is very complex, and deciphering the molecular mechanisms contributing to GI in CTCs remains crucial. The advancements in FISH analysis have strongly contributed to the unveiling of increased CIN in CTCs and its potential role in resistance mechanisms. CNAs successfully assessed via single-cell sequencing of CTCs indicated various sources of GI, such as oncogene-induced replicative stress, cell-cycle-related genes alterations or WGD, suggesting a rationale for therapeutic options. Moreover, CNA events reveal common DNA-repair-related gene alterations detected across tumor types. Those DDR alterations increase GI and thus may constitute novel therapeutic targets. Single CTC sequencing may therefore provide insight into the mechanistic origins and consequences of DDR deficiency in cancer (Figure 3). Finally, CTC-based monitoring of DDR-related biomarkers was proven to inform about therapeutic progress, but it also indicates first signals of acquiring resistance. Therefore, though investigating GI mechanisms through CTC monitoring is challenging, it is becoming particularly useful for tracking tumor heterogeneity and may present a critical element for precision medicine.

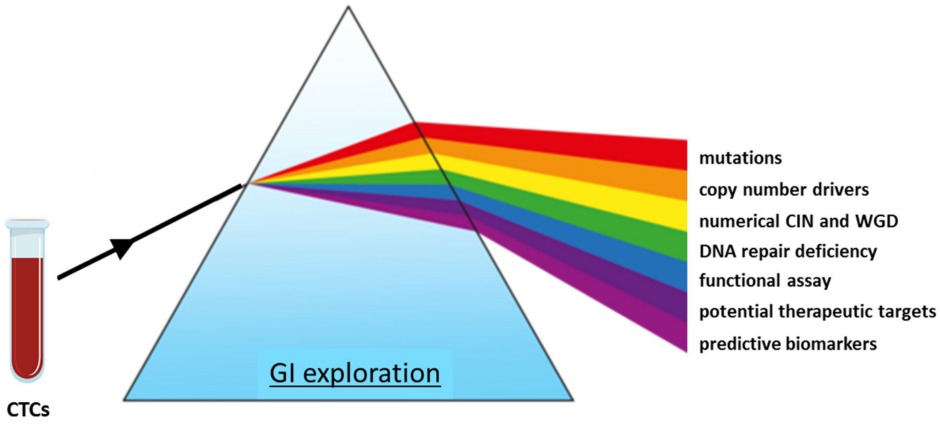


Figure 3. Schematic model of state-of-the-art strategies for the investigation of genome instability in CTCs.

Funding: T.T. is supported by La Ligue Nationale Contre le Cancer.

Institutional Review Board Statement: Not applicable.

Informed Consent Statement: Not applicable.

Data Availability Statement: Not applicable.

Acknowledgments: We are grateful to the patients and their families.

Conflicts of Interest: The authors declare no conflict of interest.

References

1. Bidard, F.-C.; Peeters, D.J.; Fehm, T.; Nolé, F.; Gisbert-Criado, R.; Mavroudis, D.; Grisanti, S.; Generali, D.; Garcia-Saenz, J.A.; Stebbing, J.; et al. Clinical Validity of Circulating Tumour Cells in Patients with Metastatic Breast Cancer: A Pooled Analysis of Individual Patient Data. *Lancet Oncol.* **2014**, *15*, 406–414. [CrossRef]
2. Lindsay, C.R.; Blackhall, F.H.; Carmel, A.; Fernandez-Gutierrez, F.; Gazzaniga, P.; Groen, H.J.M.; Hiltermann, T.J.N.; Krebs, M.G.; Loges, S.; López-López, R.; et al. EPAC-Lung: Pooled Analysis of Circulating Tumour Cells in Advanced Non-Small Cell Lung Cancer. *Eur. J. Cancer* **2019**, *117*, 60–68. [CrossRef] [PubMed]

3. Kobayashi, J.; Antoccia, A.; Tauchi, H.; Matsuura, S.; Komatsu, K. NBS1 and Its Functional Role in the DNA Damage Response. *DNA Repair* **2004**, *3*, 855–861. [CrossRef]
4. Hari, F.J.; Spycher, C.; Jungmichel, S.; Pavic, L.; Stucki, M. A Divalent FHA/BRCT-Binding Mechanism Couples the MRE11-RAD50-NBS1 Complex to Damaged Chromatin. *EMBO Rep.* **2010**, *11*, 387–392. [CrossRef] [PubMed]
5. Sharma, A.; Singh, K.; Almasan, A. Histone H2AX Phosphorylation: A Marker for DNA Damage. *Methods Mol. Biol.* **2012**, *920*, 613–626. [CrossRef] [PubMed]
6. Matthaios, D.; Hountis, P.; Karakitsos, P.; Bouros, D.; Kakolyris, S. H2AX a Promising Biomarker for Lung Cancer: A Review. *Cancer Investig.* **2013**, *31*, 582–599. [CrossRef]
7. Nagelkerke, A.; Span, P.N. Staining Against Phospho-H2AX (γ-H2AX) as a Marker for DNA Damage and Genomic Instability in Cancer Tissues and Cells. *Adv. Exp. Med. Biol.* **2016**, *899*, 1–10. [CrossRef] [PubMed]
8. Kaufman, B.; Shapira-Frommer, R.; Schmutzler, R.K.; Audeh, M.W.; Friedlander, M.; Balmaña, J.; Mitchell, G.; Fried, G.; Stemmer, S.M.; Hubert, A.; et al. Olaparib Monotherapy in Patients with Advanced Cancer and a Germline BRCA1/2 Mutation. *J. Clin. Oncol.* **2015**, *33*, 244–250. [CrossRef] [PubMed]
9. Pujade-Lauraine, E.; Ledermann, J.A.; Selle, F.; Gebski, V.; Penson, R.T.; Oza, A.M.; Korach, J.; Huzarski, T.; Poveda, A.; Pignata, S.; et al. Olaparib Tablets as Maintenance Therapy in Patients with Platinum-Sensitive, Relapsed Ovarian Cancer and a BRCA1/2 Mutation (SOLO2/ENGOT-Ov21): A Double-Blind, Randomised, Placebo-Controlled, Phase 3 Trial. *Lancet Oncol.* **2017**, *18*, 1274–1284. [CrossRef]
10. Robson, M.; Im, S.-A.; Senkus, E.; Xu, B.; Domchek, S.M.; Masuda, N.; Delaloge, S.; Li, W.; Tung, N.; Armstrong, A.; et al. Olaparib for Metastatic Breast Cancer in Patients with a Germline BRCA Mutation. *N. Engl. J. Med.* **2017**, *377*, 523–533. [CrossRef]
11. Lord, C.J.; Ashworth, A. BRCAness Revisited. *Nat. Rev. Cancer* **2016**, *16*, 110–120. [CrossRef]
12. Knijnenburg, T.A.; Wang, L.; Zimmermann, M.T.; Chambwe, N.; Gao, G.F.; Cherniack, A.D.; Fan, H.; Shen, H.; Way, G.P.; Greene, C.S.; et al. Genomic and Molecular Landscape of DNA Damage Repair Deficiency across The Cancer Genome Atlas. *Cell Rep.* **2018**, *23*, 239–254.e6. [CrossRef] [PubMed]
13. Cruz, C.; Castroviejo-Bermejo, M.; Gutiérrez-Enríquez, S.; Llop-Guevara, A.; Ibrahim, Y.H.; Gris-Oliver, A.; Bonache, S.; Morancho, B.; Bruna, A.; Rueda, O.M.; et al. RAD51 Foci as a Functional Biomarker of Homologous Recombination Repair and PARP Inhibitor Resistance in Germline BRCA-Mutated Breast Cancer. *Ann. Oncol.* **2018**, *29*, 1203–1210. [CrossRef] [PubMed]
14. Castroviejo-Bermejo, M.; Cruz, C.; Llop-Guevara, A.; Gutiérrez-Enríquez, S.; Ducy, M.; Ibrahim, Y.H.; Gris-Oliver, A.; Pellegrino, B.; Bruna, A.; Guzmán, M.; et al. A RAD51 Assay Feasible in Routine Tumor Samples Calls PARP Inhibitor Response beyond BRCA Mutation. *EMBO Mol. Med.* **2018**, *10*. [CrossRef]
15. Gilad, O.; Nabet, B.Y.; Ragland, R.L.; Schoppy, D.W.; Smith, K.D.; Durham, A.C.; Brown, E.J. Combining ATR Suppression with Oncogenic Ras Synergistically Increases Genomic Instability, Causing Synthetic Lethality or Tumorigenesis in a Dosage-Dependent Manner. *Cancer Res.* **2010**, *70*, 9693–9702. [CrossRef] [PubMed]
16. Primo, L.M.F.; Teixeira, L.K. DNA Replication Stress: Oncogenes in the Spotlight. *Genet Mol. Biol.* **2019**, *43*, e20190138. [CrossRef]
17. Helbling-Leclerc, A.; Dessarps-Freichey, F.; Evrard, C.; Rosselli, F. Fanconi Anemia Proteins Counteract the Implementation of the Oncogene-Induced Senescence Program. *Sci. Rep.* **2019**, *9*, 17024. [CrossRef]
18. Wilhelm, T.; Olziersky, A.-M.; Harry, D.; De Sousa, F.; Vassal, H.; Eskat, A.; Meraldi, P. Mild Replication Stress Causes Chromosome Mis-Segregation via Premature Centriole Disengagement. *Nat. Commun.* **2019**, *10*. [CrossRef]
19. Wangsa, D.; Quintanilla, I.; Torabi, K.; Vila-Casadesús, M.; Ercilla, A.; Klus, G.; Yuce, Z.; Galofré, C.; Cuatrecasas, M.; Lozano, J.J.; et al. Near-Tetraploid Cancer Cells Show Chromosome Instability Triggered by Replication Stress and Exhibit Enhanced Invasiveness. *FASEB J.* **2018**, *32*, 3502–3517. [CrossRef]
20. Greil, C.; Krohs, J.; Schnerch, D.; Follo, M.; Felthaus, J.; Engelhardt, M.; Wäsch, R. The Role of APC/C(Cdh1) in Replication Stress and Origin of Genomic Instability. *Oncogene* **2016**, *35*, 3062–3070. [CrossRef]
21. Bianco, J.N.; Bergoglio, V.; Lin, Y.-L.; Pillaire, M.-J.; Schmitz, A.-L.; Gilhodes, J.; Lusque, A.; Mazières, J.; Lacroix-Triki, M.; Roumeliotis, T.I.; et al. Overexpression of Claspin and Timeless Protects Cancer Cells from Replication Stress in a Checkpoint-Independent Manner. *Nat. Commun.* **2019**, *10*, 910. [CrossRef] [PubMed]
22. Dewhurst, S.M.; McGranahan, N.; Burrell, R.A.; Rowan, A.J.; Grönroos, E.; Endesfelder, D.; Joshi, T.; Mouradov, D.; Gibbs, P.; Ward, R.L.; et al. Tolerance of Whole-Genome Doubling Propagates Chromosomal Instability and Accelerates Cancer Genome Evolution. *Cancer Discov.* **2014**, *4*, 175–185. [CrossRef] [PubMed]
23. Jamal-Hanjani, M.; Wilson, G.A.; McGranahan, N.; Birkbak, N.J.; Watkins, T.B.K.; Veeriah, S.; Shafi, S.; Johnson, D.H.; Mitter, R.; Rosenthal, R.; et al. Tracking the Evolution of Non–Small-Cell Lung Cancer. *N. Engl. J. Med.* **2017**, *376*, 2109–2121. [CrossRef] [PubMed]
24. Godinho, S.A.; Picone, R.; Burute, M.; Dagher, R.; Su, Y.; Leung, C.T.; Polyak, K.; Brugge, J.S.; Thery, M.; Pellman, D. Oncogene-like Induction of Cellular Invasion from Centrosome Amplification. *Nature* **2014**, *510*, 167–171. [CrossRef] [PubMed]
25. Rhys, A.D.; Monteiro, P.; Smith, C.; Vaghela, M.; Arnandis, T.; Kato, T.; Leitinger, B.; Sahai, E.; McAinsh, A.; Charras, G.; et al. Loss of E-Cadherin Provides Tolerance to Centrosome Amplification in Epithelial Cancer Cells. *J. Cell Biol.* **2018**, *217*, 195–209. [CrossRef]
26. Bakhoum, S.F.; Ngo, B.; Laughney, A.M.; Cavallo, J.-A.; Murphy, C.J.; Ly, P.; Shah, P.; Sriram, R.K.; Watkins, T.B.K.; Taunk, N.K.; et al. Chromosomal Instability Drives Metastasis through a Cytosolic DNA Response. *Nature* **2018**, *553*, 467–472. [CrossRef]
27. Kwon, J.; Bakhoum, S.F. The Cytosolic DNA-Sensing CGAS-STING Pathway in Cancer. *Cancer Discov.* **2020**, *10*, 26–39. [CrossRef]

28. Mullard, A. Can Innate Immune System Targets Turn up the Heat on "cold" Tumours? *Nat. Rev. Drug Discov.* **2018**, *17*, 3–5. [CrossRef]
29. Chabanon, R.M.; Muirhead, G.; Krastev, D.B.; Adam, J.; Morel, D.; Garrido, M.; Lamb, A.; Hénon, C.; Dorvault, N.; Rouanne, M.; et al. PARP Inhibition Enhances Tumor Cell–Intrinsic Immunity in ERCC1-Deficient Non–Small Cell Lung Cancer. *J. Clin. Investig.* **2019**, *129*, 1211–1228. [CrossRef]
30. Sanchez-Vega, F.; Mina, M.; Armenia, J.; Chatila, W.K.; Luna, A.; La, K.C.; Dimitriadoy, S.; Liu, D.L.; Kantheti, H.S.; Saghafinia, S.; et al. Oncogenic Signaling Pathways in The Cancer Genome Atlas. *Cell* **2018**, *173*, 321–337.e10. [CrossRef]
31. Gao, Y.; Ni, X.; Guo, H.; Su, Z.; Ba, Y.; Tong, Z.; Guo, Z.; Yao, X.; Chen, X.; Yin, J.; et al. Single-Cell Sequencing Deciphers a Convergent Evolution of Copy Number Alterations from Primary to Circulating Tumor Cells. *Genome Res.* **2017**, *27*, 1312–1322. [CrossRef]
32. McGranahan, N.; Burrell, R.A.; Endesfelder, D.; Novelli, M.R.; Swanton, C. Cancer Chromosomal Instability: Therapeutic and Diagnostic Challenges. *EMBO Rep.* **2012**, *13*, 528–538. [CrossRef] [PubMed]
33. Swennenhuis, J.F.; Tibbe, A.G.J.; Levink, R.; Sipkema, R.C.J.; Terstappen, L.W.M.M. Characterization of Circulating Tumor Cells by Fluorescence in Situ Hybridization. *Cytom. A* **2009**, *75*, 520–527. [CrossRef] [PubMed]
34. Attard, G.; Swennenhuis, J.F.; Olmos, D.; Reid, A.H.M.; Vickers, E.; A'Hern, R.; Levink, R.; Coumans, F.; Moreira, J.; Riisnaes, R.; et al. Characterization of ERG, AR and PTEN Gene Status in Circulating Tumor Cells from Patients with Castration-Resistant Prostate Cancer. *Cancer Res.* **2009**, *69*, 2912–2918. [CrossRef]
35. Massard, C.; Oulhen, M.; Le Moulec, S.; Auger, N.; Foulon, S.; Abou-Lovergne, A.; Billiot, F.; Valent, A.; Marty, V.; Loriot, Y.; et al. Phenotypic and Genetic Heterogeneity of Tumor Tissue and Circulating Tumor Cells in Patients with Metastatic Castrationresistant Prostate Cancer: A Report from the PETRUS Prospective Study. *Oncotarget* **2016**, *7*, 55069–55082. [CrossRef] [PubMed]
36. Leversha, M.A.; Han, J.; Asgari, Z.; Danila, D.C.; Lin, O.; Gonzalez-Espinoza, R.; Anand, A.; Lilja, H.; Heller, G.; Fleisher, M.; et al. Fluorescence in Situ Hybridization Analysis of Circulating Tumor Cells in Metastatic Prostate Cancer. *Clin. Cancer Res.* **2009**, *15*, 2091–2097. [CrossRef] [PubMed]
37. Danila, D.C.; Anand, A.; Sung, C.C.; Heller, G.; Leversha, M.A.; Cao, L.; Lilja, H.; Molina, A.; Sawyers, C.L.; Fleisher, M.; et al. TMPRSS2-ERG Status in Circulating Tumor Cells as a Predictive Biomarker of Sensitivity in Castration-Resistant Prostate Cancer Patients Treated With Abiraterone Acetate. *Eur. Urol.* **2011**, *60*, 897–904. [CrossRef] [PubMed]
38. Ilie, M.; Long, E.; Butori, C.; Hofman, V.; Coelle, C.; Mauro, V.; Zahaf, K.; Marquette, C.H.; Mouroux, J.; Paterlini-Bréchot, P.; et al. ALK-Gene Rearrangement: A Comparative Analysis on Circulating Tumour Cells and Tumour Tissue from Patients with Lung Adenocarcinoma. *Ann. Oncol.* **2012**, *23*, 2907–2913. [CrossRef] [PubMed]
39. Pailler, E.; Adam, J.; Barthélémy, A.; Oulhen, M.; Auger, N.; Valent, A.; Borget, I.; Planchard, D.; Taylor, M.; André, F.; et al. Detection of Circulating Tumor Cells Harboring a Unique ALK Rearrangement in ALK-Positive Non-Small-Cell Lung Cancer. *J. Clin. Oncol.* **2013**, *31*, 2273–2281. [CrossRef] [PubMed]
40. Tan, C.L.; Lim, T.H.; Lim, T.K.; Tan, D.S.-W.; Chua, Y.W.; Ang, M.K.; Pang, B.; Lim, C.T.; Takano, A.; Lim, A.S.-T.; et al. Concordance of Anaplastic Lymphoma Kinase (ALK) Gene Rearrangements between Circulating Tumor Cells and Tumor in Non-Small Cell Lung Cancer. *Oncotarget* **2016**, *7*, 23251–23262. [CrossRef] [PubMed]
41. Pailler, E.; Oulhen, M.; Borget, I.; Remon, J.; Ross, K.; Auger, N.; Billiot, F.; Ngo Camus, M.; Commo, F.; Lindsay, C.R.; et al. Circulating Tumor Cells with Aberrant ALK Copy Number Predict Progression-Free Survival during Crizotinib Treatment in ALK-Rearranged Non-Small Cell Lung Cancer Patients. *Cancer Res.* **2017**, *77*, 2222–2230. [CrossRef]
42. Pailler, E.; Auger, N.; Lindsay, C.R.; Vielh, P.; Islas-Morris-Hernandez, A.; Borget, I.; Ngo-Camus, M.; Planchard, D.; Soria, J.-C.; Besse, B.; et al. High Level of Chromosomal Instability in Circulating Tumor Cells of ROS1-Rearranged Non-Small-Cell Lung Cancer. *Ann. Oncol.* **2015**, *26*, 1408–1415. [CrossRef]
43. Yanagita, M.; Redig, A.J.; Paweletz, C.P.; Dahlberg, S.E.; O'Connell, A.; Feeney, N.; Taibi, M.; Boucher, D.; Oxnard, G.R.; Johnson, B.E.; et al. A Prospective Evaluation of Circulating Tumor Cells and Cell-Free DNA in EGFR-Mutant Non-Small Cell Lung Cancer Patients Treated with Erlotinib on a Phase II Trial. *Clin. Cancer Res.* **2016**, *22*, 6010–6020. [CrossRef]
44. Zhang, T.; Boominathan, R.; Foulk, B.; Rao, C.; Kemeny, G.; Strickler, J.H.; Abbruzzese, J.L.; Harrison, M.R.; Hsu, D.S.; Healy, P.; et al. Development of a Novel C-MET-Based CTC Detection Platform. *Mol. Cancer Res.* **2016**, *14*, 539–547. [CrossRef]
45. Shoji, H.; Yamada, Y.; Taniguchi, H.; Nagashima, K.; Okita, N.; Takashima, A.; Honma, Y.; Iwasa, S.; Kato, K.; Hamaguchi, T.; et al. Clinical Impact of C-MET Expression and Genetic Mutational Status in Colorectal Cancer Patients after Liver Resection. *Cancer Sci.* **2014**, *105*, 1002–1007. [CrossRef]
46. Mayer, J.A.; Pham, T.; Wong, K.L.; Scoggin, J.; Sales, E.V.; Clarin, T.; Pircher, T.J.; Mikolajczyk, S.D.; Cotter, P.D.; Bischoff, F.Z. FISH-Based Determination of HER2 Status in Circulating Tumor Cells Isolated with the Microfluidic CEE^{TM} Platform. *Cancer Genet.* **2011**, *204*, 589–595. [CrossRef] [PubMed]
47. Munzone, E.; Nolé, F.; Goldhirsch, A.; Botteri, E.; Esposito, A.; Zorzino, L.; Curigliano, G.; Minchella, I.; Adamoli, L.; Cassatella, M.C.; et al. Changes of HER2 Status in Circulating Tumor Cells Compared with the Primary Tumor during Treatment for Advanced Breast Cancer. *Clin. Breast Cancer* **2010**, *10*, 392–397. [CrossRef] [PubMed]
48. Frithiof, H.; Aaltonen, K.; Rydén, L. A FISH-Based Method for Assessment of HER-2 Amplification Status in Breast Cancer Circulating Tumor Cells Following CellSearch Isolation. *Onco Targets Ther.* **2016**, *9*, 7095–7103. [CrossRef] [PubMed]

49. Brouwer, A.; De Laere, B.; van Dam, P.-J.; Peeters, D.; Van Haver, J.; Sluydts, E.; El Moussaoui, A.; Mendelaar, P.; Kraan, J.; Peeters, M.; et al. HER-2 Status of Circulating Tumor Cells in a Metastatic Breast Cancer Cohort: A Comparative Study on Characterization Techniques. *PLoS ONE* **2019**, *14*, e0220906. [CrossRef]
50. Punnoose, E.A.; Ferraldeschi, R.; Szafer-Glusman, E.; Tucker, E.K.; Mohan, S.; Flohr, P.; Riisnaes, R.; Miranda, S.; Figueiredo, I.; Rodrigues, D.N.; et al. PTEN Loss in Circulating Tumour Cells Correlates with PTEN Loss in Fresh Tumour Tissue from Castration-Resistant Prostate Cancer Patients. *Br. J. Cancer* **2015**, *113*, 1225–1233. [CrossRef]
51. McDaniel, A.S.; Ferraldeschi, R.; Krupa, R.; Landers, M.; Graf, R.; Louw, J.; Jendrisak, A.; Bales, N.; Marrinucci, D.; Zafeiriou, Z.; et al. Phenotypic Diversity of Circulating Tumour Cells in Patients with Metastatic Castration-Resistant Prostate Cancer. *BJU Int.* **2017**, *120*, E30–E44. [CrossRef] [PubMed]
52. Pailler, E.; Oulhen, M.; Billiot, F.; Galland, A.; Auger, N.; Faugeroux, V.; Laplace-Builhé, C.; Besse, B.; Loriot, Y.; Ngo-Camus, M.; et al. Method for Semi-Automated Microscopy of Filtration-Enriched Circulating Tumor Cells. *BMC Cancer* **2016**, *16*. [CrossRef] [PubMed]
53. Zhang, J.; Shi, H.; Jiang, T.; Liu, Z.; Lin, P.P.; Chen, N. Circulating Tumor Cells with Karyotyping as a Novel Biomarker for Diagnosis and Treatment of Nasopharyngeal Carcinoma. *BMC Cancer* **2018**, *18*, 1133. [CrossRef] [PubMed]
54. Chen, Y.; Yang, Z.; Wang, Y.; Wang, J.; Wang, C. Karyotyping of Circulating Tumor Cells for Predicting Chemotherapeutic Sensitivity and Efficacy in Patients with Esophageal Cancer. *BMC Cancer* **2019**, *19*, 651. [CrossRef]
55. Zong, C.; Lu, S.; Chapman, A.R.; Xie, X.S. Genome-Wide Detection of Single-Nucleotide and Copy-Number Variations of a Single Human Cell. *Science* **2012**, *338*, 1622–1626. [CrossRef] [PubMed]
56. Ni, X.; Zhuo, M.; Su, Z.; Duan, J.; Gao, Y.; Wang, Z.; Zong, C.; Bai, H.; Chapman, A.R.; Zhao, J.; et al. Reproducible Copy Number Variation Patterns among Single Circulating Tumor Cells of Lung Cancer Patients. *Proc. Natl. Acad. Sci. USA* **2013**, *110*, 21083–21088. [CrossRef]
57. Ferrarini, A.; Forcato, C.; Buson, G.; Tononi, P.; Del Monaco, V.; Terracciano, M.; Bolognesi, C.; Fontana, F.; Medoro, G.; Neves, R.; et al. A Streamlined Workflow for Single-Cells Genome-Wide Copy-Number Profiling by Low-Pass Sequencing of LM-PCR Whole-Genome Amplification Products. *PLoS ONE* **2018**, *13*, e0193689. [CrossRef]
58. Greene, S.B.; Dago, A.E.; Leitz, L.J.; Wang, Y.; Lee, J.; Werner, S.L.; Gendreau, S.; Patel, P.; Jia, S.; Zhang, L.; et al. Chromosomal Instability Estimation Based on Next Generation Sequencing and Single Cell Genome Wide Copy Number Variation Analysis. *PLoS ONE* **2016**, *11*, e0165089. [CrossRef]
59. Gupta, S.; Li, J.; Kemeny, G.; Bitting, R.L.; Beaver, J.; Somarelli, J.A.; Ware, K.E.; Gregory, S.; Armstrong, A.J. Whole Genomic Copy Number Alterations in Circulating Tumor Cells from Men with Abiraterone or Enzalutamide-Resistant Metastatic Castration-Resistant Prostate Cancer. *Clin. Cancer Res.* **2017**, *23*, 1346–1357. [CrossRef]
60. Hodara, E.; Morrison, G.; Cunha, A.; Zainfeld, D.; Xu, T.; Xu, Y.; Dempsey, P.W.; Pagano, P.C.; Bischoff, F.; Khurana, A.; et al. Multiparametric Liquid Biopsy Analysis in Metastatic Prostate Cancer. *JCI Insight* **2019**, *4*. [CrossRef]
61. Malihi, P.D.; Graf, R.P.; Rodriguez, A.; Ramesh, N.; Lee, J.; Sutton, R.; Jiles, R.; Ruiz Velasco, C.; Sei, E.; Kolatkar, A.; et al. Single-Cell Circulating Tumor Cell Analysis Reveals Genomic Instability as a Distinctive Feature of Aggressive Prostate Cancer. *Clin. Cancer Res.* **2020**, *26*, 4143–4153. [CrossRef]
62. Lambros, M.B.; Seed, G.; Sumanasuriya, S.; Gil, V.; Crespo, M.; Fontes, M.; Chandler, R.; Mehra, N.; Fowler, G.; Ebbs, B.; et al. Single-Cell Analyses of Prostate Cancer Liquid Biopsies Acquired by Apheresis. *Clin. Cancer Res.* **2018**, *24*, 5635–5644. [CrossRef]
63. Beltran, H.; Rickman, D.S.; Park, K.; Chae, S.S.; Sboner, A.; MacDonald, T.Y.; Wang, Y.; Sheikh, K.L.; Terry, S.; Tagawa, S.T.; et al. Molecular Characterization of Neuroendocrine Prostate Cancer and Identification of New Drug Targets. *Cancer Discov.* **2011**, *1*, 487–495. [CrossRef]
64. Paoletti, C.; Cani, A.K.; Larios, J.M.; Hovelson, D.H.; Aung, K.; Darga, E.P.; Cannell, E.M.; Baratta, P.J.; Liu, C.-J.; Chu, D.; et al. Comprehensive Mutation and Copy Number Profiling in Archived Circulating Breast Cancer Tumor Cells Documents Heterogeneous Resistance Mechanisms. *Cancer Res.* **2018**, *78*, 1110–1122. [CrossRef]
65. Carter, L.; Rothwell, D.G.; Mesquita, B.; Smowton, C.; Leong, H.S.; Fernandez-Gutierrez, F.; Li, Y.; Burt, D.J.; Antonello, J.; Morrow, C.J.; et al. Molecular Analysis of Circulating Tumor Cells Identifies Distinct Copy-Number Profiles in Patients with Chemosensitive and Chemorefractory Small-Cell Lung Cancer. *Nat. Med.* **2017**, *23*, 114–119. [CrossRef] [PubMed]
66. Su, Z.; Wang, Z.; Ni, X.; Duan, J.; Gao, Y.; Zhuo, M.; Li, R.; Zhao, J.; Ma, Q.; Bai, H.; et al. Inferring the Evolution and Progression of Small-Cell Lung Cancer by Single-Cell Sequencing of Circulating Tumor Cells. *Clin. Cancer Res.* **2019**, *25*, 5049–5060. [CrossRef]
67. Tayoun, T.; Faugeroux, O.; Aberlenc, P. Farace CTC-Derived Models: A Window into the Seeding Capacity of Circulating Tumor Cells (CTCs). *Cells* **2019**, *8*, 1145. [CrossRef] [PubMed]
68. Baccelli, I.; Schneeweiss, A.; Riethdorf, S.; Stenzinger, A.; Schillert, A.; Vogel, V.; Klein, C.; Saini, M.; Bäuerle, T.; Wallwiener, M.; et al. Identification of a Population of Blood Circulating Tumor Cells from Breast Cancer Patients That Initiates Metastasis in a Xenograft Assay. *Nat. Biotechnol.* **2013**, *31*, 539–544. [CrossRef]
69. Hodgkinson, C.L.; Morrow, C.J.; Li, Y.; Metcalf, R.L.; Rothwell, D.G.; Trapani, F.; Polanski, R.; Burt, D.J.; Simpson, K.L.; Morris, K.; et al. Tumorigenicity and Genetic Profiling of Circulating Tumor Cells in Small-Cell Lung Cancer. *Nat. Med.* **2014**, *20*, 897–903. [CrossRef]
70. Morrow, C.J.; Trapani, F.; Metcalf, R.L.; Bertolini, G.; Hodgkinson, C.L.; Khandelwal, G.; Kelly, P.; Galvin, M.; Carter, L.; Simpson, K.L.; et al. Tumourigenic Non-Small-Cell Lung Cancer Mesenchymal Circulating Tumour Cells: A Clinical Case Study. *Ann. Oncol.* **2016**, *27*, 1155–1160. [CrossRef] [PubMed]

71. Girotti, M.R.; Gremel, G.; Lee, R.; Galvani, E.; Rothwell, D.; Viros, A.; Mandal, A.K.; Lim, K.H.J.; Saturno, G.; Furney, S.J.; et al. Application of Sequencing, Liquid Biopsies, and Patient-Derived Xenografts for Personalized Medicine in Melanoma. *Cancer Discov.* **2016**, *6*, 286–299. [CrossRef]
72. Faugeroux, V.; Pailler, E.; Oulhen, M.; Deas, O.; Brulle-Soumare, L.; Hervieu, C.; Marty, V.; Alexandrova, K.; Andree, K.C.; Stoecklein, N.H.; et al. Genetic Characterization of a Unique Neuroendocrine Transdifferentiation Prostate Circulating Tumor Cell-Derived EXplant Model. *Nat. Commun.* **2020**, *11*, 1884. [CrossRef] [PubMed]
73. Stewart, C.A.; Gay, C.M.; Xi, Y.; Sivajothi, S.; Sivakamasundari, V.; Fujimoto, J.; Bolisetty, M.; Hartsfield, P.M.; Balasubramaniyan, V.; Chalishazar, M.D.; et al. Single-Cell Analyses Reveal Increased Intratumoral Heterogeneity after the Onset of Therapy Resistance in Small-Cell Lung Cancer. *Nat. Cancer* **2020**, *1*, 423–436. [CrossRef] [PubMed]
74. Zhang, Z.; Shiratsuchi, H.; Lin, J.; Chen, G.; Reddy, R.M.; Azizi, E.; Fouladdel, S.; Chang, A.C.; Lin, L.; Jiang, H.; et al. Expansion of CTCs from Early Stage Lung Cancer Patients Using a Microfluidic Co-Culture Model. *Oncotarget* **2014**, *5*, 12383–12397. [CrossRef] [PubMed]
75. Yu, M.; Bardia, A.; Aceto, N.; Bersani, F.; Madden, M.W.; Donaldson, M.C.; Desai, R.; Zhu, H.; Comaills, V.; Zheng, Z.; et al. Cancer Therapy. Ex Vivo Culture of Circulating Breast Tumor Cells for Individualized Testing of Drug Susceptibility. *Science* **2014**, *345*, 216–220. [CrossRef]
76. Gao, D.; Vela, I.; Sboner, A.; Iaquinta, P.J.; Karthaus, W.R.; Gopalan, A.; Dowling, C.; Wanjala, J.N.; Undvall, E.A.; Arora, V.K.; et al. Organoid Cultures Derived from Patients with Advanced Prostate Cancer. *Cell* **2014**, *159*, 176–187. [CrossRef] [PubMed]
77. Cayrefourcq, L.; Mazard, T.; Joosse, S.; Solassol, J.; Ramos, J.; Assenat, E.; Schumacher, U.; Costes, V.; Maudelonde, T.; Pantel, K.; et al. Establishment and Characterization of a Cell Line from Human Circulating Colon Cancer Cells. *Cancer Res.* **2015**, *75*, 892–901. [CrossRef]
78. Koch, C.; Kuske, A.; Joosse, S.A.; Yigit, G.; Sflomos, G.; Thaler, S.; Smit, D.J.; Werner, S.; Borgmann, K.; Gärtner, S.; et al. Characterization of Circulating Breast Cancer Cells with Tumorigenic and Metastatic Capacity. *EMBO Mol. Med.* **2020**, *12*, e11908. [CrossRef] [PubMed]
79. Alix-Panabières, C.; Cayrefourcq, L.; Mazard, T.; Maudelonde, T.; Assenat, E.; Assou, S. Molecular Portrait of Metastasis-Competent Circulating Tumor Cells in Colon Cancer Reveals the Crucial Role of Genes Regulating Energy Metabolism and DNA Repair. *Clin. Chem.* **2017**, *63*, 700–713. [CrossRef] [PubMed]
80. Wang, L.H.; Pfister, T.D.; Parchment, R.E.; Kummar, S.; Rubinstein, L.; Evrard, Y.A.; Gutierrez, M.E.; Murgo, A.J.; Tomaszewski, J.E.; Doroshow, J.H.; et al. Monitoring Drug-Induced GammaH2AX as a Pharmacodynamic Biomarker in Individual Circulating Tumor Cells. *Clin. Cancer Res.* **2010**, *16*, 1073–1084. [CrossRef] [PubMed]
81. Martin, O.A.; Anderson, R.L.; Russell, P.A.; Cox, R.A.; Ivashkevich, A.; Swierczak, A.; Doherty, J.P.; Jacobs, D.H.M.; Smith, J.; Siva, S.; et al. Mobilization of Viable Tumor Cells into the Circulation during Radiation Therapy. *Int. J. Radiat. Oncol. Biol. Phys.* **2014**, *88*, 395–403. [CrossRef] [PubMed]
82. Reiss, K.A.; Herman, J.M.; Zahurak, M.; Brade, A.; Dawson, L.A.; Scardina, A.; Joffe, C.; Petito, E.; Hacker-Prietz, A.; Kinders, R.J.; et al. A Phase I Study of Veliparib (ABT-888) in Combination with Low-Dose Fractionated Whole Abdominal Radiation Therapy in Patients with Advanced Solid Malignancies and Peritoneal Carcinomatosis. *Clin. Cancer Res.* **2015**, *21*, 68–76. [CrossRef] [PubMed]
83. Adams, D.L.; Adams, D.K.; He, J.; Kalhor, N.; Zhang, M.; Xu, T.; Gao, H.; Reuben, J.M.; Qiao, Y.; Komaki, R.; et al. Sequential Tracking of PD-L1 Expression and RAD50 Induction in Circulating Tumor and Stromal Cells of Lung Cancer Patients Undergoing Radiotherapy. *Clin. Cancer Res.* **2017**, *23*, 5948–5958. [CrossRef] [PubMed]
84. Chen, S.-H.; Chang, J.-Y. New Insights into Mechanisms of Cisplatin Resistance: From Tumor Cell to Microenvironment. *Int. J. Mol. Sci.* **2019**, *20*, 4136. [CrossRef]
85. Das, M.; Riess, J.W.; Frankel, P.; Schwartz, E.; Bennis, R.; Hsieh, H.B.; Liu, X.; Ly, J.C.; Zhou, L.; Nieva, J.J.; et al. ERCC1 Expression in Circulating Tumor Cells (CTCs) Using a Novel Detection Platform Correlates with Progression-Free Survival (PFS) in Patients with Metastatic Non-Small-Cell Lung Cancer (NSCLC) Receiving Platinum Chemotherapy. *Lung Cancer* **2012**, *77*, 421–426. [CrossRef]
86. Kasimir-Bauer, S.; Bittner, A.-K.; König, L.; Reiter, K.; Keller, T.; Kimmig, R.; Hoffmann, O. Does Primary Neoadjuvant Systemic Therapy Eradicate Minimal Residual Disease? Analysis of Disseminated and Circulating Tumor Cells before and after Therapy. *Breast Cancer Res.* **2016**, *18*, 20. [CrossRef] [PubMed]
87. Kuhlmann, J.D.; Wimberger, P.; Bankfalvi, A.; Keller, T.; Schöler, S.; Aktas, B.; Buderath, P.; Hauch, S.; Otterbach, F.; Kimmig, R.; et al. ERCC1-Positive Circulating Tumor Cells in the Blood of Ovarian Cancer Patients as a Predictive Biomarker for Platinum Resistance. *Clin. Chem.* **2014**, *60*, 1282–1289. [CrossRef]
88. Chebouti, I.; Kuhlmann, J.D.; Buderath, P.; Weber, S.; Wimberger, P.; Bokeloh, Y.; Hauch, S.; Kimmig, R.; Kasimir-Bauer, S. ERCC1-Expressing Circulating Tumor Cells as a Potential Diagnostic Tool for Monitoring Response to Platinum-Based Chemotherapy and for Predicting Post-Therapeutic Outcome of Ovarian Cancer. *Oncotarget* **2017**, *8*, 24303–24313. [CrossRef]
89. Zoppoli, G.; Regairaz, M.; Leo, E.; Reinhold, W.C.; Varma, S.; Ballestrero, A.; Doroshow, J.H.; Pommier, Y. Putative DNA/RNA Helicase Schlafen-11 (SLFN11) Sensitizes Cancer Cells to DNA-Damaging Agents. *Proc. Natl. Acad. Sci. USA* **2012**, *109*, 15030–15035. [CrossRef]

90. Barretina, J.; Caponigro, G.; Stransky, N.; Venkatesan, K.; Margolin, A.A.; Kim, S.; Wilson, C.J.; Lehár, J.; Kryukov, G.V.; Sonkin, D.; et al. The Cancer Cell Line Encyclopedia Enables Predictive Modelling of Anticancer Drug Sensitivity. *Nature* **2012**, *483*, 603–607. [CrossRef]
91. Lok, B.H.; Gardner, E.E.; Schneeberger, V.E.; Ni, A.; Desmeules, P.; Rekhtman, N.; de Stanchina, E.; Teicher, B.A.; Riaz, N.; Powell, S.N.; et al. PARP Inhibitor Activity Correlates with SLFN11 Expression and Demonstrates Synergy with Temozolomide in Small Cell Lung Cancer. *Clin. Cancer Res.* **2017**, *23*, 523–535. [CrossRef]
92. Conteduca, V.; Ku, S.-Y.; Puca, L.; Slade, M.; Fernandez, L.; Hess, J.; Bareja, R.; Vlachostergios, P.J.; Sigouros, M.; Mosquera, J.M.; et al. SLFN11 Expression in Advanced Prostate Cancer and Response to Platinum-Based Chemotherapy. *Mol. Cancer Ther.* **2020**, *19*, 1157–1164. [CrossRef]
93. Troncarelli Flores, B.C.; Souza, E.; Silva, V.; Ali Abdallah, E.; Mello, C.A.L.; Gobo Silva, M.L.; Gomes Mendes, G.; Camila Braun, A.; Aguiar Junior, S.; Thomé Domingos Chinen, L. Molecular and Kinetic Analyses of Circulating Tumor Cells as Predictive Markers of Treatment Response in Locally Advanced Rectal Cancer Patients. *Cells* **2019**, *8*, 641. [CrossRef]

Aims and Approaches

In an effort to investigate mechanisms underpinning the tumor-initiating capacities of CTCs and unravel new potential therapeutic targets of metastasis, our laboratory sought to develop two different functional cancer models that may recapitulate CTC biology: the chick embryo chorioallantoic membrane (CAM) (Pawlikowska et al., 2020) and the CDX mouse model (Tayoun et al., 2022).

RESEARCH ARTICLE 1. Exploitation of the chick embryo chorioallantoic membrane (CAM) as a platform for anti-metastatic drug testing. *Scientific Reports* 2020; 10:16876
Open access publication.

We put significant effort into optimizing the use of the CAM for modeling and targeting CTC metastatic potential *in ovo*. Being a naturally immunodeficient host, it is amenable to transplantations without specie- or tissue-specific restrictions (Ribatti, 2016). Moreover, the CAM presents a rich vascular network, offering great advantage for the growth of grafted tumor cells, as it has already been widely demonstrated. Another key advantage of this system is the rapid tumor formation in contrast to mouse models, which significantly shortens the time frame for a standard experiment. In Pawlikowska *et al*, we provide a step-by-step assay for the quantitative analysis of metastatic growth from a low number of characterized tumor cells on the CAM. Our work also puts forward the feasibility of preclinical testing of anti-tumoral agents such as chemotherapy and targeted therapies on metastatic tumors established in the CAM model (Pawlikowska et al., 2020).

RESEARCH ARTICLE 2. Targeting genome integrity dysfunctions impedes metastatic potency in non-small cell lung cancer circulating tumor cell-derived explants. *JCI Insight* 2022; 7(11):155804
Open access publication.

In parallel to this development, we performed functional studies to investigate CTC tumorigenicity and characterize its driving force, by developing CDX mouse models from NSCLC CTCs (Tayoun et al., 2022). Only one CDX was established previously in

this highly metastatic malignancy (as mentioned in **Introduction section III. 3)a.** (Morrow et al., 2016)), where CellSearch-detectable epithelial CTC counts are considerably low. For this project, blood samples were collected from a cohort of 55 patients with advanced NSCLC, at clinical progression time point – *i.e.* either at a change or at the end of a treatment course – to increase the probability of CTC detection. CTCs were enriched by RosetteSep-Ficoll gradient and subsequently implanted into immunodeficient Nod/Scid-IL2Rγ$^{-/-}$ (NSG) mice. Four NSCLC CDX models GR-CDXL1, GR-CDXL2, GR-CDXL3 and GR-CDXL4 were established, presenting a low tumor take rate of 4/55; ~ 7.3%. Additionally, three cell lines were expanded *in vitro* from dissociated GR-CDXL1, GR-CDXL3 and GR-CDXL4 CDX tumors.

To ensure clinical relevance of our models, preliminary work using IHC analysis was performed and has shown an epithelial phenotype in the four CDX, similarly to matched patient tumor histology. Moreover, *in vivo* drug assays demonstrated that CDX tumors recapitulated patient clinical response to chemotherapeutic treatment. An extensive molecular and functional characterization of the four CDX models and the three CDX-derived cell lines was then achieved to elucidate the mechanistic basis of CTC tumorigenic potential and is presented in **Part C. Results**.

As discussed in the introduction, NSCLC tumors carry defects in effectors of the DDR, which may constitute targetable vulnerabilities. However, the therapeutic efficacy of DDR-based agents is still poor in this malignancy; in-depth understanding of the underlying mechanisms and identification of novel biomarkers of response are urgently needed. In this PhD project, we hypothesized that dysfunctions in DDR mechanisms and genome integrity maintenance are critical processes underlying CTC metastatic potency in NSCLC and may present potential targets for anti-metastatic therapies. To test this hypothesis, the following aims were pursued:

Aim 1: Identification of genomic alterations and in-depth comparative genomic analysis using WES data.

To examine the molecular fidelity of our CDX *vs* matched patient tumors, WES was performed on CDX tumors, CDX-derived cell lines, matched patient TBs and/or isolated

CTCs and we compared mutational profiles following WES analysis. Multiple genetic alterations (mutations and CNAs) in driver genes implicated in genome integrity maintenance mechanisms and the DDR were revealed, notably *BRCA2* mutation and *FANCA* promoter deletion in GR-CDXL1, suggestive of potential HRD; *ARID1A* loss in GR-CDXL2 and GR-CDXL3 samples; gain of *MDM4* in GR-CDXL1, GR-CDXL3 and GR-CDXL4, among others.

Aim 2: Functional characterization of DDR activity and CIN events.

The identification of DDR-related genetic abnormalities by WES (aim 1) led us to the second aim, which consisted in detecting potential DDR defects in the three CDX-derived cell lines. First, we evaluated and quantified DNA damage levels in the CDX-derived cell lines. For this, we performed immunofluorescence (IF) staining of 53BP1 recruitment at DSBs and DNA damage marker γH2AX, as well as western blot analysis of cell cycle checkpoint activation. The activity of the main DSB repair pathways HR and NHEJ in CDX-derived cell lines was also assessed through IF foci analysis of major repair proteins RAD51, phosphorylated RPA32 (S33) (pRPA) and pDNA-PKcs (T2609). We also monitored CIN: most notably mitotic defects and clustering of extra centrosomes. These features subsequently provided a biological rationale for the selection of drug candidates (aim 3).

Aim 3: *In vitro* drug assays targeting DDR defects and CIN.

To investigate new DDR-based therapeutic strategies in NSCLC, we performed *in vitro* pharmacological assays targeting identified cancer cell vulnerabilities (aim 2). The sensitivity of several agents was tested in CDX-derived cell lines, including platinum-based chemotherapy (cisplatin), PARPi and DDR inhibitors. In this aim, we also investigated SLFN11, a potential predictive biomarker of CDX-derived cell response to olaparib beyond *BRCA1/2* mutations.

Aim 4: 3D modeling and targeting of CDX-derived cell line dissemination potency in the CAM model (*in ovo*) and (*in vivo*) in immunodeficient mice.

We then sought to assess the tumorigenic potential of GR-CDXL1, GR-CDXL3 and GR-CDXL4 CDX-derived cell lines in the chick CAM model and immunodeficient mice. To achieve this aim, CDX-derived cells were infected with mCherry-expressing plasmid or a luciferase lentivirus and stable cell lines were subsequently implanted on the CAM or in NSG mice respectively. Tumor growth and metastatic dissemination were monitored using 3D imaging. Next, we validated our therapeutic targets assessed *in vitro* (aim 3) by evaluating *in ovo* and *in vivo* tumor response to DDR-based therapies.

Overall, using CDX models, our work elucidated distinct DDR-related mechanisms involved in CTC tumorigenicity that provide a rationale for their therapeutic targeting in NSCLC. In cisplatin-resistant GR-CDXL1, *BRCA2* mutation was detected and mechanistic findings revealed HRD and PARPi olaparib sensitivity. This previously undescribed context suggests that resistance to chemotherapy does not exclude PARPi efficacy in HR-deficient NSCLC tumors, in contrast with the current chemosensitivity prerequisite for the selection of NSCLC patients for PARPi trials. GR-CDXL3 cells carried supernumerary chromosomes and high levels of CIN, including centrosome clustering events, a targetable promoter of CIN. Finally, GR-CDXL4 cells presented HRD and were highly sensitive to olaparib but lacked *BRCA1/2* mutations. Interestingly, olaparib sensitivity was concordant with high SLFN11 expression in GR-CDXL4, which we suggest as a potential predictor of sensitivity to PARPi in NSCLC independently of BRCAness. SLFN11 overexpression was also associated with neuroendocrine marker expression, which may also be a predictor of histological transformation of NSCLC adenocarcinoma into SCLC, for which biomarkers are currently lacking.

Part B. Additional Materials and Methods

All materials and methods used in this project have already been described in Tayoun & Faugeroux *et al* (**Part C. Results**, **pages 139-196**). Herein, I provide additional detailed experimental protocols.

1) Western blot analysis

a. Whole-cell protein extraction

Cells were seeded in a tissue culture dish 60 (TPP™) 48 hours prior to protein extraction at a concentration of 1 000 000 cells/mL for CDX-derived cell lines and 500 000 cells/mL for NSCLC cell lines. At day 2, cells were washed twice with ice-cold phosphate buffer saline (PBS) 1X, scraped off the dish on ice and centrifuged for five minutes in a 15 mL tube (Falcon®) at 250 g at 4°C. After aspirating the supernatant, cells were then immediately resuspended in NETN (NaCl EDTA Tris NP40) lysis buffer [150 mM NaCl, 1 mM EDTA, 50 mM Tris pH 7.5, 0.5% NP40, H_2O], supplemented with protease and phosphatase inhibitors (Roche). Lysates were transferred to 1.5 mL tubes (Eppendorf) and incubated for 30 minutes on ice, while stirring every five to 10 minutes. Whole-cell protein extracts were then sonicated for 15 seconds at 30% amplitude to fragment DNA, before centrifugation at maximum speed for 20 minutes at 4°C. Protein concentrations were estimated using the Micro BCA™ Protein Assay (Thermo Scientific) followed by bioluminescence reading at 562 nm on the spectrophotometer (Victor X4 Series Multilabel Plate Readers (PerkinElmer)). Laemmli buffer (4X) containing β-mercaptoethanol was added and samples were subsequently denatured by boiling at 95°C for 10 minutes.

b. Protein separation by gel electrophoresis

25-30 µg of proteins from cell lysates were then subjected to electrophoresis on a handcast 6%, 8% or 10% sodium dodecyl sulfate (SDS)-polyacrylamide gel (Bio-Rad), using the tris-glycine-SDS (TGS) 10X running buffer (Bio-Rad) diluted to 1X in water, with Precision Plus Protein™ Kaleidoscope™ Prestained Protein Standards (Bio-Rad) as

a molecular weight ladder. After migration, the proteins were transferred to a nitrocellulose membrane using the Trans-Blot™ Turbo Transfer System (Bio-Rad). Non-specific binding was blocked by incubation of the membrane in 5% non-fat dry milk in PBS 1X, 0.1% Tween®20 detergent, H_2O (PBS-T) for one hour at room temperature, on the shaker. The membrane was subsequently probed with primary antibodies diluted in PBS-milk or PBS-bovine serum albumin (BSA) at 4°C overnight. The next day, membranes were washed with PBS-T (three five-minute washes) followed by incubation with horseradish peroxidase-conjugated secondary antibodies (GE Healthcare) diluted in PBS-milk (5%) (1:5000) for one hour at room temperature, on the shaker. Membranes were washed again three times with PBS-T before incubation with WesternBright™ ECL (Advansta). Blots were then imaged either on X-ray films or more frequently using the high-resolution ChemiDoc™ XRS+ system with the Image Lab™ software (Bio-Rad).

2) Metaphase chromosome spreads

For chromosome counting, GR-CDXL1, GR-CDXL3 and GR-CDXL4 cells were treated with 0.15 µg/mL of colcemid (Roche) for three hours before fixation, which inhibits mitotic spindle formation and arrests dividing cells in metaphase. Cells were then collected, washed with PBS 1X and subsequently incubated in a hypotonic solution (75 mM KCl) for 15 minutes in a 37°C water bath. Next, cells were fixed by adding freshly prepared ethanol/acetic acid fixative solution (3:1 ratio). Cells were then subjected to several rounds of fixation, dropped carefully onto slides and left to dry at room temperature. Slides were then stored at -20°C overnight, followed by staining and mounting before microscopy.

3) *In vitro* pharmacological assays

Short-term drug testings were performed *in vitro* on GR-CDXL1, GR-CDXL3 and GR-CDXL4 cells. NSCLC cell line A549 was used as control. At day 0, cells were seeded in quadruplicates at a concentration of 500 cells/well (for A549 and GR-CDXL1) and 1000

cells/well (for GR-CDXL3 and GR-CDXL4) in 25 microliters (µL) in a 384-well test microplate (Greiner Bio-One). The microplate was subsequently incubated at 37°C, 5% CO_2 for a period of 24 or 48 hours. 24 or 48 hours after seeding (at day 2), drug dilutions in cell culture medium were added to make a total volume of 50 µL/well (**Figure 17**).

	1↔6	**7**	**8**	**9↔17**	**18**	**19↔24**
A	PBS 1X	NT	[min]	[drug] →	[max]	PBS 1X
B	PBS 1X	NT	[min]		[max]	PBS 1X
C	PBS 1X	NT	[min]		[max]	PBS 1X
D	PBS 1X	NT	[min]		[max]	PBS 1X
E	PBS 1X	NT	[min]		[max]	PBS 1X
F	PBS 1X	NT	[min]		[max]	PBS 1X
G	PBS 1X	NT	[min]		[max]	PBS 1X
H	PBS 1X	NT	[min]		[max]	PBS 1X
I ↕ P	PBS 1X	NT	[min]		[max]	PBS 1X

Figure 17. Example of a 384-well microplate layout for *in vitro* pharmacological assays. Different colors are used for different cell lines. NT, non-treated; min, minimum concentration; max, maximum concentration; PBS, phosphate buffer saline.

All drug dilutions were prepared in an Eppendorf Deepwell plate 96 (Eppendorf). Total drug volume required from stock solution ($V_{initial}$) to achieve maximum desired drug dosage (C_{final}) was determined according to the following formula:

$$V_{initial} = \frac{C\ final \times V\ final \times dilution\ factor}{C\ initial}$$

$V_{initial}$ = volume of stock transferred in µL
C_{final} = maximum drug concentration in micromolars (µM)
V_{final} = final volume in µL
$C_{initial}$ = initial concentration of stock drug solution in µM

In each well, 25 µL of the prepared drug dilution was added to 25 µL of the cell suspension with a dilution factor of 2. Several drug testings were performed with the following molecules: cisplatin (Mylan Pharma), olaparib (Selleckchem), alisertib (Aurora A inhibitor, Selleckchem), AZ82 (KIFC1 inhibitor, Clinisciences), BYL719 (PI3Kα inhibitor, Novartis) and NU7441 (DNA-PK inhibitor, Selleckchem) with initial concentrations of 3.33 mM, 100 mM, 100 mM, 10 mM, 35.67 mM, 10 mM and 5 mM respectively. Drugs

concentrations were prepared by serial dilutions of the stock solution from the highest to the lowest concentration (**Table 4**). In column 7, the drug diluent was added to the cells as control (NT wells). Then, from column 8 to 18, 25 µL of the drug solution at the appropriate concentration was administered in each well (four wells per concentration) as annotated in the microplate layout in **Figure 17**. Cells were then incubated at 37°C, 5% CO_2 for 96 hours. At day 5, cell viability was estimated using CellTiter-Glo® Luminescent Cell Viability Assay (Promega). 12.5 µL of CellTiter-Glo reagent was added per well (diluted 1:4); the microplate was shaken for 20 minutes at room temperature according to manufacturer's protocol and luminescence was subsequently measured using Victor X4 Series Multilabel Plate Readers (PerkinElmer).

In parallel, at day 0, cells from each tested cell line were seeded in quadruplicates in a second control microplate and then incubated at 37°C, 5% CO_2 for 48 hours. Luminescence was measured at day 2, *i.e.* the day of drug administration in the test microplate as described above. Measurements were then compared to the NT control wells in the test microplate containing the drug diluent, to make sure that cells grew at least two-fold throughout drug incubation period. If this was not the case, experimental data was considered uninterpretable. Cell viability and the half maximal inhibitory concentration (IC_{50}) were calculated by normalizing luminescence measurement values according to NT control wells and viability curves were plotted using GraphPad Prism V7 "log(inhibitor) *vs* response-variable slope (4 parameters)" model.

Table 4. Drug concentrations *in vitro*.

	Molecule	Concentrations													
nM	**Alisertib**	0.02	0.06	0.17	0.51	1.52	4.57	13.72	41.15	123.46	370.37	1111.11	3333.33	10000.00	30000.00
µM	**Cisplatin**	0.02	0.06	0.18	0.56	1.67	5.00	15.00	45.00	135.00					
µM	**Olaparib**	0.02	0.06	0.18	0.56	1.67	5.00	15.00	45.00	135.00	405.00	1215.00			
µM	**BYL719**	0.02	0.06	0.18	0.56	1.67	5.00	15.00	45.00	135.00					
µM	**AZ82**	0.28	0.41	0.94	1.45	2.11	3.16	4.74	7.11	10.67	16.00	24.00	36.00	54.00	81.00
µM	**NU7441**	0.01	0.04	0.11	0.33	1.00	3.00	9.00	27.00	81.00	243.00				

Part C. Results

RESEARCH ARTICLE 1. Exploitation of the chick embryo chorioallantoic membrane (CAM) as a platform for anti-metastatic drug testing. Scientific Reports 2020; 10:16876
Open access publication.

RESEARCH ARTICLE 2. Targeting genome integrity dysfunctions impedes metastatic potency in non-small cell lung cancer circulating tumor cell-derived explants. *JCI Insight* 2022; 7(11):155804
Open access publication.

SCIENTIFIC REPORTS
nature research

Check for updates

OPEN

Exploitation of the chick embryo chorioallantoic membrane (CAM) as a platform for anti-metastatic drug testing

P. Pawlikowska[1,2], T. Tayoun[1,2], M. Oulhen[2], V. Faugeroux[1,2], V. Rouffiac[3], A. Aberlenc[2], A. L. Pommier[2], A. Honore[4], V. Marty[5], O. Bawa[5], L. Lacroix[4], J. Y. Scoazec[5], A. Chauchereau[1], C. Laplace-Builhe[3] & F. Farace[1,2]✉

The establishment of clinically relevant models for tumor metastasis and drug testing is a major challenge in cancer research. Here we report a physiologically relevant assay enabling quantitative analysis of metastatic capacity of tumor cells following implantation into the chorioallantoic membrane (CAM). Engraftment of as few as 10^3 non-small cell lung cancer (NSCLC) and prostate cancer (PCa) cell lines was sufficient for both primary tumor and metastasis formation. Standard 2D-imaging as well as 3D optical tomography imaging were used for the detection of fluorescent metastatic foci in the chick embryo. H2228- and H1975-initiated metastases were confirmed by genomic analysis. We quantified the inhibitory effect of docetaxel on LNCaP, and that of cisplatin on A549- and H1299-initiated metastatic growths. The CAM assay also mimicked the sensitivity of *ALK*-rearranged H2228 and *EGFR*-mutated H1975 NSCLC cells to tyrosine kinase inhibitors crizotinib and gefitinib respectively, as well as sensitivity of LNCaP cells to androgen-dependent enzalutamide therapy. The assay was suggested to reconstitute the bone metastatic tropism of PCa cells. We show that the CAM chick embryo model may be a powerful preclinical platform for testing and targeting of the metastatic capacity of cancer cells.

Metastasis is the major cause of death from cancer. Uncovering new therapeutic targets in metastatic cancer inevitably relies on suitable and functional models amenable to pharmacological assays. Different immunodeficient mouse strains allowed human cells engraftment and opened possibilities for developing models. Over the past few years, tremendous effort has been put into establishing different patient-derived xenografts (PDX) to model patient disease and decipher novel therapeutic strategies[1]. PDX are currently the most clinically relevant models but difficulty to obtain the metastatic growth from PDX tumors makes functional studies and screening approaches challenging. Depending on research purposes, diverse sites of tumor engraftment were applied, such as orthotopically or directly in the vascular system. However, both rarely reflect the real patient metastatic disease[1]. Furthermore, costs related to establishment and husbandry of mouse models and ethical issues considerably limit their use. Recently, 3D organoids have emerged as novel robust tools to model tumor heterogeneity and perform drug screening assays[2]. Great efforts have been put into generating 3D co-cultures to simulate tumor microenvironment ex vivo. However, the lack of in vivo host complexity renders modeling metastatic disease incomplete. To overcome some of these limitations and to bridge the gap between in vitro and in vivo study of metastasis, we and others attempted to use a chorioallantoic membrane (CAM) chick embryo model.

[1]U981 "Identification of Molecular Predictors and New Targets for Cancer Treatment", INSERM, 94805 Villejuif, France. [2]"Circulating Tumor Cells" Translational Platform, UMS AMMICa CNRS 3655-INSERM US23, Gustave Roussy, Université Paris-Saclay, 94805 Villejuif, France. [3]Flow Cytometry and Imaging Platform, UMS AMMICa CNRS 3655-INSERM US23, Gustave Roussy, Université Paris-Saclay, 94805 Villejuif, France. [4]Genomic Platform, CNRS UMS3655 – INSERM US23 AMMICA, Gustave Roussy, Université Paris-Saclay, 94805 Villejuif, France. [5]Experimental and Translational Pathology Platform, CNRS UMS3655 – INSERM US23 AMMICA, Gustave Roussy, Université Paris-Saclay, 94805 Villejuif, France. ✉email: francoise.farace@gustaveroussy.fr

The first applications of the chick embryo and CAM in oncology research were announced more than a century ago[3,4]. The chicken egg model has fundamentally contributed to the most significant discoveries and some Nobel laureates, including the discovery of the first known oncogene (c-src)[5]. The chick embryo develops for 21 days until hatching. The CAM is formed within 4 to 5 incubation days (ID) through the fusion of mesodermal layers of outgrowing allantois and the chorion. The highly vascularized nature of the CAM is a considerable advantage, it greatly stimulates the growth of grafted cells. Notably, this avian model is a naturally immunodeficient host; a feature which allows implantation of tumor cells and tissues without species-specific restrictions. The extraembryonic membranes connected to the embryo through a continuous extraembryonic vessel system are easily accessible for manipulation and observation. According to European law (Directive 2010/63/EU of the European Parliament and of the Council of 22 September 2010 on the protection of animals used for scientific purposes), the CAM model system does not raise any ethical or legal concerns, thus being an attractive alternative to other animal experiments. The CAM model is maintained in an incubator at 37 °C requiring limited space. This significantly limits animal husbandry requirements compared to immunodeficient mice breeding and reduces experimentation costs. The availability of the CAM model for screening is beneficial compared to in vitro cultures, where the role of tumor vasculature and tissue tropism cannot be accounted for.

Several previous reports show the feasibility of obtaining tumor growth in the form of nodules on the CAM, starting from different tumor cell lines or tissues[4,6,7]. These studies usually aim to evaluate the morphological and morphometric characteristics of tumor nodules. Indeed, tumor growth has been evaluated by measuring the size and weight of nodules as well as the extent of the vascular network[8,9] or by immunohistochemical studies on isolated CAM primary tumors[10,11]. Technological development, especially in the field of imaging, opened up new possibilities to quantify the primary tumor growth[11,12] and study tumor cell migration[13,14]. Up until now, metastatic tumor evolution was analyzed by quantitative Alu-PCR for the detection of human tumor cells in the isolated organs of the chick embryo[15,16]. The fluorescent tumor cells were also detected at tissue sections of isolated organs[17,18]. Here, we investigated whether the CAM model may be used to evaluate the metastatic capacity of cells and serve as a potential preclinical anti-metastatic drug test. We report a step by step technology to obtain metastatic growth starting from a limited number of well-characterized tumor cells. We show the quantitative assessment of metastasis using whole-animal 3D tomography optical imaging. Finally, we provide a proof-of-concept for the feasibility of a preclinical assay of anti-metastatic compounds in the chick embryo model.

Results

Primary tumor nodule formation starting with limited cell quantities. Most previous studies showed the advantages of cell implantation at ID 10 for primary tumor nodule formation[4,6,8]. We adapted a similar protocol to a panel of non-small cell lung cancer (NSCLC) and prostate cancer (PCa) cell lines (Supplementary Table 1). The general scheme followed in all experiments is presented in Fig. 1A. In contrast to previous research, we challenged the eggs with a highly limited number of H1299 cells starting from 10^6 and successively reducing cell quantities (Fig. 1B). Reproducible results were obtained by implantation of 10^3 cells per egg, resulting in up to 80% of successfully formed nodules in the case of lung cancer cell lines (Fig. 1B) and 100% for prostate cancer cell lines (data not shown). Engrafted cell lines were engineered to express fluorescent markers. Tumor growth was evaluated by fluorescence detection in vivo using MacroFluo Nikon macroscope (Fig. 1C). Hematoxylin staining together with anti-human antibodies against Ki67 and tumor marker vimentin was further performed to confirm the human origin of tumor growth on the CAM (Fig. 1D). These results demonstrate the ability of the CAM system to form tumor nodules from as low as 10^3 cells.

Evaluation of metastasis formation in the chick embryo. We then focused on the quantitative evaluation of metastatic seeding capacities of tumor cells. As the duration of the CAM assay is limited to 7–9 days before the chick hatches, most tumor cells cannot produce macroscopically visible tumor metastasis masses before the end of the assay. However, they form small metastatic foci detectable by fluorescence imaging. We thus aimed to adapt the imaging tomography IVIS Spectrum system—most often used for visualizing tumor growth in small rodents—to detect the metastases formed by fluorescent cell lines implanted on the chick embryo. We first engrafted the GFP-expressing LNCaP and IGR-CaP1 PCa cells (10^3 cells), for which the tumorigenic potential has been reported in mice[19–21]. LNCaP primary nodules were also reported to grow on the CAM[9]. As previously observed in mouse models[19,20], IGR-CaP1-GFP appeared to display significantly increased disseminating capacity compared to standard androgen-dependent LNCaP-GFP cell line, as measured by fluorescence intensity obtained using 2D scans performed by IVIS Spectrum system (Fig. 2A,B). However, significant autofluorescence of the chick embryo was repeatedly observed throughout the analysis of GFP-expressing cells, which can hamper signal interpretation for less aggressive disseminating cells when using the GFP spectral range. Indeed, some of the embryos that were implanted with LNCaP-GFP cells presented fluorescence intensity equal to the one in negative control embryos, making the interpretation difficult. Since green fluorochrome is often used in in vivo research, we would like to point out that based on these results, GFP expression—although well-distinguished in the tumor nodule on the CAM—is not really suitable to evaluate the metastasis seeding inside the chick embryos using the fluorescence scan system. As much more limited autofluorescence is obtained in the red fluorescence spectra, further experiments were pursued with mCherry-expressing cells (after retroviral infection, Fig. 2C) or PKH26-stained cells (described below, Supplementary Table 2, Supplementary Figures 2 and 3). The protocol of cell labeling with fluorescent cell linker PKH26 was adapted to extend the use of the model for tumor cells that were not engineered to express fluorescent markers. Engraftment of 10^3 mCherry-expressing NSCLC cells produced identifiable metastatic foci (Fig. 2C,D). The most aggressive cell line was *NRAS*-mutated H1299. *KRAS*-mutated A549, *EGFR*-mutated H1975 and *ALK*-rearranged H2228 cell lines also produced significantly higher fluorescent signals compared to negative control chick embryos (Fig. 2C,D). Notably, heterogeneity in

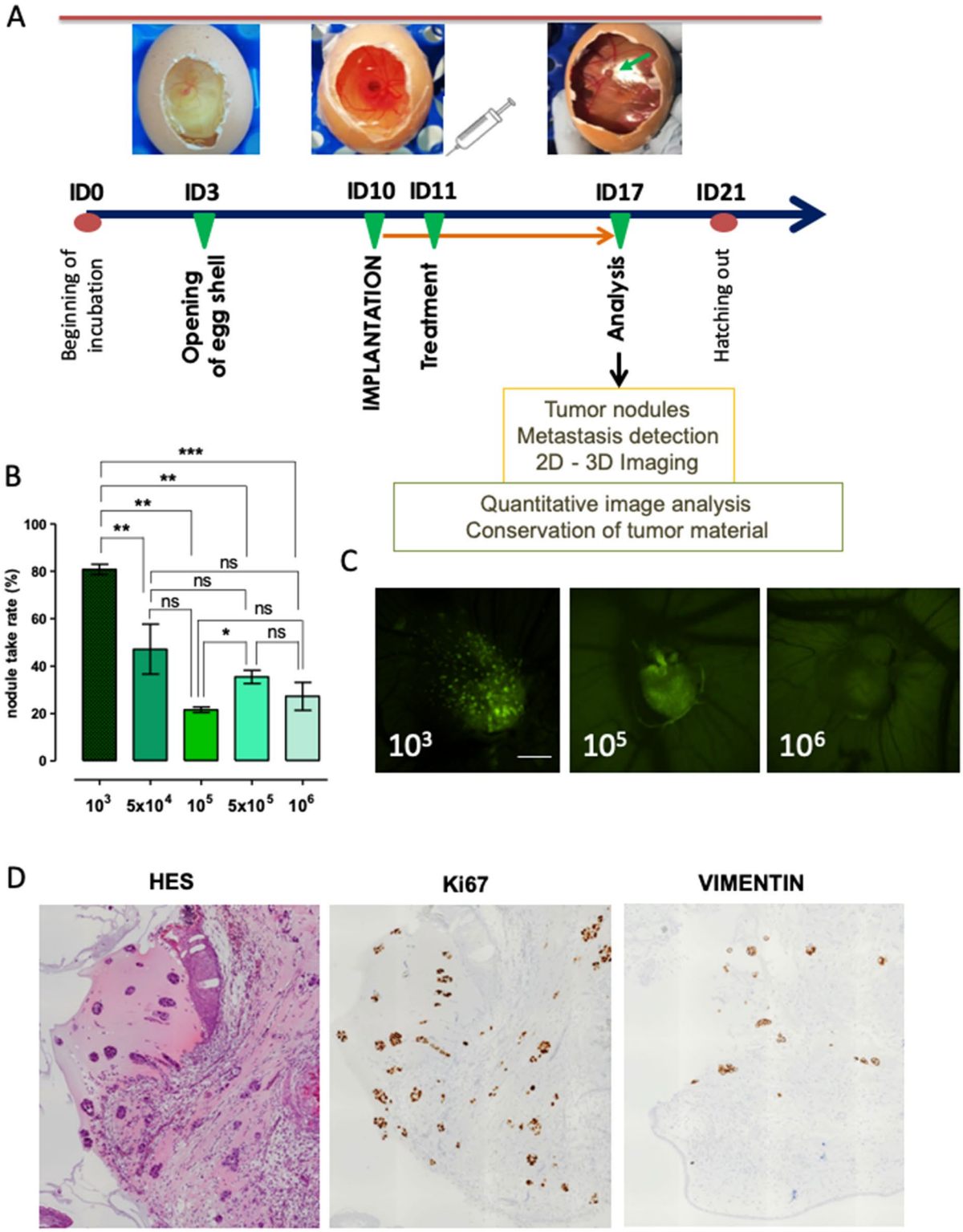


Figure 1. Chorioallantoic membrane (CAM) chick embryo model and primary tumor detection. (**A**) Schematic model embedding our timeline of standard experiment, supplemented by the images representing incubation day (ID) 3, 10 and 17. (**B**) Graph displaying percentage of eggs presenting fluorescence-positive nodules at ID 17 after implantation of indicated number of cells. Data are represented as mean ± SEM obtained from 14 experiments with 10^3 cells, 4 experiments with 5×10^4, 10^5 and 5×10^5 cells, and 8 experiments with 10^6 cells. In each experiment, a minimum of 8 eggs were evaluated. (**C**) Representative images of the fluorescent tumor nodules of H1299-GFP obtained at ID 17. (**D**) Tumor nodules obtained at ID 17 after implantation of 10^3 H1299-GFP cells, FFPE sections stained with HES, anti-human Ki67 and anti-human Vimentin antibodies.

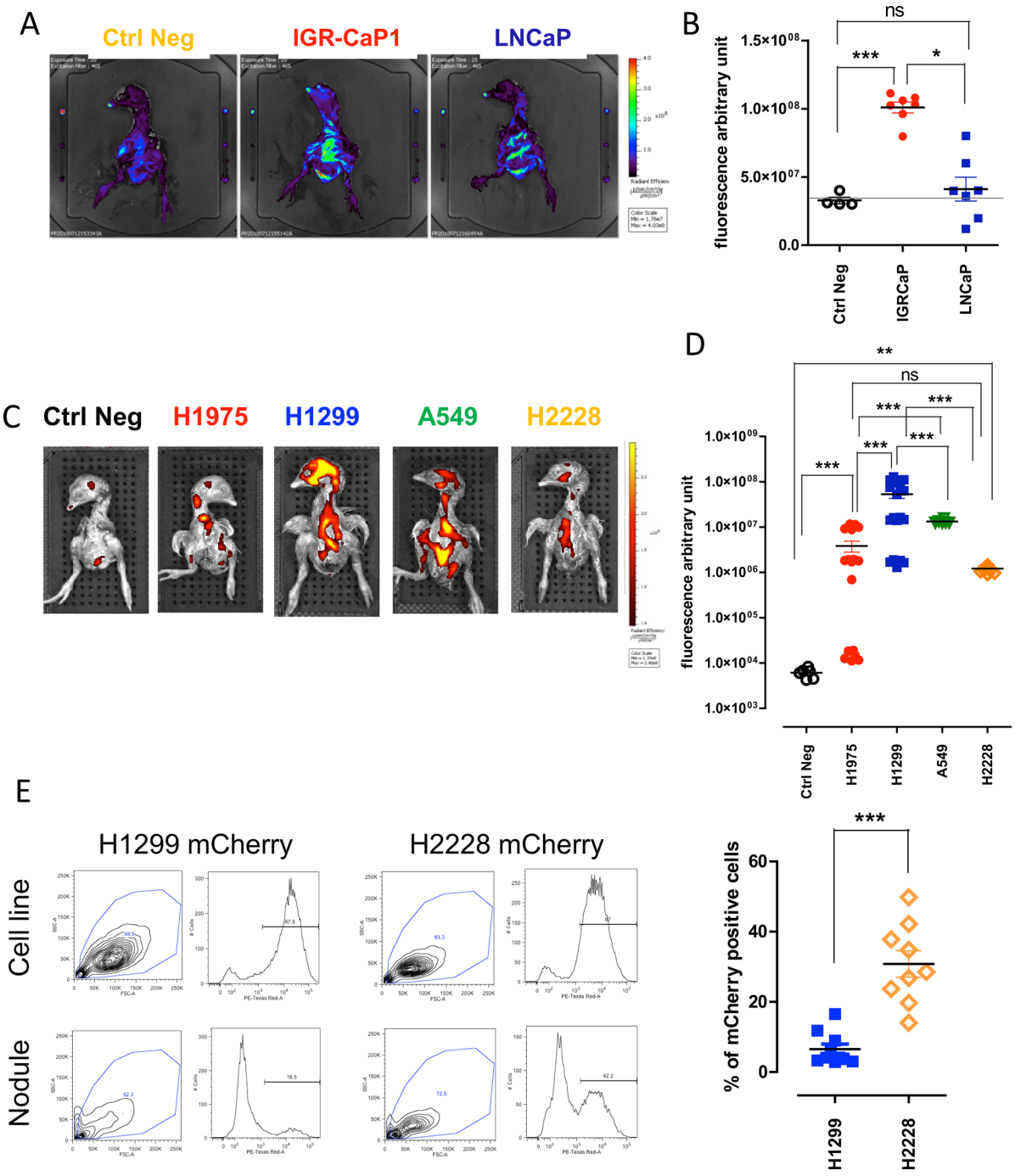


Figure 2. Metastatic capacities of prostate and lung cancer cell lines. (**A**) 2D representative images of chick embryo expressing GFP originating from eggs implanted at ID 10 with medium only (without cells, left), IGR-CaP1-GFP (middle), LNCaP-GFP (right). (**B**) Quantitative analysis of average fluorescence intensity of chick embryos presenting PCa metastases measured after 2D scan. Each point represents a single embryo. Two separate experiments were performed. (**C**) 2D representative images of chick embryos expressing mCherry originating from eggs implanted at ID 10 with NSCLC cell lines. (**D**) Quantitative analysis of average fluorescence intensity obtained after 3D scans of chick embryos presenting metastases formed after implantation of lung cancer cell lines. At least two separate experiments were performed for each cell line. Each point represents a single embryo. Numbers of analyzed embryos were for Negative Controls: 6, H1299: 21, H1975: 8, A549: 6, H2228: 14. (**E**) Representative FACS plots obtained after mCherry expression analysis in control in vitro cell lines and tumor nodules obtained at ID 17 from CAM implanted with H1299-mCherry and H2228-mCherry respectively. Right panel represents graphical quantification of H1299 and H2228 mCherry-expressing cells obtained from nodules at ID 17 after mechanistic and enzymatic dissociations. Two separate experiments were performed for each cell line. Each point represents a single embryo.

the mean fluorescence of metastatic foci from H1975 cells was observed. Average fluorescence intensity was measured in a region of interest (ROI) including the whole embryo. To further confirm metastasis foci formation, we investigated known H1975 and H1299 mutations (Supplementary Table 1) in CAM nodules and chick embryo metastases, in comparison to control cell lines. $EGFR^{T790M}$, $EGFR^{L858R}$ and $TP53^{R273H}$ homozygous mutations were detected in tested tumor nodules and metastasis samples from chick embryos engrafted with H1975 cells (Table 1). Furthermore, we detected homozygous $CDKN2A^{E69^{*}}$mutation in H1975 metastatic samples. In the case of H1299, the most aggressive cell line according to fluorescence measurements in the chick embryo, we detected the characteristic heterozygous mutation $NRAS^{Q61K}$ only in the organs invaded by metastasis and not in primary nodules (Table 1). This suggested that, at ID 17, all H1299 cells from the primary tumor site had migrated to embryo organs. To further evaluate whether some cell lines presented higher migration capacities than others, we implanted, in parallel, H1299-mCherry cells—the most aggressive cells according to fluorescence analysis of the chick embryo—and the less aggressive H2228-mCherry cells. Indeed, the metastatic fluorescence signal obtained from the chick embryos at ID 17 was statistically different (Fig. 2D). Moreover, dissociated primary nodules evaluated by FACS from the same eggs presented negative correlation with the fluorescent metastatic foci intensities. Less mCherry-positive cells were found in primary nodules of aggressive H1299 cells compared to H2228, which were predominantly present in nodules but displayed lower intensity of fluorescent metastatic foci in corresponding chick embryos (Fig. 2E).

Fluorescent imaging acquisitions providing 3-dimensional (3D) reconstitution of the embryo allowed us to precisely evaluate metastasis formation both in terms of localization and quantification (Fig. 3A). The acquisition of 3D computer tomography (CT) data combined to fluorescence images aids to localize the metastatic foci in the chick embryo and thus determine the organ with tumor lesions (Fig. 3A). Fluorescent signal was collected in specified wavelengths during serial acquisitions to filter specifically the fluorescence from GFP-, mCherry- or PKH26-positive cells. Here, we provided the example of PCa cell line (DU145) labeled with PKH26 and either cultured in vitro or implanted into the CAM (2×10^3 cells per egg). We detected the fluorescent signal from metastatic foci of the chick embryo (Fig. 3B,C; Supplementary Figure 3C) and cultured cells (Fig. 3D, Supplementary Figure 2) 7 days later. These results show that 3D reconstitution of chick embryos allows us to detect even a limited number of fluorescent cells in the whole embryo, suggesting that our system might be used as a preclinical model of metastasis.

Effect of the chemotherapeutics on metastasis formation in the chick embryo. Since we have shown the feasibility of using chick embryo as an efficient and sensitive model for metastasis seeding for different type of cancers, we thought that it might be particularly useful to assess therapeutics targeting metastasis. We implanted LNCaP-mCherry cells into the CAM at ID 10. Docetaxel (2 µg/kg), standard-of-care for PCa patients, was topically added on the surface of the CAM 24 h later (ID 11). The eggs were analyzed 6 days later (ID 17). The dose of docetaxel has been previously estimated by serial treatments (data not shown). Both 2D and 3D imaging showed that cell migration and metastasis formation into distant organs of the chick embryo was hampered by docetaxel treatment (Fig. 3E). We quantified the effect of docetaxel on the metastasis seeding capacities of LNCaP by measuring the average fluorescence intensity from images obtained after 2D scanning of chick embryos (Fig. 3F). These data showed a significant decrease in fluorescence intensity between chick embryos engrafted with LNCaP versus LNCaP treated by docetaxel.

A similar experiment was performed with NSCLC A549 and H1299 cell lines which are known to be sensitive to cisplatin treatment *in vitro*[22]. Implantation of 10^3 A549 or H1299 mCherry-expressing cells resulted in the emission of fluorescence signals on 3D reconstructed images 7 days later in different organs of the chick embryo (Fig. 3G, Supplementary Figure 1B). Treatment of chick embryos with cisplatin (10 µg/kg), 24 h after cell implantation, significantly decreased the fluorescence signal from both tested NSCLC cell lines (Fig. 3H, Supplementary Figure 1C). Cisplatin dose did not affect neither viability nor development of embryos. For all evaluated drugs chick embryo mobility as well as increasing vascularization of the CAM (the two indicators of chick embryo viability) were evaluated and compared to non-treated eggs throughout experiments. The effect of the therapeutics on chick embryo development was also estimated. Distinctly smaller embryonic size, unilateral or bilateral microphthalmia, microcephaly or ancephaly, acrania, malformations of limbs, gastroschisis or other visible malformations if detected in more than 10% of treated embryos, the drug dose was decreased.

To demonstrate that the observed reduction of metastatic signal after cisplatin treatment is not simply the result of tumor cell death at the primary site, we directly injected tumor cells into the chick embryo circulation to bypass the stage of primary tumor formation. This technically-advanced manipulation evidently increases the mortality of chick embryos. However, protection of the manipulated vein by silicon ring facilitated the healing process and allowed an adequate chick embryo development, as well as metastatic growth. No primary nodules were observed on the CAM in this experiment, however fluorescent metastatic foci were found in the chick embryo injected with mCherry-expressing H1299 cells (2×10^3) and fluorescence of less intensity was detected after cisplatin treatment (Fig. 3I,J). These data showed that the CAM chick embryo system is a sensitive model capable of recapitulating the effect of standard-of-care chemotherapies frequently used against metastatic PCa and NSCLC.

Effects of targeted therapies on metastasis formation. Then we wondered if targeted therapy efficacy could also be evaluated using the CAM system. We established first a safe dose of 2 mg/kg for tyrosine kinase inhibitors crizotinib and gefitinib (data not shown). As previously, 10^3 mCherry *ALK*-rearranged H2228 and *EGFR*-mutant H1650 NSCLC cells were implanted into the CAM at ID 10. Similarly to patients' therapy, groups of eggs were treated daily with respective therapeutics. 7 days later, the embryos treated with targeted therapies presented a significantly lower fluorescence intensity compared to non-treated ones (Fig. 4A-D), show-

Figure 3. Effect of chemotherapeutics on metastasis formation. (**A**) Representation of the methodology adapted to fluorescence intensity measurement on 3D reconstructed images. Region of interest was defined manually, using an adapted embryo size area in each case (blue box). (**B**) 3D representative images of chick embryos expressing PKH26 (bottom) 7 days after implantation with DU145 PKH26-positive cells. (**C**) Quantitative analysis of PKH26 positive and negative chick embryos. Each point represents a single embryo. (**D**) Representative images of DU145 cells 7 days after induction with PKH26 fluorescent tracer. Bar = 10 µm. (**E**) Representative images of 2D (left) and 3D (right) reconstructions of chick embryos obtained from eggs implanted with LNCaP-mCherry cells with or without docetaxel treatment. (**F**) Quantitative analysis of mean fluorescence intensity on 3D reconstructed images. Each point represents a single embryo. (**G**) Representative images of fluorescent metastatic foci seeded by H1299 cells with or without cisplatin treatment. (**H**) Quantitative analysis of mCherry-positive embryos obtained from implantation of H1299 mCherry-expressing cells, with or without cisplatin treatment. At least two separate experiments were performed for each therapeutic treatment and the graph presents the most representative one. (**I**) Representative images of metastatic foci obtained after injection of H1299-mCherry cells directly into the chick embryo circulation and treatment with or without cisplatin. (**J**) Quantitative analysis of mean fluorescence of chick embryos obtained from two separate experiments after injection of H1299-mCherry cells directly into the chick embryo circulation and treatment with or without cisplatin.

ing the inhibitory effects of crizotinib and gefitinib on the metastatic growth of H2228 and H1650 cell lines respectively.

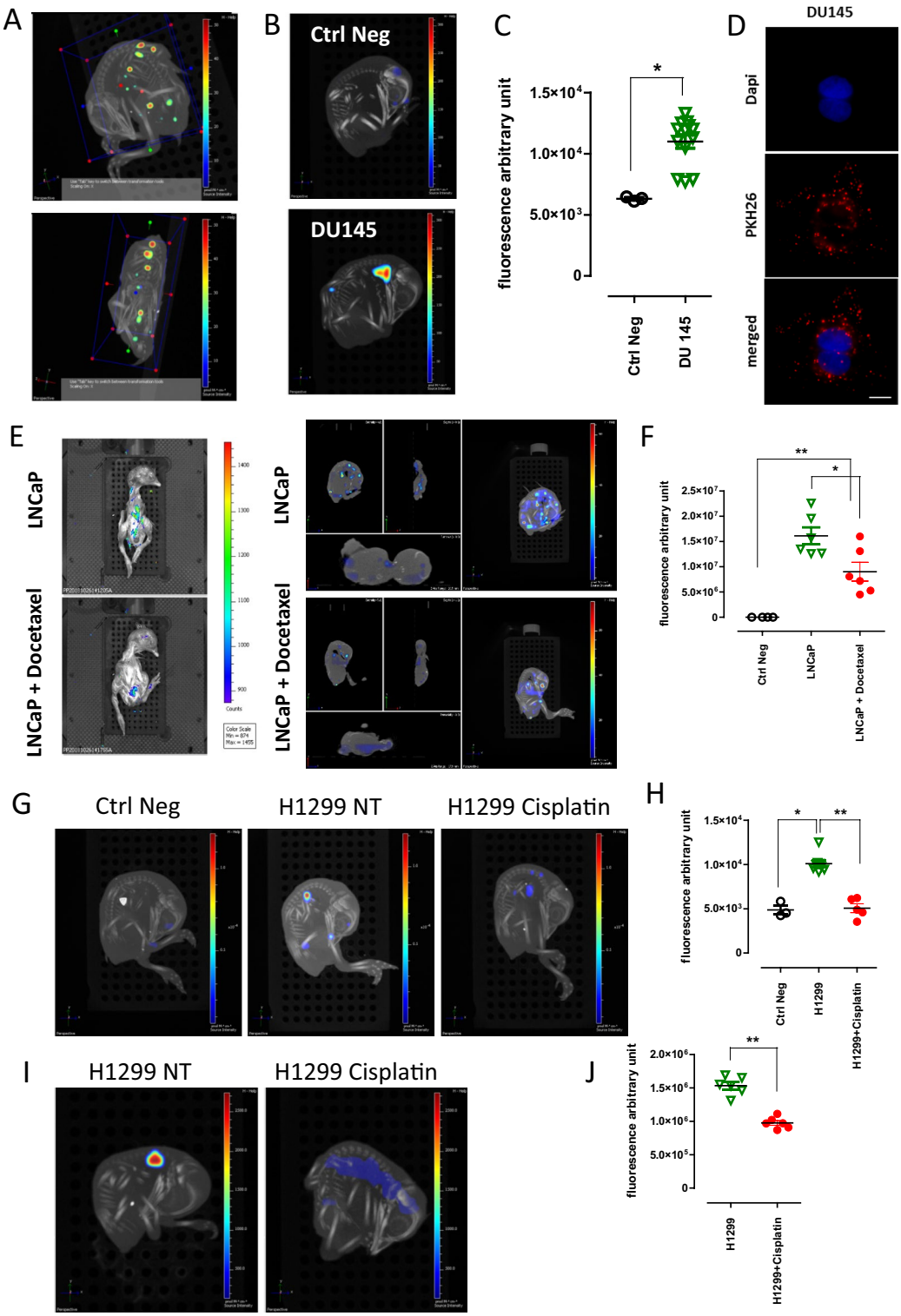
Finally, the metastatic capacity of androgen-responsive LNCaP and—unresponsive DU145 PCa cells was challenged with enzalutamide (400 µg/kg). Before implantation, cells were stained with PKH26 fluorescent tracer. The pattern and intensity of PKH26 labeling in LNCaP cell line were analyzed in vitro for 7 days, the length of chick embryo experiments (Supplementary Figure 2) and no substantial differences were observed. The characteristic punctate pattern of staining was maintained throughout the whole experiment. 2×10^3 cells were implanted per egg into the CAM at ID 10. Enzalutamide was topically administered daily for 6 days starting 24 h after cell implantation. LNCaP and DU145 both formed metastasis in the chick embryo bodies at ID 17 (Fig. 4E,F). As expected, the androgen-unresponsive DU145 cells remained resistant to enzalutamide treatment, while the drug statistically diminished metastatic capacities of LNCaP cells (Fig. 4E,F). Overall, these results demonstrate that the CAM system might be successfully used for efficacy evaluation of targeted therapies in NSCLC and PCa cells.

The chick embryo represents the specificity of PCa metastatic bone tropism. Difficulty to obtain a representative model of PCa bone metastasis hampers the development of new treatments for metastatic PCa patients. To evaluate whether the chick embryo may represent a relevant model of PCa metastatic evolution, we retrospectively compared the 3D reconstitution images of metastatic foci seeded by LNCaP, IGR-CaP1, DU145 cells to metastases formed by the NSCLC cell lines (H1975, H1299, A549, H2228 and H1650). Additionally, we tested GR-CDX P1, a unique cell line established in the laboratory from circulating tumor cell-derived explant (CDX) model of castration resistant prostate cancer (CRPC)[23]. LNCaP cells were found to metastasize to the bones of the chick embryo with 50% incidence (Fig. 5A,B). The more aggressive IGR-CaP1 cells were always localized within the bones. 75% and 54% of tumor foci obtained after implantation of GR-CDX P1 and DU145 cells respectively were found co-localized with the skeleton after image reconstruction. Indeed, this evaluation is rather approximative and based on the overlapping fluorescent spot with the CT image of the chick skeleton. However, the same type of evaluation using lung cancer cell lines shows that metastatic foci disseminated in the bones never exceed 20%, for all cell lines tested. To further confirm the presence of human PCa metastatic foci in the bones of the chick embryo, we collected the long bones from chick embryos implanted with IGR-CaP1 cell line. Bones were cleaned and RNA was extracted from the flushed bone marrows and crashed bones. We detected the expression of human genes that were described as characteristics of the metastatic process of this cell line[19]. 6 bone samples out of 8 presented high expression of TNFSRFIIB, SPP1 and Vimentin evidencing the presence of human tumor cells inside the chick embryo bones. Samples marked 'bones 2′ and 'bones 6′ most probably contained very few IGR-CaP1 cells since only two genes out of three tested were found at detectable levels (Fig. 5C). Although requiring further investigation, these data suggest that the CAM chick model may potentially represent a system able to reconstitute the particular metastatic tropism of prostate tumors to the bones.

Discussion

Further development in the establishment of novel in vivo preclinical models is needed to increase knowledge about tumor seeding and offer new insights into therapeutic strategies. In this study we show that metastases in the organs of the chick embryos can be obtained following the engraftment of a number as low as 10^3 of tumor cells into the CAM. Standard 2D and 3D optical tomography imaging enabled highly sensitive detection of fluorescent metastatic foci within 7 days from cell engraftment. Metastasis formation in the chick embryo was confirmed by molecular studies. We quantified the inhibitory effects of a variety of standard-of-care treatments including chemotherapy and targeted therapies using several NSCLC and PCa cell lines. We also observed that the CAM chick embryo system may allow the reconstitution of the bone metastatic tropism of PCa cell lines. Our data show that the CAM system may provide a rapid and sensitive method to evaluate the metastatic activity of cancer cells and assess the efficacy of anti-metastatic compounds.

Until now, analysis of tumor growth on the CAM has relied on visual inspection by microscopy and quantification of nodule size or weight[8,9]. These methods have been continuously optimized. Two studies have reported


A
B
Ctrl Neg
DU145
C
fluorescence arbitrary unit
1.5×10⁴
1.0×10⁴
5.0×10³
0
*
Ctrl Neg
DU 145
D
DU145
Dapi
PKH26
merged
E
LNCaP
LNCaP + Docetaxel
LNCaP
LNCaP + Docetaxel
F
fluorescence arbitrary unit
2.5×10⁷
2.0×10⁷
1.5×10⁷
1.0×10⁷
5.0×10⁶
0
**
*
Ctrl Neg
LNCaP
LNCaP + Docetaxel
G
Ctrl Neg
H1299 NT
H1299 Cisplatin
H
fluorescence arbitrary unit
1.5×10⁴
1.0×10⁴
5.0×10³
0
*
**
Ctrl Neg
H1299
H1299+Cisplatin
I
H1299 NT
H1299 Cisplatin
J
fluorescence arbitrary unit
2.0×10⁶
1.5×10⁶
1.0×10⁶
5.0×10⁵
0
**
H1299
H1299+Cisplatin

Cell line	Sample	Gene	Protein change	Exon	Variant Allele frequency (%)
NCI-H1975	gDNA	*EGFR*	T790M	20	76
		EGFR	L858R	21	75
		TP53	R273H	8	100
		CDKN2A	E69*	2	100
	Nodule N1	*EGFR*	T790M	20	52
		EGFR	L858R	21	67
		TP53	R273H	8	100
		CDKN2A	E69*	2	Not covered
	Nodule N4	*EGFR*	T790M	20	19
		EGFR	L858R	21	32
		TP53	R273H	8	75
		CDKN2A	E69*	2	Not covered
	Metastasis M1	*EGFR*	T790M	20	79
		EGFR	L858R	21	78
		TP53	R273H	8	99
		CDKN2A	E69*	2	100
	Metastasis M2	*EGFR*	T790M	20	76
		EGFR	L858R	21	75
		TP53	R273H	8	100
		CDKN2A	E69*	2	100
	Metastasis M3	*EGFR*	T790M	20	74
		EGFR	L858R	21	74
		TP53	R273H	8	100
		CDKN2A	E69*	2	100
	Metastasis M4	*EGFR*	T790M	20	73
		EGFR	L858R	21	72
		TP53	R273H	8	100
		CDKN2A	E69*	2	100
NCI-H1299	gDNA	*NRAS*	Q61K	3	44
	Nodule N1	*NRAS*	Q61K	3	0
	Nodule N3	*NRAS*	Q61K	3	0
	Metastasis M1	*NRAS*	Q61K	3	35
	Metastasis M2	*NRAS*	Q61K	3	40
	Metastasis M3	*NRAS*	Q61K	3	45
	Metastasis M5	*NRAS*	Q61K	3	44

Table 1. Genomic analysis of tumor nodules and metastases as well as corresponding cell lines with NGS Ampli1 CHP Custom (Menarini Silicon Biosystems) and home-made NSCLC Panel.

the successful measurement of bioluminescence of human tumors growing in the CAM[11,12]. The dynamics of primary tumor growth using a luciferase reporter was shown for PCa and osteosarcoma[12]. In our work, the primary nodule growth was visualized, similarly to others[10,17,24], by fluorescence. Microscopic evaluation of primary tumors on the CAM reveals extremely dynamic cellular interactions between fluorescent tumor cells and the microenvironment[13]. During the first days of incubation, the CAM contains three layers: the ectoderm attached to the shell membrane, the mesoderm which is enriched in blood vessels and the endoderm. At ID 10, when tumor cells are implanted, the ectoderm of the CAM is characterized by a highly developed capillary system, which is crucial for tumor seeding and dissemination. An improved technique of microscopic assessment of tumor angiogenesis confirmed these observations using CAM optical sectioning next to classic histological and fluorescent stainings[25]. Tumor cell motility and migration were visualized in the CAM using intravital imaging[10,13]. This methodology was particularly useful for studying the initial migration of cells on the CAM and required large numbers of implanted cells varying from 10^6[25] up to 8×10^6[10]. The lower cell number implanted into the CAM to follow metastatic foci formation started at 2×10^4 per egg[9]. However the most frequently used concentration of engrafted tumor cells was 2×10^6 per egg[18,26]. Here we described a protocol which requires only 10^3 tumor cells to obtain visible nodule growth on CAM and metastasis development in the chick embryo. This result highlights the sensitivity of our method and detection technique, which may have a particular importance in applications with limited number of cells. For example, this approach may be of interest to evaluate rare subpopulations of cancer stem cells or genetically modified tumorigenic subclones.

Our protocol is both highly favorable for metastasis establishment and sensitive for their detection compared to other studies using the CAM system. We adapted the number of tumor cells able to survive the period of

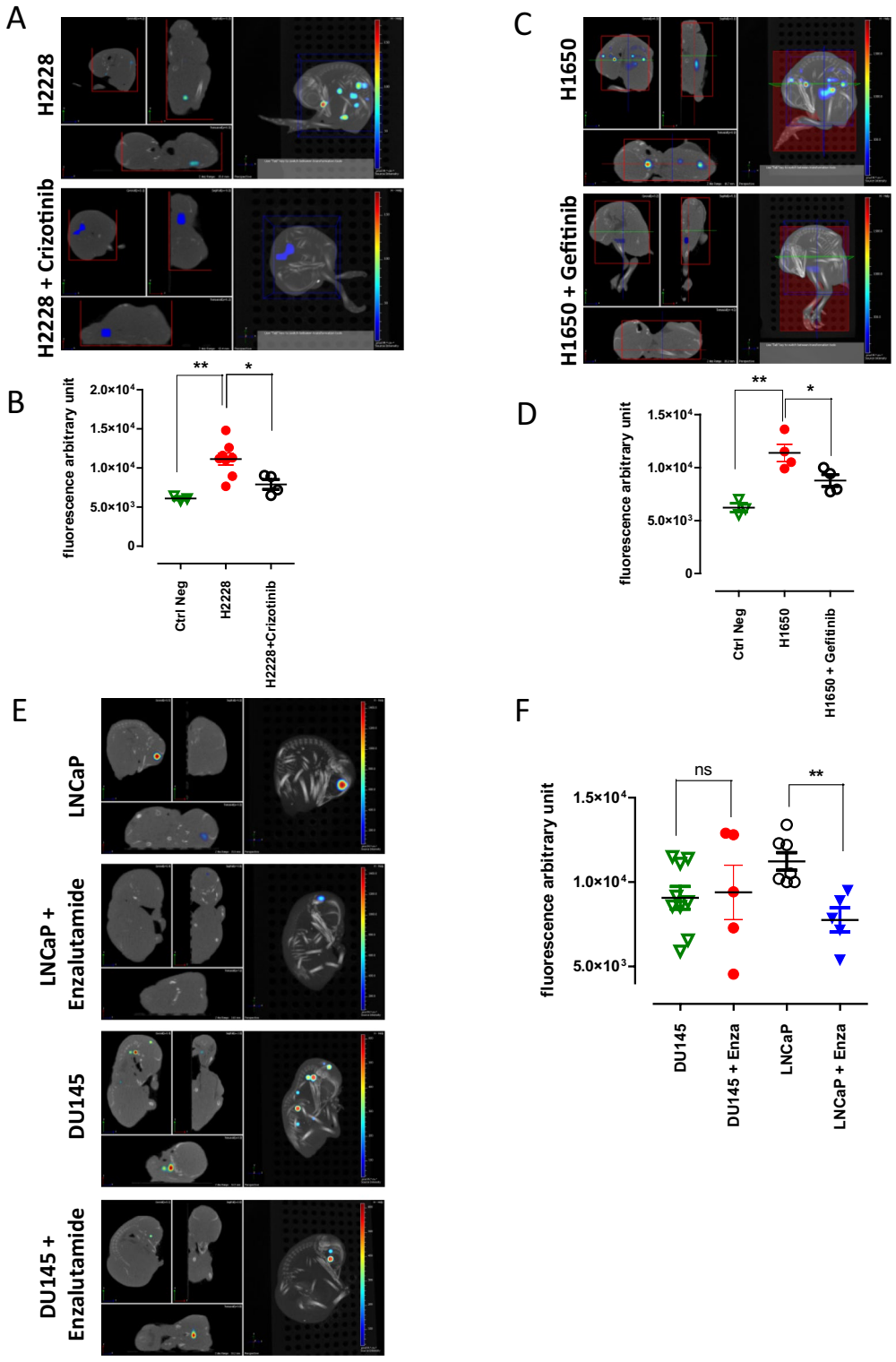


Figure 4. Effect of targeted therapies on metastasis formation. (**A**) Representative images of 3D views of chick embryos originating from eggs implanted with H2228 mCherry-expressing cells with or without crizotinib treatment. (**B**) Analysis of chick embryos coming from eggs implanted with H2228-mCherry with or without crizotinib. (**C**) Representative images of 3D views of chick embryos from eggs implanted with H1650 cells with or without gefitinib treatment. (**D**) Analysis of metastasis from eggs implanted with H1650 cells with or without gefitinib treatment. At least two separate experiments were performed for each therapeutic treatment and the graph presents the most representative one. (**E**) 3D representative images of chick embryos expressing PKH26 and originating from eggs implanted at ID 10 with LNCaP or DU145 PKH26-positive cells; with or without enzalutamide treatment. (**F**) Quantitative analysis of average fluorescence intensity from eggs implanted with PCa cells, with or without enzalutamide treatment. Each point represents a single embryo. Graph represents results obtained from two separate experiments.

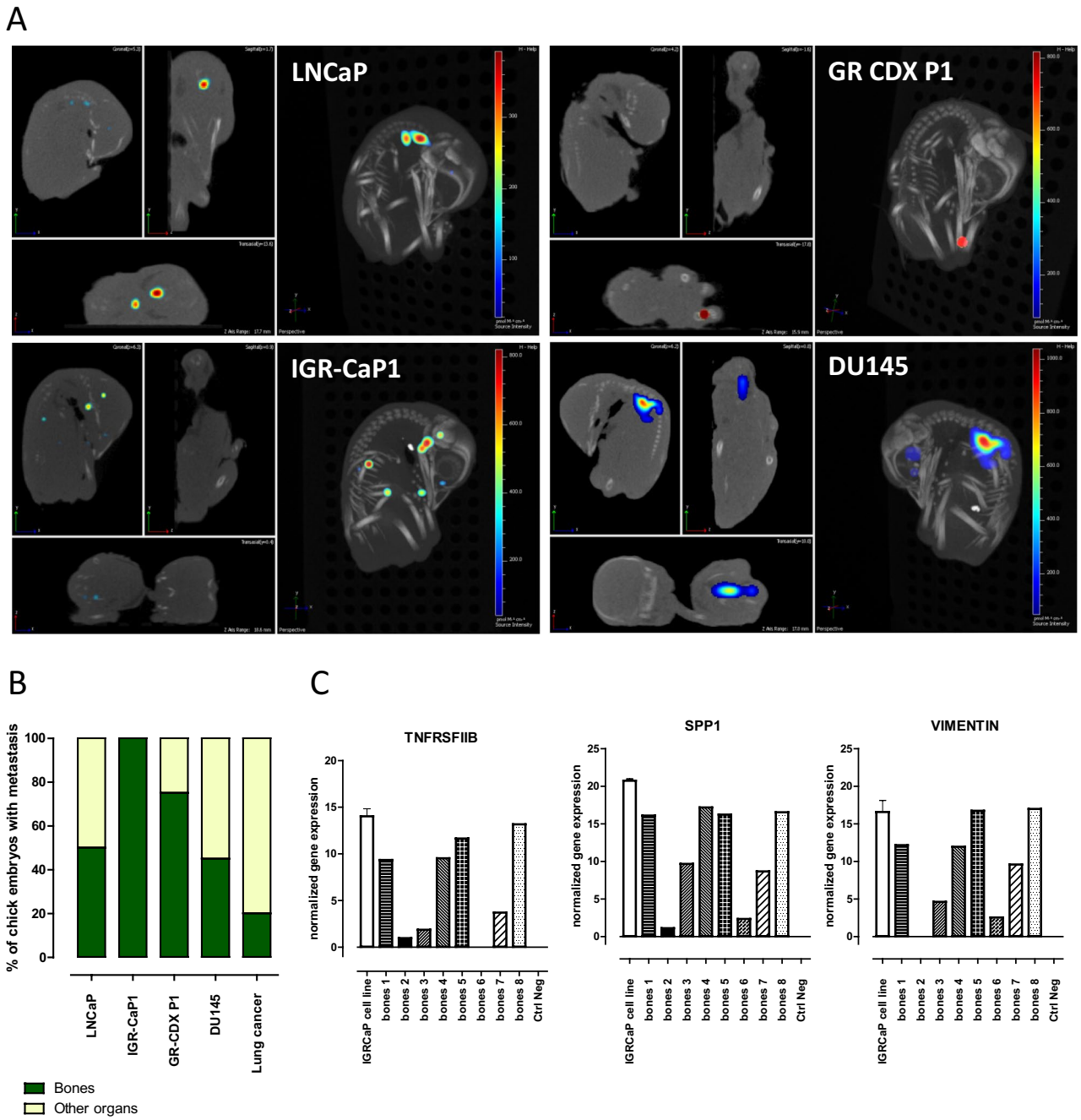


Figure 5. Prostate cancer tropism in chick embryo. (**A**) Representative examples of 3D reconstructions of chick embryos presenting bone-localized metastatic foci. (**B**) Proportions of metastatic sites recovered in bones of the chick embryo. Number of evaluated embryos for LNCaP: 10; IGR-CaP1: 13, GR-CDX P1: 8; DU145: 11; lung cancer: 28. The analysis was performed retrospectively from the images collected during different experiments using PCa cells. (**C**) qRT-PCR analysis of bones isolated from chick embryos after implantation of IGR-CaP1-GFP cells, expression of human TNFRSFIIB, SPP1 and Vimentin was normalized to negative control of bones from non-implanted chick embryos. The positive control was an in vitro collected IGR-CaP1 cell line. Experiment was performed twice with two different negative and positive controls and 4 bones tested in each.

implantation and healing using the growth factor-reduced matrigel medium. Importantly, we applied a micro-hemorrhage induction step to facilitate tumor cell migration. This procedure increases the risk of chick embryo mortality but is nonetheless crucial for stimulation of vascularization, tumor cell migration and seeding. Additionally, we noticed that a high number of rapidly proliferating cancer cells were accompanied by necrosis in the primary nodule. Evidently, the capacity to form metastatic foci is highly dependent on cell type as we showed in the case of two different lung tumor cell lines (H1299 and H2228). Although implantation conditions were

exactly the same, the two cell lines differed in metastatic seeding capacities. Finally, the sensitivity of fluorescence detection of the imaging technique used is also an important factor.

To increase our knowledge on metastatic seeding, a deeper observation into the chick embryo is required. However, due to the presence of eggshell, most visualization techniques are usually limited to the CAM and its closely attached areas. Previously reported metastasis formation in the chick embryo was evaluated by immunohistochemical analysis of organ sections[10,27–29]. Otherwise, the tumor burden was estimated by qPCR of ALU sequences from DNA of isolated organs[15,16]. Today, the chick embryo and metastatic cells may be visualized thanks to sensitive imaging modality. The first application of computer tomography (CT) was reported in 2013. CT imaging was combined with PET in order to visualize the tumor tracer uptake[30]. Another interesting report showed that tumor cells labeled with magnetic polymers might be visualized in different organs of the chick embryo using Magnetic Resonance Imaging (MRI[31]). However, this method requires an adapted contrast agent and a high number of cells to be implanted on the CAM, due to the substantial loss of signal resulting from intensive cell proliferation. In some cases, to avoid the eggshell barrier, experiments were performed *ex ovo* to present dynamic tumor cells motility by videomicroscopy[14]. In the *in ovo* experiments reported here, since fluorescence signals are undetectable throughout the eggshell, we measured metastatic foci *post mortem* inside the chick embryo using 3D fluorescence imaging. Additionally, combining fluorescence acquisition to 3D CT allowed the specific localization of metastatic foci in the embryo. It is important to state that, as observed using most *in ovo* techniques, our method does not directly address the size of tumor lesion. Indeed, backscattered signals depend on the number of fluorescent cells, the intracellular level of fluorescent protein expression and the thickness of embryo tissues. Additional imaging modality is required to fulfill this need.

We are fully aware that the model proposed here does not fully recapitulate human disease. Indeed, the metastatic process may be stimulated by the chick embryonic environment and the very short time leading to metastasis formation most likely influences the final features of tumors. However, our results highlight the potential utility of the chick embryo CAM model as an in vivo tool to assess tumor sensitivity to therapeutic compounds. Highly sensitive 3D fluorescence and CT imaging allows the localization of metastasis in the chick embryo but also gives possibilities to quantify the metastatic foci signals in comparison to negative controls or treated chick embryos. Thus the CAM system emerges as a complementary assay for drug testing.

Recently, optimization of 3D primary cultures has provided biologically relevant information on tumor growth and response to various stimuli[32]. However, the complex interactions within the organism are hardly mimicked in 3D co-culture techniques[2] and complementary preclinical tools are needed. Up until now, many successful drug tests were performed on primary nodules of the CAM and confirm utilization of this model as a reliable preclinical model for testing novel therapeutics[17,26,33]. The effect of nanoparticle-based anticancer drugs on ovarian cancer cells in the CAM model has also been reported[18]. Here we focus on targeting metastatic capacities of tumor cells in the chick embryo. First, we demonstrate the effects of common chemotherapeutics such as docetaxel and cisplatin on prostate and lung cancer metastatic growths. Then we mimicked the response of *ALK*-positive NSCLC to tyrosine kinase inhibitor crizotinib. The pharmacological growth inhibition of pancreatic ductal adenocarcinoma by crizotinib was previously reported by measuring luciferase activity in primary nodules on the CAM[11]. The possibility to use a CAM model to test targeted therapies was confirmed quantitatively using two others molecules, namely gefitinib (EGFR inhibitor) and enzalutamide (androgen receptor inhibitor) to treat eggs implanted with H1650 and LNCaP cells respectively. This suggests that, with the combination of fluorescence and 3D CT whole-embryo imaging, the chick embryo assay may serve as a rapid and efficient method to perform a first screening of potential therapeutic molecules.

One of the seldom recapitulated events in metastatic models is tumor tissue tropism[34]. Indeed, specific bone tropism of advanced PCa hardly occurs in spontaneous PCa models. Up until now, the most representative models were obtained after intracardiac or intraosseous injection of tumor cells in immunodeficient mice[35] or, as recently reported, in bioengineered mouse models with humanized bones[36]. Recently CAM xenografts from PCa were successfully established[37]. Previous studies on PCa using the CAM were based on visualization of the primary tumor and intravasation process[9]. The metastatic foci of PC3 PCa cells were found in the brain of chick embryos[17] and bone evaluation was not mentioned. In this study, the most aggressive IGR-CaP1 and GR-CDX P1 PCa cell lines preferentially formed metastases in the developing bones of the chick embryo, which suggests the relevance of the CAM in modeling PCa metastatic progression and its tropism.

Conclusion. The chick embryo model is a powerful tool to improve understanding of basic principles of metastatic colonization with new possibilities for improving precision medicine approaches for metastatic cancer patients. This report shows that the CAM model, formerly used in embryogenesis and angiogenesis studies, provides a platform for functional characterization of metastatic tumors and therapeutic compound screening approaches when combined with advanced CT and spectral imaging. Indeed, evaluation of cancer spread beyond the primary lesion using sensitive imaging technologies continues to improve today. In addition to preclinical studies, future work should focus on using the CAM as a platform to graft different primary cell and tissue types, which has already been started[6,24,37].

Methods

Cell cultures. All cell lines, except IGR-CaP1-GFP, LNCaP-GFP and GR-CDX P1-GFP, were obtained from ATCC collection and maintained in RPMI medium supplemented with 1% penicillin/streptomycin and 10% fetal bovine serum at 37 °C in 5% CO_2. LNCaP-GFP and IGR-CaP1-GFP were a gift from A Chauchereau[19,20] and GR-CDX P1-GFP cell line was established and characterized in the laboratory[23].

The chick embryo metastasis model. Fertilized chicken eggs were purchased from a certified hatchery and incubated for 3 days at 37 °C with 60% humidity. At ID 3, eggs were cleaned and a window of an approximate 2 cm-diameter was drilled into the eggshell to lower the CAM by creating an air pocket between the separated shell membrane and the CAM. This window allows to manipulate and implant the cells. Before closing it, 100 µL of penicillin (10^4 U/mL) and streptomycin (10 mg/mL) were added into the CAM. The whole procedure was performed under aseptic conditions. The window was then covered with parafilm and the egg was placed back in the incubator. At ID 10, 10^3 (unless stated differently) tumor cells per egg diluted in 20 µL of medium were mixed with 20 µL of matrigel. The mix was incubated as a drop for 30 min at 37 °C. The CAM was lacerated gently using a sterile cotton swab to facilitate engraftment, and the semisolid mix of matrigel and cells was subsequently implanted at the place of laceration into the CAM. Again the window was covered with parafilm and the egg was placed back in the incubator. Tumor growth and embryo viability were examined daily until the day of imaging analysis i.e. ID 17. At ID 17 (day 7 post-implantation) the complete analysis of tumor and embryo was performed.

Fluorescent Macroscopy imaging. Fluorescent tumor nodules were visualized in vivo using the AZ100 fluorescent macroscope (Nikon, Tokyo, JP) equipped with the NIS software. GFP- and mCherry-expressing cells in the primary tumor nodules were imaged on the CAM using Ex 482/35 nm, DM506, Em 536/40 nm and ex543/22 nm, DM562, Em593/40 filter sets respectively.

Whole 3D-chick embryo Fluorescence imaging and quantification. Chick embryos were scanned post mortem for fluorescence detection. Fluorescence and CT scans were performed simultaneously using the IVIS Spectrum Imager (PerkinElmer, MA, USA). The system is equipped with 10 narrow band excitation filters (30 nm bandwidth) and 18 narrow band emission filters (20 nm bandwidth) and gives possibility to read fluorescence in spanning wavelengths: 430–840 nm. 2D fluorescent images were acquired in epi-illumination using the adequate filters for GFP or mCherry fluorophores and displayed as an overlay of a black/white photograph and fluorescent signals. In 3D, the chick embryo was first scanned in CT before being examined in trans-illumination through 15 spots of excitation (with GFP or mCherry excitation filters) on average and covering the entire chick embryo. For 2D and 3D images, fluorescent signals were acquired with a 12-cm field of view, a binning (resolution) factor of 8, and a 2/*f* stop-and-open filter. The acquisition time was automatically computed by the software in order to obtain a minimum of 600 counts/pixel. In post-treatment using the Living Image software, tumoral fluorescent foci were reconstructed on the CT images. Regions of interest (ROI) were then defined manually on images (using an adapted to embryo size area in each case), and signal intensities were calculated using the Living Image software (PerkinElmer, MA, USA) and expressed as radiant efficiency or absorbance for 2D or 3D respectively.

Histochemistry. After imaging, the CAM tumor nodules were collected and fixed in 4% PFA (Electron Microscopy Sciences, Hatfield, PA) and embedded in paraffin after tissue processing. Serial 7-µm paraffin sections were processed and routinely stained with hematoxylin-eosin-safranin (HES). Immunohistochemistry staining was performed with antibodies mouse monoclonal anti-human Ki-67 (MIB 1; Dako M724001) and anti-human Vimentin (Roche, 790-2917).

Isolation of genomic DNA from cells and tumor samples. Nodules and metastases from H1299 and H1975 cells were collected at ID 17. DNA from control cell lines, tumor nodules from the CAM and metastasis from chick embryo organs were isolated according to manufacturer protocols using DNeasy Blood and tissue Kit (Qiagen).

Targeted next-generation sequencing. The extracted DNA was subjected to sequencing on selected amplicons for representative genes; the detailed process was described previously[38]. Two targeted panels were used: the Ampli1 Cancer Hotspot Panel Custom Beta adapted from Ion Ampliseq CHP v2 by Menarini Silicon Biosystems covering 2,265 COSMIC hotspots regions across 315 amplicons of 48 cancer-related genes and an in-house panel targeting the tyrosine kinase domain in *ALK* and *EGFR* genes. Sequencing was performed using appropriate Ion chips for the IonPersonal Genome Machine or the Ion S5 System.

RNA extraction and qRT-PCR analysis. RNA was extracted from 10^6 IGR-CaP1 cells for positive control and collected at ID 17 from chick embryo bones in which in the 3D scan imaging the fluorescent signal was overlapping with the CT image of bone. Bones were purified from muscle and connected tissue, then bone marrow was flushed and empty bone was crushed and put together with the bone marrow. RNA extraction was performed according to manufacturer protocol using RNAsy MicroKit (Qiagen) and reverse-transcribed using the Maxima First Strand cDNA Synthesis Kit (Thermo Scientific, K1622). qRT-PCR was performed using TaqMan Universal Master Mix (Applied Biosystems, Roche) and a CFX96 Touch Real-Time PCR Detection System (Bio-Rad). The TaqMan primers were obtained from Applied Biosystems (TNFRSF11B/OPG, Hs00900358_ml; SPP1/osteopontin, Hs00959010_ml; Vimentin, Hs00185584_ml) and were used as previously described[19].

Stable cell lines expressing mCherry. The stable tumor cell lines expressing mCherry were established after infection with mCherry-expressing retroviral vectors (plasmid: IRES-mCherry #80139, Addgene Teddington, UK). Production and titration of retroviral particles were performed as described [39]. The infection was

performed on retronectin-coated plates (TaKaRa Bio, CA, USA) and efficiency was assayed by testing mCherry expression using flow cytometry. When efficiency was below 98%, cell sorting was performed.

PKH26 staining. PKH26 linker was purchased from Sigma (St.Louis, MO) and staining was performed according to manufacturer protocol. Briefly, 10^6 cells were washed with PBS and resuspended in 500 µL of diluent buffer. 2 × Dye solution (500 nM) was prepared in 500 µL of diluent buffer. Two solutions were mixed and incubated 4 min at room temperature. Reaction was stopped by adding 1 mL of serum. Cells were subsequently washed and prepared for implantation. 2×10^5 stained cells were incubated in vitro in standard culture conditions in order to verify the fluorescence signal daily throughout the experiment (7 days).

Treatments. For dose determination, the viability of chick embryos and morphology-altering effects were systematically investigated, as reported elsewhere (11, 18, 26, 31). Cisplatin was tested at the doses of 50 µg/kg, 30 µg/kg and 10 µg/kg. Doses of 50 and 30 µg/kg were toxic for chick embryos (100% of embryos died at ID 15). All embryos were alive and no influence on their development was observed at the dose of 10 µg/kg which was selected for drug-assays. Docetaxel was tested at doses of 20, 10 and 2 µg/kg. Doses of 20 and 10 µg/kg were toxic for chick embryos and the 2 µg/kg dose was selected. Gefitinib and crizotinib were tested with doses of 20, 10 and 2 mg/kg. Important toxicity was observed with gefitinib doses of 20 mg/kg and 10 mg/kg (50% and 40% of embryos died respectively), and crizotinib dose of 20 mg/kg (60%). An important teratogenic effect was observed in 50% of eggs at crizotinib dose of 10 mg/kg. Dose of 2 mg/kg was selected for both gefitinib and crizotinib. Enzalutamide was toxic for chick embryos at 1 mg/kg (80%). The 400 µg/kg dose did not produce side effects and was selected. Tested eggs were monitored daily throughout the experiment. Chick embryo mobility as well as increasing vascularization of the CAM (the two indicators of chick embryo viability) were evaluated and compared to non-treated eggs.

Tumors originating from LNCaP, H1299, A549 cell lines were treated 24 h after cell implantation with vehicle, 2 µg/kg docetaxel, or 10 µg/kg cisplatin respectively. Tumors originating from H2228, H1650, DU145 and LNCaP were treated daily from ID 11 up to ID 16 with vehicle, 2 mg/kg crizotinib, 2 mg/kg gefitinib, or 400 µg/kg enzalutamide. The drug was administered topically on the CAM, near the tumor nodule and the final doses were calculated based on the weight of the chicken egg at ID 10.

Statistical analysis. Data are shown as means and standard error of the mean (SEM), and P values are reported as follows: $^*P < 0.05$, $^{**}P < 0.01$, and $^{***}P < 0.001$. Statistical analysis was performed using the GraphPad Prism software, version 6.0 (GraphPad Software, San Diego, CA). Data were analyzed using nonparametric Mann–Whitney test.

Received: 29 January 2020; Accepted: 16 September 2020
Published online: 09 October 2020

References

1. Hidalgo, M. *et al.* Patient-derived xenograft models: an emerging platform for translational cancer research. *Cancer Discov.* **4**, 998–1013. https://doi.org/10.1158/2159-8290.CD-14-0001 (2014).
2. Candini, O. *et al.* A novel 3D in vitro platform for pre-clinical investigations in drug testing, gene therapy, and immuno-oncology. *Sci. Rep.* **9**, 7154. https://doi.org/10.1038/s41598-019-43613-9 (2019).
3. Murphy, J. B. & Rous, P. The behavior of chicken sarcoma implanted in the developing embryo. *J. Exp. Med.* **15**, 119–132. https://doi.org/10.1084/jem.15.2.119 (1912).
4. Kain, K. H. *et al.* The chick embryo as an expanding experimental model for cancer and cardiovascular research. *Dev. Dyn.* **243**, 216–228. https://doi.org/10.1002/dvdy.24093 (2014).
5. Stehelin, D., Varmus, H. E., Bishop, J. M. & Vogt, P. K. DNA related to the transforming gene(s) of avian sarcoma viruses is present in normal avian DNA. *Nature* **260**, 170–173. https://doi.org/10.1038/260170a0 (1976).
6. Dohle, D. S. *et al.* Chick ex ovo culture and ex ovo CAM assay: how it really works. *J. Vis. Exp.* https://doi.org/10.3791/1620 (2009).
7. Uloza, V. *et al.* Effect of laryngeal squamous cell carcinoma tissue implantation on the chick embryo chorioallantoic membrane: morphometric measurements and vascularity. *Biomed. Res. Int.* **2015**, 629754. https://doi.org/10.1155/2015/629754 (2015).
8. Chambers, A. F., Shafir, R. & Ling, V. A model system for studying metastasis using the embryonic chick. *Cancer Res.* **42**, 4018–4025 (1982).
9. Kunzi-Rapp, K. *et al.* Chorioallantoic membrane assay: vascularized 3-dimensional cell culture system for human prostate cancer cells as an animal substitute model. *J. Urol.* **166**, 1502–1507. https://doi.org/10.1016/s0022-5347(05)65820-x (2001).
10. Deryugina, E. I. & Quigley, J. P. Chick embryo chorioallantoic membrane model systems to study and visualize human tumor cell metastasis. *Histochem. Cell. Biol.* **130**, 1119–1130. https://doi.org/10.1007/s00418-008-0536-2 (2008).
11. Rovithi, M. *et al.* Development of bioluminescent chick chorioallantoic membrane (CAM) models for primary pancreatic cancer cells: a platform for drug testing. *Sci. Rep.* **7**, 44686. https://doi.org/10.1038/srep44686 (2017).
12. Jefferies, B. *et al.* Non-invasive imaging of engineered human tumors in the living chicken embryo. *Sci. Rep.* **7**, 4991. https://doi.org/10.1038/s41598-017-04572-1 (2017).
13. Zijlstra, A., Lewis, J., Degryse, B., Stuhlmann, H. & Quigley, J. P. The inhibition of tumor cell intravasation and subsequent metastasis via regulation of in vivo tumor cell motility by the tetraspanin CD151. *Cancer Cell* **13**, 221–234. https://doi.org/10.1016/j.ccr.2008.01.031 (2008).
14. Stoletov, K. *et al.* Quantitative in vivo whole genome motility screen reveals novel therapeutic targets to block cancer metastasis. *Nat. Commun.* **9**, 2343. https://doi.org/10.1038/s41467-018-04743-2 (2018).
15. Zijlstra, A. *et al.* A quantitative analysis of rate-limiting steps in the metastatic cascade using human-specific real-time polymerase chain reaction. *Cancer Res.* **62**, 7083–7092 (2002).
16. Palmer, T. D., Lewis, J. & Zijlstra, A. Quantitative analysis of cancer metastasis using an avian embryo model. *J. Vis. Exp.* https://doi.org/10.3791/2815 (2011).

17. Menen, R. *et al.* Inhibition of metastasis of circulating human prostate cancer cells in the chick embryo by an extracellular matrix produced by foreskin fibroblasts in culture. *Anticancer Res.* **32**, 1573–1577 (2012).
18. Vu, B. T. *et al.* Chick chorioallantoic membrane assay as an in vivo model to study the effect of nanoparticle-based anticancer drugs in ovarian cancer. *Sci. Rep.* **8**, 8524. https://doi.org/10.1038/s41598-018-25573-8 (2018).
19. Al Nakouzi, N. *et al.* The IGR-CaP1 xenograft model recapitulates mixed osteolytic/blastic bone lesions observed in metastatic prostate cancer. *Neoplasia* **14**, 376–387. https://doi.org/10.1593/neo.12308 (2012).
20. Al Nakouzi, N. *et al.* Targeting CDC25C, PLK1 and CHEK1 to overcome Docetaxel resistance induced by loss of LZTS1 in prostate cancer. *Oncotarget* **5**, 667–678. https://doi.org/10.18632/oncotarget.1574 (2014).
21. Yang, F. *et al.* Combination of quercetin and 2-methoxyestradiol enhances inhibition of human prostate cancer LNCaP and PC-3 cells xenograft tumor growth. *PLoS ONE* **10**, e0128277. https://doi.org/10.1371/journal.pone.0128277 (2015).
22. Li, M. *et al.* Inhibition of AMPK-related kinase 5 (ARK5) enhances cisplatin cytotoxicity in non-small cell lung cancer cells through regulation of epithelial-mesenchymal transition. *Am. J. Transl. Res.* **9**, 1708–1719 (2017).
23. Faugeroux, V. *et al.* Genetic characterization of a unique neuroendocrine transdifferentiation prostate circulating tumor cell-derived eXplant model. *Nat. Commun.* **11**, 1884. https://doi.org/10.1038/s41467-020-15426-2 (2020).
24. Moreno-Jimenez, I. *et al.* The chorioallantoic membrane (CAM) assay for the study of human bone regeneration: a refinement animal model for tissue engineering. *Sci. Rep.* **6**, 32168. https://doi.org/10.1038/srep32168 (2016).
25. Mangir, N., Raza, A., Haycock, J. W., Chapple, C. & Macneil, S. An improved in vivo methodology to visualise tumour induced changes in vasculature using the chick chorionic allantoic membrane assay. *In Vivo* **32**, 461–472. https://doi.org/10.21873/invivo.11262 (2018).
26. Swadi, R. *et al.* Optimising the chick chorioallantoic membrane xenograft model of neuroblastoma for drug delivery. *BMC Cancer* **18**, 28. https://doi.org/10.1186/s12885-017-3978-x (2018).
27. Ossowski, L. In vivo invasion of modified chorioallantoic membrane by tumor cells: the role of cell surface-bound urokinase. *J Cell Biol* **107**, 2437–2445. https://doi.org/10.1083/jcb.107.6.2437 (1988).
28. Cimpean, A. M., Ribatti, D. & Raica, M. The chick embryo chorioallantoic membrane as a model to study tumor metastasis. *Angiogenesis* **11**, 311–319. https://doi.org/10.1007/s10456-008-9117-1 (2008).
29. Liu, M. *et al.* The histone methyltransferase EZH2 mediates tumor progression on the chick chorioallantoic membrane assay, a novel model of head and neck squamous cell carcinoma. *Transl. Oncol.* **6**, 273–281. https://doi.org/10.1593/tlo.13175 (2013).
30. Warnock, G. *et al.* In vivo PET/CT in a human glioblastoma chicken chorioallantoic membrane model: a new tool for oncology and radiotracer development. *J. Nucl. Med.* **54**, 1782–1788. https://doi.org/10.2967/jnumed.112.117150 (2013).
31. Herrmann, A., Taylor, A., Murray, P., Poptani, H. & See, V. Magnetic resonance imaging for characterization of a chick embryo model of cancer cell metastases. *Mol. Imaging* **17**, 1536012118809585. https://doi.org/10.1177/1536012118809585 (2018).
32. Padhye, A. *et al.* A novel ex vivo tumor system identifies Src-mediated invasion and metastasis in mesenchymal tumor cells in non-small cell lung cancer. *Sci. Rep.* **9**, 4819. https://doi.org/10.1038/s41598-019-41301-2 (2019).
33. Pink, D. *et al.* High efficacy vasopermeability drug candidates identified by screening in an ex ovo chorioallantoic membrane model. *Sci. Rep.* **5**, 15756. https://doi.org/10.1038/srep15756 (2015).
34. Berish, R. B., Ali, A. N., Telmer, P. G., Ronald, J. A. & Leong, H. S. Translational models of prostate cancer bone metastasis. *Nat. Rev. Urol.* **15**, 403–421. https://doi.org/10.1038/s41585-018-0020-2 (2018).
35. Power, C. A. *et al.* A novel model of bone-metastatic prostate cancer in immunocompetent mice. *Prostate* **69**, 1613–1623. https://doi.org/10.1002/pros.21010 (2009).
36. Landgraf, M. *et al.* Humanized bone facilitates prostate cancer metastasis and recapitulates therapeutic effects of zoledronic acid in vivo. *Bone Res.* **7**, 31. https://doi.org/10.1038/s41413-019-0072-9 (2019).
37. Hu, J. *et al.* Establishment of xenografts of urological cancers on chicken chorioallantoic memebrane (CAM) to study metastasis. *Precis. Clin. Med.* **2**, 140–151 (2019).
38. Pailler, E. *et al.* Acquired resistance mutations to ALK inhibitors identified by single circulating tumor cell sequencing in ALK-rearranged non-small-cell lung cancer. *Clin. Cancer Res.* **25**, 6671–6682. https://doi.org/10.1158/1078-0432.CCR-19-1176 (2019).
39. Hamelin, V., Letourneux, C., Romeo, P. H., Porteu, F. & Gaudry, M. Thrombopoietin regulates IEX-1 gene expression through ERK-induced AML1 phosphorylation. *Blood* **107**, 3106–3113. https://doi.org/10.1182/blood-2005-07-2953 (2006).

Acknowledgments

The authors thank Helene Rocheteau from the Experimental and Translational Platform of Pathology AMMICa INSERM US23/UMS CNRS3655 for help in experimental work. The authors also thank Menarini Silicon Biosystems particularly Nicolò Manaresi to provide us the Ampli1 Cancer Hotspot Panel Custom Beta.

Author contributions

Conceptualization: P.P. and F.F.; Experimental work: P.P., T.T., M.O., A.A., V.F., A.L.P.; A.H., V.M., O.B.; Data analysis and interpretation: P.P.; V.R.; C.L.B.; M.O.; V.F. JY. S.; Funding Acquisition: F.F.; Supervision: F.F.; Writing: P.P. and F.F.; Revising manuscript content: P.P.; T.T.; M.O.; V.F.; V.R.; A.A.; A.L.P; A.C.; L.L.; JY. S.; C.L.B.; F.F.

Competing interests

The authors declare no competing interests.

Additional information

Supplementary information is available for this paper at https://doi.org/10.1038/s41598-020-73632-w.

Correspondence and requests for materials should be addressed to F.F.

Reprints and permissions information is available at www.nature.com/reprints.

Publisher's note Springer Nature remains neutral with regard to jurisdictional claims in published maps and institutional affiliations.

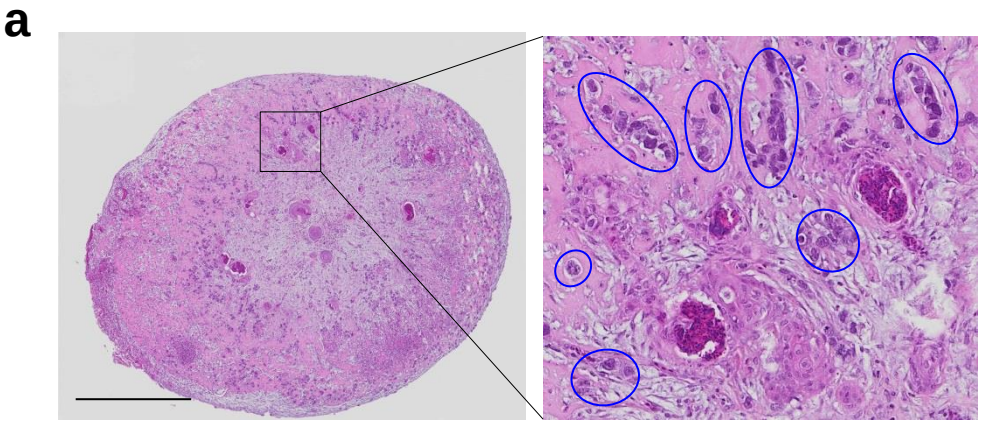
Open Access This article is licensed under a Creative Commons Attribution 4.0 International License, which permits use, sharing, adaptation, distribution and reproduction in any medium or format, as long as you give appropriate credit to the original author(s) and the source, provide a link to the Creative Commons licence, and indicate if changes were made. The images or other third party material in this article are included in the article's Creative Commons licence, unless indicated otherwise in a credit line to the material. If material is not included in the article's Creative Commons licence and your intended use is not permitted by statutory regulation or exceeds the permitted use, you will need to obtain permission directly from the copyright holder. To view a copy of this licence, visit http://creativecommons.org/licenses/by/4.0/.

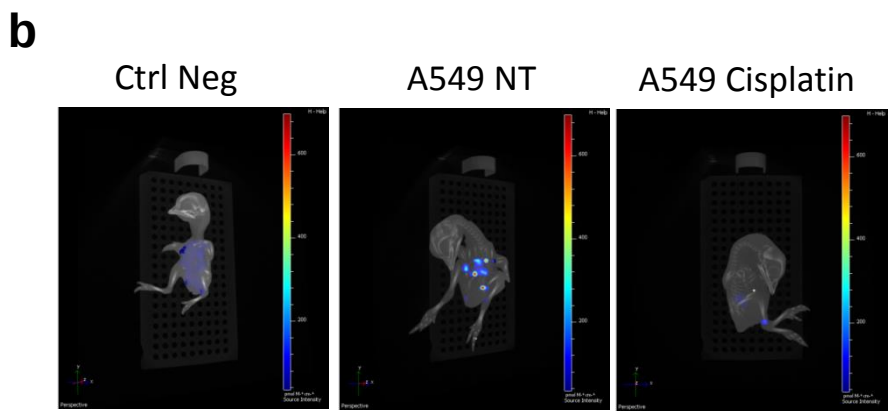
© The Author(s) 2020

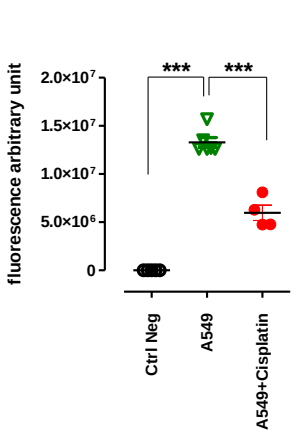
Exploitation of the chick embryo chorioallantoic membrane (CAM) as a platform for anti-metastatic drug testing

Pawlikowska P, Tayoun T, Oulhen M, Faugeroux V, Rouffiac V, Aberlenc A, Pommier AL, Honore A, Marty V, Bawa O, Lacroix L, Scoazec JY, Chauchereau A, Laplace-Builhe C, Farace F

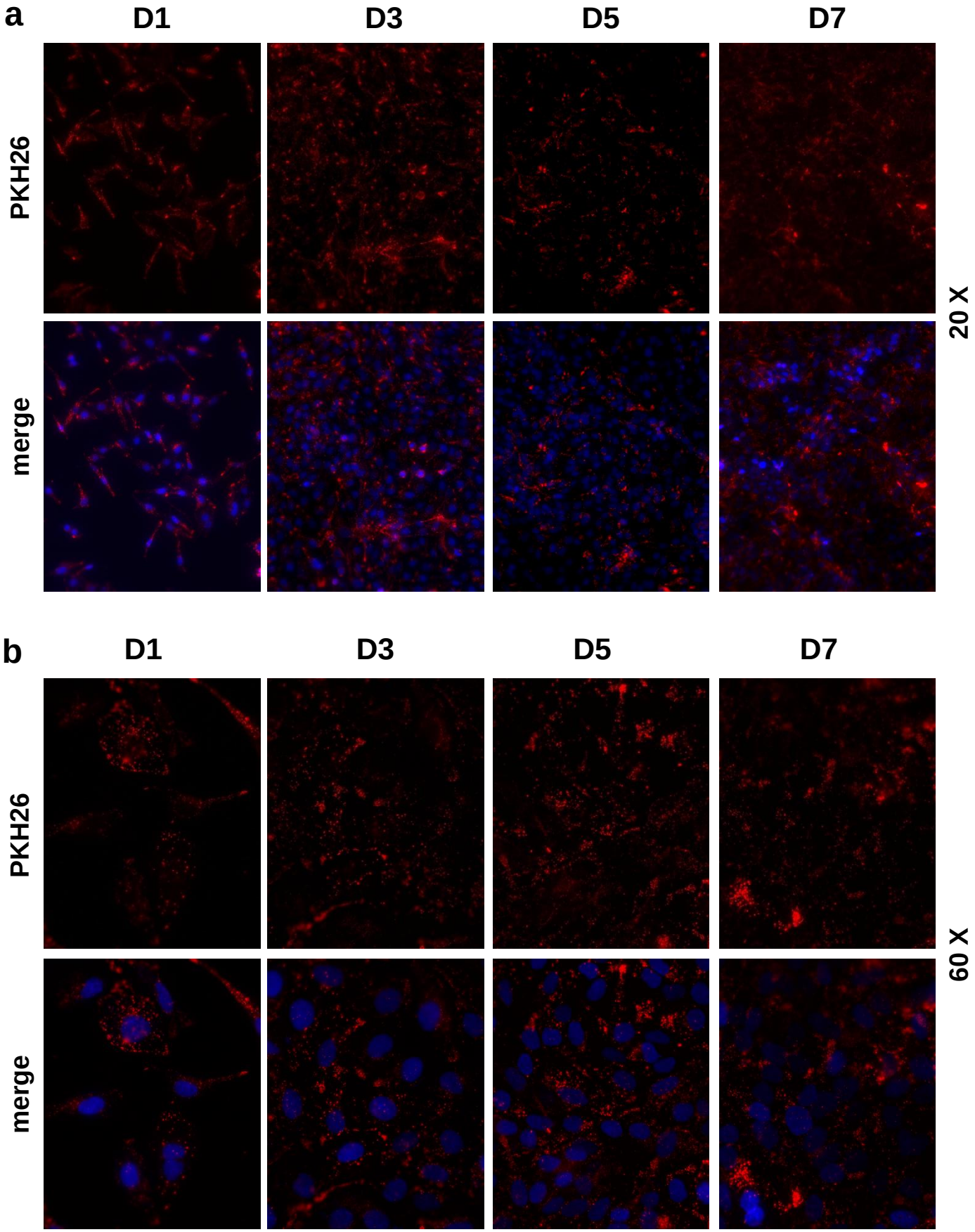
Supplementary Material



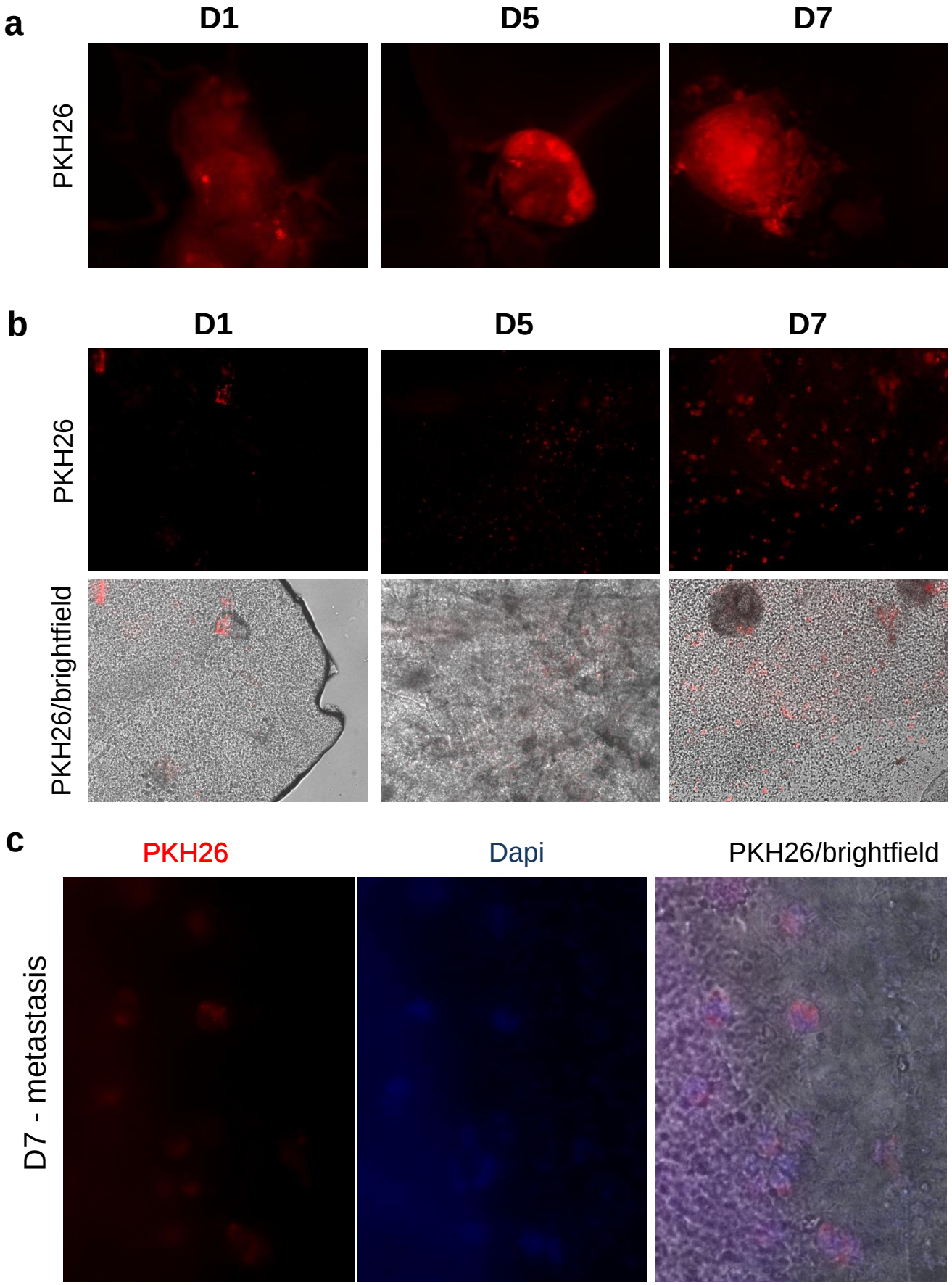




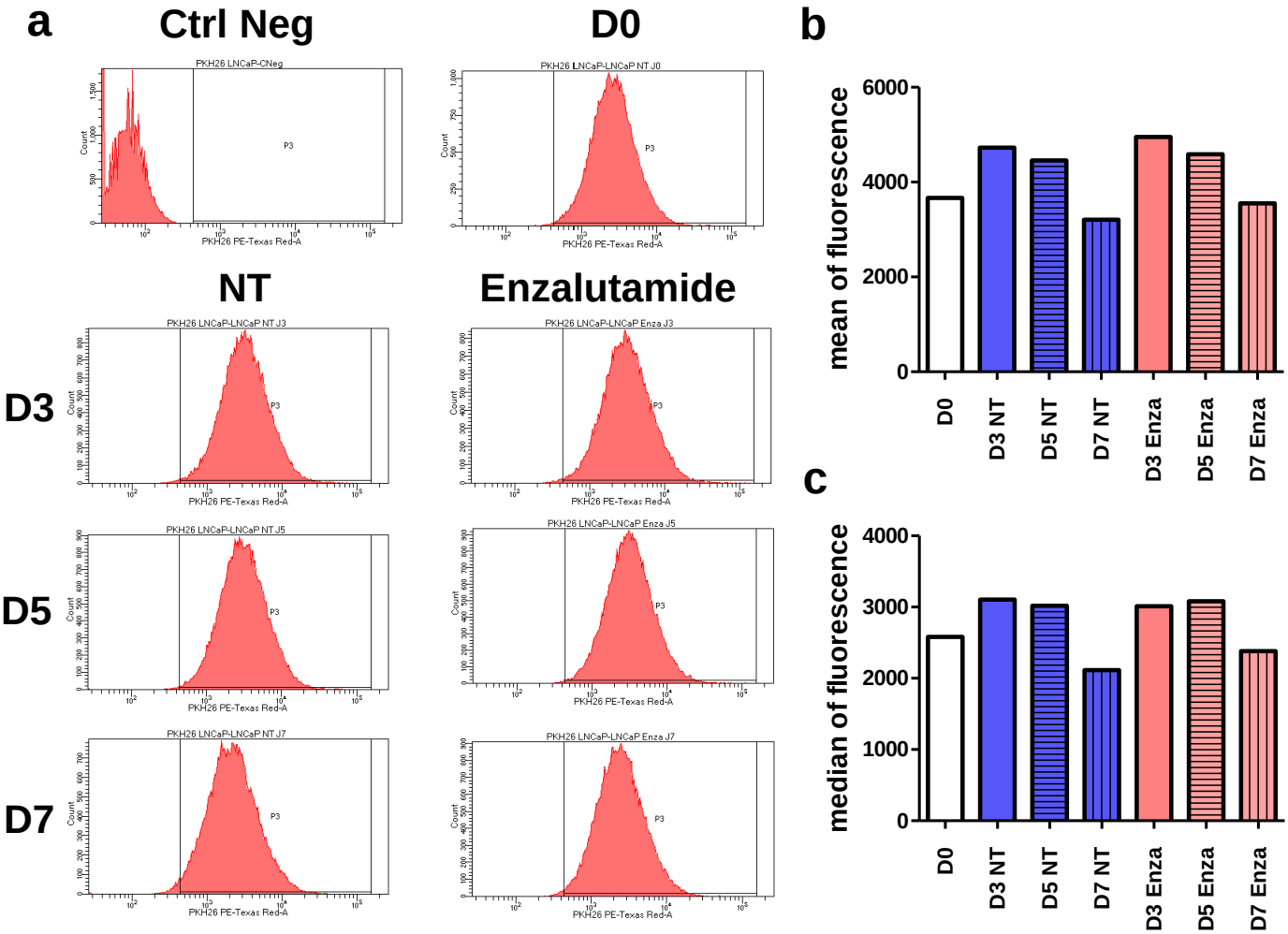
Supplementary Figure 1.



Supplementary Figure 2.



Supplementary Figure 3.



Supplementary Figure 4.

Supplementary Figures

Fig. 1. a. Tumor nodules of H1299-GFP, FFPE sections stained with HES. Areas with tumor cells were framed. b. Representative images of fluorescent metastatic foci formed by A549 mCherry cells with or without cisplatin treatment. c. Quantitative analysis of mean fluorescence from 3D analysis of chick embryos after implantation of A549 mCherry cells. Experiment was performed twice and the representative one is shown. Each point represents a single embryo.

Fig. 2. Representative images showing the pattern and intensity of PKH26 staining during 7 days of *in vitro* culture of LNCaP cell line. Magnification 20x a, and 60x b. Images were captured using NIS Elements software Version 4.0; AR Ver4.00.05 for 64bit edition (Nikon Instruments Inc., https://www.microscope.healthcare.nikon.com/products/software/nis-elements).

Fig. 3. Representative images showing a. tumor nodules obtained from LNCaP stained with PKH26 and collected at different time-points; examined *in vivo* by a fluorescence macroscope. Images were captured using NIS Elements software Version 3.2; BR Ver for 64bit edition (Nikon Instruments Inc., https://www.microscope.healthcare.nikon.com/products/software/nis-elements). b. PKH26 fluorescent cells presented in tumor nodules using fluorescent microscope (20x) with the corresponding bright field images. c. Example of metastatic foci in esophagus inner membrane of chick embryo 7 days after implantation of LNCaP cells stained with PKH26. Images obtained using fluorescent microscope (20x) with the corresponding bright field images. Images were captured using NIS Elements software Version 4.0; AR Ver4.00.05 for 64bit edition (Nikon Instruments Inc., https://www.microscope.healthcare.nikon.com/products/software/nis-elements).

Fig. 4. *In vitro* analysis of LNCaP cells stained at D0 with PKH26 and treated or not with enzalutamide (500 nM) during 7 days. PKH26 fluorescence intensity was measured by FACS. a. FACS histograms showing PKH26 fluorescence at different days of the experiment and negative control presenting non-stained cells. b. Graph representing mean of PKH26 fluorescence at each day of experiment. c. Graph representing median of PKH26 fluorescence at each day of experiment.

Cell line	Tumor type	alteration	origin
NCI-H1299	Large cell carcinoma	NRAS Q61K	ATCC
NCI-H1975	Non-small cell lung carcinoma	EGFR T790M EGFR L858R TP53 R273H CDKN2A E69*	ATCC
A549	Non-small cell lung carcinoma	KRAS G12S	ATCC
NCI-H2228	Non-small cell lung carcinoma	EML4-ALK fusion	ATCC
NCI-H1650	Non-small cell lung carcinoma	EGFR delE746-A750	ATCC
LNCaP	Prostate carcinoma Androgen receptor positive	PTEN loss	ATCC
DU145	Prostate carcinoma Androgen-independent	8q gain	ATCC
IGR-CaP1	Prostate carcinoma	TP53 Y126C	[19]Al Nakouzi *et al.* 2012
GR-CDX P1	Prostate carcinoma	TP53, RB1, PTEN loss	[23]Faugeroux *et al.* 2020

Supplementary Table 1. List of used cell lines with their short characteristics.

Fluorescent protein/dye	**Excitation** (nm)	**Emission** (nm)	**Advantages in context of CAM model**	**Disadvantages in context of CAM model**
GFP	465	520	Very stable and non-toxic	Sensitivity of fluorescent imaging is limited by strong and heterogeneous auto-fluorescence signal of the chick embryo
mCherry	570	620	Compatible with deep imaging, low auto-fluorescent background, resistant to photo-bleaching	Possibly less stable than GFP
PKH26	535	580	Compatible with deep, imaging, low auto-fluorescent background, useful for *in vivo* long-lasting studies (here 7 days), compatible with 3D IVIS Spectrum Imaging	Toxicity, required dose adaptation to cell/tissue types, Localized in lipid regions of the intracellular membranes

Supplementary Table 2. Advantages and disadvantages of used fluorescent markers in the contexts of the CAM model.

JCI insight

Targeting genome integrity dysfunctions impedes metastatic potency in non–small cell lung cancer circulating tumor cell–derived explants

Tala Tayoun,[1,2] Vincent Faugeroux,[1,2] Marianne Oulhen,[1,2] Olivier Déas,[3] Judith Michels,[4] Laura Brulle-Soumare,[3] Stefano Cairo,[3] Jean-Yves Scoazec,[5] Virginie Marty,[5] Agathe Aberlenc,[1,2] David Planchard,[4] Jordi Remon,[6] Santiago Ponce,[2,4] Benjamin Besse,[4] Patricia L. Kannouche,[7] Jean-Gabriel Judde,[3] Patrycja Pawlikowska,[2] and Françoise Farace[1,2]

[1]Gustave Roussy, Paris-Saclay University, "Circulating Tumor Cells" Translational Platform, CNRS UMS3655 – INSERM US23 AMMICA, Villejuif, France. [2]INSERM, U981 "Identification of Molecular Predictors and new Targets for Cancer Treatment", Villejuif, France. [3]XenTech, Evry, France. [4]Gustave Roussy, Paris-Saclay University, Department of Cancer Medicine, Villejuif, France. [5]Gustave Roussy, Paris-Saclay University, "Histo-Cytopathology" Translational Platform, CNRS UMS3655 – INSERM US23 AMMICA, Villejuif, France. [6]Department of Medical Oncology, Clara Campal Comprehensive Oncology Center (HM-CIOCC), Hospital HM New Delphi, HM Hospitals, Barcelona, Spain. [7]Paris-Saclay University, CNRS UMR9019 "Genome Integrity and Cancers", Gustave Roussy, Villejuif, France.

DNA damage and genomic instability contribute to non–small cell lung cancer (NSCLC) etiology and progression. However, their therapeutic exploitation is disappointing. CTC-derived explants (CDX) offer systems for mechanistic investigation of CTC metastatic potency and may provide rationale for biology-driven therapeutics. Four CDX models and 3 CDX-derived cell lines were established from NSCLC CTCs and recapitulated patient tumor histology and response to platinum-based chemotherapy. CDX (GR-CDXL1, GR-CDXL2, GR-CDXL3, GR-CDXL4) demonstrated considerable mutational landscape similarity with patient tumor biopsy and/or single CTCs. Truncal alterations in key DNA damage response (DDR) and genome integrity–related genes were prevalent across models and assessed as therapeutic targets in vitro, in ovo, and in vivo. GR-CDXL1 presented homologous recombination deficiency linked to biallelic *BRCA2* mutation and *FANCA* deletion, unrepaired DNA lesions after mitosis, and olaparib sensitivity, despite resistance to chemotherapy. SLFN11 overexpression in GR-CDXL4 led to olaparib sensitivity and was in coherence with neuroendocrine marker expression in patient tumor biopsy, suggesting a predictive value of SLFN11 in NSCLC histological transformation into small cell lung cancer (SCLC). Centrosome clustering promoted targetable chromosomal instability in GR-CDXL3 cells. These CDX unravel DDR and genome integrity–related defects as a central mechanism underpinning metastatic potency of CTCs and provide rationale for their therapeutic targeting in metastatic NSCLC.

Introduction

Advanced non–small cell lung cancer (NSCLC) has a poor prognosis, owing to severe metastatic spread and acquired treatment resistance, with no curative therapy (1). Over the past 2 decades, genomic profiling has become a standard diagnostic tool in NSCLC and the implementation of targeting oncogenic alterations of tyrosine kinases (e.g., epidermal growth factor receptor [EGFR], anaplastic lymphoma kinase [*ALK*] or c-ros oncogene 1 [*ROS1*] fusions) has demonstrated unprecedented clinical benefits in corresponding patient subsets (2). In the majority of advanced-stage NSCLC lacking targetable mutations, platinum-based chemotherapy remains a cornerstone in first-line treatment, with or without immunotherapy (3). DNA damage and genome instability in response to mutagenic insults in NSCLC have received considerable attention and represent an attractive therapeutic target (4). Synthetic lethality approaches to cancer therapy and the clinical development of poly(ADP-ribose) polymerase inhibitors (PARPi) have been a major breakthrough in the treatment of *BRCA1/2*-mutant cancers (5, 6) (ovary,

Authorship note: TT and VF contributed equally to the work. PP and FF contributed equally to the work.

Conflict of interest: DP provides consulting, an advisory role, or lectures for the following: AstraZeneca, Bristol-Myers Squibb, Boehringer Ingelheim, Celgene, Daiichi Sankyo, Eli Lilly, Merck, Novartis, Pfizer, prIME Oncology, Peer CME, Roche, and Samsung. DP has honoraria for the following: AstraZeneca, Bristol-Myers Squibb, Boehringer Ingelheim, Celgene, Eli Lilly, Merck, Novartis, Pfizer, prIME Oncology, Peer CME, Roche, and Samsung. DP has done clinical trials research for the following: AstraZeneca, Bristol-Myers Squibb, Boehringer Ingelheim, Eli Lilly, Merck, Novartis, Pfizer, Roche, Medimmun, Sanofi-Aventis, Taiho Pharma, Novocure, and Daiichi Sankyo. DP has traveled for and/or received accommodations and had expenses paid from the following: AstraZeneca, Roche, Novartis, prIME Oncology, and Pfizer. BB has sponsored research at Gustave Roussy Cancer Center, as well as 4D Pharma, Abbvie, Amgen, Aptitude Health, AstraZeneca, BeiGene, Blueprint Medicines, BMS, Boehringer Ingelheim, Celgene, Cergentis, Cristal Therapeutics, Daiichi-Sankyo, Eli Lilly, GSK, Inivata, Janssen, Onxeo, OSE immunotherapeutics, Pfizer, Roche-Genentech, Sanofi, Takeda, and Tolero Pharmaceuticals.

Copyright: © 2022, Tayoun et al. This is an open access article published under the terms of the Creative Commons Attribution 4.0 International License.

Submitted: October 21, 2021
Accepted: April 27, 2022
Published: May 5, 2022

Reference information: *JCI Insight*. 2022;7(11):e155804. https://doi.org/10.1172/jci.insight.155804.

breast, pancreas, and prostate) and are highly effective in potentiating chemotherapy, based on the biological rationale that the deficiency in DNA repair machinery modulates tumor response to platinum chemotherapy (7–10). However, clinical studies assessing PARPi efficacy either in combination with chemotherapy or as maintenance treatment have failed to yield any significant benefit in chemosensitive NSCLC tumors with or without *BRCA* mutations (11, 12).

Genome integrity is constantly threatened by different types of DNA lesions, with DNA double-stranded breaks (DSBs) being the most cytotoxic and mainly repaired by homologous recombination (HR) (13). Failure to resolve DSBs owing to loss-of-function mutations in genes encoding key players in the DNA damage response (DDR) — such as *BRCA1*, *BRCA2* — and HR deficiency (HRD) has paved the way toward DDR-directed therapeutic strategies in several cancers (6). Although *BRCA* mutations are not very common in NSCLC, *BRCAness* — a state of defect in the DNA repair machinery mimicking *BRCA1*/*BRCA2* loss — has been reported several times in NSCLC. However, its therapeutic implications remain to be elucidated (14). To this end, in-depth mechanistic understanding of DDR mechanisms contributing to genome stability maintenance is crucial to evaluate their impact in NSCLC and offer greater DDR-based therapeutic windows.

The main route to metastatic spread is by circulating tumor cell (CTC) dissemination from the primary tumor and/or distinct metastatic foci (15). CTC count is a negative prognostic marker in several malignancies, including NSCLC (16–19). The metastasis-initiating capacity of a minor subset of patient CTCs with cancer stem cell properties has been reported in immunodeficient mice and CTC-derived explant (CDX) models were established in different cancer types (20–24). CDX may provide relevant insight into the biology of metastasis, serve to examine mechanisms underpinning metastatic disease, and provide a platform to decipher biology-driven treatment strategies (25). Nevertheless, their development remains extremely difficult due to CTC paucity in the bloodstream and technical challenges related to their phenotypic heterogeneity (26). In NSCLC, only one CDX model has been generated to date (22).

Here, we hypothesized that genome integrity-related dysfunctions are critical processes in CTC metastatic potency and NSCLC progression. CDX models can offer a platform for the functional characterization of DDR and genome integrity maintenance mechanisms, as well as the testing of biology-driven therapeutic hypotheses. We report the development of 4 NSCLC CDX models and 3 in vitro CDX-derived cell lines, which recapitulate patient tumor pathology and chemoresponse. Genomic analysis of the CDX, cell line, their matching tumor biopsy (TB), and patient single CTCs indicated an important overlap of mutational landscapes. Phylogenetic reconstruction revealed clonal alterations in genes involved in the DDR and genome integrity across all models. Through mechanistic analysis, we detected HRD in GR-CDXL1 — concordant with biallelic somatic *BRCA2* mutation and *FANCA* deletion — and GR-CDXL4 cell lines. Both responded to PARPi olaparib treatment, consistent with SLFN11 overexpression in GR-CDXL4 cells, which has been described as a predictor of sensitivity to PARPi in several cancers (27, 28). On the other hand, mitotic defects with centrosome clustering events were prevalent in GR-CDXL3 and successfully assessed as therapeutic targets in vitro, in ovo, and in vivo. Our results open up perspectives for a therapeutic exploitation of the DDR and genome stability maintenance defects, as well as for predictive biomarker identification in metastatic NSCLC.

Results

Patient donors and establishment of NSCLC CDX models. Blood samples were collected from 55 patients with advanced NSCLC. Among them, 82% presented adenocarcinoma, and all but 10 patients were smokers (Table 1 and Supplemental Table 1; supplemental material available online with this article; https://doi.org/10.1172/jci.insight.155804DS1). After hematopoietic blood cell depletion, the CTC-enriched fraction was implanted into NSG (NOD.Cg-*Prkdc*^{scid}*Il2rg*^{tm1Wjl}/SzJ) mice. The average number of EpCAM$^+$ CTCs detected by the CellSearch system in a 7.5 mL blood sample was 163 with a median of 2 CTCs (range, 0–3903 CTCs). The average number of implanted epithelial CTCs (EpCAM$^+$/cytokeratin$^+$, CD45$^-$) estimated based on CellSearch CTC counts was 693 with a median of 9 CTCs (range, 0–17694 CTCs). CTCs from patients P8 (termed L1), P37 (termed L2), P48 (termed L3), and P50 (termed L4) (3 adenocarcinomas, 1 squamous cell carcinoma) successfully generated 4 CDX tumors in mice called GR-CDXL1, GR-CDXL2, GR-CDXL3, and GR-CDXL4, respectively (Figure 1, A and B). Patients L1, L3, and L4 had high EpCAM$^+$/pan-cytokeratin$^+$ CTC counts (750, 177, and 243 CTCs per 7.5 mL blood, respectively) at the moment of implantation, while patient L2 presented

Table 1. Patient demographics

Clinical parameters	Patients	Patients with CDX
Age[A]	59 (37–81)	51 (39–66)
Sex (%)		
Female	21 (38)	2 (50)
Male	34 (62)	2 (50)
Smoking status (%)		
Nonsmoker	10 (18)	0
Smoker <15 PY	10 (18)	0
Smoker ≥ 15 PY	37 (67)	4 (100)
Histology (%)		
Adenocarcinoma	45 (82)	3 (75)
Squamous cell carcinoma	7 (13)	1 (25)
Large cell carcinoma	3 (5)	0
Number of metastatic sites (%)		
0	4 (7)	0
1	17 (31)	0
≥ 2	34 (62)	4 (100)
Number of lines of therapy[A]		
0	6 (11)	0
1	20 (36)	2 (50)
≥ 2	29 (53)	2 (50)

CDX, circulating tumor cell-derived explant; PY, pack per year. [A]Results obtained at blood collection.

only 10 CTCs (Supplemental Table 1). Indeed, 3500, 330, and 1102 CTCs were implanted in NSG mice for the establishment of GR-CDXL1, GR-CDXL3, and GR-CDXL4, respectively, while only 35 CTCs were injected in the case of GR-CDXL2 (Figure 1B). CDX were generated at a single time point, after first-line therapy (GR-CDXL3, GR-CDXL4) or second-line therapy (GR-CDXL1, GR-CDXL2). All 4 patients had unresected tumors, and their clinical history is summarized in Supplemental Figure 1. A TB was obtained at diagnosis for patients L2, L3, and L4. An additional TB at disease progression (at the time of CTC injection) was obtained for patient L4 (Figure 1A). Patient L2 had a *KRAS*-mutated tumor, and patient L4 had a *MET*-amplified tumor, while no known oncogenic driver alteration was detected for patient L3 (Supplemental Table 1 and Supplemental Figure 2A). Unfortunately, tumor cell content in patient L1 TB was not sufficient to perform routine molecular diagnosis.

At CDX passage 1, human origin of the tumor was validated by FISH testing of Alu element genetic marker (data not shown). Tumor fragments were used for CDX propagation in successive generations of NSG mice. Histopathology of the 4 CDX was assessed in comparison with available corresponding TB specimens. All TB and CDX tumors were of epithelial origin (positive for EpCAM and/or CK8/18), and none of the CDX expressed vimentin (Figure 1C and Supplemental Figure 2C). Poorly differentiated lung adenocarcinoma cells were detected in GR-CDXL1, GR-CDXL2 (Supplemental Figure 2C), and GR-CDXL4 (Figure 1C) tumors by HES stain, while in patient L3, TB 10% of tumor cells were positive for p40 and CK5/6 squamous markers (Supplemental Figure 2C). GR-CDXL1 CDX expressed neuroendocrine markers chromogranin A and synaptophysin in 10% of the cells (Supplemental Figure 2C). Foci of neuroendocrine cells expressing chromogranin A were detected in patient L4 diagnostic TB (10%), in TB at progression (20%), and in 50% and 30% of tumor cells in the CDX and the cell line, respectively. Synaptophysin was not expressed in patient L4 diagnostic TB, while it was detected in 60% of tumor cells in the TB at progression, in 40% of CDX tumor cells, and in 25% of the cell line (Figure 1C).

To evaluate whether CDX mimic patient responses to chemotherapy, in vivo drug assays were conducted in NSG mice (Supplemental Figure 3). GR-CDXL1 was resistant to cisplatin, mirroring patient L1 clinical progression at 2 months, while GR-CDXL2 showed tumor regression, recapitulating corresponding patient response to platinum salts (Supplemental Figure 1). In GR-CDXL3, the CDX tumor slowly progressed over the course of cisplatin treatment, similarly to patient L3, who progressed after 6 cycles of chemotherapy combination. In GR-CDXL4, cisplatin treatment resulted in delayed CDX tumor growth before

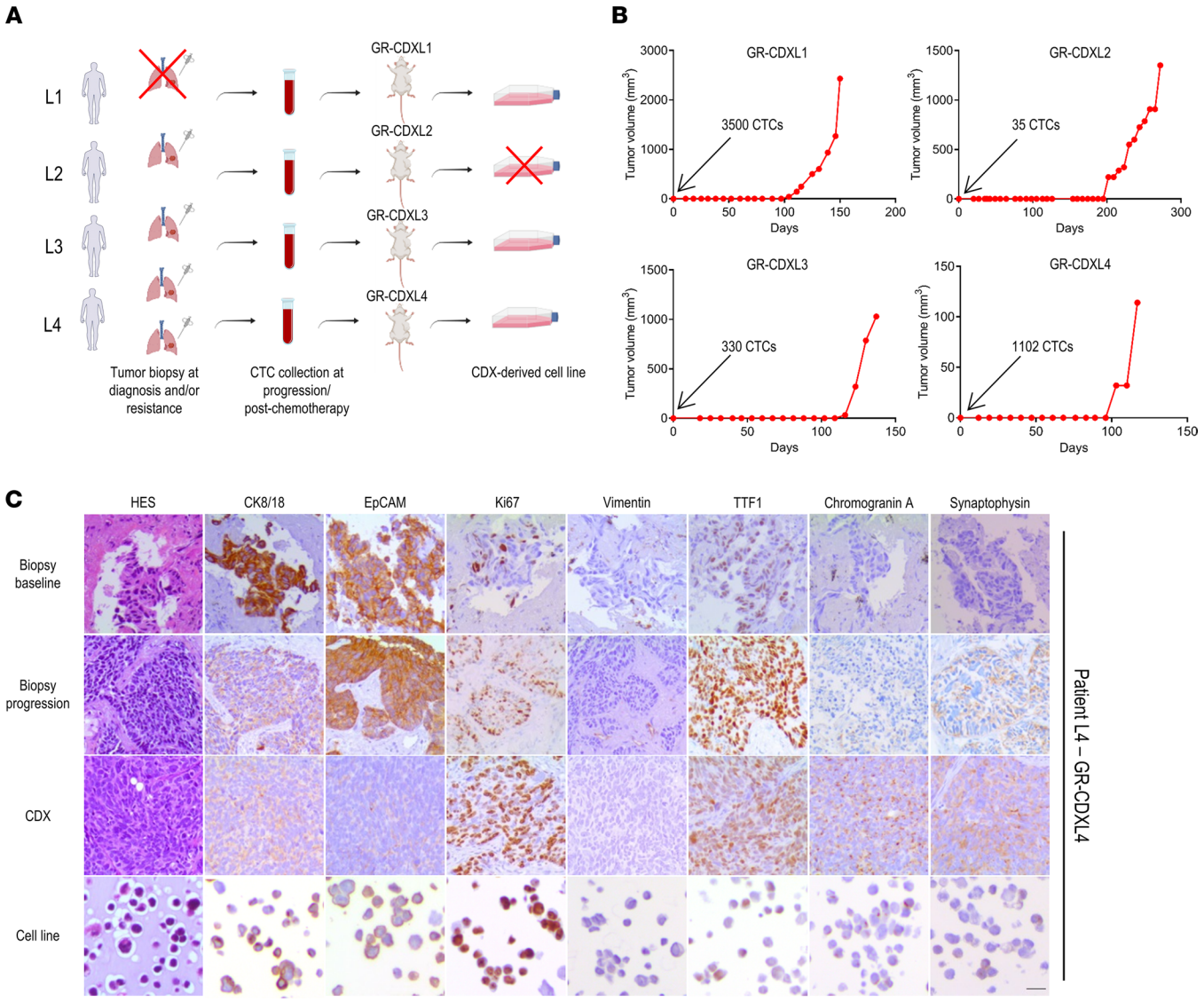


Figure 1. Establishment and characterization of CDX and CDX-derived cell lines. (**A**) Schematic of available patient samples and established CDX and CDX-derived cell lines (red cross = not available). (**B**) CDX tumor growth curves. Indicated number of CTCs was injected in NSG mice. Palpable CDX tumors were obtained after 100, 200, 116, and 100 days in GR-CDXL1, GR-CDXL2, GR-CDXL3, and GR-CDXL4, respectively. (**C**) IHC characterization of patient L4 TB at baseline and disease progression, GR-CDXL4 CDX tumor and CDX-derived cell line. Representative images of HES, CK8/18, EpCAM, Ki67, Vimentin, TTF1, Chromogranin A, and Synaptophysin stainings are shown at a total magnification of ×200. Scale bar: 10 μm.

progression after day 20, in accordance with patient L4's partial response after 4 cycles of chemotherapy (Supplemental Figure 1). Paclitaxel treatment promoted tumor stabilization in GR-CDXL1, in accordance with a stable disease in patient L1. GR-CDXL2 exhibited tumor stabilization before sudden progression, which reflects patient initial tolerance to paclitaxel over a 2-month treatment course followed by disease progression. The GR-CDXL4 tumor was a nonresponder (Supplemental Figures 1 and 3). Overall, chemoresponse of the 4 CDX tumors mirrored that of corresponding patient tumors, which validated our models.

Establishment of CDX-derived cell lines and in vivo and in ovo metastatic modeling. At passage 2, CDX tumors were dissociated and human tumor cells were cultured in vitro. GR-CDXL1 and GR-CDXL4 cells grew as adherent microspheres, while GR-CDXL3 formed an adherent monolayer (Supplemental Figure 2B). Despite several attempts of cell expansion at different passages, GR-CDXL2 cells did not grow in vitro. Overall, 3 permanent CDX-derived cell lines were established with an average doubling time of 4 days. They all expressed a phenotype similar to their corresponding CDX (Figure 1C and Supplemental Figure 2C). Interestingly, CDX-derived cells expressed stem cell markers CD133 and CD166. ABCG2 and ALDH activity were detected in GR-CDXL1 cells, while CD90 was expressed by GR-CDXL1 and GR-CDXL3

cells (Supplemental Figure 2D). To assess the tumorigenicity and metastatic capacity of CDX-derived cell lines, we reinjected CDX-derived cells in the chorioallantoic membrane (CAM) of the chick embryo and NSG mice. For in ovo experiments, cells were infected with mCherry-expressing retroviral particles before engraftment on the CAM, as previously reported (29). The 3 CDX-derived cell lines formed tumor nodules, and GR-CDXL3 cells showed increased disseminating capacity compared with GR-CDXL1 and GR-CDXL4 (Figure 2A). To evaluate later stages of metastatic spread, intracardiac (IC) injection of luciferase-expressing cells was performed in NSG mice. All CDX-derived cell lines were tumorigenic. GR-CDXL1 cells formed localized single tumors, while GR-CDXL3 and GR-CDXL4 cells seeded multiple metastases (Figure 2B and Supplemental Figure 4).

Genome characterization and phylogenetic analysis of TB, CTCs, CDX, and CDX-derived cell lines. To determine the extent to which the CDX is representative of the TB and evaluate genome alterations potentially associated with tumorigenic activity, we performed whole-exome sequencing (WES) analysis of TB of patients L2 and L3 at diagnosis and patient L4 TB at progression; we analyzed single CTCs from patients L1 and L3, and we analyzed the CDX models and the CDX-derived cell lines. Due to the lower quality of collected material, patient L4 diagnostic TB was excluded from WES analysis, and material was conserved for IHC. Single CTCs with satisfactory whole genome amplification quality controls could not be obtained for patients L2 and L4. All samples submitted for sequencing are annotated in Supplemental Figure 5. All WES data are available in Supplemental Data Sets 1–6. Sequencing depth, coverage, and number of variants identified in the TB, CTCs, CDX, and CDX-derived cell lines are provided in Supplemental Table 2 and Supplemental Table 3. In total, 52.24% (303 of 580) of mutations detected in the patient L2 TB specimen were found in the CDX (Figure 3A). Amino acid sequence variation of driver genes in the different samples is listed in Figure 3C. Patient L2 TB and CDX presented a *KRAS*-mutant tumor with concurring mutations in genes *KEAP1*, *STK11*, and *RBM10*. Driver mutation in the cell cycle checkpoint kinase and DDR gene *CHEK2* was also found in these samples (Figure 3, B and C). In total, 56.7% (161 of 284) of patient L3 TB alterations were conserved in GR-CDXL3 CDX, including driver *TP53* and DNA repair gene *DDB1* mutations (Figure 3, A, C, and D). A total of 75.8% (213 of 281) of mutations detected in patient L4 TB at progression was found in GR-CDXL4 CDX, including loss-of-function in tumor suppressor genes *RB1*, *TP53*, and *NF1* (Figure 3A). Overall, the important overlap of mutations between the CDX and the corresponding TB validates the clinical relevance of the CDX models. Importantly, these data reveal aberrations in genes involved in genome integrity maintenance through DNA repair mechanisms and the DDR.

Statistics of allele drop-out and false-positive rate of patients L1 and L3 single CTCs are shown in Supplemental Figure 11. Using variant calling criteria (present in at least 1 other tumor sample), a set of 24 unique variants with high variant allele frequencies was identified in L1-CTC1. All mutations were conserved in GR-CDXL1 CDX (Supplemental Table 3). Five single CTCs from patient L3 were analyzed by WES, and *TP53* driver mutation was recurrent in CTCs 1, 2, and 5; the TB; and the CDX. *ASPM*, a gene involved in mitotic spindle formation, was mutated in CTCs 2, 3, and 5; the TB; and the CDX, while a driver mutation in *DDB1* was detected in CTC5, the TB, and the CDX.

We then focused on the mutational profiles of the CDX, as these models may not only recapitulate primary tumor molecular characteristics, but also help track metastatic disease through tumorigenic CTCs. We therefore examined the mutations exclusive to the CDX (not in the corresponding TB), which may be potentially acquired during metastatic progression. In GR-CDXL2, 33.5% (153 of 456) of the detected mutations were exclusive to the CDX. In GR-CDXL3, 29% (66 of 227) of mutations were found in the CDX and the cell line (Figure 3E), including driver mutations in *ERBB2* and *MED23* (Figure 3, F and G). Finally, 36% (120 of 333) of mutations found in GR-CDXL4 CDX were exclusive to the CDX and the cell line (Figure 3, E–G). Overall, in all CDX models, approximately 30% of mutations were likely acquired during metastatic progression.

To evaluate the relevance of our CDX-derived cell lines, we performed a comparative genomic analysis with the corresponding CDX. The GR-CDXL1 CDX mutational profile presented 91.4% similarity with the cell line, including driver mutations in genes involved in DNA repair such as *ATRX*, *BRCA2*, and *TP53BP1*, along with chromatin remodeling genes, including *ARID1A* and *ARID1B* (Supplemental Figure 6, A–C). GR-CDXL3 and GR-CDXL4 CDX had 81.9% and 72% mutational overlap, respectively, with their corresponding cell line (Supplemental Figure 6A). These results reveal important mutational landscape similarities between the CDX and the CDX-derived cell line, as identified through hierarchical clustering of all variant genes (Supplemental Figure 7), thus validating our models of study.

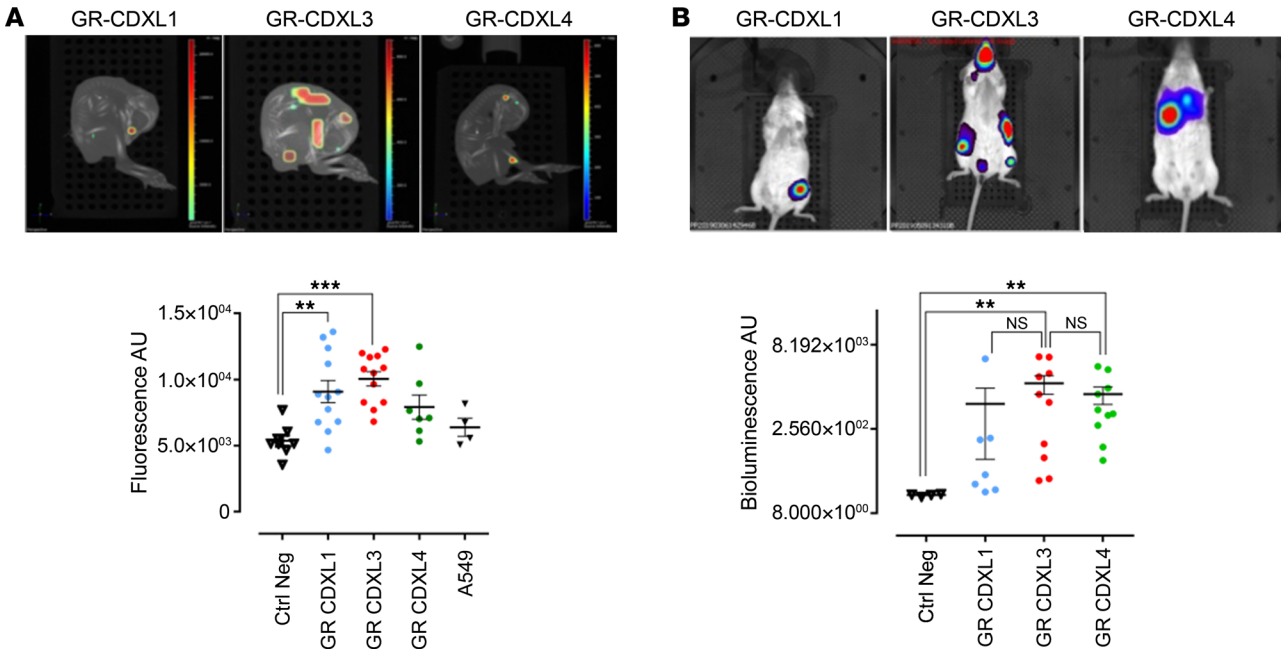


Figure 2. Evaluation of CDX-derived cell line metastatic potency in ovo and in vivo. (**A**) Metastatic capacity of CDX-derived cell lines in the CAM. mCherry-expressing CDX-derived cells were implanted into the CAM, and metastatic fluorescent signal was analyzed at day 7. Representative fluorescence/CT images of GR-CDXL1–, GR-CDXL3–, and GR-CDXL4–generated tumors are shown (top). Quantitative analysis of average fluorescence intensity (bottom); each point represents a single embryo. (**B**) Metastatic capacity of CDX-derived cell lines in NSG mice. Luciferase-expressing CDX-derived cells were grafted into NSG mice by IC to generate metastases. Representative BLI images of GR-CDXL1–, GR-CDXL3–, and GR-CDXL4–generated tumors are shown (top). Quantitative analysis of average BLI intensity (bottom); each point represents a single mouse. Data are mean ± SEM; $^{**}P < 0.01$, $^{***}P < 0.001$ by Kruskall Wallis and post hoc Dunn's test.

Next, we performed copy number alteration (CNA) analysis and examined shared alterations between TB specimen, the CDX, and the CDX-derived cell line for each model. Multiple CNAs were detected across the 4 models, highlighting chromosomal instability (CIN) (Figure 4 and Supplemental Figures 8 and 9). Unsupervised hierarchical clustering of all CNAs identified a single cluster in patients L1 samples, composed of the CDX and the cell line, and a single cluster in patient L2 samples, consisting of the patient TB and the CDX, with predominant copy number losses. On the other hand, 2 separate clusters were depicted among each sample from patients L3 and L4; the first was composed of the TB, and the second was composed of the CDX and the cell line, with predominant copy number gains (Figure 4). As commonly observed in lung cancer, loss of tumor suppressor genes *TP53* and *MAP2K4* and gain of *TERT* were identified in all samples; *PTEN* and *APC* losses were detected in GR-CDXL1 and GR-CDXL4 tumor samples and in GR-CDXL3 CDX and its cell line. Moreover, *RB1* loss was detected in GR-CDXL3 and GR-CDXL4, while *STK11* loss was detected in GR-CDXL1 and GR-CDXL2 samples. Several unstable chromosomal regions occurring across CDX models included DNA repair and DDR-related genes. Notably, the deletion of *FANCA* promoter (segment 16q24.3) in GR-CDXL1 samples (Supplemental Figure 8), *FHIT* loss (GR-CDXL1, GR-CDXL2, and GR-CDXL3 samples), *ARID1A* loss (GR-CDXL2 and GR-CDXL3 samples), and proto-oncogene *MDM4* gain (GR-CDXL1 and GR-CDXL4 CDX and cell line; GR-CDXL3 TB, CDX, and cell line). Large-scale alterations including gain in 7q containing *CDK6* (patient L2 TB and GR-CDXL2 CDX, GR-CDXL3, and GR-CDXL4 CDX and cell line) were also found. In addition, *AKT1* gain was found in GR-CDXL3 CDX and cell line, as well as *ERBB2* (chr 17) amplification (Supplemental Figure 8). Comparing WES data with significantly altered genes in adenocarcinoma and squamous cell carcinoma from 11 cBioPortal studies in NSCLC showed that our models were highly representative of these histologies (Supplemental Figure 10, A and B). These variants were also predominant in other types of metastatic malignancies (Supplemental Figure 10C) (30). In addition, key DDR-related alterations that emerge from our CDX model WES analysis are found at a low frequency in cBioPortal NSCLC studies (31–35).

Finally, using driver alterations, we investigated cell lineage tracing of the CDX and CDX-derived cell lines. Phylogenetic inference from somatic mutations and CNA data was used to map the clones from TB

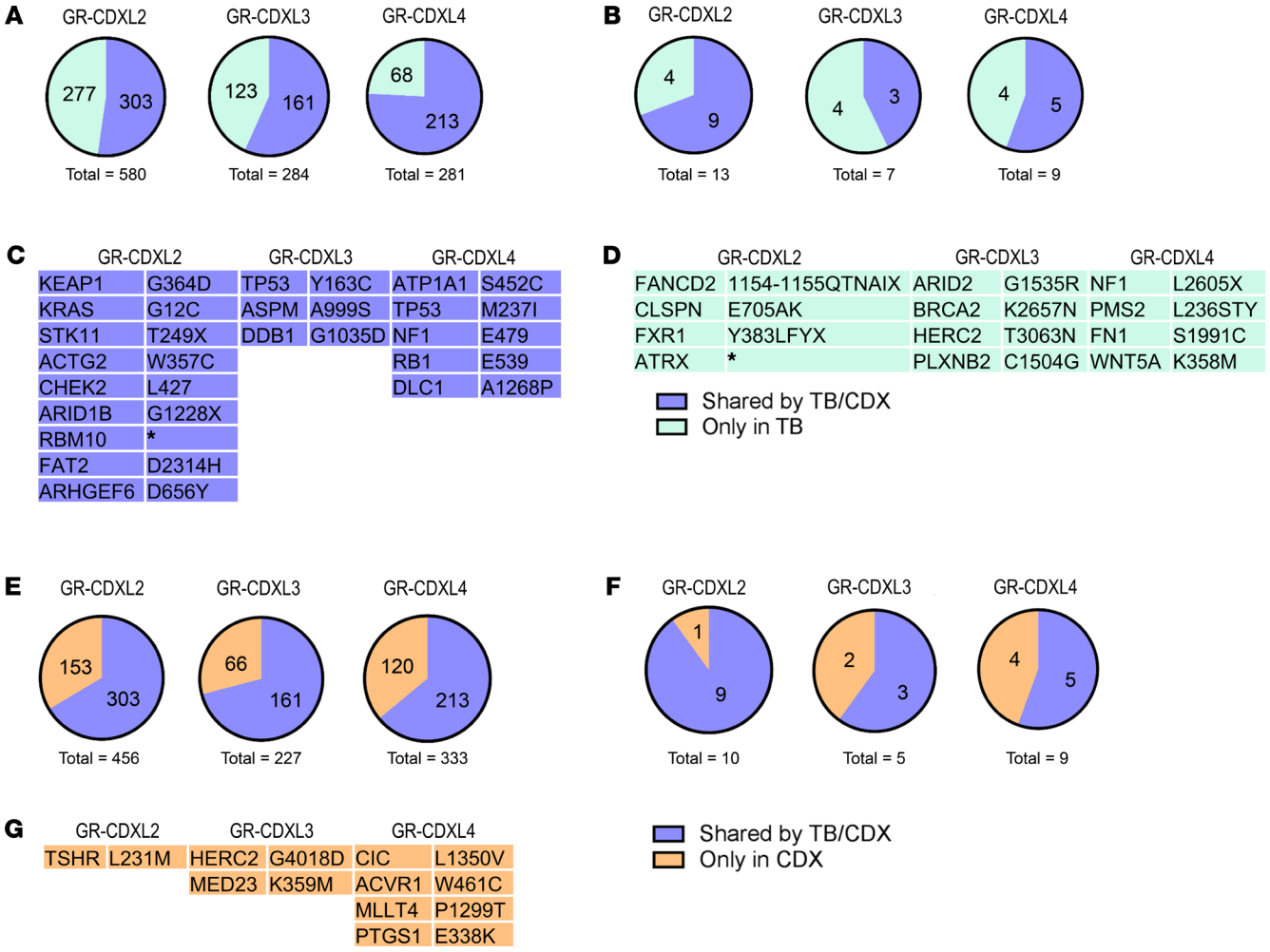


Figure 3. Comparative genomic analysis of biopsies and the CDX. (**A**) Fraction of TB mutations detected and undetected in the CDX. (**B**) Fraction of TB driver mutations detected and undetected in the CDX. (**C**) Mutated driver genes and their amino acid sequence variation in the biopsy and the CDX. (**D**) Mutated driver genes and amino acid sequence variation in the TB only. (**E**) Fraction of CDX mutations issued or not from the TB. (**F**) Fraction of CDX driver mutations issued or not from the TB. (**G**) Mutated driver genes and amino acid sequence variation in the CDX only.

and tumorigenic CTCs that contributed to CDX tumors (Figure 5). In the 4 CDX models, loss of tumor suppressor genes such as *TP53*, *STK11*, and *MAP2K4* was an early event. Subclonal mutations in *TP53*, *ARID1B*, and *BRCA2* genes were detected in GR-CDXL1 CDX and cell line (Figure 5A). Subclonal loss of the 16q region harboring DNA repair–related *WWOX* and *FANCA* was also observed in this model (Figure 5A). Truncal cooccuring mutations were found in oncogenic driver genes *KRAS*, *KEAP1*, *STK11*, *ARID1B*, *RBM10*, and *TSHR* in patient L2 TB and GR-CDXL2 CDX (Figure 5B). Moreover, truncal driver alterations were detected in DDR pathway genes *CHEK2* and *ARID1B* (Figure 5B). In GR-CDXL3, truncal *TP53* mutation and early whole-genome doubling (WGD) were detected, as were clonal *MDM4* and *PARP10* gains (Figure 5C). Two ramifications were observed: the first one containing patient L3 single CTCs 2-5, the CDX, and the cell line — which acquired *PTEN* loss, *BRCA1* loss, *ERBB2* amplification, and *AKT1* gain — and the second one carrying the TB (Figure 5C). In GR-CDXL4, *TP53*, *RB1*, *NF1*, *ACVR1*, and *ATP1A1* driver mutations were clonal, while gains of DNA repair–related genes *MDM2* and *MDM4* were subclonal in the CDX and the cell line (Figure 5D). Overall, phylogenetic reconstruction of the 4 models reveals the clonality of mutations in DDR- and repair-related genes, suggesting their potential implication in metastatic disease progression and interest as therapeutic targets. CNAs in key DNA repair genes are also acquired in CDX and cell lines, recapitulating important CIN in our models.

DDR and DNA repair mechanisms activity in CDX-derived cell lines. The recurrence of DDR-related genomic alterations revealed by WES led us to the mechanistic characterization of DDR mechanisms in our models.

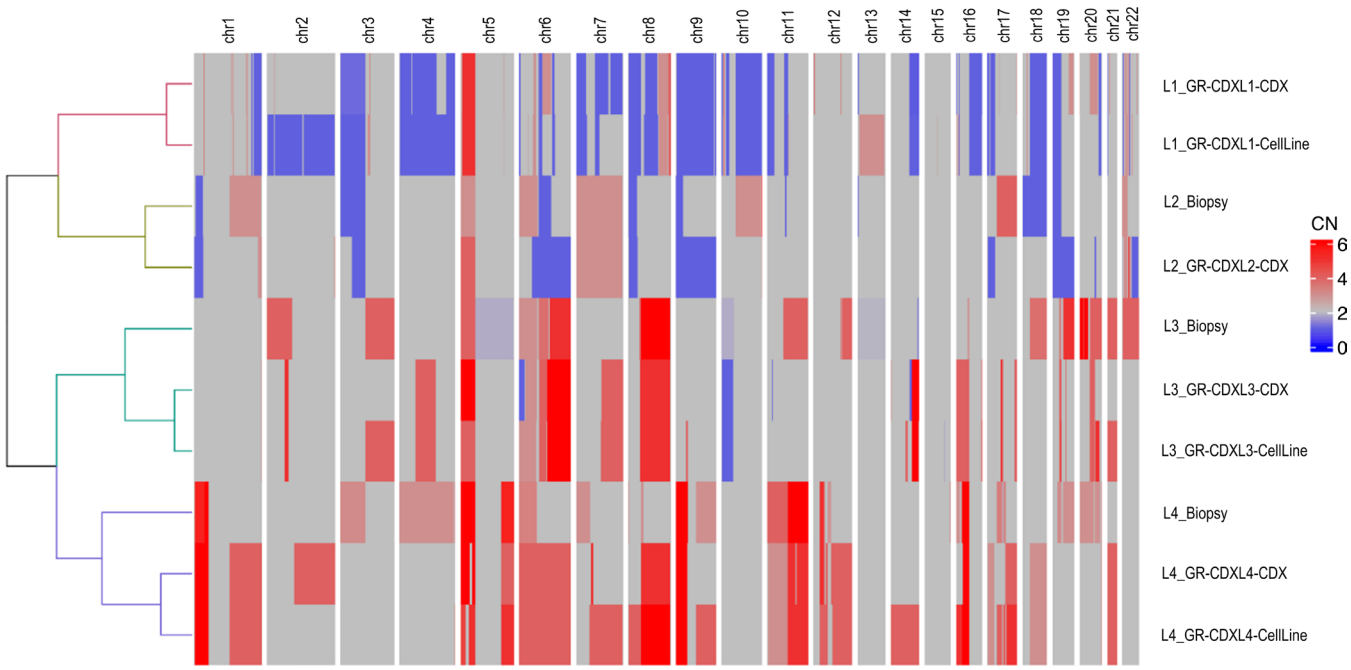


Figure 4. Heatmap of the CNA analysis of the TB, the CDX, and the CDX-derived cell lines. Unsupervised hierarchical clustering of CNA profiles was performed. Copy gains are shown in red, and copy losses are shown in blue. CN, copy number.

To estimate DSB frequency in CDX-derived cell lines, a dual cyclin A (S/G2 phase marker)/p53-binding protein 1 (53BP1-mediator of DSB repair) staining was performed. 53BP1 localizes to lesions and forms foci during S/G2 phases (Figure 6A). The incidence of DSBs in S/G2 is significantly higher in CDX-derived cells (ranging from 38%–58% of cells) compared with control NSCLC adenocarcinoma cell lines (Figure 6A). Phosphorylation of histone H2AX was also assessed to monitor DNA damage in cancer cells undergoing mitosis. We observed important levels of damaged mitotic DNA in GR-CDXL1 and in GR-CDXL4 compared with control (Figure 6B). Notably, GR-CDXL1 G1 cells harbored a significant proportion of 53BP1 nuclear bodies, which indicates the persistence of unrepaired damage after mitosis in G1 (Figure 6C). Furthermore, persistent DNA damage in GR-CDXL1 induced constitutive activation of checkpoint kinase 1 (*CHEK1*) shown by increased phosphorylation at Ser-345 distinctly in GR-CDXL1 cells (Figure 6D).

Next, we monitored nuclear foci of key actors in HR and nonhomologous end joining (NHEJ) to evaluate DSB repair in the CDX-derived cell lines. HR activity was assessed through RAD51 and phosphorylated RPA32 (pRPA) recruitment. RAD51 foci were detected in geminin-expressing S-phase cells after induction of DSBs by ionizing radiation (IR). While HR was activated upon IR in ~80% of GR-CDXL3 cells, RAD51 recruitment was negligible in GR-CDXL1 (10% of cells) and GR-CDXL4 (~20%) (Figure 6E). Similarly, pRPA32 failed to be recruited at lesion sites in GR-CDXL1 cells after aphidicolin (APH; replicative DNA polymerase inhibitor) treatment (Figure 6F). On the other hand, GR-CDXL1, GR-CDXL3, and GR-CDXL4 cells were NHEJ proficient in response to APH-induced DNA damage, as shown by pDNA-PKc nuclear foci formation (Figure 6G). These results reveal HRD in GR-CDXL1 cells, which is concordant with somatic *BRCA2* mutation and *FANCA* loss detected by WES (Figure 5A and Supplemental Figure 6). HRD was also observed in GR-CDXL4, without any genomic rationale behind it. Interestingly, high PARP1 protein levels were detected in GR-CDXL1 and GR-CDXL4 cells, suggesting its possible targeting (Figure 6D).

Mitotic defects investigation in CDX-derived cell lines. High CIN level has been confirmed by metaphase chromosome spreads of GR-CDXL1, GR-CDXL3, and GR-CDXL4 cells, presenting 54, 110, and 59 chromosomes, respectively (Figure 7, A and B). A tetraploid DNA content was detected by WES in the GR-CDXL3 cell line only, while GR-CDXL4 exhibited a near-triploid genome (Figure 7C), recapitulating the copy number profiles of the corresponding CDX (Supplemental Figure 8 and Supplemental Figure 12A). These results, supported by the presence of centromeres into lagging DNA during mitosis

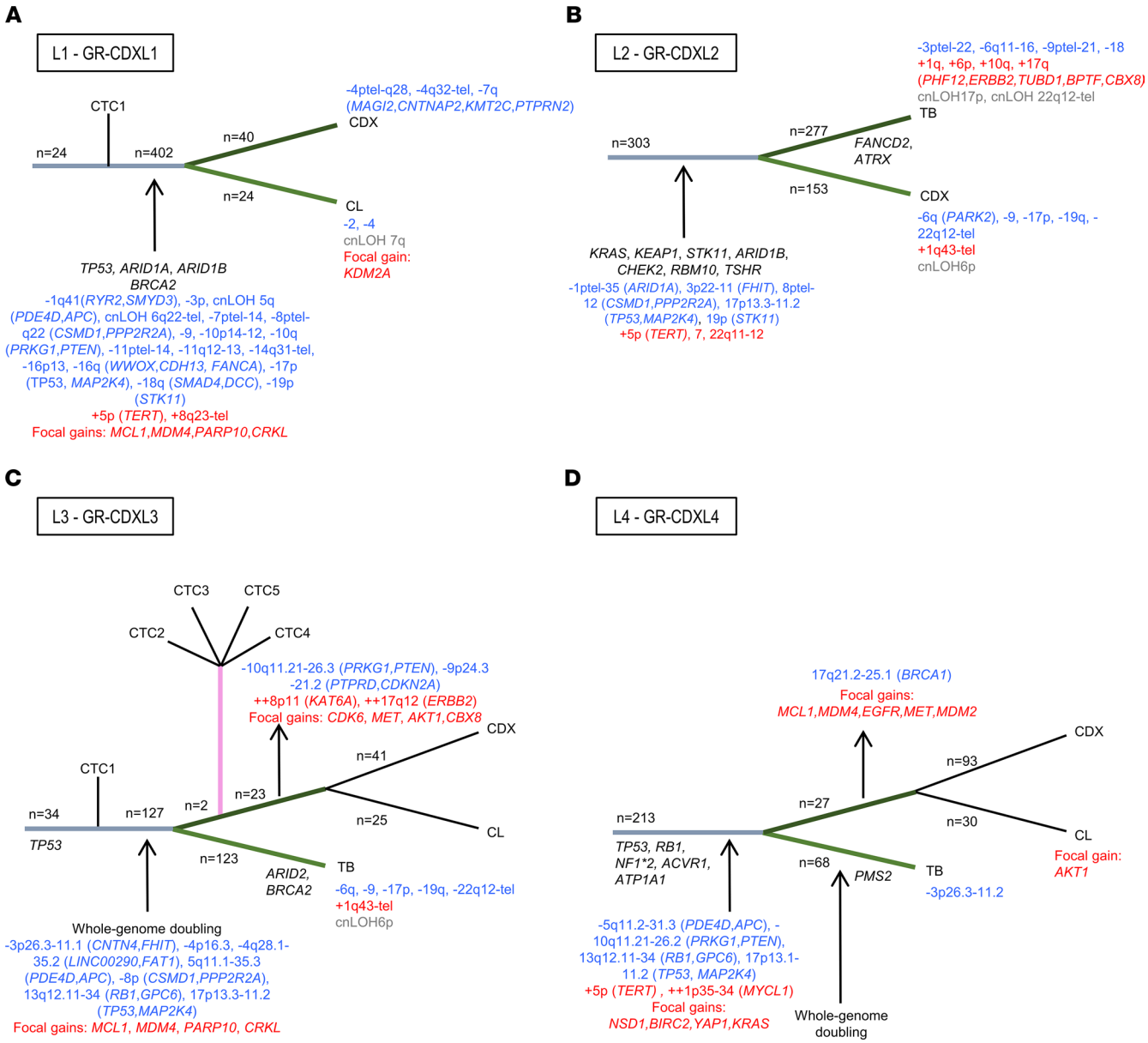


Figure 5. Phylogeny of CDX and CDX-derived cell lines. (**A**–**D**) Branches are unscaled, and their length is not proportional to the number of alterations occurring in the branch. The number of mutations (in dark) and the CNAs (gain in red and loss in blue) are mentioned on the branches of the tree. Only genes bearing driver truncal or acquired alterations (mutations or CNAs) are indicated.

(Supplemental Figure 12, B and C), highlight numerical CIN distinctly in GR-CDXL3. Furthermore, CDX-derived cells presented numerous mitotic defects including multipolar divisions, anaphase bridges and lagging chromosomes (Figure 7E). We, thus, focused next on centrosome abnormalities, which are frequent in cancer and contribute to CIN (36). Clustering of supernumerary centrosomes has been previously reported as a coping mechanism of cancer cells, enabling them to form bipolar spindles and survive (37). To investigate whether this event is a common feature in our models, dual α-tubulin/centrin IF staining was performed (Figure 7E). Interestingly, GR-CDXL3 exhibited high proportions of cells with centrosome clustering (~85%) compared with control A549, GR-CDXL1 and GR-CDXL4 cells. This phenomenon is known to protect cancer cells from otherwise lethal multipolar divisions, which is consistent with their low incidence level in GR-CDXL3 cells (Figure 7, D and E).

In vitro, in ovo, and in vivo therapeutic targeting of CDX-derived cell lines. WES-based mutation landscape and subsequent mechanistic studies highlighted CIN and genome instability propagation across all CDX models, suggesting cancer cell vulnerabilities. This, thus, provided a biological rationale for the selection

of drug candidates targeting DNA repair and DDR defects (Supplemental Figure 13). First, GR-CDXL1 resistance to cisplatin and sensitivity in GR-CDXL4 observed in vivo were confirmed in vitro (Figure 8A). HRD in GR-CDXL1 and GR-CDXL4 cell lines (Figure 6, E and F) led us to assess the efficacy of PARPi olaparib. In spite of cisplatin resistance but in concordance with its HRD features, GR-CDXL1 responded to olaparib. GR-CDXL4 was also extremely sensitive to olaparib compared with A549 and GR-CDXL3 cells (Figure 8B). As no biological explanation was provided for drug response in GR-CDXL4, we explored a hypothesis based on a protein biomarker. We, therefore, assessed SLFN11 expression in our cell lines and its possible correlation with GR-CDXL4 cell sensitivity to olaparib. Interestingly, GR-CDXL4 cells overexpressed SLFN11 protein, while it was not detected in A549, GR-CDXL1, or GR-CDXL3 cells (Figure 8C). *SLFN11* mRNA levels were also significantly higher in GR-CDXL4 cells (8-fold) compared with other cell lines (Figure 8D). These findings led us to further investigate SLFN11 expression in olaparib-sensitive GR-CDXL1 and GR-CDXL4 samples. To this end, we performed IHC on GR-CDXL1 CDX and cell line, patient L4 TB specimens at diagnosis and progression, and GR-CDXL4 CDX and cell line. Representative samples from NSG mice metastases (see Figure 2B) from both CDX models were also analyzed. IHC analysis revealed that 60% of tumor cells in patient L4 TB (diagnosis and progression) were positive for SLFN11. GR-CDXL4 samples also strongly expressed SLFN11 with 70%, 90%, and 90% cell positivity in the CDX, the CDX-derived cell line, and the mouse metastatic tumor, respectively. In contrast, GR-CDXL1 tumor samples were all negative for this marker (Figure 8E). Together, these data indicate that SLFN11 overexpression may be implicated in reduced HR activity in GR-CDXL4 cells, conferring olaparib sensitivity independently of *BRCA1/2* mutation status.

In ovo, both GR-CDXL1 and GR-CDXL4 mCherry-expressing tumors responded to a 6-day course of olaparib monotherapy (100 μg/kg). Indeed, the metastatic fluorescence signals obtained by GR-CDXL1 and GR-CDXL4 tumors on the CAM were significantly reduced at ID17 (Figure 8G and Supplemental Figure 14B). In vivo, significantly delayed tumor growth was observed in treated groups as expected, while nontreated GR-CDXL1-Luc and GR-CDXL4-Luc tumors were unresponsive, reaching respectively twice and 4 times the initial tumor volume over the experimental course (Figure 8, H and I, and Supplemental Figure 14C).

A panel of DDR and cell cycle inhibitors including NHEJ key factor DNA-dependent protein kinase (DNAPK) inhibitor NU7441 and Aurora A inhibitor alisertib was evaluated in our CDX-derived cell lines. However, no significant effects have been noted (data not shown). GR-CDXL3 cells were highly sensitive to PI3KA inhibitor BYL719 in vitro compared with control, in accordance with *AKT* amplification and *PTEN* loss detected in CNA analysis (Figure 8F and Supplemental Figure 14A). We next tested whether centrosome clustering inhibition would impact GR-CDXL3 cell survival by targeting kinesin family member C1 (KIFC1), a critical factor in this mechanism. No significant effect of KIFC1 inhibitor AZ82 on GR-CDXL3 cells was found in vitro (data not shown). We then sought to compare GR-CDXL3 tumor response to BYL719 and AZ82 as monotherapy versus combination therapy in the CAM (Figure 8J). The effect of BYL719 was not statistically significant, while tumors were slightly more responsive to AZ82 alone. Interestingly, a notable synergistic effect of the drug combination was observed on GR-CDXL3 tumors compared with monotherapy (Figure 8J). In contrast to the in ovo assay, AZ82 monotherapy did not have a noticeable effect on tumor growth in NSG mice, while tumor response to BYL719 was statistically significant (Figure 8K). Most importantly, tumors were highly sensitive to the AZ82/BYL719 combination targeting 2 different mechanisms of tumor adaptation in GR-CDXL3, in concordance with the synergy obtained in ovo (Figure 8, K and L, and Supplemental Figure 14, D and E).

Discussion

Defective DDR and genome instability are common in NSCLC and a potential therapeutic opportunity, but clinical data have so far been disappointing (14). In this study, we report the comprehensive analysis of 4 CDX models established from advanced-stage NSCLC patient CTCs — which recapitulated patient tumor pathology and chemoresponse — and 3 CDX-derived cell lines. Genomic analysis by WES unraveled a characteristic mutational spectrum from which several DNA repair-related deleterious alterations emerged, associated with CTC-mediated metastatic progression. Mechanistic studies revealed high levels of DNA damage in our CDX-derived cell lines, notably in GR-CDXL1 where DSBs remain unrepaired after mitosis. Subsequent functional assessment evaluation of DNA repair activity showed impaired RAD51 foci formation in GR-CDXL1 and GR-CDXL4 cells, accompanied by sensitivity to PARPi in vitro, in the

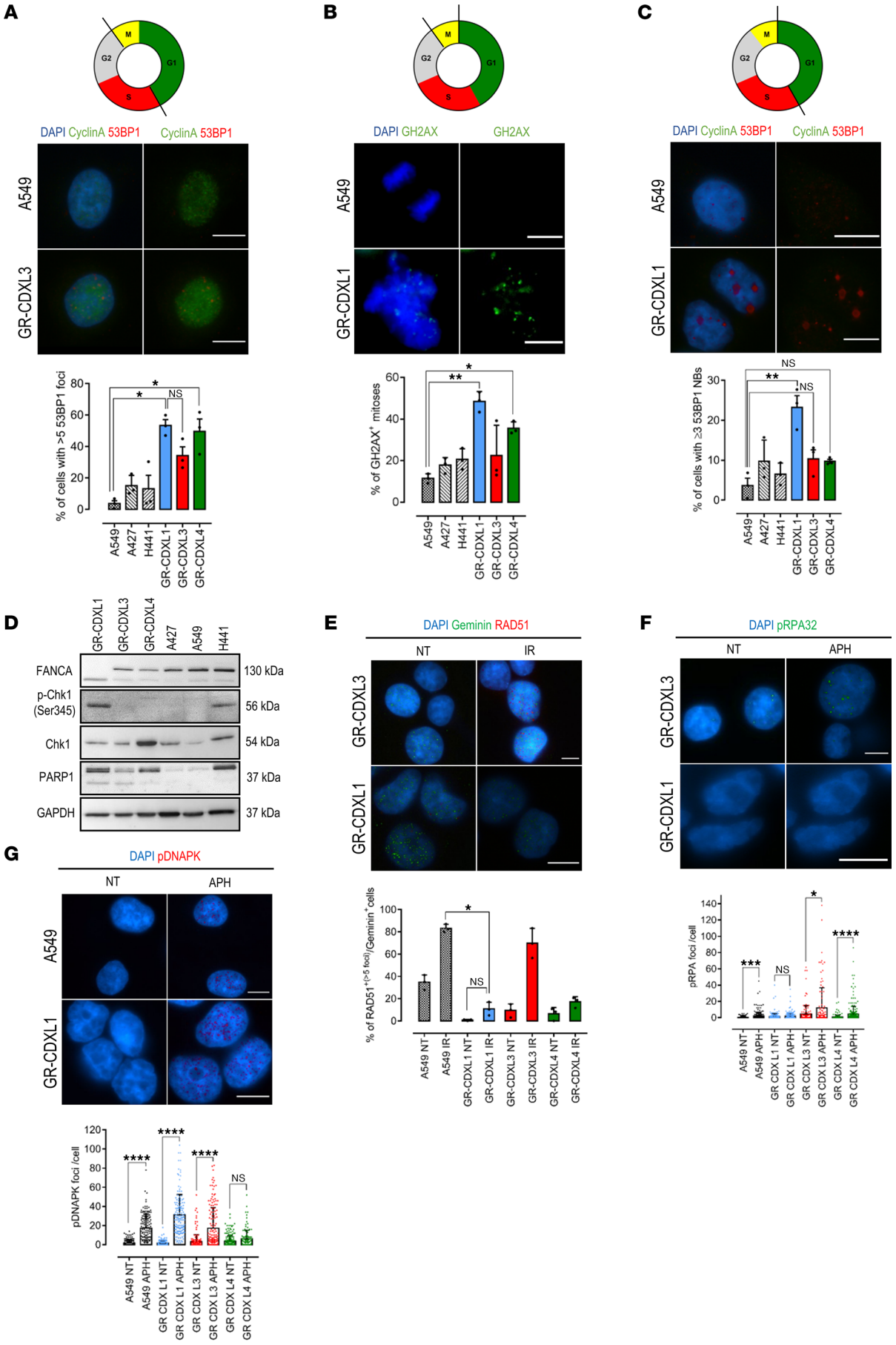

A
M
G2
G1
S
DAPI CyclinA 53BP1
CyclinA 53BP1
A549
GR-CDXL3
% of cells with >5 53BP1 foci
A549
A427
H441
GR-CDXL1
GR-CDXL3
GR-CDXL4
B
DAPI GH2AX
GH2AX
A549
GR-CDXL1
% of GH2AX+ mitoses
C
DAPI CyclinA 53BP1
CyclinA 53BP1
A549
GR-CDXL1
% of cells with ≥3 53BP1 NBs
NS
D
GR-CDXL1
GR-CDXL3
GR-CDXL4
A427
A549
H441
FANCA
130 kDa
p-Chk1 (Ser345)
56 kDa
Chk1
54 kDa
PARP1
37 kDa
GAPDH
37 kDa
E
DAPI Geminin RAD51
NT
IR
GR-CDXL3
GR-CDXL1
% of RAD51+(>5 foci)/Geminin+ cells
A549 NT
A549 IR
GR-CDXL1 NT
GR-CDXL1 IR
GR-CDXL3 NT
GR-CDXL3 IR
GR-CDXL4 NT
GR-CDXL4 IR
F
DAPI pRPA32
NT
APH
GR-CDXL3
GR-CDXL1
pRPA foci /cell
A549 NT
A549 APH
GR CDX L1 NT
GR CDX L1 APH
GR CDX L3 NT
GR CDX L3 APH
GR CDX L4 NT
GR CDX L4 APH
G
DAPI pDNAPK
NT
APH
A549
GR-CDXL1
pDNAPK foci /cell
A549 NT
A549 APH
GR CDX L1 NT
GR CDX L1 APH
GR CDX L3 NT
GR CDX L3 APH
GR CDX L4 NT
GR CDX L4 APH

Figure 6. DNA damage response activation in CDX-derived cell lines. (**A**) Representative images of 53BP1 foci (red) in A549 and GR-CDXL3 cells (top). Proportion of S/G2 (cyclinA$^+$) cells with more than 5 53BP1 foci (bottom). (**B**) Representative images of GH2AX$^+$ (green) mitotic cells in GR-CDXL1 and A549 (top). Proportion of H2AX$^+$ mitoses (bottom). (**C**) Representative images of 53BP1 NB (red) in A549 and GR-CDXL1 cells (top). Proportion of G1 (cyclinA$^-$) cells with more than 3 53BP1 NB (bottom). (**D**) Western blot analysis of the levels of p-CHK1, CHK1, FANCA, and PARP1 in CDX-derived and NSCLC cell lines. (**E**) Representative images of IR-induced RAD51 foci (red) in S phase (geminin$^+$) GR-CDXL1 and GR-CDXL3 cells (top). Proportion of RAD51$^+$/geminin$^+$ NT and IR cells (bottom). (**F**) Representative images of APH-induced pRPA32 foci (green) in GR-CDXL1 and GR-CDXL3 cells (top). Level of pRPA32 foci per cell in NT and APH-treated (bottom). (**G**) Representative images of APH-induced pDNA-PK foci (red) in A549 and GR-CDXL1 cells (top). Level of pDNAPK foci per cell in NT and APH-treated (bottom). For **E**–**G**, we kept only A549 NSCLC cell line as a comparator, as the other control had equivalent levels of DNA damage. Data are shown as mean ± SD from at least 3 independent experiments; $*P < 0.05$, $**P < 0.01$, $***P < 0.001$, $****P < 0.0001$ by Kruskall Wallis and post hoc Dunn's test. NB, nuclear body; NT, nontreated, IR, irradiated; APH, aphidicolin. Scale bar: 10 μm.

CAM model and immunodeficient mice, thus inferring HRD. This was supported by a genomic rationale in GR-CDXL1 involving *BRCA2* mutation and *FANCA* deletion, while *SLFN11* overexpression was elucidated as a molecular rationale predictive of olaparib sensitivity in GR-CDXL4. GR-CDXL3 presented supernumerary chromosomes and centrosome clustering, leading to CIN propagation and promoting highly aggressive tumor seeding in ovo and in vivo. Moreover, GR-CDXL3 tumors were highly sensitive to the drug combination targeting centrosome clustering and AKT signaling.

One fundamental limitation is the low prevalence of CellSearch-detected epithelial CTCs in some metastatic cancers (e.g., NSCLC, pancreatic cancer). Only 1 CDX model has been previously generated in NSCLC, displaying a predominant mesenchymal phenotype (22). Here, we report the comprehensive analysis of 4 CDX models established from advanced-stage NSCLC patient EpCAM$^+$ CTCs and 3 CDX-derived cell lines. CTC counts as low as 35 were sufficient for CDX tumor growth, indicating that, even at low concentrations, CTCs may contain subpopulations with important tumorigenic potential. Overall engraftment rate was low (4 of 55, ~7%) as expected. We observed that it was higher for squamous cell carcinoma (1 of 7 patients; 14.3%) than adenocarcinoma (3 of 45 patients; 6.67%). However, it is difficult to draw a correlation between success rates and tumor histologies based on such a low number of successful attempts. In our study, all CDX tumors and established cell lines presented an epithelial phenotype, which shows that EpCAM$^+$ CTCs presented tumorigenic potential in our 4 models. In vivo drug assays recapitulated patient responses to first-line chemotherapy, thus validating our models. CDX-derived cell lines have demonstrated strong tumorigenic activity both in ovo and in vivo. Notably, GR-CDXL3 and GR-CDXL4 cells were highly metastatic, in concordance with their CIN profiles, showing their relevance as a tool to investigate mechanisms underlying metastatic progression, as was previously reported using small cell lung cancer (SCLC) CDX-derived cells (38). WES analysis showed that GR-CDXL2 and GR-CDXL3 CDX recapitulated the corresponding patient diagnostic TB, while GR-CDXL4 was representative of the TB at progression, with 52%, 57%, and 76 % mutational profile similarity. Moreover, 34%, 29%, and 36% of mutations were found exclusively in the GR-CDXL2, GR-CDXL3, and GR-CDXL4 CDX, respectively, possibly issued from metastasis. The patient L1 biopsy specimen was insufficient for molecular profiling, as biopsy material is often scarce in NSCLC. The relevance of GR-CDXL1, thus, relies on the molecular similarity with patient L1 CTC1 represented by 24 shared mutations. In accordance with NSCLC cBioPortal studies, we found that genes harboring truncal mutations in GR-CDXL1, GR-CDXL2, and GR-CDXL4 were found in 79% of genes altered in lung adenocarcinoma, while truncal mutations in GR-CDXL3 are found in 61% of genes altered in squamous cell carcinoma. Therefore, our models were found to be representative of NSCLC histologies, displaying alterations exclusive to this malignancy (e.g., *TP53*, *KRAS*, *KEAP1*, *STK11*). Key DDR-related mutations emerge from WES analysis, including *TP53*, *BRCA2* (GR-CDXL1), *CHEK2* (GR-CDXL2), and *ARID1B* (GR-CDXL1, GR-CDXL2), and reconstruction of phylogenetic trees infers their clonality. In addition, important subclonal CNA diversification in DDR-related genes was revealed across our models. Overall, genomic analysis supports the hypothesis that defects in genome maintenance mechanisms fuel CTC-driven tumor progression in NSCLC models.

Based on the rationale that DNA repair impairment may sensitize tumor cells to DNA-damaging chemotherapy, several clinical trials were conducted to assess PARPi efficacy in combination with chemotherapy in NSCLC patients (11). Despite encouraging phase II results in metastatic squamous NSCLC, phase III evaluation of veliparib in association with chemotherapy failed to show any survival benefits (34, 35). In the maintenance setting, PIN and PIPSeN trials have shown that olaparib also failed to improve survival in platinum-sensitive NSCLC patients (39, 40). However, patients were not included based on

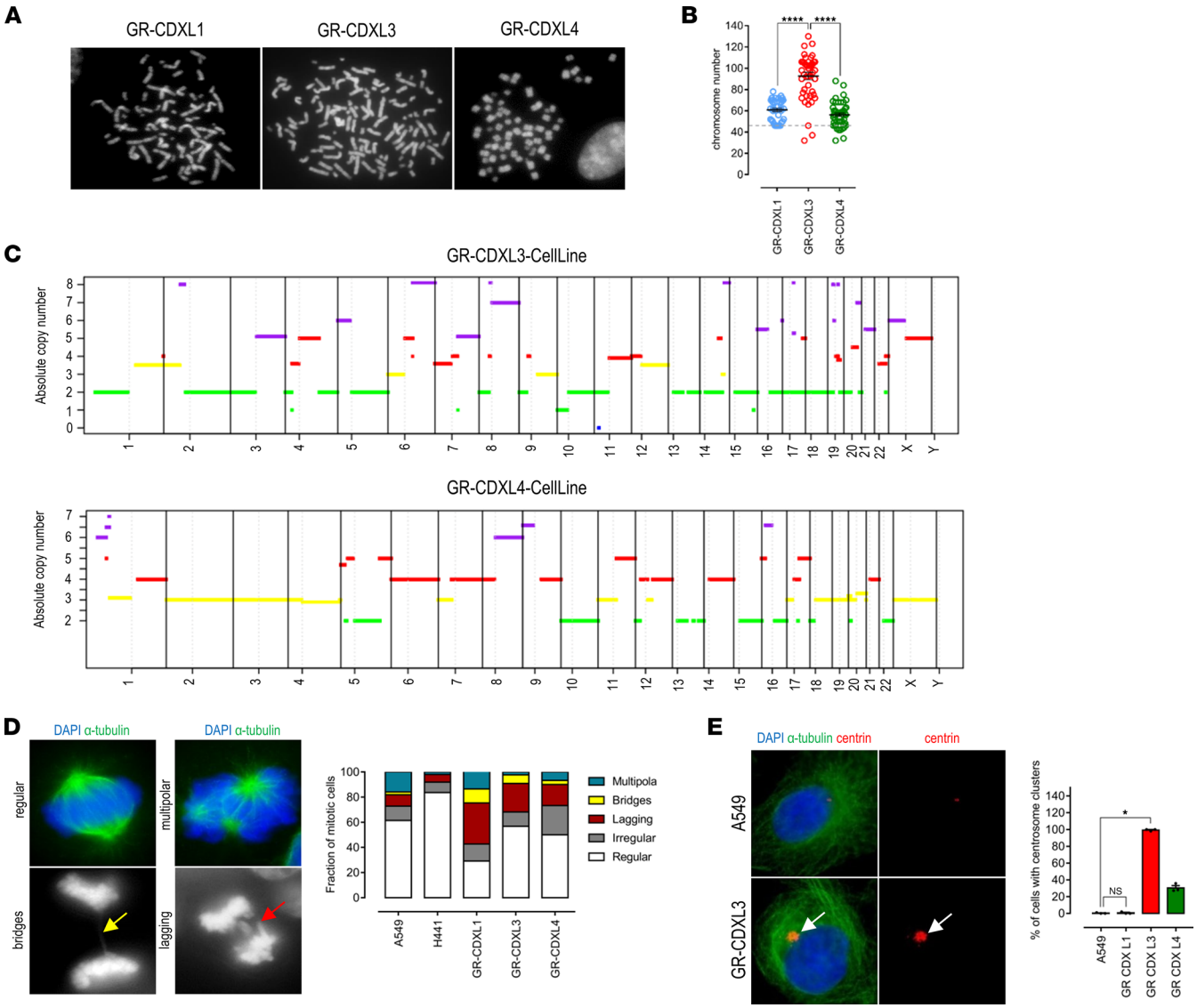


Figure 7. Mitotic defects in CDX-derived cell lines. (**A**) Metaphase spreads of GR-CDXL1, GR-CDXL3, and GR-CDXL4 chromosomes, shown at a total magnification of ×150. (**B**) Chromosome numbers. (**C**) Absolute copy number profiles showing whole-genome duplication of GR-CDXL3 (top) and GR-CDXL4 (bottom) cell lines. (**D**) IF analyses of mitotic defects in NSCLC and CDX-derived cells; yellow arrow indicates anaphasic bridge, and red arrow indicates lagging chromosome (left). Fraction of mitotic cells presenting defects (right). (**E**) Representative images of dual α-tubulin/centrin immunostaining revealing clustering of extra centrosomes in GR-CDXL3 cells (white arrows) (left). Proportion of cells presenting centrosome clusters (right). Statistical significance was assessed using Kruskall Wallis and post hoc Dunn's test for **B** and **E**. Data are shown as mean ± SEM; $*P < 0.05$, $***P < 0.0001$ from $n = 3$ experiments.

HRD status. Others are currently evaluating PARPi activity with or without chemotherapy in NSCLC patients, harboring HRD or not (12). In a recent study assessing the occurrence of HR-related mutations across several cancers, HRD was reported in 5% of NSCLC patients and 2% of *BRCA1/2* variants were pathogenic in this population (41). Here, we report that GR-CDXL1 displays a somatic biallelic mutation in *BRCA2* and promoter deletion of Fanconi anemia pathway gene *FANCA*. The 2 pathways are in cross-talk for DNA lesion repair, and *BRCA2* and *FANCA* inactivation promote HRD, which is also evident through unrepaired damage after mitosis, constitutive activation of *CHEK1*, and failure in RAD51 foci formation in GR-CDXL1 cells. Interestingly, similarly to patient L1, the GR-CDXL1 model is resistant to chemotherapy but, as predicted by molecular and functional profiling, highly sensitive to olaparib in vitro, in ovo, and in mice. This previously undescribed clinical context suggests that resistance to chemotherapy does not exclude PARPi efficacy in HR-deficient NSCLC tumors. A deeper understanding of the biological basis of HRD is, thus, crucial to expand patient screening beyond chemosensitivity for a more adequate selection of patients with HRD features and optimize PARPi efficacy in NSCLC malignancies.

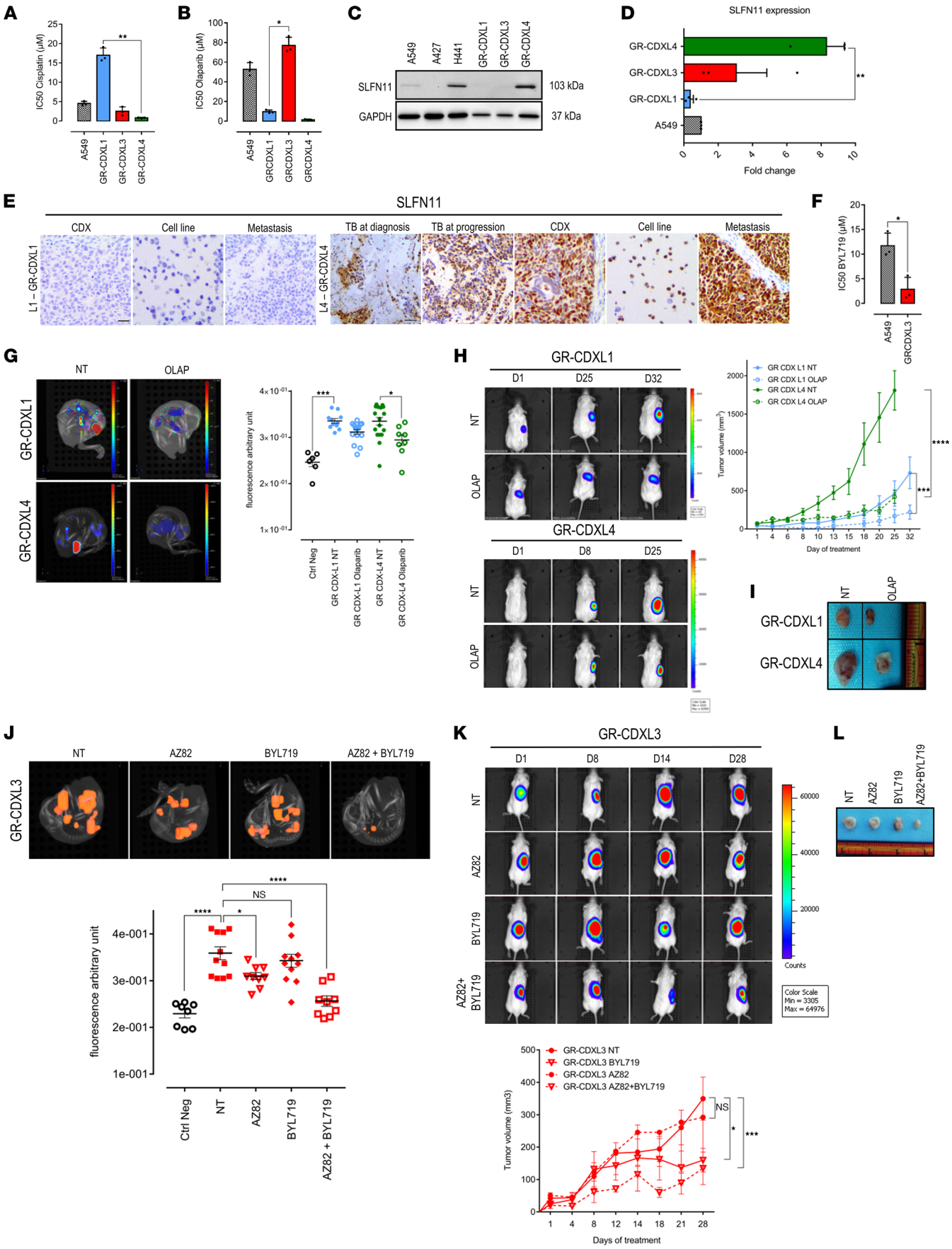

A
IC50 Cisplatin (uM)
A549
GR-CDXL1
GR-CDXL3
GR-CDXL4
B
IC50 Olaparib (uM)
A549
GRCDXL1
GRCDXL3
GRCDXL4
C
A549
A427
H441
GR-CDXL1
GR-CDXL3
GR-CDXL4
SLFN11
GAPDH
103 kDa
37 kDa
D
SLFN11 expression
GR-CDXL4
GR-CDXL3
GR-CDXL1
A549
Fold change
E
SLFN11
CDX
Cell line
Metastasis
TB at diagnosis
TB at progression
CDX
Cell line
Metastasis
L1 – GR-CDXL1
L4 – GR-CDXL4
F
IC50 BYL719 (uM)
A549
GRCDXL3
G
NT
OLAP
GR-CDXL1
GR-CDXL4
fluorescence arbitrary unit
Ctrl Neg
GR CDX-L1 NT
GR CDX-L1 Olaparib
GR CDX-L4 NT
GR CDX-L4 Olaparib
H
GR-CDXL1
D1
D25
D32
NT
OLAP
GR-CDXL4
D1
D8
D25
GR CDX L1 NT
GR CDX L1 OLAP
GR CDX L4 NT
GR CDX L4 OLAP
Tumor volume (mm3)
Day of treatment
I
NT
OLAP
GR-CDXL1
GR-CDXL4
J
NT
AZ82
BYL719
AZ82 + BYL719
GR-CDXL3
fluorescence arbitrary unit
NS
Ctrl Neg
NT
AZ82
BYL719
AZ82 + BYL719
K
GR-CDXL3
D1
D8
D14
D28
NT
AZ82
BYL719
AZ82+ BYL719
Counts
Color Scale
Min = 3305
Max = 64976
GR-CDXL3 NT
GR-CDXL3 BYL719
GR-CDXL3 AZ82
GR-CDXL3 AZ82+BYL719
Tumor volume (mm3)
Days of treatment
L
NT
AZ82
BYL719
AZ82+BYL719

Figure 8. In vitro, in ovo, and in vivo drug assays. (**A**) Mean in vitro IC_{50} values of cisplatin for control and CDX-derived cell lines. (**B**) Mean in vitro IC_{50} values of olaparib. (**C**) Western blot showing SLFN11 expression levels in GR-CDXL1, GR-CDXL3, GR-CDXL4, and NSCLC cell lines. (**D**) qPCR for SLFN11 gene expression in A549 and CDX-derived cell lines normalized to GAPDH expression level. Data are fold change and are shown as mean ± SEM. $n = 3$ experiments; $^{**}P < 0.01$ by Kruskall-Wallis and Dunn's test. (**E**) IHC staining of SLFN11 in patients L1 (CDX, cell line, and metastatic mouse tumor) and L4 (TB, CDX, cell line, metastatic mouse tumor) samples. Scale bar: 30 μm. (**F**) Mean in vitro IC_{50} values of BYL719 for control and GR-CDXL3 cell line. For **A**, **B**, and **F**, data are shown as mean ± SD. $n = 3$ experiments; $^{*}P < 0.05$, $^{**}P < 0.01$, Kruskall-Wallis and Dunn's test (**A** and **B**), 2-tailed unpaired *t* test with Welch's correction (**F**). (**G**) Three-dimensional representative images at ID17 (left) and quantitative analysis of average fluorescent tumor foci (right) of GR-CDXL1 or GR-CDXL4 mCherry-expressing CAM tumors, treated or not with olaparib. (**H**) Luciferase-expressing GR-CDXL1 (left, upper panel) or GR-CDXL4 (left, lower panel) tumors treated with olaparib. Representative BLI images (left) and tumor volumes (right) obtained at indicated days of treatment are shown. (**I**) Tumors at day 32 (GR-CDXL1-Luc) and day 25 (GR-CDXL4-Luc). (**J**) Three-dimensional representative images obtained at ID17 (left) and quantitative analysis of average fluorescent tumor foci (right) of GR-CDXL3 mCherry-expressing CAM tumors treated or not with AZ82 and/or BYL719. For **G** and **J**, data are shown as mean ± SEM. $n = 3$ experiments; $^{*}P < 0.05$, $^{**}P < 0.01$, $^{***}P < 0.001$, $^{****}P < 0.0001$ by Kruskall-Wallis and Dunn's test. Each point represents a single embryo. (**K**) Representative BLI images of GR-CDXL3 luciferase–expressing mouse tumors treated or not with AZ82 and/or BYL719. Tumor volume is shown (lower panel). For **H** and **K**, data are shown as mean ± SEM. $n = 5$; $^{*}P < 0.05$, $^{***}P < 0.001$, $^{****}P < 0.0001$ by 2-way ANOVA. (**L**) GR-CDXL3 luciferase–expressing tumors obtained at day 28.

We report a second HR-deficient CDX model GR-CDXL4, sensitive to olaparib but lacking an HRD-related mutation. SLFN11, an acknowledged DNA/RNA helicase recruited at replication forks via replication protein A (RPA) in response to genotoxic stress, has recently emerged as a candidate biomarker of sensitivity to platinum-based chemotherapies and PARPi (39–41). In SCLC, SLFN11 expression correlated with PARPi olaparib and talazoparib activity in preclinical models, while it was associated with improved survival in patients treated with PARPi/chemotherapy combination (28, 42, 43). To our knowledge, its significance in NSCLC has not been reported yet. Interestingly, in this study, we detected high *SLFN11* mRNA levels and SLFN11 protein overexpression in GR-CDXL4 cells. IHC analysis indicated a strong expression of SLFN11 in patient L4 TB at progression and in the corresponding CDX tumor. This prompted us to evaluate SLFN11 expression in patient L4 TB at diagnosis, which revealed strong expression, as well. Basal SLFN11 expression may, thus, be predictive of tumor sensitivity to PARPi. Nevertheless, additional investigations are warranted to confirm the correlation between SLFN11 overexpression and NSCLC tumor response to olaparib. Initially, the patient L4 TB specimen at diagnosis was classified as *MET*-amplified adenocarcinoma, and additional analysis showed positive neuroendocrine staining in a few tumor cells, in addition to *SLFN11*$^{+}$ cells. At progression, neuroendocrine marker levels were intensified along with strong SLFN11 expression, suggesting a potential SCLC transformation. Histological transformation of lung adenocarcinoma into SCLC is a rare event, which has been described as a key resistance mechanism to tyrosine kinase inhibitor (TKI) treatment in around 5% *EGFR*-mutant and few *ALK*-rearranged NSCLC cases (44, 45). Furthermore, phylogenetic analysis by Lee et al. suggested that early divergent evolution of EGFR TKI-resistant SCLC from adenocarcinoma is predisposed by the complete inactivation of *RB1* and *TP53* (46). In the present case, we showed that all L4 tumor samples harbored loss-of-function *RB1* and *TP53* mutations. We propose that early tumor screening for SLFN11 expression can aid in the selection of NSCLC patients eligible for PARPi treatment. In addition to its predictive value of sensitivity, our data raise the hypothesis that SLFN11 expression may be a histologic biomarker to predict phenotypic transformation of adenocarcinoma into SCLC. Further investigation is needed to confirm this predictive role of SLFN11 in NSCLC malignancy.

WGD was observed as a clonal event in GR-CDXL3 model, consistent with previous work in NSCLC (47). The cell line displayed important CIN and was, thus, highly tumorigenic and seeded multiple metastases when injected in mice and chick embryo CAM. This ensued notably due to clustering of supernumerary centrosomes mediated by KIFC1, promoting bipolar divisions in cancer cells allowing their survival (48, 49). Since KIFC1 inhibition alone had no significant anticancer activity, we sought to improve its efficacy by adding PI3KA inhibitor BYL719, targeting AKT1 in GR-CDXL3 tumors. Synergy was observed between the 2 molecules, showing significant tumor response in ovo and in vivo. However, we acknowledge limitations to these data, as the AZ82 molecule has been shown to have unfavorable cytotoxic effects and none of the other KIFC1 inhibitors currently available exhibit enough potency (50). Nevertheless, encouraging findings recently reported by Fan et al. elucidated a potential role of KIFC1 as a biomarker of cancer recurrence. The authors show that DNA-damaging therapies promote centrosome clustering through ATM and Rad3-related–mediated (ATR-mediated) and Ataxia-Telangiectasia mutated–mediated (ATM-mediated) phosphorylation of KIFC1, suggesting this mechanism as a therapeutic target (50).

In conclusion, in-depth characterization and functional analysis of CDX systems elucidate a biological rationale for DDR and genome instability–directed therapeutics in NSCLC (Supplemental Figure 13). All

our CDX models display a characteristic mutation spectrum for genome integrity regulator genes, highlighting their implication in CTC tumorigenic potential. Mechanistic studies unravel CTC-specific DNA repair dysfunctionality in 3 CDX and their corresponding cell line, which provides insight into the importance of DNA repair management in NSCLC. Importantly, our findings shed light on the necessity to broaden screening approaches in NSCLC beyond chemosensitivity in order to expand the category of patients who may benefit from PARPi. We suggest *SLFN11* as a predictive biomarker of sensitivity to PARPi in NSCLC. Additionally, we put forward its potential role as a predictor of NSCLC adenocarcinoma transformation into SCLC.

Methods

Supplemental Methods are available online with this article.

Patient samples

Blood was drawn in CellSave (Menarini Silicon Biosystems) and EDTA tubes and were immediately transferred to the laboratory.

CTC enumeration

Blood samples collected in CellSave tubes were run with the CellSearch platform (Menarini) using the CTC kit (Menarini) according to manufacturer's instructions and training.

CTC enrichment before implantation into mice

In total, 50 μL of the RosetteSep cocktail (StemCell Technologies) was added per 1mL of blood and incubated 20 minutes at room temperature (RT). After incubation, the sample was diluted with an equal volume of HBSS (Invitrogen) supplemented with 2% FBS (Invitrogen). The solution was then carefully layered on top of 15 mL Ficoll-Plaque Plus (GE-Healthcare) and centrifuged for 20 minutes at 1200*g* at 20°C without brake. Enriched cells were collected, washed with 50 mL HBSS/2% FBS, and centrifuged for 5 minutes at 250*g* at 20°C. Cells were resuspended in 100 μL of cold HBSS supplemented with 100 μL cold Matrigel (Corning) and kept on ice until implantation in mice.

Growth of CDX in immunocompromised mice

Before CTC implantation, NSG 6-week-old male mice (Charles River Laboratories) were anesthetized by peritoneal injection of 10 mg/mL ketamine and 1 mg/mL xylazine at a dose of 10 mL/kg. The upper dorsal regions of mice were shorn, and the skin was aseptized with a chlorhexidine solution, incised at the level of the interscapular region, and CTCs were injected in 200 μL HBSS/Matrigel in the interscapular fat pad. Mice were monitored every day. Palpable tumors were monitored once a week, and tumor volume was determined as the following: (tumor length × tumor width^2)/2. When it reached 1770 mm^3 or when mice presented signs of deteriorated health status, tumors were aseptically excised and dissected into fragments of approximately 20 mm^3. Tumor fragments were passaged into NSG mice, and the remainder of the tumor was used for Alu sequence detection, IHC, molecular analysis, and cell line establishment. Mice were housed in pathogen-free animal housing at the Center for Exploration and Experimental Functional Research (CERFE; Evry, France) animal facility in individually ventilated cages of Polysulfone plastic (213 × 362 × 185 mm) with sterilized and dust-free bedding cobs; they were provided access to sterilized food and water ad libitum, under a light-dark cycle (14-hour circadian cycle of artificial light) and with controlled RT and humidity. Mice were housed in groups with a maximum of 6 animals during a 7-day acclimation period and groups of a maximum of 6 animals during the experimental phase.

Enrichment, detection and isolation of single CTCs

Individual CTC isolation was performed by combining different methods described in Supplemental Methods.

WES

Genomic DNA is captured using Agilent in-solution enrichment methodology (SureSelect XT Clinical Research Exome, Agilent) with their biotinylated oligonucleotides probes library (SureSelect XT Clinical Research Exome 54 Mb, Agilent), followed by paired-end 75 bases massively parallel sequencing on Illumina HiSeq4000. For the detailed process, see Gnirke et al. (51). Sequence capture, enrichment and

elution are performed according to manufacturer's instruction and protocols (SureSelect, Agilent) without modification except for library preparation performed with NEBNext Ultra kit (New England Biolabs). For library preparation, 600 ng of each genomic DNA are fragmented by sonication and purified to yield fragments of 150–200 bp. Paired-end adaptor oligonucleotides from the NEB kit are ligated on repaired, A-tailed fragments and then purified and enriched by 8 PCR cycles. In total, 1200 ng of these purified libraries are then hybridized to the SureSelect oligo probe capture library for 72 hours. After hybridization, washing, and elution, the eluted fraction is PCR amplified with 9 cycles; it is then purified and quantified by quantitative PCR (qPCR) to obtain sufficient DNA template for downstream applications. Each eluted-enriched DNA sample is then loaded on an Illumina HiSeq4000 for 75b paired-end sequencing. Image analysis and base calling were performed using Illumina Real Time Analysis (2.7.6) with default parameters.

Heatmap

CNA absolute profiles were clustered using the inverse Spearman correlation coefficient as distance, and Ward's aggregation method. The heatmap was built using the complexHeatmap R package and in-house codes. All computation and figure processings were performed using R v4.0.2.

Phylogenetic inference

All nonsilent somatic mutations present in at least 2 tumor samples were considered for determining phylogenetic trees. Tree construction is detailed in Supplemental Methods.

CDX-derived cell line establishment and cell culture

CDX tumor dissociation and cultures are described in Supplemental Methods.

Immunofluorescence

Cells were seeded on coverslips in 6-well plates. After 48 hours, cells were either left untreated, irradiated (6 Gray) or treated with APH at the indicated doses. Twenty-four hours later, cells were washed with PBS 1×, fixed with 4% paraformaldehyde (15 minutes at RT), and permeabilized with 0.5 Triton X-100 (Roche; 10 minutes at RT). Nonspecific binding sites were blocked with BSA for 30 minutes. Primary antibody staining (Supplemental Table 7) was performed at 37°C for 1 hour, followed by a secondary antibody (anti–rabbit Alexa Fluor 555 [clone Poly4064, 406412, BioLegend]; anti–mouse Alexa Fluor 488 [polyclonal, A-11029, Invitrogen]) incubation of 30 minutes at 37°C. Scanning and image analysis were done on an Ariol scanning system (Leica Biosystems Richmond Inc.) including a Leica DM6000 B microscope with multibay stages (MB 8).

RNA extraction and qPCR analysis

For *SLFN11* gene expression analysis, total RNA was isolated, and qPCR was performed as described in Supplemental Methods.

In vitro drug assays

CDX-derived and A549 cells were seeded in quadruplicates into 384-well plates. Twenty four or 48 hours after seeding, cells were treated with cisplatin, olaparib, BYL719, or AZ82 for 5 days. Drugs were diluted in Advanced DMEM (Invitrogen). Cell viability assays were performed using CellTiter-Glo Luminescent Cell Viability assay kit (Promega). Luminescence was measured by Victor X4 Series Multilabel Plate Readers (Perkin Elmer). Generation of drug-response curves and determination of IC_{50} values were performed using Prism software.

In vivo modeling of metastasis and drug assays

CAM. Fertilized chicken eggs were purchased (EARL Les Bruyères) and incubated for 3 days at 37°C with 60% humidity. Metastasis evaluation and drug assays in the CAM chick embryo model were performed as previously described (29). Briefly, 2×10^3 mCherry-expressing cells were implanted into the CAM at incubation day 10 (ID10). Tumor growth and embryo viability were examined daily until imaging analysis at ID17. Treatments were administered topically starting at ID11 as follows: olaparib via single administration (100 μg/kg), and AZ82 (20 μg/kg) and BYL719 (10 μg/kg) every other day. The final doses were calculated based on the weight of the chicken egg at ID11. At ID17, fluorescence and CT scans of

the chick embryo were performed simultaneously using the IVIS Spectrum Imager (PerkinElmer). A 3D reconstitution of images was performed using Living Image software (PerkinElmer).

Mice. In total, 5×10^5 luciferase-expressing CDX-derived cells were grafted by IC injection into NSG mice (Charles River Laboratories). Metastatic progression was monitored once a week by bioluminescence imaging (BLI) evaluation under anesthesia and after i.p. injection of D-luciferin (15 μg/kg; Promega) using IVIS Spectrum imaging (PerkinElmer). To test in vivo drug efficacy, 2×10^6 cells were injected s.c. into NSG mice. Once tumors reached an average volume of 100 mm^3, mice were randomized into groups and treated with vehicle DMSO (1%), olaparib (50 mg/kg, i.p. injection, 3 times per week), BYL719 (20 mg/kg, oral gavage, 3 times per week), AZ82 (10 mg/kg, oral gavage, 3 times per week), or a combination of BYL719 and AZ82. S.c. tumor dimensions were measured by caliper. For BLI evaluation, i.p. with D-luciferin (15 μg/kg; Promega) was performed, and mice were scanned using IVIS Spectrum imaging (PerkinElmer) under anesthesia.

Statistics

Unpaired 2-tailed Student's *t* test with Welch's correction was used to compare 2 groups, and Kruskall-Wallis followed by post hoc Dunn's test was used for multiple comparisons. Two-way ANOVA was used to analyze tumor growth data in vivo. All statistical tests were performed using GraphPad Prism 7 software and are specified in figure legends. Data are shown as mean values ± SD or SEM, as indicated; 95% CI was used, and significance was considered when *P* value was less than 0.05.

Study approval

Human studies. The study (IDRCB2008-A00585-50) was conducted at Gustave Roussy, authorized by the French national regulation agency Agence Nationale de Sécurité du Médicament et des produits de santé (ANSM), and approved by the Ethics Committee and our IRB (CSET number 2008/1370). All patients provided written informed consent allowing for the collection of 10 blood samples (30 mL) over 3 years.

Animal studies. Animal experimentation was approved by the Animal Experimentation Ethics Committee (no. 26, project 2018_019_13999) and performed according to European laws and regulations. The animal care, housing, and all experiments were performed in accordance with French legislation concerning the protection of laboratory animals and in accordance with a currently valid license for experiments on vertebrate animals, issued by the French Ministry of Higher Education, Research and Innovation (MESRI).

Author contributions

TT, VF, and PP conducted experiments and contributed to experimental design, data analysis, and manuscript editing with the assistance of MO. AA provided technical assistance. OD, LBS, SC, and JGJ contributed to CDX establishment and characterization. PLK and PP provided DNA repair expertise. JR and SP contributed to data analysis and manuscript editing. JM, DP, and BB supported patient recruitment and sample management, and provided clinical support for the study. VM performed immunohistopathology experiments and analysis under the supervision of JYS. FF directed the research and manuscript editing.

Acknowledgments

We are very grateful for the patients and their families. The authors thank Emma Pailler for her valuable contribution to this study. We also thank Sophie Postel-Vinay and Francesco Facchinetti for very helpful discussions; Integragen GeCo (Evry, France), Marc Deloger, and Bastien Job for bioinformatics analysis; and Stefan Michiels and Nusaïbah Ibrahimi for their help with statistical analysis. TT is supported by La Ligue Contre le Cancer and Fondation pour la Recherche médicale (grant no. FDT202106012817). The study was supported by ANR-15-CE17-0006-01.

Address correspondence to: Françoise Farace, Gustave Roussy, Université Paris-Saclay, "Rare Circulating Cells" Translational Platform, CNRS UMS3655 — INSERM US23 AMMICA, F-94805, Villejuif, France. Phone: 33.142115198; Email: francoise.farace@gustaveroussy.fr.

1. Sung H, et al. Global Cancer Statistics 2020: GLOBOCAN estimates of incidence and mortality worldwide for 36 cancers in 185 countries. *CA Cancer J Clin*. 2021;71(3):209–249.
2. Reck M, Rabe KF. Precision diagnosis and treatment for advanced non-small-cell lung cancer. *N Engl J Med*. 2017;377(9):849–861.
3. Gandhi L, et al. Pembrolizumab plus chemotherapy in metastatic non-small-cell lung cancer. *N Engl J Med*. 2018;378(22):2078–2092.

4. Postel-Vinay S, et al. The potential of exploiting DNA-repair defects for optimizing lung cancer treatment. *Nat Rev Clin Oncol*. 2012;9(3):144–155.
5. Lord CJ, Ashworth A. PARP inhibitors: synthetic lethality in the clinic. *Science*. 2017;355(6330):1152–1158.
6. Pilié PG, et al. State-of-the-art strategies for targeting the DNA damage response in cancer. *Nat Rev Clin Oncol*. 2019;16(2):81–104.
7. Robson M et al. Olaparib for metastatic breast cancer in patients with a germline BRCA mutation. *N Engl J Med*. 2017;377(6):523–533.
8. Moore K, et al. Maintenance olaparib in patients with newly diagnosed advanced ovarian cancer. *N Engl J Med*. 2018;379(26):2495–2505.
9. Golan T, et al. Maintenance olaparib for germline BRCA-mutated metastatic pancreatic cancer. *N Engl J Med*. 2019;381(4):317–327.
10. De Bono J, et al. Olaparib for metastatic castration-resistant prostate cancer. *N Engl J Med*. 2020;382(22):2091–2102.
11. Remon J, et al. Somatic and germline BRCA 1 and 2 mutations in advanced NSCLC from the SAFIR02-lung trial. *JTO Clin Res Rep*. 2020;1(3):100068.
12. Passiglia F, et al. Repositioning PARP inhibitors in the treatment of thoracic malignancies. *Cancer Treat Rev*. 2021;99:102256.
13. Ceccaldi R, et al. Repair pathway choices and consequences at the double-strand break. *Trends Cell Biol*. 2016;26(1):52–64.
14. Knijnenburg TA, et al. Genomic and molecular landscape of DNA damage repair deficiency across The Cancer Genome Atlas. *Cell Rep*. 2018;23(1):239–254.
15. Massagué J, Obenauf AC. Metastatic colonization by circulating tumour cells. *Nature*. 2016;529(7586):298–306.
16. Cristofanilli M, et al. Circulating tumor cells, disease progression, and survival in metastatic breast cancer. *N Eng J Med*. 2004;351(8):781–791.
17. De Bono JS, et al. Circulating tumor cells predict survival benefit from treatment in metastatic castration-resistant prostate cancer. *Clin Cancer Res*. 2008;14(19):6302–6309.
18. Krebs MG, et al. Evaluation and prognostic significance of circulating tumor cells in patients with non-small-cell lung cancer. *J Clin Oncol*. 2011;29(12):1556–1563.
19. Lindsay CR, et al. EPAC-lung: pooled analysis of circulating tumour cells in advanced non-small cell lung cancer. *Eur J Cancer*. 2019;117:60–68.
20. Baccelli I, et al. Identification of a population of blood circulating tumor cells from breast cancer patients that initiates metastasis in a xenograft assay. *Nat Biotechnol*. 2013;31(6):539–544.
21. Hodgkinson CL, et al. Tumorigenicity and genetic profiling of circulating tumor cells in small-cell lung cancer. *Nat Med*. 2014;20(8):897–903.
22. Morrow CJ, et al. Tumourigenic non-small-cell lung cancer mesenchymal circulating tumour cells: a clinical case study. *Ann Oncol*. 2016;27(6):1155–1160.
23. Drapkin BJ, et al. Genomic and functional fidelity of small cell lung cancer patient-derived xenografts. *Cancer Discov*. 2018;8(5):600–615.
24. Faugeroux V, et al. Genetic characterization of a unique neuroendocrine transdifferentiation prostate circulating tumor cell-derived eXplant model. *Nat Commun*. 2020;11(1):1884.
25. Tayoun T, et al. CTC-derived models: a window into the seeding capacity of circulating tumor cells (CTCs). *Cells*. 2019;8(10):1145.
26. Alix-Panabières C, Pantel K. Challenges in circulating tumour cell research. *Nat Rev Cancer*. 2014;14(9):623–631.
27. Murai J, et al. Resistance to PARP inhibitors by SLFN11 inactivation can be overcome by ATR inhibition. *Oncotarget*. 2016;7(47):76534–76550.
28. Lok BH, et al. PARP inhibitor activity correlates with SLFN11 expression and demonstrates synergy with temozolomide in small cell lung cancer. *Clin Cancer Res*. 2017;23(2):523–535.
29. Pawlikowska P, et al. Exploitation of the chick embryo chorioallantoic membrane (CAM) as a platform for anti-metastatic drug testing. *Sci Rep*. 2020;10(1):16876.
30. Robinson DR, et al. Integrative clinical genomics of metastatic cancer. *Nature*. 2017;548(7667):297–303.
31. Ding L, et al. Somatic mutations affect key pathways in lung adenocarcinoma. *Nature*. 2008;455(7216):1069–1075.
32. Imielinski M, et al. Mapping the hallmarks of lung adenocarcinoma with massively parallel sequencing. *Cell*. 2012;150(6):1107–1120.
33. Rizvi NA, et al. Cancer immunology. Mutational landscape determines sensitivity to PD-1 blockade in non-small cell lung cancer. *Science*. 2015;348(6230):124–128.
34. Jordan EJ, et al. Prospective comprehensive molecular characterization of lung adenocarcinomas for efficient patient matching to approved and emerging therapies. *Cancer Discov*. 2017;7(6):596–609.
35. Caso R, et al. Preoperative clinical and tumor genomic features associated with pathologic lymph node metastasis in clinical stage I and II lung adenocarcinoma. *NPJ Precis Oncol*. 2021;5(1):70.
36. Ganem NJ, et al. A mechanism linking extra centrosomes to chromosomal instability. *Nature*. 2009;460(7252):278–282.
37. Rhys AD, et al. Loss of E-cadherin provides tolerance to centrosome amplification in epithelial cancer cells. *J Cell Biol*. 2018;217(1):195–209.
38. Lallo A, et al. Ex vivo culture of cells derived from circulating tumour cell xenograft to support small cell lung cancer research and experimental therapeutics. *Br J Pharmacol*. 2019;176(3):436–450.
39. Fennell DA, et al. A randomized phase II trial of olaparib maintenance versus placebo monotherapy in patients with chemo-sensitive advanced non-small cell lung cancer. *J Clin Oncol*. 2020;38(15 suppl):e21649.
40. Postel-Vinay S, et al. 100MO Olaparib maintenance vs placebo in platinum-sensitive non-small cell lung cancer: the phase II randomized PIPSeN trial. *J Thorac Oncol*. 2021;16(4):S752.
41. Heeke AL, et al. Prevalence of homologous recombination-related gene mutations across multiple cancer types. *JCO Precis Oncol*. 2018;2:PO.17.00286.
42. Stewart CA, et al. Dynamic variations in epithelial-to-mesenchymal transition (EMT), ATM, and SLFN11 govern response to PARP inhibitors and cisplatin in small cell lung cancer. *Oncotarget*. 2017;8(17):28575–28587.
43. Pietanza MC, et al. Randomized, double-blind, phase ii study of temozolomide in combination with either veliparib or placebo in patients with relapsed-sensitive or refractory small-cell lung cancer. *J Clin Oncol*. 2018;36(23):2386–2394.

44. Aldea M, et al. Overcoming resistance to tumor-targeted and immune-targeted therapies. *Cancer Discov*. 2021;11(4):874–899.
45. Marcoux N, et al. EGFR-mutant adenocarcinomas that transform to small-cell lung cancer and other neuroendocrine carcinomas: clinical outcomes. *J Clin Oncol*. 2019;37(4):278–285.
46. Lee J-K, et al. Clonal history and genetic predictors of transformation into small-cell carcinomas from lung adenocarcinomas. *J Clin Oncol*. 2017;35(26):3065–3074.
47. Jamal-Hanjani M, et al. Tracking the evolution of non-small-cell lung cancer. *N Engl J Med*. 2017;376(22):2109–2121.
48. Rath O, Kozielski F. Kinesins and cancer. *Nat Rev Cancer*. 2012;12(8):527–539.
49. Wu J, et al. Discovery and mechanistic study of a small molecule inhibitor for motor protein KIFC1. *ACS Chem Biol*. 2013;8(10):2201–2208.
50. Fan G, et al. The ATM and ATR kinases regulate centrosome clustering and tumor recurrence by targeting KIFC1 phosphorylation. *Nat Commun*. 2021;12(1):20.
51. Gnirke A, et al. Solution hybrid selection with ultra-long oligonucleotides for massively parallel targeted sequencing. *Nat Biotechnol*. 2009;27(2):182–189.

SUPPLEMENTARY FIGURES

Supplementary Table 1: Clinicobiological characteristics of NSCLC cohort.

Supplementary Table 2: Number of variants identified in TB specimens, CDXs and CDX-derived cell lines.

Supplementary Table 3: Number of high-confidence variants identified in CTC samples.

Supplementary Table 4: List of antibodies used for IHC and staining conditions.

Supplementary Table 5: List of antibodies used for FACS analysis.

Supplementary Table 6: List of antibodies used for western blot.

Supplementary Table 7: List of antibodies used for immunofluorescence.

Supplementary Figure 1: Clinical timelines of patients L1, L2, L3 and L4. The length of each segment is proportional to the duration of treatment (1cm = 1 month). Patients L2, L3 and L4 biopsy at diagnosis was issued from the left latero-tracheal lymph node, the right inferior lobe and the left superior lobe of the lung respectively. Patient L4 biopsy at progression was sampled in the lung.

Supplementary Figure 2: Phenotypic characterization of patient samples, CDX and CDX-derived cell lines. (**A**) Number of CTCs detected by CellSearch according to tumor molecular status of the 55 NSCLC patients. (**B**) Representative images of cell morphology in the three CDX-derived cell lines at 10X, 20X and 40 X magnifications. Scale bar: 50 µm. (**C**) Immunohistochemical stainings on GR-CDXL1 CDX tumor and CDX-derived cell line (scale bar: 20 µm), patient L2 biopsy and GR-CDXL2 CDX tumor (scale bar: 30 µm) (HES, CK8/18, EpCAM, Ki67, Vimentin, TTF1,

Chromogranin A and synaptophysin) and on patient L3 biopsy, GR-CDXL3 CDX tumor and CDX-derived cell line (scale bar: 20 µm) (HES, chromogranin A, synaptophysin, P40, CK5/6, EpCAM, Vimentin, Ki67). All images are shown at 20X magnification. (**D**) Flow cytometry analyses of epithelial (EpCAM, panCK, E-cadherin), mesenchymal (vimentin) and cancer stem cell markers (ALDH, CD133, CD90, ABCG2 and CD166) in the three CDX-derived cell lines.

Supplementary Figure 3: In vivo drug assays. Palpable subcutaneous tumors of GR-CDXL1 (n=10), GR-CDXL2 (n=6), GR-CDXL3 (n=6) and GR-CDXL4 (n=9) at passages P11, P5, P5 and P4 respectively were treated once every week (intraperitoneal injection) with paclitaxel (15 mg/kg) and/or cisplatin (5 mg/kg) or the vehicle as indicated by the arrows. Tumor volumes were determined by caliper according to the formula (width^2×length)/2. Data are presented as mean tumor volumes ± SEM.

Supplementary Figure 4: Metastatic tumor detection in mice. GR-CDXL1, GR-CDXL3 and GR-CDXL4 tumor FFPE sections stained with HES, and anti-human CK7 and anti-human Ki67.

Supplementary Figure 5: Flow diagram of samples available for WES analysis for each patient.

Supplementary Figure 6: Comparative genomic analysis of the CDX and the CDX-derived cell lines. (**A**) Fraction of CDX mutations shared with the corresponding cell line. (**B**) Fraction of CDX driver mutations shared with the corresponding cell line. (**C**) Mutated driver genes and their amino acid sequence variation in the CDX and the CDX-derived cell line. (**D**) Mutated driver genes and their amino acid sequence variation in the CDX only.

Supplementary Figure 7: Dendograms resulting from hierarchical clustering analysis of all mutations detected by WES among patients L1, L3 and L4 samples.

Supplementary Figure 8: Comparative CNA analysis of the biopsies, the CDX and the CDX-derived cell lines. Circos plot of CNAs detected in the biopsy, the CDX and the CDX-derived cell line (when available) for each model (GR-CDXL1, GR-CDXL2, GR-CDXL3 and GR-CDXL4).

Supplementary Figure 9: Comparative CNA analysis of the CDX models. Circos plot of CNAs detected in the four CDX models (gain in red, normal in black, loss in blue) (1: GR-CDXL1, 2: GR-CDXL2, 3: GR-CDXL3, 4: GR-CDXL4).

Supplementary Figure 10: Frequency of CDX gene alterations in lung cancer histologies according to cBioPortal studies. (**A**) Genes harboring truncal mutations in GR-CDXL1, GR-CDXL2 and GR-CDXL4 were found in 79% of genes altered in lung adenocarcinoma. (**B**) Genes harboring truncal mutations in GR-CDXL3 are found in 61% of genes altered in squamous cell carcinoma. All CDX models displayed functional inactivation of *TP53* found at 53.8%. GR-CDXL1 harbored a deleterious *KMT2C* (9.4%), *ARID1A* (6.4%), *ATRX* (5.4%), *BRCA2* mutation (3.2%) and *FANCA* deletion (0.9%). GR-CDXL2 had a *KRAS*-mutant profile which included co-occurring mutations in *KEAP1* (14.5%), *STK11* (15.7%) and *RBM10* (9.5%) genes, exclusive of adenocarcinoma. Genomic characterization revealed DDR-related *CHEK2* and *ARID1B* driver mutations found at 1.4% and 3.4% respectively (1–5). (**C**) Genes harboring truncal mutations in GR-CDXL1, GR-CDXL2, GR-CDXL3 and GR-CDXL4 are predominant in other types of metastatic cancers.

Supplementary Figure 11: Statistics of allele drop-out and false-positive rate of single CTCs. (**A**) and (**B**) Representation of allelic drop-out (ADO) in GR-CDXL1 (**A.** left) and GR-CDXL3 (**B.** left). Reliable variants (green) were defined by an equal variant allele frequency (VAF) in both germline DNA and WBC bulk samples. Variants in ADO (red) were defined by a VAF ranging from 0.2 to 0.8 in germline DNA and <0.1 or >0.9 in WBC bulk. False-positive rates in one P8 CTC (**A.** right) and in five P51 CTCs (**B.** right) are shown. To estimate false-positive rates, we divided the number of reliable somatic variants not present in bulk tumor samples (TBs and CDX) by the number of target bases covered ≥8X in the same sample.

Supplementary Figure 12: Chromosomal instability of GR-CDXL3 and GR-CDXL4 CDX models. (**A**) Absolute copy number profiles of GR-CDXL3 and GR-CDXL4 CDX models. Yellow=normal/major copy number, red=gain, green=loss, purple=amplification. (**B**) Representative images of mitotic lagging chromosome analysis in GR-CDXL1 and GR-CDXL3 cells after 4'6-diamidino-2-phenylindole (DAPI, blue) and centromere staining with anti-CENPA (green). (**C**) Lagging DNA analysis obtained from scoring at least 50 anaphases per cell line in three independent experiments. Data are presented as mean ± SEM, *p<0.05 (unpaired t-test with Welch's correction).

Supplementary Figure 13: Diagram of DDR-related pathways implicated in CDX-derived cell line vulnerabilities and targeting strategies. DNA damage in the three CDX-derived cell lines results in the activation of several repair cascades prone to defects. Olaparib-induced PARP trapping leads to synthetic lethality in *BRCA2*/*FANCA*-defective GR-CDXL1 cells. Dual targeting of AKT1 gain through the inhibition of PI3KA (by BYL719) and centrosome clustering via KIFC1 inhibition (by AZ82) leads to GR-CDXL3 cell death. In GR-CDXL4 cells, SLFN11 overexpression

may lead to olaparib sensitivity. SSB, single-strand DNA break; DSB, double-strand DNA break; HR, homologous recombination.

Supplementary Figure 14: *In vivo* parameters. (**A**) Western blot analysis of the levels of p-AKT and AKT in CDX-derived (GR-CDXL1, GR-CDXL3 and GR-CDXL4) and NSCLC (A427, A549 and H441) cell lines. (**B**) Average body weight of mice injected with GR-CDXL1 or GR-CDXL4 Luc cells measured over the course of treatment. (**C**) Quantitative analysis of BLI. (**D**) Average body weight of mice injected with GR-CDXL3 Luc cells measured over the course of treatment. (**E**) Quantitative analysis of BLI. Each point represents a single mouse. For **B-E**, n=5 for all groups except GR-CDXL1 NT where n=4. Data are presented as mean ± SEM, ***p<0.001, ****p<0.0001 (two-way ANOVA).

SUPPLEMENTARY METHODS

***Enrichment, detection and isolation of single CTCs*.** Individual CTC isolation was performed by combining different methods. Either: (i) isolation by size of epithelial tumor cells (ISET) filtration, immunofluorescence staining and scanning of filters, followed by laser microdissection $CD45^+$ cells, or (ii) enrichment via RosetteSep, immunofluorescence staining followed by FACS isolation, or (iii) CTC detection using CellSearch followed by CTC isolation using self-seeding microwell chips. The methods are described in detail in previous reports (6, 7).

***WGA, quality control, dsDNA*.** Whole genome amplification (WGA) of CTCs and CD45-positive cells was performed using the Ampli1 WGA kit (Menarini) according to manufacturer's instructions. The quality of Ampli1 WGA products was checked by multiplex PCR as described by Polzer *et al.* (8). To increase total dsDNA content in Ampli1 WGA products, ssDNA molecules were converted into dsDNA molecules using the Ampli1 ReAmp/ds kit (Menarini).

***Isolation of genomic DNA from blood, TB, CDX and CDX-derived cell line*.** DNA from formalin-fixed paraffin-embedded tumor biopsies was purified with QIAamp DNA FFPE Tissue kit (Qiagen, Hilden, Germany) according to manufacturer's protocol. DNA from the CDX was extracted with AllPrep DNA/RNA kit (Qiagen) and germline DNA and cell line DNA was purified with QIAamp DNA blood kit (Qiagen).

***Sequence alignment and variant calling*.** Base calling was performed using the Real-Time Analysis software sequence pipeline (2.7.7) from Illumina with default parameters. Sequence reads from amplified DNA (circulating T cells and CD45 pools) were trimmed for Ampli1 adapters with Cutadapt (1.14) (9). Human reads from xenograft samples were extracted by bamcmp (10). Reads were then aligned to the

human genome build hg38/GRCh38.p7 using the Burrows-Wheeler Aligner (BWA) tool (11). Duplicated reads were removed using Sambamba (12). Variant calling of single nucleotide variants (SNVs) and small insertions/deletions (indels) was performed using the Broad Institute's GATK Haplotype Caller GVCF tool (3.7) (13, 14) for germline variants and MuTect2 tool (2.0, --max_alt_alleles_in_normal_count=2; --max_alt_allele_in_normal_fraction=0.04) (15) for somatic variants. To keep only reliable somatic variants, we then applied the following post-filtering steps:

- Variants classified as "PASS" or "t_lod_fstar" by MuTect2 (and not flagged as PID).
- Coverage ≥8 in the tumor and matched normal sample.
- QSS score ≥ 20.
- Variant allele fraction in the tumor (VAFT) ≥ 0.05 with ≥ 5 mutated reads, variant allele fraction in the normal sample (VAFN) = 0.

Additional criteria were applied to generate a high-confidence set of variants from CTCs. Variants had to be present in either the primary tissue (at least 1 TB specimen) or the CDX.

Bam-readcount (https://github.com/genome/bam-readcount) was used to rescue reliable variants that were present in at least two tumor samples and were not detected by Mutect2 because of their low VAF. Ensembl's Variant Effect Predictor (VEP, release 87) (16) was used to annotate variants with respect to functional consequences (type of mutation and prediction of the functional impact on the protein by SIFT.2.2 and PolyPhen 2.2.2) and frequencies in public (dbSNP147, 1000 Genomes phase 3, ExAC r3.0, COSMIC v79) and in-house databases. We used the Cancer Genome Interpreter (17) to predict driver and passenger mutations.

***Dendrogram*.** SNV mutations were aggregated as a binary score (1 if a non-synonymous or frameshifting, exonic or on a splice-site was observed, else 0) at the gene level. Resulting profiles were clusterized using the binary distance and Ward's aggregation method. All computation and figure processings were performed using R v4.0.2.

***ADO and false-positive rate estimation*.** CTC and $CD45^+$ pool DNA were amplified before sequencing. To estimate ADO, we selected all reliable variants in germline or CD45 DNA using HaplotypeCaller with the following post-filtering: coverage ≥8 in both samples, ≥5 variant reads representing ≥5% of sequenced reads at that position, genotype quality ≥20. We then compared the proportions of normal/variant reads in the germline and CD45 DNA using Fisher's exact test. Variants with a significant difference ($p < 0.05$), a variant allele fraction between 0.2 and 0.8 in germline DNA and <0.1 or >0.9 in the CD45 DNA were considered to have undergone ADO. To estimate the false-positive rates in CTC samples, we divided the number of potentially false-positive events by the number of target bases covered ≥8X in the same sample. We adopted a conservative approach and considered as false-positive all events not found in the TB and the CDX.

***Copy number analysis*.** To identify copy-number alterations (CNAs), we identified germline single-nucleotide polymorphisms (SNPs) in each sample and we calculated the coverage log-ratio (LRR) and B allele frequency (BAF) at each SNP site. Genomic profiles were divided into homogeneous segments by applying the circular binary segmentation algorithm, as implemented in the Bioconductor package *DNAcopy* (18), to both LRR and BAF values. We then used the Genome Alteration Print (GAP) method (19) to determine the ploidy of each sample, the level of

contamination with normal cells and the allele-specific copy number of each segment. Ploidy was estimated as the median copy-number across the genome. Chromosome aberrations were then defined using empirically determined thresholds as follows: gain, copy number > ploidy + 0.5; loss, copy number < ploidy – 0.5; high-level amplification, copy number > ploidy + 2; homozygous deletion, copy number < 0.5. Finally, we considered a segment to have undergone LOH when the copy number of the minor allele was equal to 0. CIRCOS plots were generated using CIRCOS (20).

***Characterization of known copy number changes in CTCs*.** As expected, the log-ratio (LRR) and B allele frequency (BAF) profiles of CTC samples were too noisy to obtain reliable pangenomic copy-number profiles. However, we observed that many chromosome segments displayed allelic imbalances consistent with the presence of chromosome aberrations identified in other samples, in particular PDX and cell line samples. We used these allelic imbalances to detect chromosome aberrations identified in other samples as follows:

1) For each CTC and each chromosome aberration, we counted the number of SNPs with consistent (e.g. BAF > 0.5 in the CTC and tumor samples) and discordant allelic imbalance

2) We used Fisher's exact test to identify chromosome segments with a significant enrichment in consistent SNPs

3) We considered an aberration to be present in a CTC sample if the Fisher test was significant (p-value < 0.05) with ≥80% consistent SNPs.

***Phylogenetic inference*.** Trees were built using a binary presence/absence matrix built from the VAF of each sample (present = VAF > 0). The R Bioconductor package

phangorn v2.3.1 (21) was used to perform the parsimony ratchet method (22), generating unrooted trees. The number of mutations and driver mutations on each branch were then determined by selecting mutations present in all samples downstream the branch.

***CDX-derived cell line establishment and cell culture*.** After resection, tumor fragments were conserved in RPMI 1640 medium (Life Technologies, Carlsbad, CA, USA) and immediately transferred to the laboratory. After two washes in 1X PBS (Life Technologies) and incubation for 10min in a 10 mL 1X PBS solution containing 1:10 penicillin/streptomycin (penicillin 10,000 units/mL, streptomycin 10,000 µg/mL, Life Technologies), tumor fragments were first mechanically dissociated using a scalpel before enzymatic dissociation with the Tumor Dissociation Human Kit (Miltenyi Biotech, Köln, Germany) according to manufacturer's protocol. Cell suspension was then successively filtered on 100-µm and 40-µm cell strainer and washed with PBS 1X before counting. Depletion of mouse cells was performed with the Mouse Cell Depletion Kit according to manufacturer's protocol using an AutoMacs Pro Separator (Miltenyi Biotec). Tumor cells were then centrifuged and resuspended in Advanced DMEM/F12 medium (Life Technologies) supplemented with 10% FBS, 1% antibiotics (penicillin-streptomycin) and 1% ultraglutamine (Lonza, Basel, Switzerland). After counting, cells were plated in six-well plates (TPP, Trasadingen, Switzerland) coated with poly-L-lysine (Merck, Sigma-Aldrich LLC., Saint-Louis, MO, USA). For GR-CDXL3 and GR-CDXL4 cells, culture medium is supplemented with ROCK1 inhibitor 10nM (Y-27632; Selleckchem, Houston, TX, USA). Cells were observed three times a week and passaged in tissue culture flasks for cell expansion, freezing or characterization; cells were detached using 0.005% trypsin-EDTA (Life Technologies) before centrifugation and counting. The same

normal-serum culture medium was used for cell expansion and permanent culture. Human adenocarcinoma NSCLC cell lines A549 (derived from primary lung tumor) and H441 (derived from pericardial fluid) were obtained through the CANCER-ID consortium and grown in RPMI 1640 medium. Lung A427 cell line (derived from primary lung tumor) was obtained from the American Type culture Collection (ATCC) and grown in MEM medium (Sigma Aldrich) supplemented with 10% FBS, 1% antibiotics, 1% ultraglutamine and 1% sodium pyruvate (Thermo Scientific). All cell lines were regularly verified for mycoplasma contamination using MycoAlert (Lonza).

***Immunohistochemistry*.** IHC staining was performed on formalin-fixed, paraffin-embedded (FFPE) tissue from patient biopsy specimens, CDX and CDX-derived cell lines with antibodies to CK8/18, EpCAM, Ki67 antigen, Vimentin, CD44, TTF1, p40, CK5/6, Chromogranin A, Synaptophysin and SLFN11 (**Supplementary Table 4**). All primary antibody incubations were carried out at RT for 1h except incubation with CK5/6 and SLFN11, which was performed at 37°C. IHC stains were examined by an experienced pathologist (JYS).

***FACS analysis*.** Aldehyde dehydrogenase (ALDH) activity was performed using the Aldefluor kit (StemCell Technologies) according to manufacturer's instructions. EpCAM, CD133, CD166, pan-cytokeratins and E-cadherin antibodies were used according to manufacturer's protocol. Fixation and permeabilization steps were performed for pan-cytokeratins and E-cadherin antibodies using the Fix&Perm kit (ThermoFisher) according to the manufacturer's instructions. $2x10^5$ cells were incubated with each antibody or corresponding negative control isotype antibodies (**Supplementary Table 5**) at RT for 20 min. Acquisition was performed with LSR

Fortessa cytometer (BD Biosciences) equipped with BD FACS Diva software. Data were analyzed using the Kaluza software (Beckman Coulter).

***Protein extraction and western blot analysis*.** Cells were lysed in 1% NP40 lysis buffer [150 mM NaCl, 1 mM EDTA, 50 mM Tris pH7.5, 0.5% NP40, H_2O] supplemented with protease and phosphatase inhibitors (Roche) for 30min on ice. Protein concentrations were measured using the Micro BCA™ protein assay kit (Thermo Scientific). Laemmli buffer (4X) containing β-mercaptoethanol was added and samples were subsequently denatured by boiling at 95°C. Proteins were resolved by 6, 8 or 10% SDS-polyacrylamide gels and transferred onto a nitrocellulose membrane (Bio-Rad), followed by a PBS-milk (5%)-blocking step (1h). Signals were detected using WesternBright ECL (Advansta) on the ChemiDoc XRS+ System (Bio-Rad). The antibodies used in this study are listed in **Supplementary Table 6**.

***RNA extraction and quantitative real-time PCR analysis*.** Total RNA was isolated using the ReliaPrep RNA Cell Miniprep System (Promega) and 1 µg of RNA was used to synthesize cDNA using the High-capacity RNA-to-cDNA™ kit (Thermo Scientific) according to manufacturer's instructions. The primers used were as follows:

- *SLFN11* (forward 5'-GGCCCAGACCAAGCCTTAAT-3' and reverse 5'-CACTGAAAGCCAGGGCAAAC-3')
- *GAPDH* (forward 5'-CCTCAACGACCACTTTGTCA-3' and reverse 5'-TTCCTCTTGTGCTCTTGCTG-3')

Quantitative real-time PCR was carried out using Maxima SYBR Green/ROX qRT-PCR Master Mix (Thermo Scientific) on the Viia7 PCR system (Applied Biosystems).

Relative gene expression was calculated according to the ΔΔCq method and normalized to *GAPDH* expression.

Drugs and chemicals. Aphidicolin (CAS 38966-21-1, Calbiochem) was purchased from Merck. Cisplatin (Mylan Pharma) and PI3KA inhibitor BYL719 (Novartis) were kind gifts from Dr S. Postel-Vinay and Dr Fabrice Andre (INSERM U981, Gustave Roussy, Villejuif) respectively. The PARPi olaparib (AZD-2281, AstraZeneca) was purchased from Selleck Chemicals. KIFC1 inhibitor AZ82 (AOB4872-5) was obtained from CliniSciences. All stock solutions were prepared in DMSO.

***Stable cell lines expressing mCherry-Luc or GFP-Luc*.** Stable tumor cell lines were established after infection with retroviral/lentiviral vectors (plasmids: MI-Luc-IRES-mCherry #75020, Addgene Teddington, UK; lentivirus: RediFect^{TM} Red-FLuc-GFP, PerkinElmer). Production and titration of retroviral particles were performed as previously described (23). Infection was performed on retronectin-coated plates (TaKaRa Bio, CA, USA) and efficiency was assayed by testing mCherry expression using flow cytometry. When efficiency was below 98%, cell sorting was performed.

Additional References

1. Imielinski M et al. Mapping the Hallmarks of Lung Adenocarcinoma with Massively Parallel Sequencing. *Cell* 2012;150(6):1107–1120.

2. Rizvi NA et al. Mutational landscape determines sensitivity to PD-1 blockade in non–small cell lung cancer. *Science* 2015;348(6230):124–128.

3. Caso R et al. Preoperative clinical and tumor genomic features associated with pathologic lymph node metastasis in clinical stage I and II lung adenocarcinoma. *npj Precis. Onc.* 2021;5(1):1–8.

4. Jordan NV et al. HER2 expression identifies dynamic functional states within circulating breast cancer cells. *Nature* 2016;537(7618):102–106.

5. Ding L et al. Somatic mutations affect key pathways in lung adenocarcinoma. *Nature* 2008;455(7216):1069–1075.

6. Pailler E et al. Acquired Resistance Mutations to ALK Inhibitors Identified by Single Circulating Tumor Cell Sequencing in ALK-Rearranged Non–Small-Cell Lung Cancer. *Clin Cancer Res* 2019;25(22):6671–6682.

7. Faugeroux V et al. An Accessible and Unique Insight into Metastasis Mutational Content Through Whole-exome Sequencing of Circulating Tumor Cells in Metastatic Prostate Cancer. *European Urology Oncology* 2020;3(4):498–508.

8. Polzer B et al. Molecular profiling of single circulating tumor cells with diagnostic intention. *EMBO Mol Med* 2014;6(11):1371–1386.

9. Martin M. Cutadapt removes adapter sequences from high-throughput sequencing reads. *EMBnet.journal* 2011;17(1):10–12.

331 10. Khandelwal G et al. Next-Generation Sequencing Analysis and Algorithms for
332 PDX and CDX Models. *Mol Cancer Res* 2017;15(8):1012–1016.

333 11. Li H, Durbin R. Fast and accurate short read alignment with Burrows–Wheeler
334 transform. *Bioinformatics* 2009;25(14):1754–1760.

335 12. Tarasov A, Vilella AJ, Cuppen E, Nijman IJ, Prins P. Sambamba: fast processing
336 of NGS alignment formats. *Bioinformatics* 2015;31(12):2032–2034.

337 13. DePristo MA et al. A framework for variation discovery and genotyping using
338 next-generation DNA sequencing data. *Nat Genet* 2011;43(5):491–498.

339 14. Auwera GAV der et al. From FastQ Data to High-Confidence Variant Calls: The
340 Genome Analysis Toolkit Best Practices Pipeline. *Current Protocols in Bioinformatics*
341 2013;43(1):11.10.1-11.10.33.

342 15. Cibulskis K et al. Sensitive detection of somatic point mutations in impure and
343 heterogeneous cancer samples. *Nat Biotechnol* 2013;31(3):213–219.

344 16. McLaren W et al. The Ensembl Variant Effect Predictor. *Genome Biology*
345 2016;17(1):122.

346 17. Tamborero D et al. Cancer Genome Interpreter annotates the biological and
347 clinical relevance of tumor alterations. *Genome Medicine* 2018;10(1):25.

348 18. Venkatraman ES, Olshen AB. A faster circular binary segmentation algorithm for
349 the analysis of array CGH data. *Bioinformatics* 2007;23(6):657–663.

19. Popova T et al. Genome Alteration Print (GAP): a tool to visualize and mine complex cancer genomic profiles obtained by SNP arrays. *Genome Biology* 2009;10(11):R128.

20. Krzywinski M et al. Circos: An information aesthetic for comparative genomics. *Genome Res.* 2009;19(9):1639–1645.

21. Schliep KP. phangorn: phylogenetic analysis in R. *Bioinformatics* 2011;27(4):592–593.

22. Nixon KC. The Parsimony Ratchet, a New Method for Rapid Parsimony Analysis. *Cladistics* 1999;15(4):407–414.

23. Hamelin V, Letourneux C, Romeo P-H, Porteu F, Gaudry M. Thrombopoietin regulates IEX-1 gene expression through ERK-induced AML1 phosphorylation. *Blood* 2006;107(8):3106–3113.

Abbreviations

CTC: circulating tumor cell

CDX: CTC-derived eXplant

NSCLC: non-small cell lung cancer

DDR: DNA damage response

HR: homologous recombination

HRD: homologous recombination deficiency

NHEJ: non-homologous end joining

PARPi: poly-ADP polymerase inhibitor

TB: tumor biopsy

NB: nuclear body

CAM: chick embryo chorioallantoic membrane

CNA: copy number analysis

CIN: chromosomal instability

WGD: whole-genome doubling

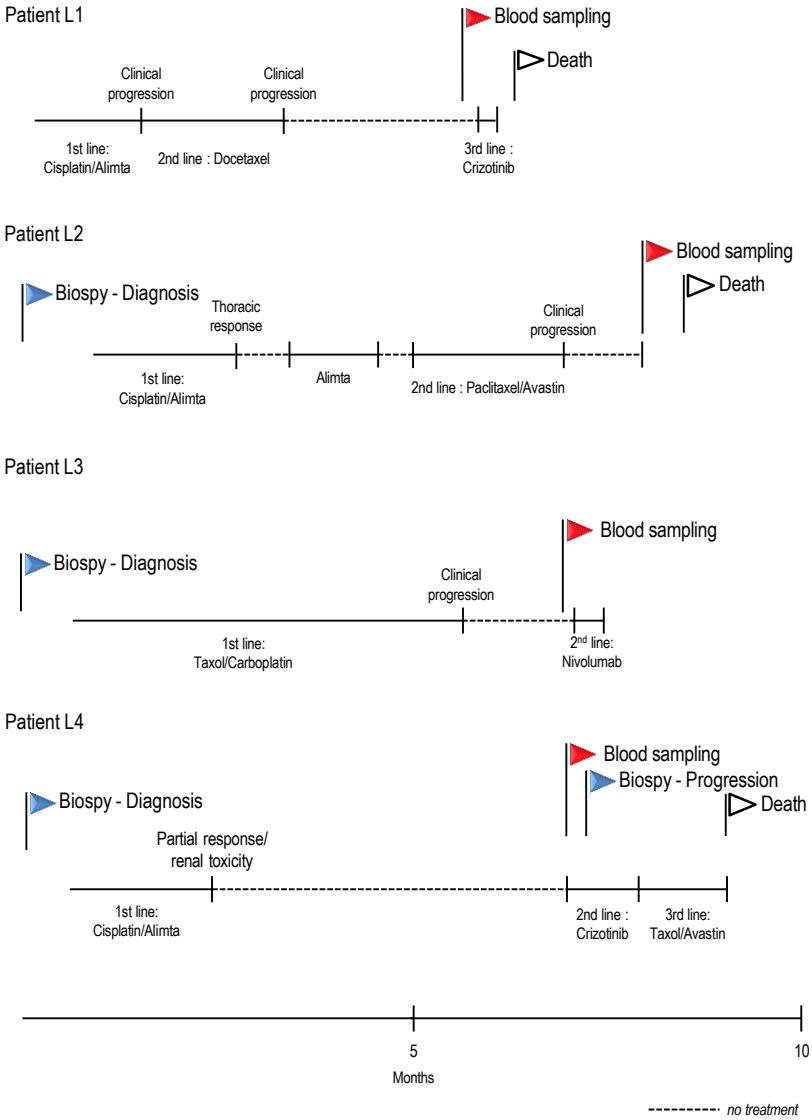
WES: whole-exome sequencing

IHC: immunohistochemistry

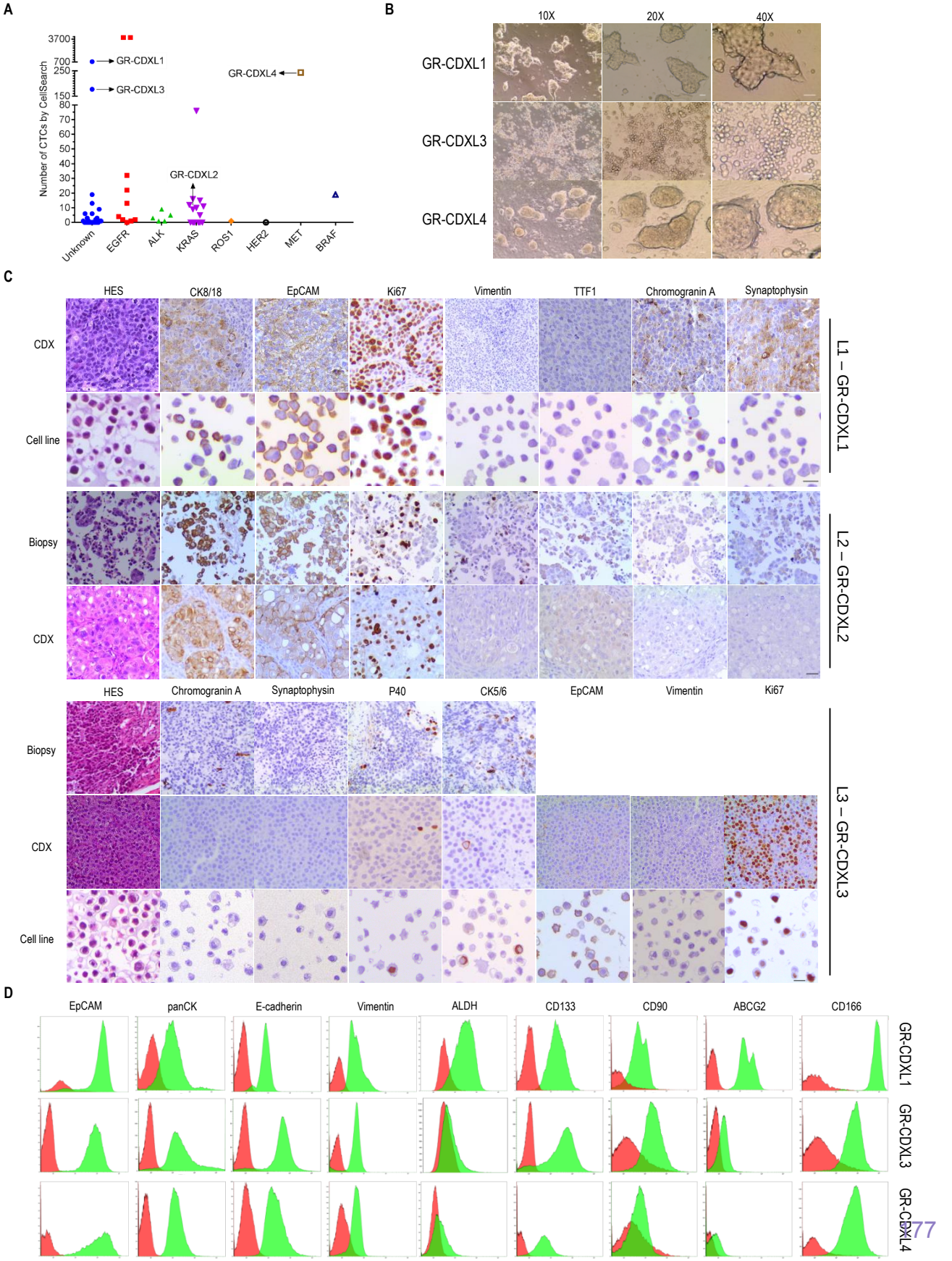
RT: room temperature

BLI: bioluminescence imaging

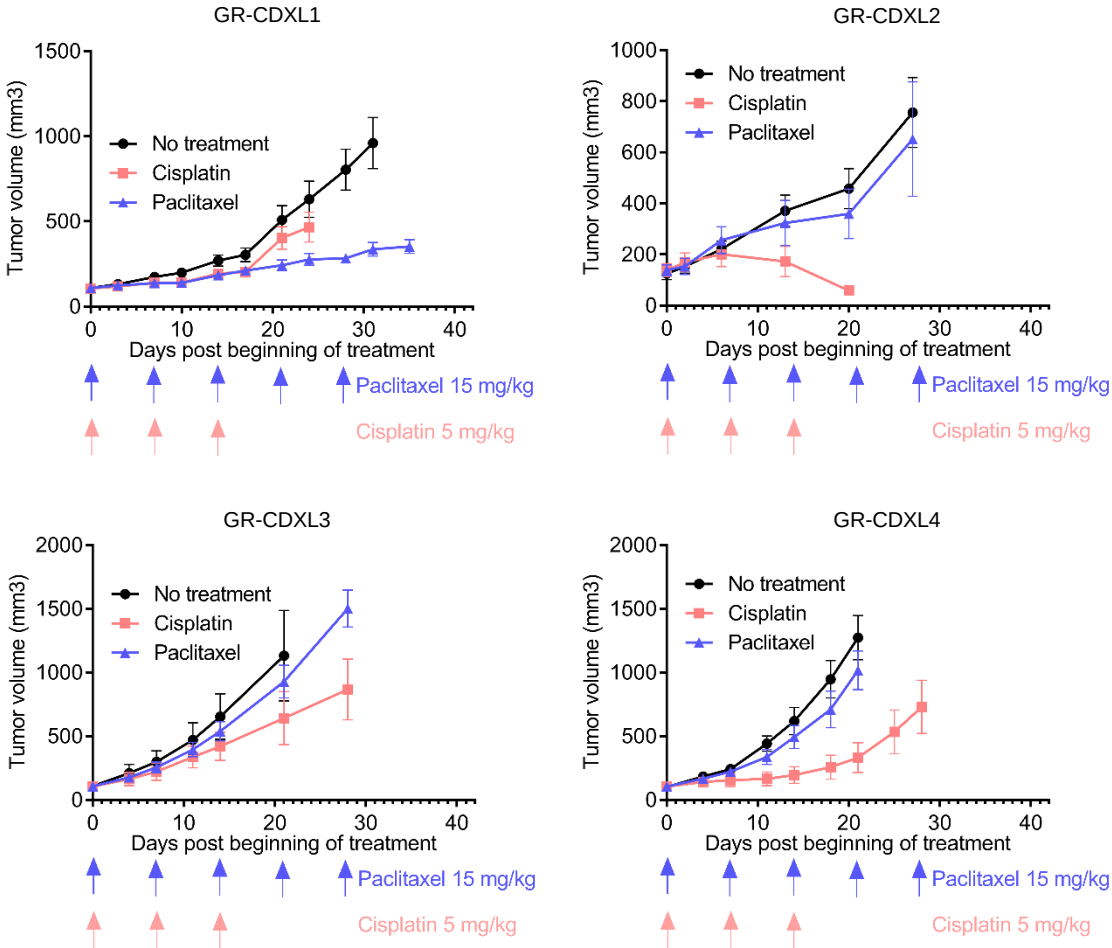
Supplementary Figure 1



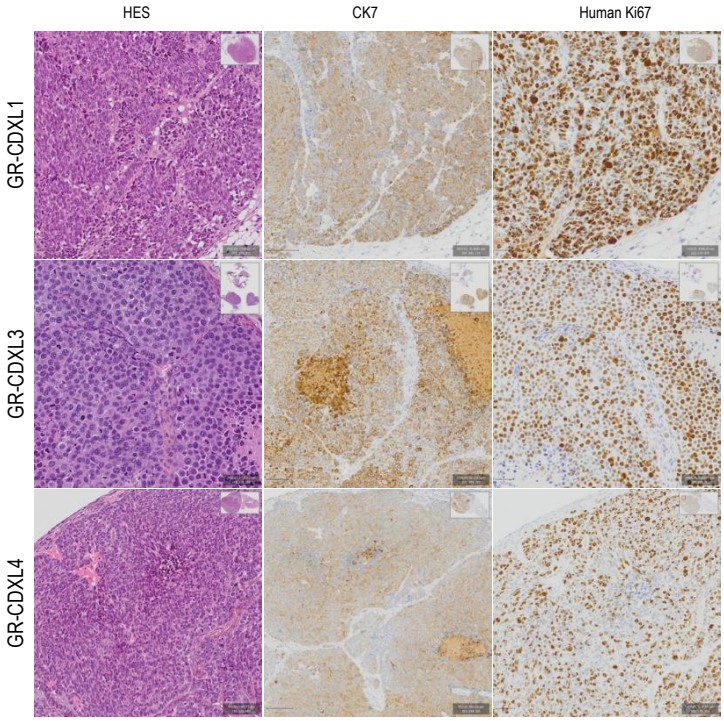
Supplementary Figure 2



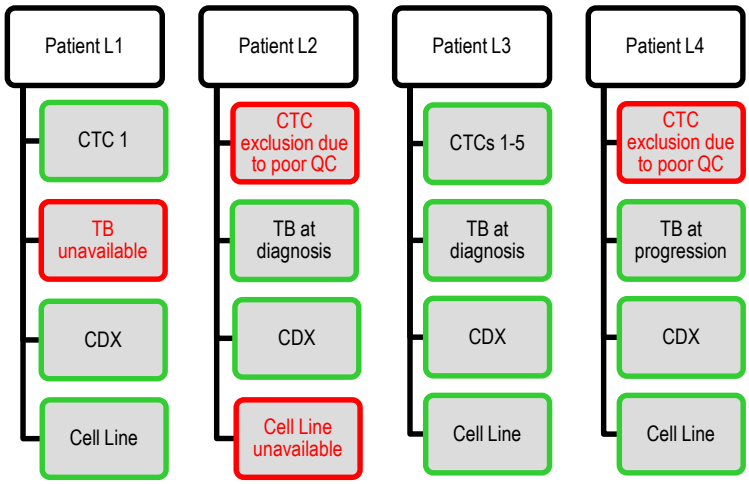
Supplementary Figure 3



Supplementary Figure 4

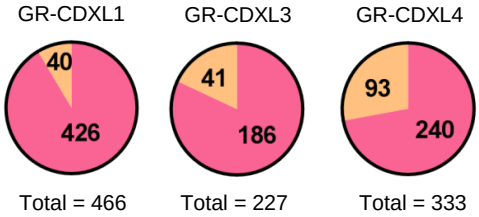


Supplementary Figure 5

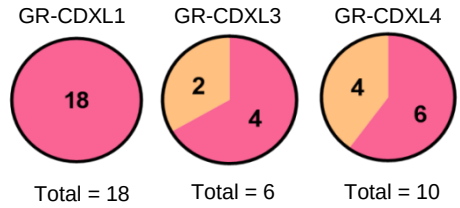


Supplementary Figure 6

A



B



C

GR-CDXL1	
SPEN	D3584H
ARID1A	S696X
ARID1A	1711-1712X
ABL2	Y486F
ABL2	D371Y
TP53	R196P
SETBP1	V1430L
RHOA	E40Q
ARID1B	M874K
KMT2C	E4543K
UBR5	G2560C
ATRX	V1568F
EIF4G3	D1165H
BRCA2	H3010Y
TP53BP1	S207C
SOX9	V115L
EPHA4	R209C
PIK3R4	R103W

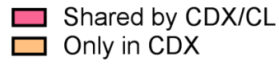
GR-CDXL3	
TP53	Y163C
ASPM	A999S
DDB1	G1035D
HERC2	G4018D

GR-CDXL4	
ATP1A1	S452C
TP53	M237I
NF1	E479
ACVR1	W461C
RB1	E539
DLC1	A1268P

D

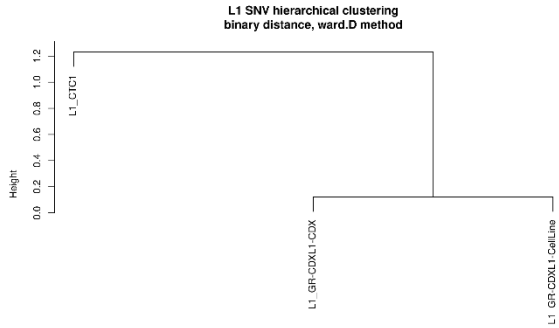
GR-CDXL3	
HERC2	G4018D
MED23	K359M

GR-CDXL4	
CIC	L1350V
ACVR1	W461C
MLLT4	P1299T
PTGS1	E338K

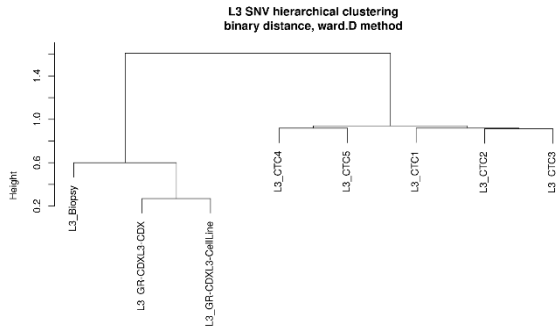


Supplementary Figure 7

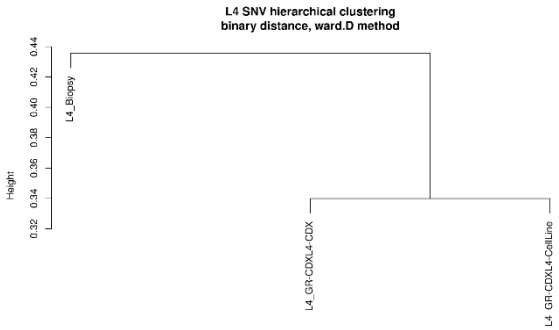
A



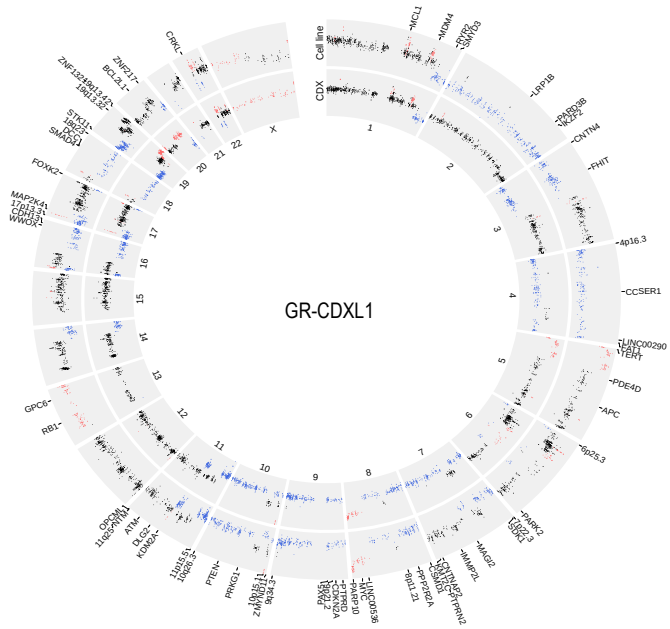
B

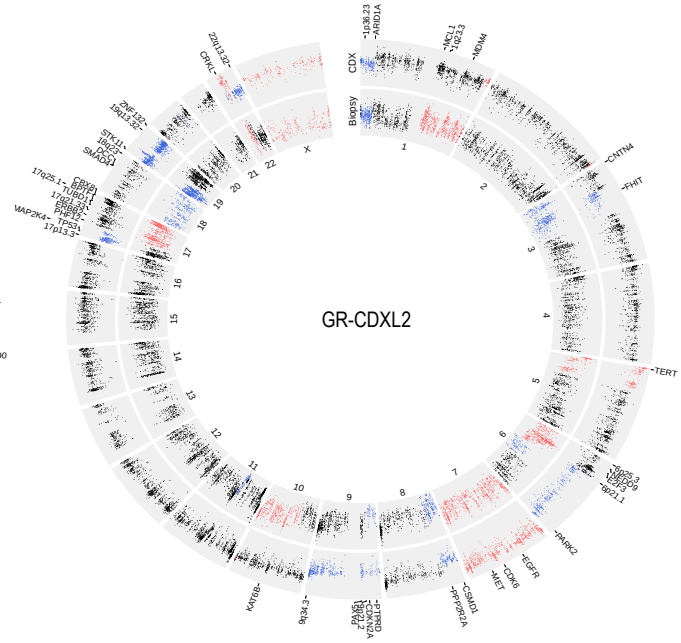


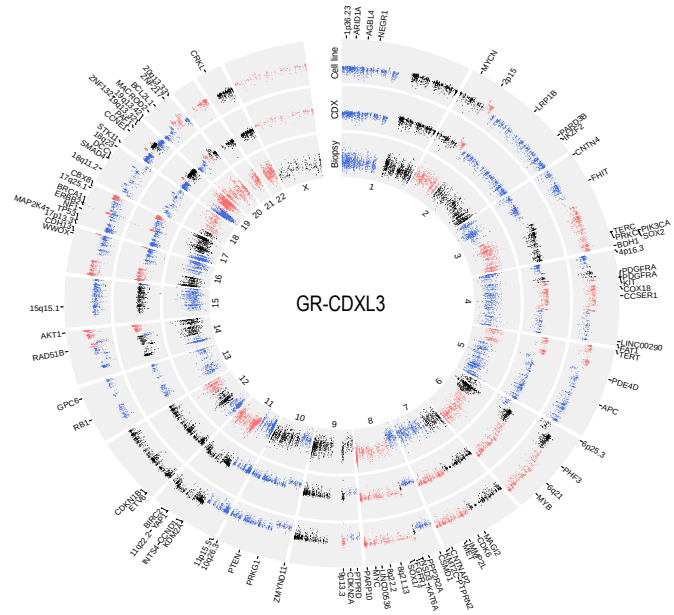
C

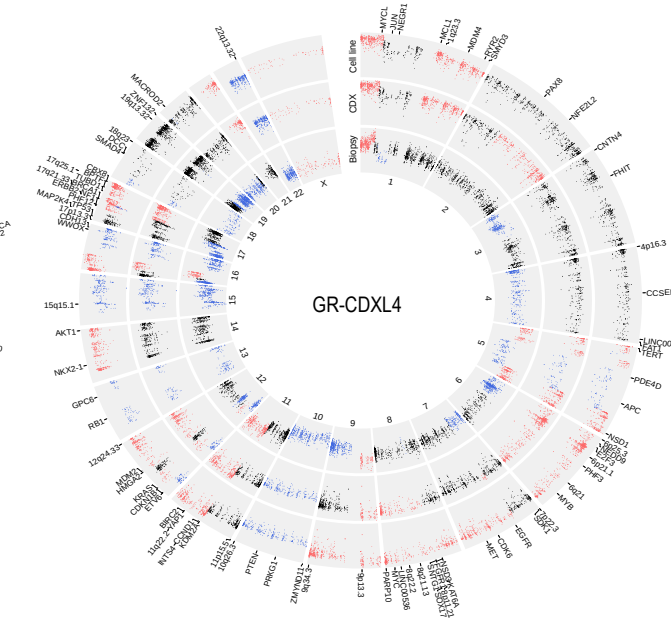


Supplementary Figure 8

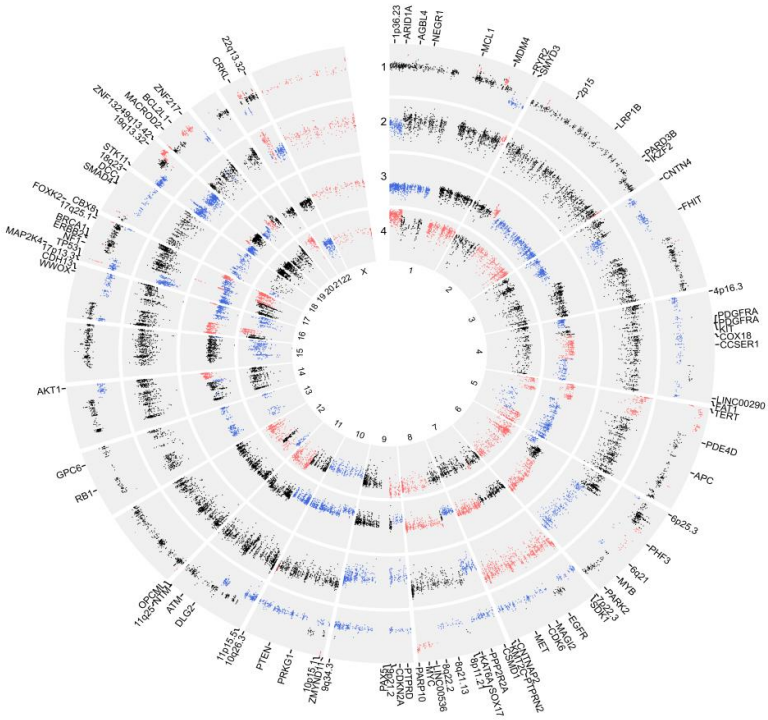




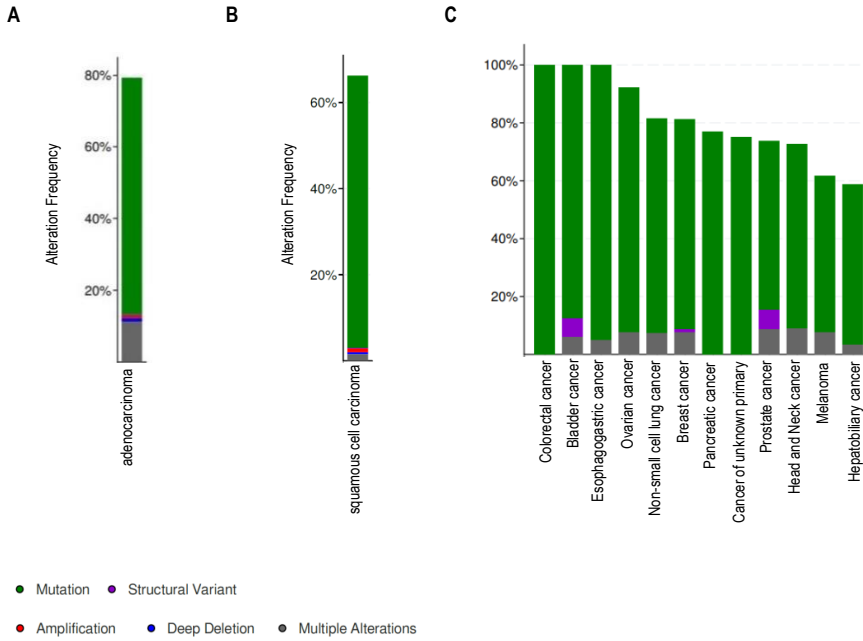




Supplementary Figure 9

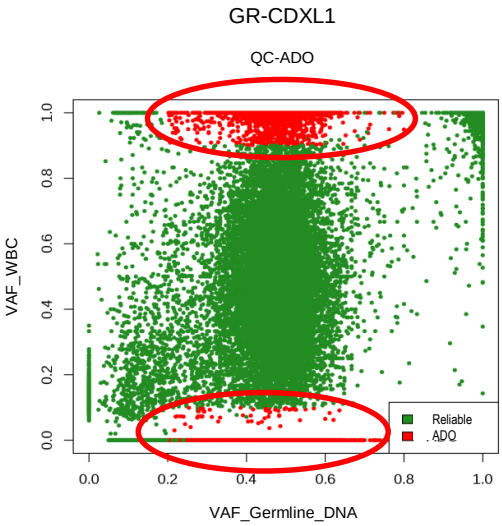


Supplementary Figure 10



Supplementary Figure 11

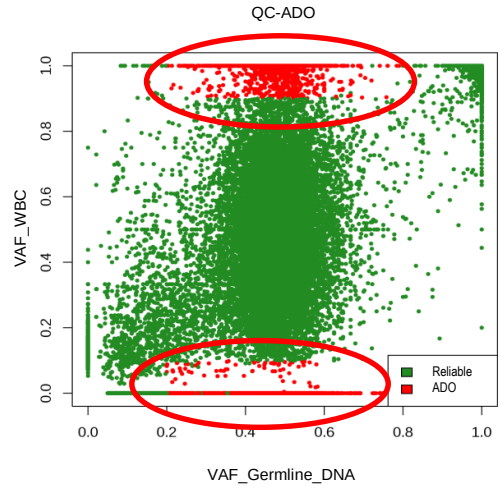
A



Proportion of germline variants with ADO
0,157515487

Sample	Number of false-positive variants	Number of target bases covered ≥8X	False-positive rate
L1-CTC1	1306	10465312	0,0001247

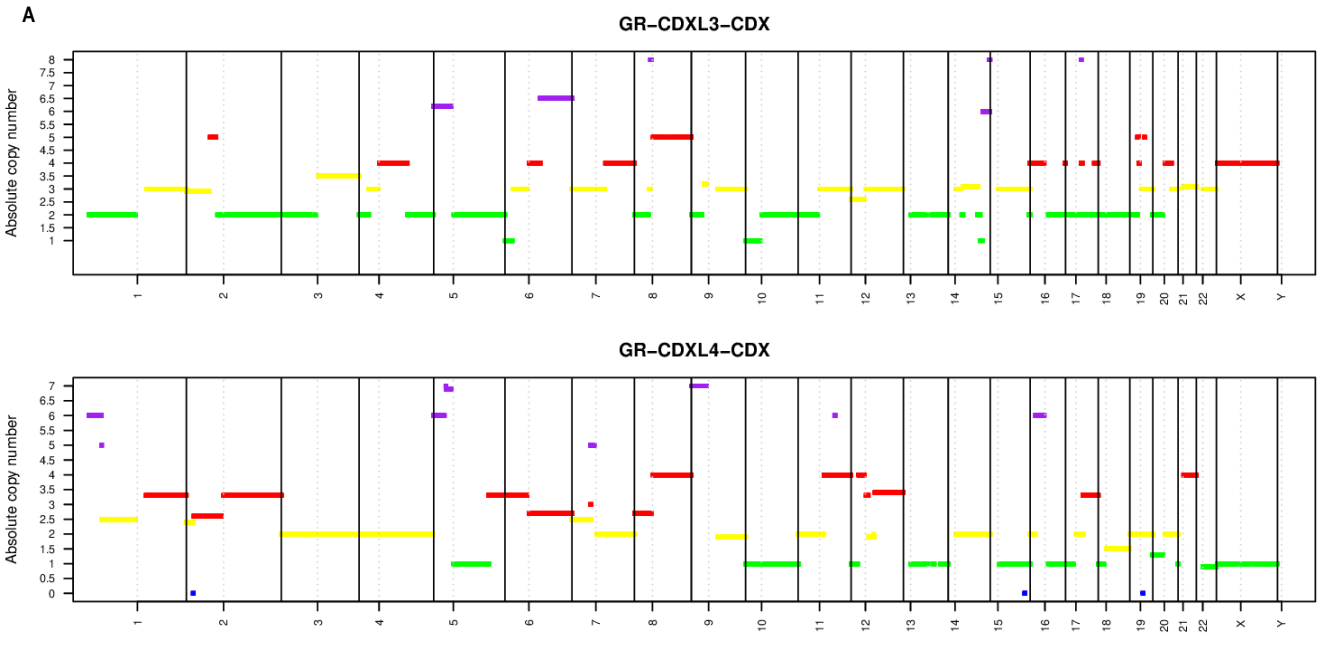
B

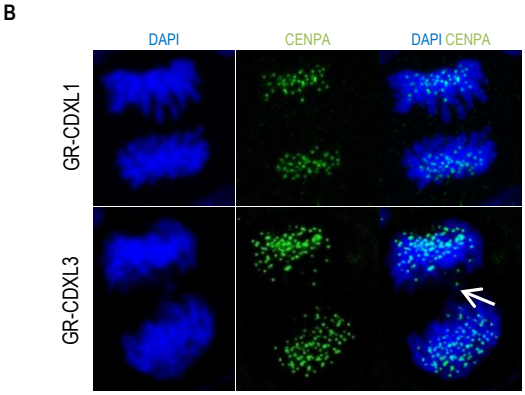


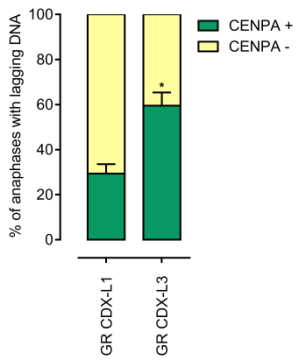
Proportion of germline variants with ADO
0,09321979

Sample	Number of false-positive variants	Number of target bases covered ≥8X	False-positive rate
L3-CTC1	1647	35136861	4,68739E-05
L3-CTC2	1396	29505812	4,73127E-05
L3-CTC3	1599	32123746	4,97763E-05
L3-CTC4	1295	36725416	3,52617E-05
L3-CTC5	932	32677245	2,85214E-05

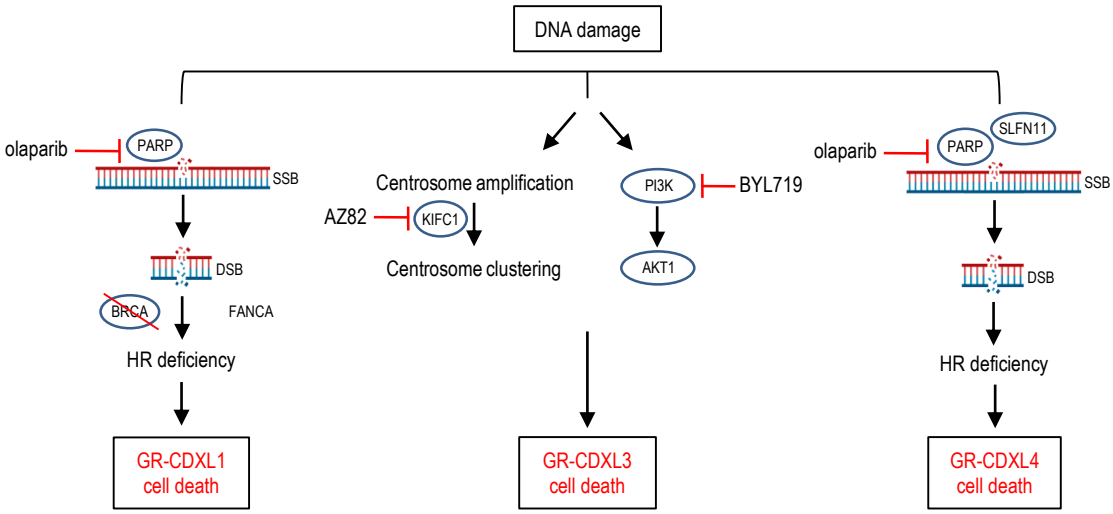
Supplementary Figure 12



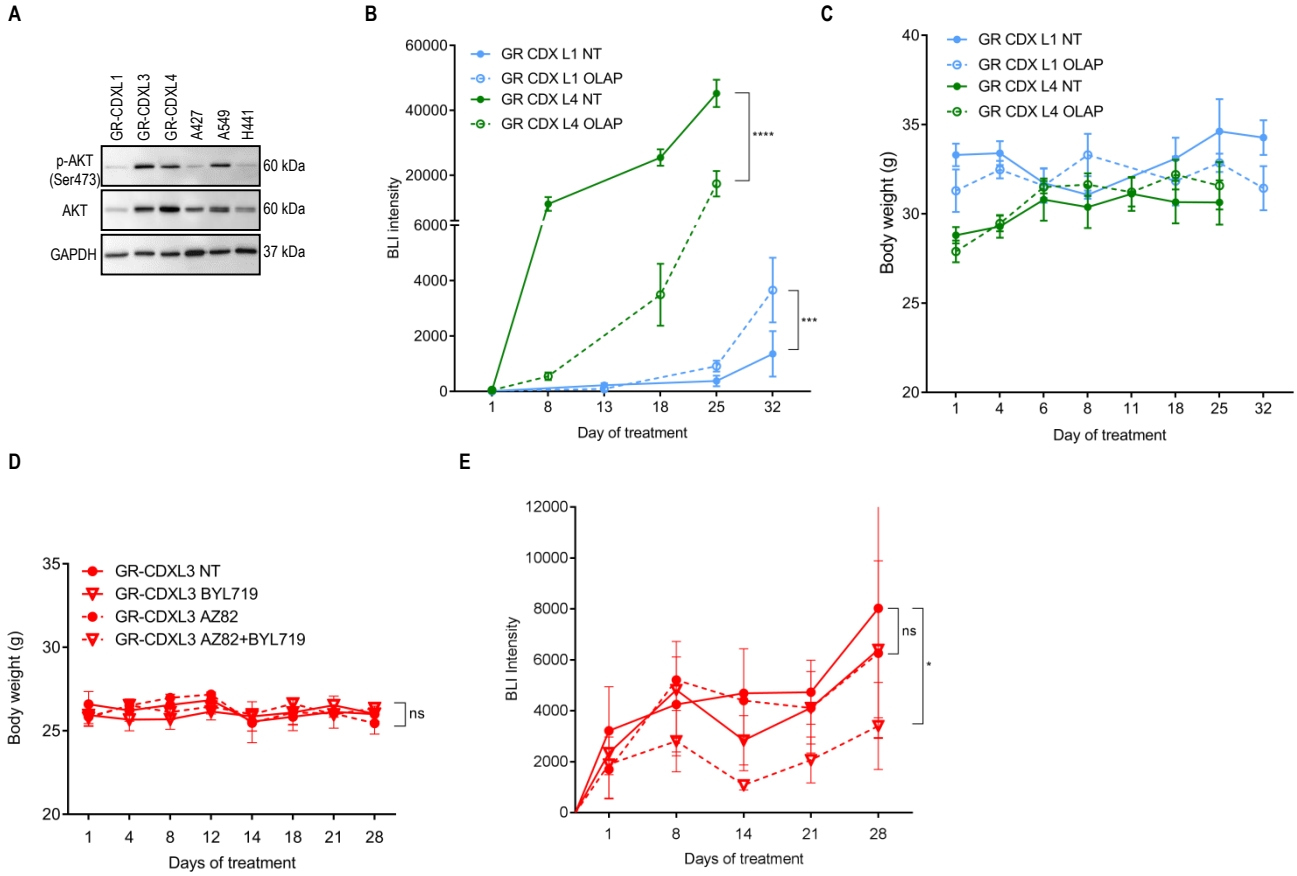




Supplementary Figure 13



Supplementary Figure 14



Supplementary Table 1

Patient	Age	Gender	Histology	Smoking status (PY)	# lines of therapy	# metastatic sites	Oncogenic drivers	# CTCs by CS /7.5 mL blood	# CTCs injected	Model
P1	45	F	Adenocarcinoma	nonsmoker	6	4	-	9	23	
P2	52	M	Adenocarcinoma	25	4	1	*BRAF*	1	3	
P3	64	F	Adenocarcinoma	nonsmoker	4	3	*EGFR*	22	62	
P4	53	M	Adenocarcinoma	40	1	1	*KRAS*	5	17	
P5	40	M	Adenocarcinoma	20	0	2	-	ND	ND	
P6	62	F	Adenocarcinoma	nonsmoker	1	3	*EGFR*	0	0	
P7	72	M	Adenocarcinoma	1	7	0	*KRAS*	0	0	
P8 (termed L1)	39	M	Adenocarcinoma	50	2	2	-	750	3500	GR-CDXL1
P9	37	M	Large cell carcinoma	4-5	1	2	*ROS1*	1	5	
P10	61	F	Adenocarcinoma	35	7	1	*KRAS*	0	0	
P11	55	M	Adenocarcinoma	20	1	2	-	0	0	
P12	51	M	Large cell carcinoma	50	1	0	-	0	0	
P13	64	M	Adenocarcinoma	45	1	3	*KRAS*	0	0	
P14	55	M	Adenocarcinoma	10	2	1	*ALK*	9	38	
P15	56	M	Adenocarcinoma	*	1	3	*BRAF*	0	0	
P16	62	F	Adenocarcinoma	25	6	2	*KRAS*	0	0	
P17	66	F	Adenocarcinoma	nonsmoker	2	2	*EGFR*	2	9	
P18	46	F	Adenocarcinoma	nonsmoker	1	1	*EGFR*	32	137	
P19	42	F	Adenocarcinoma	20	2	2	*c-MET*	1	4	
P20	61	F	Adenocarcinoma	35	3	2	-	3	13	
P21	74	M	Adenocarcinoma	80	2	4	-	0	0	
P22	61	M	Adenocarcinoma	60	4	3	*ALK*	5	19	
P23	69	M	Squamous cell carcinoma	50	2	0	-	0	0	
P24	68	M	Adenocarcinoma	100	0	3	-	2	8	
P25	52	F	Adenocarcinoma	32	3	3	*KRAS*	15	62	
P26	56	F	Adenocarcinoma	35	1	2	*KRAS*	76	253	
P27	56	F	Squamous cell carcinoma	40	5	1	-	1	4	
P28	65	M	Adenocarcinoma	30	2	1	-	6	22	
P29	58	M	Adenocarcinoma	50	4	1	*ALK*	1	4	
P30	65	M	Adenocarcinoma	15	1	3	*KRAS*	12	42	
P31	55	F	Adenocarcinoma	7	5	0	*ALK, MET*	1	4	
P32	66	M	Adenocarcinoma	8	1	1	*EGFR*	13	49	
P33	64	M	Adenocarcinoma	5	0	2	*EGFR*	4	17	
P34	65	M	Adenocarcinoma	70	1	1	-	0	0	
P35	59	M	Squamous cell carcinoma	15	1	3	-	19	86	
P36	56	M	Squamous cell carcinoma	40	3	4	-	6	19	
P37 (termed L2)	45	F	Adenocarcinoma	25	2	3	*KRAS*	10	35	GR-CDXL2
P38	53	M	Adenocarcinoma	40	1	2	*KRAS*	16	66	
P39	81	F	Adenocarcinoma	nonsmoker	2	3	*EGFR*	3903	17694	
P40	63	M	Squamous cell carcinoma	40	0	3	-	0	0	
P41	59	M	Adenocarcinoma	unknown	1	3	-	0	0	
P42	71	F	Adenocarcinoma	2	6	1	*EGFR*	1	4	
P43	51	M	Adenocarcinoma	18	1	3	*EGFR*	13	54	
P44	59	F	Adenocarcinoma	nonsmoker	0	1	-	1	4	
P45	40	F	Adenocarcinoma	15	0	1	*KRAS*	9	47	
P46	67	M	Squamous cell carcinoma	1	2	2	-	0	0	
P47	54	M	Adenocarcinoma	30	1	1	*HER2*	0	0	
P48 (termed L3)	55	M	Squamous cell carcinoma	34	1	3	-	117	330	GR-CDXL3
P49	69	F	Adenocarcinoma	nonsmoker	2	1	*ALK*	3	16	
P50 (termed L4)	66	F	Adenocarcinoma	80	1	3	*MET*	243	1102	GR-CDXL4
P51	58	M	Adenocarcinoma	35	1	2	*BRAF*	19	86	
P52	71	F	Adenocarcinoma	nonsmoker	3	1	*EGFR*	2	8	
P53	53	M	Adenocarcinoma	40	2	3	*KRAS*	0	0	
P54	64	M	Adenocarcinoma	40	2	1	*KRAS*	0	0	
P55	73	M	Large cell carcinoma	60	2	4	-	0	0	

Supplementary Table 2

Model	Sample	Mean Depth	Coverage above 25X	SNVs	INDELs	SNVs+INDELs
GR-CDXL1	L1-CDX	158	97	450	17	467
	L1-CellLine	154	97	436	14	450
GR-CDXL2	L2-TB	148	91	363	217	580
	L2-CDX	110	81	436	20	456
GR-CDXL3	L3-TB	73	92	287	7	294
	L3-CDX	97	84	232	10	242
	L3-CellLine	96	84	221	6	227
GR-CDXL4	L4-TB	110	96	282	13	295
	L4-CDX	114	88	332	11	343
	L4-CellLine	112	87	263	11	274

Supplementary Table 3

Model	Sample	Mean Depth	Coverage above 25X	SNVs+INDELs shared by at least 2 CTCs	SNVs+INDELs shared by at least 1 CTC and TB	SNVs+INDELs shared by at least 1 CTC and CDX	High-confidence SNVs+INDELs*
GR-CDXL1	L1-CTC1	32	11	N/A	N/A	24	24
GR-CDXL3	L3-CTC1	73	48	418	39	36	41
	L3-CTC2	50	39	78	57	58	64
	L3-CTC3	54	43	95	64	67	70
	L3-CTC4	76	50	72	71	69	78
	L3-CTC5	76	45	60	51	50	55

*Unique SNVs and INDELs were obtained by adding SNVs and INDELs shared by at least 1 CTC and TB and SNVs and INDELs shared by at least 1 CTC and the CDX. Duplicate values were counted only once.

Supplementary Table 4

Antibody	Manufacturer	Reference	Clone	Species	Dilution	Antigen retrieval
CK8/18	Novocastra	#NCL-L-CK5/6/8/18	5D3, LP34	mouse	1/100	40 minutes
CK5/6	DAKO	#M7237	D5/16B4	mouse	1/10	40 minutes
CK7	DAKO	#M7018	OV-TL 12/30	mouse	1/50	20 minutes
EpCAM	Cell Signaling	#2929S	VU1D9	mouse	1/500	40 minutes
Ki67	DAKO	#M7240	MIB-1	mouse	1/20	20 minutes
Vimentin	Santa Cruz	#SC-6260	V9	mouse	1/500	No retrieval
TTF1	DAKO	#M3575	8G7G3/1	mouse	1/50	60 minutes
Chromogranin A	DAKO	#M0869	DAK-A3	mouse	1/50	40 minutes
Synaptophysin	DAKO	#M7315	DAK-SYNAP	mouse	1/16	40 minutes
P40	DBS	#RP 163-05	polyclonal	rabbit	1/50	40 minutes
SLFN11	Cell Signaling	#34858	D8W1B	rabbit	1/50	20 minutes

Supplementary Table 5

Antibody	Manufacturer	Reference	Clone	Species	Fluorochrome	Dilution	Isotypes
EpCAM	BD Pharmingen	347200	EBA-1	mouse	APC	1/20	Ms IgG1
CD133-2	Miltenyi	130-098-046	293C3	mouse	PE	1/10	Ms IgG2b
CD90	BD Pharmingen	555596	5E10	mouse	PE	1/5	Ms IgG1
ABCG2	R&D system	FAB995P	5D3	mouse	PE	1/5	Ms IgG2b
CD166	R&D system	FAB6561P	105902	mouse	PE	1/100	Ms IgG1
CD24	BD Pharmingen	555428	ML5	mouse	PE	1/5	Ms IgG2a
CD44	BD Pharmingen	555478	G44-26	mouse	FITC	1/5	Ms IgG2b
Pan-cytokeratins	ebioscience	53-9003-82	AE1/AE3	mouse	AF488	1/100	Ms IgG1
E-cadherin	BD Pharmingen	560061	36/E-Cadherin	mouse	AF488	1/200	Ms IgG2a
Vimentin	Santa Cruz	sc-6260	V9	mouse	AF488	1/2	Ms IgG1

Supplementary Table 6

Antibody	Manufacturer	Reference	Clone	Species	Dilution
p-CHK1 (Ser345)	Cell Signaling	#2348	133D3	rabbit	1/500
p-AKT (Ser473)	Cell Signaling	#9271	polyclonal	rabbit	1/1000
CHK1	Santa Cruz	sc-8408	G-4	mouse	1/500
AKT	Cell Signaling	#4685	11E7	rabbit	1/1000
FANCA	Bethyl Lab	A301-980A	polyclonal	rabbit	1/500
PARP1	Cell Signaling	#9542	polyclonal	mouse	1/1000
SLFN11	Santa Cruz	sc-374339	E-4	mouse	1/500
GAPDH	Santa Cruz	sc-47724	0411	mouse	1/1000

Supplementary Table 7

Antibody	Manufacturer	Reference	Clone	Species	Dilution
Cyclin A	Santa Cruz	sc-271682	B-8	mouse	1/300
53BP1	Abcam	ab21083	polyclonal	rabbit	1/300
H2AX (Ser139)	Merck	05-636	JBW301	mouse	1/3000
Geminin	Santa Cruz	sc-74456	F-7	mouse	1/300
RAD51	Merck	PC130	polyclonal	rabbit	1/300
p-RPA32 (S33)	Bethyl Lab	A300-246A-M	polyclonal	rabbit	1/1000
p-DNAPK	Abcam	ab18356	10B1	mouse	1/1000
CENPA	Abcam	ab13939	3-19	mouse	1/1000

Part D. Discussion and Perspectives

The present work is part of a larger project undertaken by our group over the past few years, to develop functional cancer models (CAM and CDX) and provide insight into the biology of CTCs in both CRPC and NSCLC malignancies (Faugeroux, Pailler, et al., 2020; Pawlikowska et al., 2020; Tayoun et al., 2022). My doctoral research focused on the comprehensive genomic and functional characterization of four novel CDX models (GR-CDXL1, GR-CDXL2, GR-CDXL3 and GR-CDXL4) and three CDX-derived cell lines established in our laboratory in collaboration with XenTech (ANR project grant ANR-15-CE17-0006-01), from advanced-stage NSCLC patient CTCs. Only one other NSCLC CDX model has been previously reported in the litterature, harboring a mesenchymal phenotype as no CTCs were detected by CellSearch (Morrow et al., 2016). Despite the relatively high take rate observed in aggressive malignancies such as SCLC or melanoma, CDX model establishment from NSCLC patients remains particularly difficult. Low success rate in NSCLC is mostly attributed to the low counts of CellSearch-detectable CTCs, defined by EpCAM and CK positivity (5 CTCs/7.5 mL *vs* prognostic cut-off of 50 CTCs in SCLC) (Krebs et al., 2012; Lallo et al., 2017; Tayoun et al., 2019). Herein, we noted that the implantation of a substantial number of epithelial CTCs may not be the sole factor required for CDX tumor growth. Indeed, mesenchymal CTCs can also give rise to a CDX in NSCLC (Morrow et al., 2016). Using the CellSearch system, multiple studies including our own have reported the low prevalence of NSCLC CTCs even at advanced stages of the disease, due to the loss of EpCAM expression (or to a CK-low phenotype), mainly through EMT (Hou et al., 2011; Lecharpentier et al., 2011; Lindsay et al., 2017). Our group has highlighted a mesenchymal vimentin^{+} phenotype in *ALK*-rearranged NSCLC CTCs in response to ALK TKI, which may define the tumorigenic clones seeding metastasis in *ALK*-positive NSCLC (Pailler et al., 2013). This was further confirmed in a subsequent study elucidating a highly altered CNA profile in ALK^{+}/CK^{-} NSCLC CTCs (Oulhen et al., 2021). Improvements in different aspects such as CTC

enrichment approaches (*e.g.* non-EpCAM-based methods) or CTC implantation techniques are thus needed to enhance tumor take rate in NSCLC CDX models.

The establishment of permanent *in vitro* CDX-derived cell lines facilitated characterization studies, as these were more easily amenable to mechanistic and pharmacological assays in a shorter time frame compared to CDX, as well as to genetic modifications for *in vivo* metastatic monitoring. Similar tools were previously developed from SCLC CDX models, albeit as short-term *ex vivo* cultures (Lallo et al., 2019). Throughout this project, we developed and optimized the chick embryo CAM assay as a preclinical platform for the functional characterization of metastatic tumors in short time frames. This technique enabled *in ovo* monitoring of CDX-derived cell metastatic spread through the detection of fluorescent metastatic foci within seven to nine days using spectral imaging. Less aggressive cell lines remained in primary nodules and failed to migrate, thus generating higher fluorescence intensity compared to highly disseminating tumor cells, which were found at lower levels in primary nodules (Pawlikowska et al., 2020). Furthermore, we use the CAM model for pharmacological targeting of metastatic tumors, by testing and validating biology-driven therapeutic strategies in NSCLC (Tayoun et al., 2022).

DDR dysfunctions are an important hallmark of cancer contributing to tumor development. Over the years, targeting the DDR has emerged as an unprecedented therapeutic opportunity in several malignancies, but its exploitation in NSCLC is still particularly poor (Passiglia et al., 2021; Pearl et al., 2015; Pilié, Tang, et al., 2019; Remon et al., 2020). Clinical studies evaluating PARPi as maintenance treatment did not have proven efficacy in chemosensitive NSCLC tumors, even in the HRD tumor setting (Owonikoko et al., 2019; Postel-Vinay et al., 2021). A deeper understanding of DDR pathways and their implication in NSCLC tumor progression using functional models is thus required. For this purpose, our group developed novel CDX platforms to help provide relevant insight into mechanisms underlying metastatic progression and identify DDR-related vulnerabilities.

Our CDX tumors and CDX-derived cell lines faithfully recapitulated corresponding patient response to platinum-based chemotherapy. Comparative WES analysis unraveled important mutational profile similarities (52-76%) between the CDX, the CDX-derived cell line and the matched patient TB when available or patient single CTC (in the case of GR-CDXL1). These findings thus validated the clinical relevance of our models. Importantly, phylogenetic inference from genomic WES data depicted clonal driver mutations in key DDR-related genes, including *TP53*, *BRCA2*, *PARP1*, *CHK2*, *ARID1A* and *ARID1B*, as well as acquired CNAs; loss of *FANCA* and *WWOX* and gain of *MDM2* and *MDM4* DDR genes and *AKT1*. This is in line with previous findings in NSCLC tumors showing deleterious mutations in DDR pathways (Knijnenburg et al., 2018; Ricciuti et al., 2020), which led us to further investigate DDR activity in our CDX-derived cell lines.

GR-CDXL1 cells were resistant to cisplatin – mimicking patient clinical progression at two months in response to chemotherapy – and presented a somatic, bi-allelic *BRCA2* mutation as well as the deletion of the FA effector *FANCA* promoter. Additionally, these cells harbored high levels of DSBs which remained unrepaired post-mitosis, constitutively activating CHK1 signaling and the DDR. IF analysis of irradiated tumor cells showed impaired RAD51 nuclear foci formation – a surrogate marker of HR function (Graeser et al., 2010) – in both GR-CDXL1 and GR-CDXL4 proliferative (geminin^{+}) cells. These findings provided an HRD profile in both GR-CDXL1 and GR-CDXL4 tumor cells, leading to their sensitivity to olaparib *in vitro*, *in ovo* and *in vivo*. We acknowledge that the platinum-resistant/olaparib-sensitive profile of GR-CDXL1 contradicts the currently accepted predictive value of chemosensitivity for PARPi response in solid cancers (Cleary et al., 2020; Sonnenblick et al., 2015). However, in the SAFIR02-Lung cohort, pathogenic *BRCA1/2* mutations found in NSCLC tumors (~ 2.1%) were not indicative of higher platinum sensitivity (Remon et al., 2020). Evidence also shows that CTCs may have differential therapeutic responses (C. Gong et al., 2015; M. Yu et al., 2014). In breast cancer, it has been elucidated that increased reactive oxygen species production triggered by CTC detachment from the ECM promoted a partial

pre-activation of cell cycle checkpoints in CTCs, prior to chemotherapy (C. Gong et al., 2015). This partial DDR activation, rather than recruitment of effector repair proteins, potentiated their DNA repair efficiency and, in turn, their resistance to chemotherapy (C. Gong et al., 2015). GR-CDXL1 chemoresponse could therefore be possibly dictated by a similar mechanism in NSCLC. Furthermore, targeting its constitutive induction of CHK1 signaling may be an interesting approach to restore GR-CDXL1 sensitivity to cisplatin.

In order to expand clinical use and better stratify patients that may benefit from DDR-based treatments, reliable predictive biomarkers of response to DDR inhibitors are urgently needed (Michels et al., 2014; Pilié, Tang, et al., 2019). Herein, in an effort to identify a biomarker of response to olaparib in GR-CDXL4 – which presented HRD without a genomic *a priori* – and in line with current knowledge on SLFN11 (as mentioned in the **Introduction section V. 4)a.**), we detected SLFN11 protein in GR-CDXL4 cells only. Importantly, to check whether it was also found in other patient L4 samples and in GR-CDXL1 samples, we performed IHC analysis of matched patient TB at diagnosis and progression, CDX tumor and CDX-derived cell line, which showed that an important proportion of tumor cells in all patient L4 samples highly expressed SLFN11, while immunostainings of patient L1 samples were all negative for this protein. We therefore suggest SLFN11 expression as a potential predictive biomarker of response to olaparib in NSCLC. However, these findings are preliminary and require further functional correlation analysis between olaparib sensitivity and SLFN11 expression. For this, additional experiments must be performed: (i) *SLFN11* gene knock-out (KO) in GR-CDXL4 cells and establishment of a stable cell line GR-CDXL4-mCherry-KO, (ii) *in vitro* pharmacological testings using olaparib on GR-CDXL4-mCherry-KO and (iii) injection of the KO cells in immunodeficient mice to evaluate resistance to olaparib *in vivo*. Furthermore, establishing SLFN11 overexpression as a predictive biomarker in NSCLC requires investigation in additional preclinical studies, followed by clinical validation in clinical trials, as it is currently being done in SCLC (NCT04334941). In addition to its role in predicting response to PARPi, we show that SLFN11

overexpression was concordant with neuroendocrine marker expression in the matched patient TB at progression to crizotinib, which may be a potential driver of histological transformation to SCLC. Transformation from adenocarcinoma to SCLC is a recognized resistance mechanism to EGFR TKI, which has also been reported in *ALK*-mutated patients at resistance to TKI (Cha et al., 2016; Cooper et al., 2022). The biological mechanisms behind it remain unclear, but it has been demonstrated that baseline *RB1* and *TP53* inactivation increased its risk of occurrence (J.-K. Lee et al., 2017); a genomic profile that was deciphered by WES analysis in all patient L4 tumor samples. We therefore suggest another predictive role of SLFN11 overexpression in promoting NSCLC-SCLC transformation, but further investigation is warranted.

GR-CDXL3 and GR-CDXL4 presented increased CIN levels including early whole-genome doubling, a known feature of NSCLC tumors predictive of unfavorable prognosis (Jamal-Hanjani et al., 2017). Moreover, GR-CDXL3 cells harbored supernumerary chromosomes. Interestingly, we also elucidated a tumor survival mechanism of centrosome clustering in GR-CDXL3 cells, which is frequently adopted by cancer cells harboring amplified centrosomes and helps them maintain their survival *via* bipolar spindle formation (Ganem et al., 2009; Krämer et al., 2011; Sansregret et al., 2018). This CIN-promoting event thus constitutes a potential therapeutic target in cancer (Bakhoum & Compton, 2012). In our model, targeting clustering in GR-CDXL3 using kinesin motor protein KIFC1 inhibitor AZ82 did not affect tumor cell viability. However, a synergistic antitumor effect was achieved *in ovo* and *in vivo* upon association of AZ82 and PI3Kα inhibitor BYL719 targeting *AKT1* gain in GR-CDXL3 cells. Nonetheless, it is important to note that nonspecific toxicity of AZ82 was previously observed at 4 µM, which highly limits its use beyond this study (W. Zhang et al., 2016). A recent report by Fan *et al* has demonstrated that ATM/ATR kinases induce KIFC1 phosphorylation and subsequent centrosome clustering in tumor cells in response to DNA-damaging agents, leading to high CIN as well as a risk of tumor resistance to treatment and recurrence. The authors thus highlight the therapeutic potential of blocking KIFC1 phosphorylation using, for example, ATR or ATM inhibitors (Fan et al.,

2021). Overall, our data highlights tumor adaptation mechanisms of CIN in GR-CDXL3, which are implicated in tumor propagation and aggressiveness and are targetable *in ovo* and *in vivo*.

Preliminary IF analyses in CDX-derived cell lines GR-CDXL1, GR-CDXL3 and GR-CDXL4 have shown the presence of micronuclei; extra-nuclear chromatin fragments surrounded with a nuclear envelope, arising during mitosis from unresolved genome instability. Cyclic GMP–AMP synthase (cGAS), a key cytosolic DNA sensor, localizes to micronuclei in response to nuclear envelope rupture-mediated DNA release, leading to downstream immune response activation through cGAS-stimulator of interferon genes (STING) signaling (Kwon & Bakhoum, 2020; Mackenzie et al., 2017). In the context of accumulating evidence unraveling the role of DDR deficiency in determining tumor immunogenicity (Chabanon et al., 2021), we plan to explore the activation of the cGAS-STING pathway in our CDX-derived cell lines through the evaluation of: (i) protein expression of cGAS and STING by western blot, (ii) transcriptional and secretion levels of inflammatory cytokines including CCL5 and CXCL10 – which are normally upregulated in this immune response (Parkes et al., 2016) – by qRT-PCR and Enzyme-Linked Immunosorbent Assay (ELISA) respectively.

Several reports elucidated the immunomodulatory effect of PARPis and other DDR inhibitors in different DDR-deficient contexts including NSCLC, through the activation of the cGAS-STING cascade, thus providing a preclinical rationale for the therapeutic association of DDR inhibitors and ICIs (Chabanon et al., 2019; Ding et al., 2018; Pantelidou et al., 2019; Parkes et al., 2016; Sen et al., 2019). The dynamic interplay between the DDR and the tumor immune system is being extensively exploited in the clinic (Wanderley et al., 2022). Numerous trials exploring the combination of DDR inhibitors (*e.g.* PARPi, ATRi) and immune checkpoint blockade are currently ongoing in several cancer types including NSCLC, where a proof-of-concept phase I/II study is evaluating the efficacy of durvalumab in combination with olaparib (NCT02484404) (Desmond et al., 2022). Therefore, the investigation of micronuclei-induced cGAS-

STING pathway activation in our DDR-deficient models may help uncover new immuno-oncology therapeutic targets in NSCLC CTCs.

Overall, this work provides for the first time to our knowledge an in-depth molecular and functional characterization of novel CTC-derived systems in NSCLC. Genomic and mechanistic analyses elucidated distinct DDR dysfunctions underpinning CTC metastatic potency in each of our CDX-derived cell lines. Importantly, our findings suggest biology-driven targeting strategies as well as SLFN11 as a predictive biomarker of response, which may help inform patient selection for an expanded use of DDR-based therapies in NSCLC.

Finally, it is important to acknowledge here that CDX models cannot inform clinical decisions in real time, owing to the significant technical hurdles discussed above and the experimental duration. Nonetheless, the development of CDX models provides a significant asset for a more in-depth understanding of CTC biology and the mechanistic basis of metastatic development. For this and based on the comprehensive characterization of our CDX and CDX-derived cell lines, a license is currently being discussed with our collaborator XenTech to value these models and further promote their use as a tractable system in translational research. In addition, high-throughput functional studies (*i.e.* genomics, transcriptomics and proteomics) on these CDX models and single patient CTCs isolated from fresh blood samples is paramount, to identify CTC-specific vulnerabilities and develop anti-metastasis therapies.

Part E. Reference List

1. Abraham, R. T. (2001). Cell cycle checkpoint signaling through the ATM and ATR kinases. *Genes & Development*, *15*(17), 2177–2196.
2. Aceto, N., Bardia, A., Miyamoto, D. T., Donaldson, M. C., Wittner, B. S., Spencer, J. A., Yu, M., Pely, A., Engstrom, A., Zhu, H., Brannigan, B. W., Kapur, R., Stott, S. L., Shioda, T., Ramaswamy, S., Ting, D. T., Lin, C. P., Toner, M., Haber, D. A., & Maheswaran, S. (2014). Circulating Tumor Cell Clusters Are Oligoclonal Precursors of Breast Cancer Metastasis. *Cell*, *158*(5), 1110–1122.
3. Adalsteinsson, V. A., & Love, J. C. (2014). Towards Engineered Processes for Sequencing-Based Analysis of Single Circulating Tumor Cells. *Current Opinion in Chemical Engineering*, *4*, 97–104.
4. Adams, D. L., Adams, D. K., He, J., Kalhor, N., Zhang, M., Xu, T., Gao, H., Reuben, J. M., Qiao, Y., Komaki, R., Liao, Z., Edelman, M. J., Tang, C.-M., & Lin, S. H. (2017). Sequential Tracking of PD-L1 Expression and RAD50 Induction in Circulating Tumor and Stromal Cells of Lung Cancer Patients Undergoing Radiotherapy. *Clinical Cancer Research*, *23*(19), 5948–5958.
5. Adams, D. L., Stefansson, S., Haudenschild, C., Martin, S. S., Charpentier, M., Chumsri, S., Cristofanilli, M., Tang, C.-M., & Alpaugh, R. K. (2015). Cytometric characterization of Circulating Tumor Cells Captured by microfiltration and their correlation to the cellsearch® CTC test. *Cytometry Part A*, *87*(2), 137–144.
6. Aguirre-Ghiso, J. A., Liu, D., Mignatti, A., Kovalski, K., & Ossowski, L. (2001). Urokinase Receptor and Fibronectin Regulate the ERKMAPK to p38MAPK Activity Ratios That Determine Carcinoma Cell Proliferation or Dormancy In Vivo. *Molecular Biology of the Cell*, *12*(4), 863–879.
7. Alexandrov, L. B., Nik-Zainal, S., Wedge, D. C., Aparicio, S. A. J. R., Behjati, S., Biankin, A. V., Bignell, G. R., Bolli, N., Borg, A., Børresen-Dale, A.-L., Boyault, S., Burkhardt, B., Butler, A. P., Caldas, C., Davies, H. R., Desmedt, C., Eils, R., Eyfjörd, J. E., Foekens, J. A., … Stratton, M. R. (2013). Signatures of mutational processes in human cancer. *Nature*, *500*(7463), 415–421.
8. Al-Hajj, M., Wicha, M. S., Benito-Hernandez, A., Morrison, S. J., & Clarke, M. F. (2003). Prospective identification of tumorigenic breast cancer cells. *Proceedings of the National Academy of Sciences*, *100*(7), 3983–3988.
9. Alix-Panabières, C., & Pantel, K. (2014). Challenges in circulating tumour cell research. *Nature Reviews Cancer*, *14*(9), 623–631.
10. Alix-Panabières, C., & Pantel, K. (2021). Liquid Biopsy: From Discovery to Clinical Application. *Cancer Discovery*, *11*(4), 858–873.
11. Allard, W. J., Matera, J., Miller, M. C., Repollet, M., Connelly, M. C., Rao, C., Tibbe, A. G. J., Uhr, J. W., & Terstappen, L. W. M. M. (2004). Tumor cells circulate in the peripheral blood of all major carcinomas but not in healthy subjects or patients with nonmalignant diseases. *Clinical Cancer Research*, *10*(20), 6897–6904.
12. Andree, K. C., Mentink, A., Zeune, L. L., Terstappen, L. W. M. M., Stoecklein, N. H., Neves, R. P., Driemel, C., Lampignano, R., Yang, L., Neubauer, H., Fehm, T., Fischer, J. C., Rossi, E.,

Manicone, M., Basso, U., Marson, P., Zamarchi, R., Loriot, Y., Lapierre, V., … Bono, J. S. (2018). Toward a real liquid biopsy in metastatic breast and prostate cancer: Diagnostic LeukApheresis increases CTC yields in a European prospective multicenter study (CTCTrap). *International Journal of Cancer*, *143*(10), 2584–2591.

13. Ansieau, S., Bastid, J., Doreau, A., Morel, A.-P., Bouchet, B. P., Thomas, C., Fauvet, F., Puisieux, I., Doglioni, C., Piccinin, S., Maestro, R., Voeltzel, T., Selmi, A., Valsesia-Wittmann, S., Caron de Fromentel, C., & Puisieux, A. (2008). Induction of EMT by Twist Proteins as a Collateral Effect of Tumor-Promoting Inactivation of Premature Senescence. *Cancer Cell*, *14*(1), 79–89.
14. Antonia, S. J., Villegas, A., Daniel, D., Vicente, D., Murakami, S., Hui, R., Kurata, T., Chiappori, A., Lee, K. H., de Wit, M., Cho, B. C., Bourhaba, M., Quantin, X., Tokito, T., Mekhail, T., Planchard, D., Kim, Y.-C., Karapetis, C. S., Hiret, S., … Özgüroğlu, M. (2018). Overall Survival with Durvalumab after Chemoradiotherapy in Stage III NSCLC. *New England Journal of Medicine*, *379*(24), 2342–2350.
15. Antonia, S. J., Villegas, A., Daniel, D., Vicente, D., Murakami, S., Hui, R., Yokoi, T., Chiappori, A., Lee, K. H., de Wit, M., Cho, B. C., Bourhaba, M., Quantin, X., Tokito, T., Mekhail, T., Planchard, D., Kim, Y.-C., Karapetis, C. S., Hiret, S., … Özgüroğlu, M. (2017). Durvalumab after Chemoradiotherapy in Stage III Non–Small-Cell Lung Cancer. *New England Journal of Medicine*, *377*(20), 1919–1929.
16. Armstrong, A. J., Marengo, M. S., Oltean, S., Kemeny, G., Bitting, R. L., Turnbull, J. D., Herold, C. I., Marcom, P. K., George, D. J., & Garcia-Blanco, M. A. (2011). Circulating Tumor Cells from Patients with Advanced Prostate and Breast Cancer Display Both Epithelial and Mesenchymal Markers. *Molecular Cancer Research*, *9*(8), 997–1007.
17. Ashworth, A. (2008). A Synthetic Lethal Therapeutic Approach: Poly(ADP) Ribose Polymerase Inhibitors for the Treatment of Cancers Deficient in DNA Double-Strand Break Repair. *Journal of Clinical Oncology*, *26*(22), 3785–3790.
18. Ashworth, A., & Lord, C. J. (2018). Synthetic lethal therapies for cancer: What's next after PARP inhibitors? *Nature Reviews Clinical Oncology*, *15*(9), 564–576.
19. Ashworth, T. (1869). A case of cancer in which cells similar to those in the tumors were seen in blood after death. *The Medical Journal of Australia*, *14*, 146–147.
20. Attard, G., Swennenhuis, J. F., Olmos, D., Reid, A. H. M., Vickers, E., A'Hern, R., Levink, R., Coumans, F., Moreira, J., Riisnaes, R., Oommen, N. B., Hawche, G., Jameson, C., Thompson, E., Sipkema, R., Carden, C. P., Parker, C., Dearnaley, D., Kaye, S. B., … de Bono, J. S. (2009). Characterization of ERG, AR and PTEN gene status in circulating tumor cells from patients with castration-resistant prostate cancer. *Cancer Research*, *69*(7), 2912–2918.
21. Baccelli, I., Schneeweiss, A., Riethdorf, S., Stenzinger, A., Schillert, A., Vogel, V., Klein, C., Saini, M., Bäuerle, T., Wallwiener, M., Holland-Letz, T., Höfner, T., Sprick, M., Scharpff, M., Marmé, F., Sinn, H. P., Pantel, K., Weichert, W., & Trumpp, A. (2013). Identification of a population of blood circulating tumor cells from breast cancer patients that initiates metastasis in a xenograft assay. *Nature Biotechnology*, *31*(6), 539–544.

22. Bakhoum, S. F., & Compton, D. A. (2012). Chromosomal instability and cancer: A complex relationship with therapeutic potential. *The Journal of Clinical Investigation*, *122*(4), 1138–1143.
23. Baldominos, P., Barbera-Mourelle, A., Barreiro, O., Huang, Y., Wight, A., Cho, J.-W., Zhao, X., Estivill, G., Adam, I., Sanchez, X., McCarthy, S., Schaller, J., Khan, Z., Ruzo, A., Pastorello, R., Richardson, E. T., Dillon, D., Montero-Llopis, P., Barroso-Sousa, R., … Agudo, J. (2022). Quiescent cancer cells resist T cell attack by forming an immunosuppressive niche. *Cell*, *185*(10), 1694-1708.e19.
24. Banerjee, S., Stewart, J., Porta, N., Toms, C., Leary, A., Lheureux, S., Khalique, S., Tai, J., Attygalle, A., Vroobel, K., Lord, C. J., Natrajan, R., & Bliss, J. (2021). ATARI trial: ATR inhibitor in combination with olaparib in gynecological cancers with ARID1A loss or no loss (ENGOT/GYN1/NCRI). *International Journal of Gynecologic Cancer*, *31*(11), 1471–1475.
25. Barkan, D., El Touny, L. H., Michalowski, A. M., Smith, J. A., Chu, I., Davis, A. S., Webster, J. D., Hoover, S., Simpson, R. M., Gauldie, J., & Green, J. E. (2010). Metastatic Growth from Dormant Cells Induced by a Col-I–Enriched Fibrotic Environment. *Cancer Research*, *70*(14), 5706–5716.
26. Barretina, J., Caponigro, G., Stransky, N., Venkatesan, K., Margolin, A. A., Kim, S., Wilson, C. J., Lehár, J., Kryukov, G. V., Sonkin, D., Reddy, A., Liu, M., Murray, L., Berger, M. F., Monahan, J. E., Morais, P., Meltzer, J., Korejwa, A., Jané-Valbuena, J., … Garraway, L. A. (2012). The Cancer Cell Line Encyclopedia enables predictive modelling of anticancer drug sensitivity. *Nature*, *483*(7391), 603–607.
27. Bartkova, J., Hořejší, Z., Koed, K., Krämer, A., Tort, F., Zieger, K., Guldberg, P., Sehested, M., Nesland, J. M., Lukas, C., Ørntoft, T., Lukas, J., & Bartek, J. (2005). DNA damage response as a candidate anti-cancer barrier in early human tumorigenesis. *Nature*, *434*(7035), 864–870.
28. Baxter, J. S., Zatreanu, D., Pettitt, S. J., & Lord, C. J. (2022). Resistance to DNA repair inhibitors in cancer. *Molecular Oncology*, *n/a*(n/a), Article n/a.
29. Beck, C., Robert, I., Reina-San-Martin, B., Schreiber, V., & Dantzer, F. (2014). Poly(ADP-ribose) polymerases in double-strand break repair: Focus on PARP1, PARP2 and PARP3. *Experimental Cell Research*, *329*(1), 18–25.
30. Berthault, N., Bergam, P., Pereira, F., Girard, P.-M., & Dutreix, M. (2022). Inhibition of DNA Repair by Inappropriate Activation of ATM, PARP, and DNA-PK with the Drug Agonist AsiDNA. *Cells*, *11*(14), 2149.
31. Besse, B., Awad, M., Forde, P., Thomas, M., Park, K., Goss, G., Rizvi, N., Huemer, F., Hochmair, M., Bennouna, J., Cosaert, J., Szucs, Z., Mortimer, P., Hobson, R., Sachsenmeier, K., Dean, E., Ambrose, H., Hayward, C., Dressman, M., … Heymach, J. (2021). OA07.08 HUDSON: An Open-Label, Multi-Drug, Biomarker-Directed, Phase II Platform Study in Patients with NSCLC, who Progressed on Anti-PD(L)1 Therapy. *Journal of Thoracic Oncology*, *16*(3), S118–S119.
32. Bidard, F.-C., Jacot, W., Kiavue, N., Dureau, S., Kadi, A., Brain, E., Bachelot, T., Bourgeois, H., Gonçalves, A., Ladoire, S., Naman, H., Dalenc, F., Gligorov, J., Espié, M., Emile, G., Ferrero, J.-M., Loirat, D., Frank, S., Cabel, L., … Pierga, J.-Y. (2021). Efficacy of Circulating Tumor Cell

Count–Driven vs Clinician-Driven First-line Therapy Choice in Hormone Receptor–Positive, ERBB2-Negative Metastatic Breast Cancer: The STIC CTC Randomized Clinical Trial. *JAMA Oncology*, *7*(1), 34–41.

33. Bidard, F.-C., Peeters, D. J., Fehm, T., Nolé, F., Gisbert-Criado, R., Mavroudis, D., Grisanti, S., Generali, D., Garcia-Saenz, J. A., Stebbing, J., Caldas, C., Gazzaniga, P., Manso, L., Zamarchi, R., de Lascoiti, A. F., De Mattos-Arruda, L., Ignatiadis, M., Lebofsky, R., van Laere, S. J., … Michiels, S. (2014). Clinical validity of circulating tumour cells in patients with metastatic breast cancer: A pooled analysis of individual patient data. *The Lancet. Oncology*, *15*(4), 406–414.
34. Blackhall, F., Frese, K. K., Simpson, K., Kilgour, E., Brady, G., & Dive, C. (2018). Will liquid biopsies improve outcomes for patients with small-cell lung cancer? *The Lancet Oncology*, *19*(9), e470–e481.
35. Bousquet, G., & Janin, A. (2016). Patient-Derived Xenograft: An Adjuvant Technology for the Treatment of Metastatic Disease. *Pathobiology*, *83*(4), 170–176.
36. Bracken, C., Gregory, P., Kolesnikoff, N., Bert, A., Wang, J., Shannon, M., & Goodall, G. (2008). A Double-Negative Feedback Loop between ZEB1-SIP1 and the microRNA-200 Family Regulates Epithelial-Mesenchymal Transition. *Cancer Research*, *68*, 7846–7854.
37. Bragado, P., Estrada, Y., Parikh, F., Krause, S., Capobianco, C., Farina, H. G., Schewe, D. M., & Aguirre-Ghiso, J. A. (2013). TGFβ2 dictates disseminated tumour cell fate in target organs through TGFβ-RIII and p38α/β signalling. *Nature Cell Biology*, *15*(11), 1351–1361.
38. Braun, S., Vogl, F. D., Naume, B., Janni, W., Osborne, M. P., Coombes, R. C., Schlimok, G., Diel, I. J., Gerber, B., Gebauer, G., Pierga, J.-Y., Marth, C., Oruzio, D., Wiedswang, G., Solomayer, E.-F., Kundt, G., Strobl, B., Fehm, T., Wong, G. Y. C., … Pantel, K. (2005). A Pooled Analysis of Bone Marrow Micrometastasis in Breast Cancer. *New England Journal of Medicine*, *353*(8), 793–802.
39. Brown, J. S., O'Carrigan, B., Jackson, S. P., & Yap, T. A. (2017). Targeting DNA Repair in Cancer: Beyond PARP Inhibitors. *Cancer Discovery*, *7*(1), 20–37.
40. Bryant, H. E., Schultz, N., Thomas, H. D., Parker, K. M., Flower, D., Lopez, E., Kyle, S., Meuth, M., Curtin, N. J., & Helleday, T. (2005). Specific killing of BRCA2-deficient tumours with inhibitors of poly(ADP-ribose) polymerase. *Nature*, *434*(7035), 913–917.
41. Bunting, S. F., Callén, E., Wong, N., Chen, H.-T., Polato, F., Gunn, A., Bothmer, A., Feldhahn, N., Fernandez-Capetillo, O., Cao, L., Xu, X., Deng, C.-X., Finkel, T., Nussenzweig, M., Stark, J. M., & Nussenzweig, A. (2010). 53BP1 Inhibits Homologous Recombination in Brca1-Deficient Cells by Blocking Resection of DNA Breaks. *Cell*, *141*(2), 243–254.
42. Burma, S., Chen, B. P. C., & Chen, D. J. (2006). Role of non-homologous end joining (NHEJ) in maintaining genomic integrity. *DNA Repair*, *5*(9), 1042–1048.
43. Byrne, A. T., Alférez, D. G., Amant, F., Annibali, D., Arribas, J., Biankin, A. V., Bruna, A., Budinská, E., Caldas, C., Chang, D. K., Clarke, R. B., Clevers, H., Coukos, G., Dangles-Marie, V., Eckhardt, S. G., Gonzalez-Suarez, E., Hermans, E., Hidalgo, M., Jarzabek, M. A., … Trusolino, L. (2017). Interrogating open issues in cancer precision medicine with patient-derived xenografts. *Nature Reviews Cancer*, *17*(4), 254–268.

44. Camidge, D. R., Kim, H. R., Ahn, M.-J., Yang, J. C. H., Han, J.-Y., Hochmair, M. J., Lee, K. H., Delmonte, A., García Campelo, M. R., Kim, D.-W., Griesinger, F., Felip, E., Califano, R., Spira, A., Gettinger, S. N., Tiseo, M., Lin, H. M., Gupta, N., Hanley, M. J., … Popat, S. (2020). Brigatinib Versus Crizotinib in Advanced ALK Inhibitor–Naive ALK-Positive Non–Small Cell Lung Cancer: Second Interim Analysis of the Phase III ALTA-1L Trial. *Journal of Clinical Oncology*, *38*(31), 3592–3603.
45. Camidge, D. R., Kim, H. R., Ahn, M.-J., Yang, J. C.-H., Han, J.-Y., Lee, J.-S., Hochmair, M. J., Li, J. Y.-C., Chang, G.-C., Lee, K. H., Gridelli, C., Delmonte, A., Garcia Campelo, R., Kim, D.-W., Bearz, A., Griesinger, F., Morabito, A., Felip, E., Califano, R., … Popat, S. (2018). Brigatinib versus Crizotinib in ALK-Positive Non–Small-Cell Lung Cancer. *New England Journal of Medicine*, *379*(21), 2027–2039.
46. Campbell, J. D., Alexandrov, A., Kim, J., Wala, J., Berger, A. H., Pedamallu, C. S., Shukla, S. A., Guo, G., Brooks, A. N., Murray, B. A., Imielinski, M., Hu, X., Ling, S., Akbani, R., Rosenberg, M., Cibulskis, C., Ramachandran, A., Collisson, E. A., Kwiatkowski, D. J., … Meyerson, M. (2016). Distinct patterns of somatic genome alterations in lung adenocarcinomas and squamous cell carcinomas. *Nature Genetics*, *48*(6), 607–616.
47. Campbell, P. J., Getz, G., Korbel, J. O., Stuart, J. M., Jennings, J. L., Stein, L. D., Perry, M. D., Nahal-Bose, H. K., Ouellette, B. F. F., Li, C. H., Rheinbay, E., Nielsen, G. P., Sgroi, D. C., Wu, C.-L., Faquin, W. C., Deshpande, V., Boutros, P. C., Lazar, A. J., Hoadley, K. A., … The ICGC/TCGA Pan-Cancer Analysis of Whole Genomes Consortium. (2020). Pan-cancer analysis of whole genomes. *Nature*, *578*(7793), 82–93.
48. Carter, L., Rothwell, D. G., Mesquita, B., Smowton, C., Leong, H. S., Fernandez-Gutierrez, F., Li, Y., Burt, D. J., Antonello, J., Morrow, C. J., Hodgkinson, C. L., Morris, K., Priest, L., Carter, M., Miller, C., Hughes, A., Blackhall, F., Dive, C., & Brady, G. (2017). Molecular analysis of circulating tumor cells identifies distinct copy-number profiles in patients with chemosensitive and chemorefractory small-cell lung cancer. *Nature Medicine*, *23*(1), 114–119.
49. Cayrefourcq, L., Mazard, T., Joosse, S., Solassol, J., Ramos, J., Assenat, E., Schumacher, U., Costes, V., Maudelonde, T., Pantel, K., & Alix-Panabieres, C. (2015). Establishment and Characterization of a Cell Line from Human Circulating Colon Cancer Cells. *Cancer Research*, *75*(5), 892–901.
50. Ceccaldi, R., Rondinelli, B., & D'Andrea, A. D. (2016). Repair Pathway Choices and Consequences at the Double-Strand Break. *Trends in Cell Biology*, *26*(1), 52–64.
51. Ceccaldi, R., Sarangi, P., & D'Andrea, A. D. (2016). The Fanconi anaemia pathway: New players and new functions. *Nature Reviews Molecular Cell Biology*, *17*(6), 337–349.
52. Cha, Y. J., Cho, B. C., Kim, H. R., Lee, H.-J., & Shim, H. S. (2016). A Case of ALK-Rearranged Adenocarcinoma with Small Cell Carcinoma-Like Transformation and Resistance to Crizotinib. *Journal of Thoracic Oncology*, *11*(5), e55–e58.
53. Chabanon, R. M., Muirhead, G., Krastev, D. B., Adam, J., Morel, D., Garrido, M., Lamb, A., Hénon, C., Dorvault, N., Rouanne, M., Marlow, R., Bajrami, I., Cardeñosa, M. L., Konde, A., Besse, B., Ashworth, A., Pettitt, S. J., Haider, S., Marabelle, A., … Postel-Vinay, S. (2019). PARP

inhibition enhances tumor cell–intrinsic immunity in ERCC1-deficient non–small cell lung cancer. *The Journal of Clinical Investigation*, *129*(3), 1211–1228.

54. Chabanon, R. M., Rouanne, M., Lord, C. J., Soria, J.-C., Pasero, P., & Postel-Vinay, S. (2021). Targeting the DNA damage response in immuno-oncology: Developments and opportunities. *Nature Reviews Cancer*, *21*(11), 701–717.
55. Chambers, A. F., Groom, A. C., & MacDonald, I. C. (2002). Dissemination and growth of cancer cells in metastatic sites. *Nature Reviews Cancer*, *2*(8), 563–572.
56. Chaudhuri, A. A., Chabon, J. J., Lovejoy, A. F., Newman, A. M., Stehr, H., Azad, T. D., Khodadoust, M. S., Esfahani, M. S., Liu, C. L., Zhou, L., Scherer, F., Kurtz, D. M., Say, C., Carter, J. N., Merriott, D. J., Dudley, J. C., Binkley, M. S., Modlin, L., Padda, S. K., … Diehn, M. (2017). Early Detection of Molecular Residual Disease in Localized Lung Cancer by Circulating Tumor DNA Profiling. *Cancer Discovery*, *7*(12), 1394–1403.
57. Chebouti, I., Kuhlmann, J. D., Buderath, P., Weber, S., Wimberger, P., Bokeloh, Y., Hauch, S., Kimmig, R., & Kasimir-Bauer, S. (2016). ERCC1-expressing circulating tumor cells as a potential diagnostic tool for monitoring response to platinum-based chemotherapy and for predicting post-therapeutic outcome of ovarian cancer. *Oncotarget*, *8*(15), 24303–24313.
58. Chen, Y., McAndrews, K. M., & Kalluri, R. (2021). Clinical and therapeutic relevance of cancer-associated fibroblasts. *Nature Reviews Clinical Oncology*, *18*(12), 792–804.
59. Chen, Y., Yang, Z., Wang, Y., Wang, J., & Wang, C. (2019). Karyotyping of circulating tumor cells for predicting chemotherapeutic sensitivity and efficacy in patients with esophageal cancer. *BMC Cancer*, *19*(1), 651.
60. Chen, Z., Fillmore, C. M., Hammerman, P. S., Kim, C. F., & Wong, K.-K. (2014). Non-small-cell lung cancers: A heterogeneous set of diseases. *Nature Reviews Cancer*, *14*(8), 535–546.
61. Cheng, B., Pan, W., Xing, Y., Xiao, Y., Chen, J., & Xu, Z. (2022). Recent advances in DDR (DNA damage response) inhibitors for cancer therapy. *European Journal of Medicinal Chemistry*, *230*, 114109.
62. Cleary, J. M., Aguirre, A. J., Shapiro, G. I., & D'Andrea, A. D. (2020). Biomarker-Guided Development of DNA Repair Inhibitors. *Molecular Cell*, *78*(6), 1070–1085.
63. Cohen, S. J., Punt, C. J. A., Iannotti, N., Saidman, B. H., Sabbath, K. D., Gabrail, N. Y., Picus, J., Morse, M., Mitchell, E., Miller, M. C., Doyle, G. V., Tissing, H., Terstappen, L. W. M. M., & Meropol, N. J. (2008). Relationship of Circulating Tumor Cells to Tumor Response, Progression-Free Survival, and Overall Survival in Patients With Metastatic Colorectal Cancer. *Journal of Clinical Oncology*, *26*(19), 3213–3221.
64. Conteduca, V., Ku, S.-Y., Puca, L., Slade, M., Fernandez, L., Hess, J., Bareja, R., Vlachostergios, P. J., Sigouros, M., Mosquera, J. M., Sboner, A., Nanus, D. M., Elemento, O., Dittamore, R., Tagawa, S. T., & Beltran, H. (2020). SLFN11 expression in advanced prostate cancer and response to platinum-based chemotherapy. *Molecular Cancer Therapeutics*, *19*(5), 1157–1164.
65. Cooper, A. J., Sequist, L. V., & Lin, J. J. (2022). Third-generation EGFR and ALK inhibitors: Mechanisms of resistance and management. *Nature Reviews Clinical Oncology*, 1–16.

66. Coussy, F., El-Botty, R., Château-Joubert, S., Dahmani, A., Montaudon, E., Leboucher, S., Morisset, L., Painsec, P., Sourd, L., Huguet, L., Nemati, F., Servely, J.-L., Larcher, T., Vacher, S., Briaux, A., Reyes, C., La Rosa, P., Lucotte, G., Popova, T., … Marangoni, E. (2020). BRCAness, SLFN11, and RB1 loss predict response to topoisomerase I inhibitors in triple-negative breast cancers. *Science Translational Medicine*, *12*(531), eaax2625.
67. Craene, B. D., & Berx, G. (2013). Regulatory networks defining EMT during cancer initiation and progression. *Nature Reviews Cancer*, *13*(2), 97–110.
68. Cristofanilli, M., Budd, G. T., Ellis, M. J., Stopeck, A., Matera, J., Miller, M. C., Reuben, J. M., Doyle, G. V., Allard, W. J., Terstappen, L. W. M. M., & Hayes, D. F. (2004). Circulating Tumor Cells, Disease Progression, and Survival in Metastatic Breast Cancer. *New England Journal of Medicine*, *351*(8), 781–791.
69. Cristofanilli, M., Hayes, D. F., Budd, G. T., Ellis, M. J., Stopeck, A., Reuben, J. M., Doyle, G. V., Matera, J., Allard, W. J., Miller, M. C., Fritsche, H. A., Hortobagyi, G. N., & Terstappen, L. W. M. M. (2005). Circulating Tumor Cells: A Novel Prognostic Factor for Newly Diagnosed Metastatic Breast Cancer. *Journal of Clinical Oncology*, *23*(7), 1420–1430.
70. Dann, R. B., DeLoia, J. A., Timms, K. M., Zorn, K. K., Potter, J., Flake, D. D., Lanchbury, J. S., & Krivak, T. C. (2012). BRCA1/2 mutations and expression: Response to platinum chemotherapy in patients with advanced stage epithelial ovarian cancer. *Gynecologic Oncology*, *125*(3), 677–682.
71. Dantzer, F., de la Rubia, G., Ménissier-de Murcia, J., Hostomsky, Z., de Murcia, G., & Schreiber, V. (2000). Base Excision Repair Is Impaired in Mammalian Cells Lacking Poly(ADP-ribose) Polymerase-1. *Biochemistry*, *39*(25), 7559–7569.
72. Das, M., Riess, J. W., Frankel, P., Schwartz, E., Bennis, R., Hsieh, H. B., Liu, X., Ly, J. C., Zhou, L., Nieva, J. J., Wakelee, H. A., & Bruce, R. H. (2012). ERCC1 expression in circulating tumor cells (CTCs) using a novel detection platform correlates with progression-free survival (PFS) in patients with metastatic non-small-cell lung cancer (NSCLC) receiving platinum chemotherapy. *Lung Cancer*, *77*(2), 421–426.
73. Davidson, M. R., Gazdar, A. F., & Clarke, B. E. (2013). The pivotal role of pathology in the management of lung cancer. *Journal of Thoracic Disease*, *5*(Suppl 5), S463–S478.
74. Davies, K. D., & Doebele, R. C. (2013). Molecular Pathways: ROS1 Fusion Proteins in Cancer. *Clinical Cancer Research*, *19*(15), 4040–4045.
75. de Bono, J. S., Scher, H. I., Montgomery, R. B., Parker, C., Miller, M. C., Tissing, H., Doyle, G. V., Terstappen, L. W. W. M., Pienta, K. J., & Raghavan, D. (2008). Circulating Tumor Cells Predict Survival Benefit from Treatment in Metastatic Castration-Resistant Prostate Cancer. *Clinical Cancer Research*, *14*(19), 6302–6309.
76. De Vos, M., Schreiber, V., & Dantzer, F. (2012). The diverse roles and clinical relevance of PARPs in DNA damage repair: Current state of the art. *Biochemical Pharmacology*, *84*(2), 137–146.
77. Deans, A. J., & West, S. C. (2011). DNA interstrand crosslink repair and cancer. *Nature Reviews. Cancer*, *11*(7), 467–480.

78. Desitter, I., Guerrouahen, B. S., Benali-Furet, N., Wechsler, J., Jänne, P. A., Kuang, Y., Yanagita, M., Wang, L., Berkowitz, J. A., Distel, R. J., & Cayre, Y. E. (2011). A new device for rapid isolation by size and characterization of rare circulating tumor cells. *Anticancer Research*, *31*(2), 427–441.
79. Desmond, D., Vilimas, R., Mullenix, C., Zhao, C., Szabo, E., Shelat, M., Ballman, M., Sansone, S., Steinberg, S. M., Lee, J.-M., & Rajan, A. (2022). Durvalumab (D) in combination with olaparib (O) for advanced, previously treated non-small cell lung cancer (NSCLC). *Journal of Clinical Oncology*, *40*(16_suppl), e21153–e21153.
80. Dillon, M. T., Boylan, Z., Smith, D., Guevara, J., Mohammed, K., Peckitt, C., Saunders, M., Banerji, U., Clack, G., Smith, S. A., Spicer, J. F., Forster, M. D., & Harrington, K. J. (2018). PATRIOT: A phase I study to assess the tolerability, safety and biological effects of a specific ataxia telangiectasia and Rad3-related (ATR) inhibitor (AZD6738) as a single agent and in combination with palliative radiation therapy in patients with solid tumours. *Clinical and Translational Radiation Oncology*, *12*, 16–20.
81. Ding, L., Kim, H.-J., Wang, Q., Kearns, M., Jiang, T., Ohlson, C. E., Li, B. B., Xie, S., Liu, J. F., Stover, E. H., Howitt, B. E., Bronson, R. T., Lazo, S., Roberts, T. M., Freeman, G. J., Konstantinopoulos, P. A., Matulonis, U. A., & Zhao, J. J. (2018). PARP Inhibition Elicits STING-Dependent Antitumor Immunity in Brca1-Deficient Ovarian Cancer. *Cell Reports*, *25*(11), 2972-2980.e5.
82. Drapkin, B. J., George, J., Christensen, C. L., Mino-Kenudson, M., Dries, R., Sundaresan, T., Phat, S., Myers, D. T., Zhong, J., Igo, P., Hazar-Rethinam, M. H., Licausi, J. A., Gomez-Caraballo, M., Kem, M., Jani, K. N., Azimi, R., Abedpour, N., Menon, R., Lakis, S., … Farago, A. F. (2018). Genomic and Functional Fidelity of Small Cell Lung Cancer Patient-Derived Xenografts. *Cancer Discovery*, *8*(5), 600–615.
83. Dumont, N., Liu, B., DeFilippis, R. A., Chang, H., Rabban, J. T., Karnezis, A. N., Tjoe, J. A., Marx, J., Parvin, B., & Tlsty, T. D. (2013). Breast Fibroblasts Modulate Early Dissemination, Tumorigenesis, and Metastasis through Alteration of Extracellular Matrix Characteristics. *Neoplasia*, *15*(3), 249–262.
84. Durinikova, E., Reilly, N. M., Buzo, K., Mariella, E., Chilà, R., Lorenzato, A., Dias, J. M. L., Grasso, G., Pisati, F., Lamba, S., Corti, G., Degasperi, A., Cancelliere, C., Mauri, G., Andrei, P., Linnebacher, M., Marsoni, S., Siena, S., Sartore-Bianchi, A., … Arena, S. (2022). Targeting the DNA Damage Response Pathways and Replication Stress in Colorectal Cancer. *Clinical Cancer Research*, OF1–OF16.
85. Erez, N., Truitt, M., Olson, P., & Hanahan, D. (2010). Cancer-Associated Fibroblasts Are Activated in Incipient Neoplasia to Orchestrate Tumor-Promoting Inflammation in an NF-κB-Dependent Manner. *Cancer Cell*, *17*(2), 135–147.
86. Ewing, J. (1928). *Neoplastic Diseases: A treatise on Tumours.* W. B. Sanders Co.
87. Fabbri, F., Carloni, S., Zoli, W., Ulivi, P., Gallerani, G., Fici, P., Chiadini, E., Passardi, A., Frassineti, G. L., Ragazzini, A., & Amadori, D. (2013). Detection and recovery of circulating colon cancer cells using a dielectrophoresis-based device: KRAS mutation status in pure CTCs. *Cancer Letters*, *335*(1), 225–231.

88. Fan, G., Sun, L., Meng, L., Hu, C., Wang, X., Shi, Z., Hu, C., Han, Y., Yang, Q., Cao, L., Zhang, X., Zhang, Y., Song, X., Xia, S., He, B., Zhang, S., & Wang, C. (2021). The ATM and ATR kinases regulate centrosome clustering and tumor recurrence by targeting KIFC1 phosphorylation. *Nature Communications*, *12*, 20.
89. Farmer, H., Mccabe, N., Lord, C., Tutt, A., Johnson, D., Richardson, T., Santarosa, M., Dillon, K., Hickson, I., Knights, C., Martin, N., Jackson, S., Smith, G., & Ashworth, A. (2005). Targeting the DNA repair defect in BRCA mutant cells as a therapeutic strategy. *Nature*, *434*, 917–921.
90. Faugeroux, V., Lefebvre, C., Pailler, E., Pierron, V., Marcaillou, C., Tourlet, S., Billiot, F., Dogan, S., Oulhen, M., Vielh, P., Rameau, P., NgoCamus, M., Massard, C., Laplace-Builhé, C., Tibbe, A., Taylor, M., Soria, J.-C., Fizazi, K., Loriot, Y., … Farace, F. (2020). An Accessible and Unique Insight into Metastasis Mutational Content Through Whole-exome Sequencing of Circulating Tumor Cells in Metastatic Prostate Cancer. *European Urology Oncology*, *3*(4), 498–508.
91. Faugeroux, V., Pailler, E., Oulhen, M., Deas, O., Brulle-Soumare, L., Hervieu, C., Marty, V., Alexandrova, K., Andree, K. C., Stoecklein, N. H., Tramalloni, D., Cairo, S., NgoCamus, M., Nicotra, C., Terstappen, L. W. M. M., Manaresi, N., Lapierre, V., Fizazi, K., Scoazec, J.-Y., … Farace, F. (2020). Genetic characterization of a unique neuroendocrine transdifferentiation prostate circulating tumor cell-derived eXplant model. *Nature Communications*, *11*(1), 1884.
92. Felici, C., Mannavola, F., Stucci, L. S., Duda, L., Cafforio, P., Porta, C., & Tucci, M. (2022). Circulating tumor cells from melanoma patients show phenotypic plasticity and metastatic potential in xenograft NOD.CB17 mice. *BMC Cancer*, *22*(1), 1–12.
93. Fennell, D. A., Lester, J. F., Danson, S., Blackhall, F. H., Nicolson, M., Nixon, L. S., Porter, C., Gardner, G. M., White, A., Griffiths, G. O., & Casbard, A. C. (2020). A randomized phase II trial of olaparib maintenance versus placebo monotherapy in patients with chemosensitive advanced non-small cell lung cancer. *Journal of Clinical Oncology*, *38*(15_suppl), e21649–e21649.
94. Ferrarini, A., Forcato, C., Buson, G., Tononi, P., Del Monaco, V., Terracciano, M., Bolognesi, C., Fontana, F., Medoro, G., Neves, R., Möhlendick, B., Rihawi, K., Ardizzoni, A., Sumanasuriya, S., Flohr, P., Lambros, M., de Bono, J., Stoecklein, N. H., & Manaresi, N. (2018). A streamlined workflow for single-cells genome-wide copy-number profiling by low-pass sequencing of LM-PCR whole-genome amplification products. *PloS One*, *13*(3), e0193689.
95. Fidler, I. (1975). *Biological Behavior of Malignant Melanoma Cells Correlated to Their Survival in vivo*. *35*, 7.
96. Fidler, I., & Nicolson, G. (1976). Organ Selectivity for Implantation Survival and Growth of B16 Melanoma Variant Tumor Lines2. *Journal of the National Cancer Institute*, *57*, 1199–1202.
97. Fischer, K. R., Durrans, A., Lee, S., Sheng, J., Li, F., Wong, S. T. C., Choi, H., El Rayes, T., Ryu, S., Troeger, J., Schwabe, R. F., Vahdat, L. T., Altorki, N. K., Mittal, V., & Gao, D. (2015).

Epithelial-to-mesenchymal transition is not required for lung metastasis but contributes to chemoresistance. *Nature*, *527*(7579), 472–476.

98. Folkman, J. (1971). Tumor Angiogenesis: Therapeutic Implications. *New England Journal of Medicine*, *285*(21), 1182–1186.
99. Forde, P. M., Spicer, J., Lu, S., Provencio, M., Mitsudomi, T., Awad, M. M., Felip, E., Broderick, S. R., Brahmer, J. R., Swanson, S. J., Kerr, K., Wang, C., Ciuleanu, T.-E., Saylors, G. B., Tanaka, F., Ito, H., Chen, K.-N., Liberman, M., Vokes, E. E., … Girard, N. (2022). Neoadjuvant Nivolumab plus Chemotherapy in Resectable Lung Cancer. *New England Journal of Medicine*, *386*(21), 1973–1985.
100. Franses, J. W., Philipp, J., Missios, P., Bhan, I., Liu, A., Yashaswini, C., Tai, E., Zhu, H., Ligorio, M., Nicholson, B., Tassoni, E. M., Desai, N., Kulkarni, A. S., Szabolcs, A., Hong, T. S., Liss, A. S., Fernandez-del Castillo, C., Ryan, D. P., Maheswaran, S., … Ting, D. T. (2020). Pancreatic circulating tumor cell profiling identifies LIN28B as a metastasis driver and drug target. *Nature Communications*, *11*(1), 3303.
101. Friboulet, L., Li, N., Katayama, R., Lee, C. C., Gainor, J. F., Crystal, A. S., Michellys, P.-Y., Awad, M. M., Yanagitani, N., Kim, S., Pferdekamper, A. C., Li, J., Kasibhatla, S., Sun, F., Sun, X., Hua, S., McNamara, P., Mahmood, S., Lockerman, E. L., … Engelman, J. A. (2014). The ALK inhibitor ceritinib overcomes crizotinib resistance in non-small cell lung cancer. *Cancer Discovery*, *4*(6), 662–673.
102. Frithiof, H., Aaltonen, K., & Rydén, L. (2016). A FISH-based method for assessment of HER-2 amplification status in breast cancer circulating tumor cells following CellSearch isolation. *OncoTargets and Therapy*, *9*, 7095–7103.
103. Gadgeel, S., Rodríguez-Abreu, D., Speranza, G., Esteban, E., Felip, E., Dómine, M., Hui, R., Hochmair, M. J., Clingan, P., Powell, S. F., Cheng, S. Y.-S., Bischoff, H. G., Peled, N., Grossi, F., Jennens, R. R., Reck, M., Garon, E. B., Novello, S., Rubio-Viqueira, B., … Garassino, M. C. (2020). Updated Analysis From KEYNOTE-189: Pembrolizumab or Placebo Plus Pemetrexed and Platinum for Previously Untreated Metastatic Nonsquamous Non–Small-Cell Lung Cancer. *Journal of Clinical Oncology*, *38*(14), 1505–1517.
104. Gainor, J. F., Dardaei, L., Yoda, S., Friboulet, L., Leshchiner, I., Katayama, R., Dagogo-Jack, I., Gadgeel, S., Schultz, K., Singh, M., Chin, E., Parks, M., Lee, D., DiCecca, R. H., Lockerman, E., Huynh, T., Logan, J., Ritterhouse, L. L., Le, L. P., … Shaw, A. T. (2016). Molecular Mechanisms of Resistance to First- and Second-Generation ALK Inhibitors in ALK-Rearranged Lung Cancer. *Cancer Discovery*, *6*(10), 1118–1133.
105. Gandhi, L., Rodríguez-Abreu, D., Gadgeel, S., Esteban, E., Felip, E., De Angelis, F., Domine, M., Clingan, P., Hochmair, M. J., Powell, S. F., Cheng, S. Y.-S., Bischoff, H. G., Peled, N., Grossi, F., Jennens, R. R., Reck, M., Hui, R., Garon, E. B., Boyer, M., … Garassino, M. C. (2018). Pembrolizumab plus Chemotherapy in Metastatic Non–Small-Cell Lung Cancer. *New England Journal of Medicine*, *378*(22), 2078–2092.
106. Ganem, N. J., Godinho, S. A., & Pellman, D. (2009). A Mechanism Linking Extra Centrosomes to Chromosomal Instability. *Nature*, *460*(7252), 278–282.

107. Gao, D., Vela, I., Sboner, A., Iaquinta, P. J., Karthaus, W. R., Gopalan, A., Dowling, C., Wanjala, J. N., Undvall, E. A., Arora, V. K., Wongvipat, J., Kossai, M., Ramazanoglu, S., Barboza, L. P., Di, W., Cao, Z., Zhang, Q. F., Sirota, I., Ran, L., … Chen, Y. (2014). Organoid Cultures Derived from Patients with Advanced Prostate Cancer. *Cell*, *159*(1), 176–187.

108. Gao, H., Chakraborty, G., Lee-Lim, A. P., Mo, Q., Decker, M., Vonica, A., Shen, R., Brogi, E., Brivanlou, A. H., & Giancotti, F. G. (2012). The BMP Inhibitor Coco Reactivates Breast Cancer Cells at Lung Metastatic Sites. *Cell*, *150*(4), 764–779.

109. Garcés, J.-J., Cedena, M.-T., Puig, N., Burgos, L., Perez, J. J., Cordon, L., Flores-Montero, J., Sanoja-Flores, L., Calasanz, M.-J., Ortiol, A., Blanchard, M.-J., Rios, R., Martin, J., Martínez-Martinez, R., Bargay, J., Sureda, A., de la Rubia, J., Hernandez, M.-T., Rodriguez-Otero, P., … Paiva, B. (2022). Circulating Tumor Cells for the Staging of Patients With Newly Diagnosed Transplant-Eligible Multiple Myeloma. *Journal of Clinical Oncology*, JCO.21.01365.

110. Gasch, C., Bauernhofer, T., Pichler, M., Langer-Freitag, S., Reeh, M., Seifert, A. M., Mauermann, O., Izbicki, J. R., Pantel, K., & Riethdorf, S. (2013). Heterogeneity of Epidermal Growth Factor Receptor Status and Mutations of KRAS/PIK3CA in Circulating Tumor Cells of Patients with Colorectal Cancer. *Clinical Chemistry*, *59*(1), 252–260.

111. Gawad, C., Koh, W., & Quake, S. R. (2016). Single-cell genome sequencing: Current state of the science. *Nature Reviews Genetics*, *17*(3), 175–188.

112. Girotti, M. R., Gremel, G., Lee, R., Galvani, E., Rothwell, D., Viros, A., Mandal, A. K., Lim, K. H. J., Saturno, G., Furney, S. J., Baenke, F., Pedersen, M., Rogan, J., Swan, J., Smith, M., Fusi, A., Oudit, D., Dhomen, N., Brady, G., … Marais, R. (2016). Application of Sequencing, Liquid Biopsies, and Patient-Derived Xenografts for Personalized Medicine in Melanoma. *Cancer Discovery*, *6*(3), 286–299.

113. Gkountela, S., Castro-Giner, F., Szczerba, B. M., Vetter, M., Landin, J., Scherrer, R., Krol, I., Scheidmann, M. C., Beisel, C., Stirnimann, C. U., Kurzeder, C., Heinzelmann-Schwarz, V., Rochlitz, C., Weber, W. P., & Aceto, N. (2019). Circulating Tumor Cell Clustering Shapes DNA Methylation to Enable Metastasis Seeding. *Cell*, *176*(1–2), 98-112.e14.

114. Gocheva, V., Wang, H.-W., Gadea, B. B., Shree, T., Hunter, K. E., Garfall, A. L., Berman, T., & Joyce, J. A. (2010). IL-4 induces cathepsin protease activity in tumor-associated macrophages to promote cancer growth and invasion. *Genes & Development*, *24*(3), 241–255.

115. Gong, C., Liu, B., Yao, Y., Qu, S., Luo, W., Tan, W., Liu, Q., Yao, H., Zou, L., Su, F., & Song, E. (2015). Potentiated DNA Damage Response in Circulating Breast Tumor Cells Confers Resistance to Chemotherapy. *Journal of Biological Chemistry*, *290*(24), 14811–14825.

116. Gong, Z., Li, Q., Shi, J., Wei, J., Li, P., Chang, C.-H., Shultz, L. D., & Ren, G. (2022). Lung fibroblasts facilitate pre-metastatic niche formation by remodeling the local immune microenvironment. *Immunity*, *55*(8), 1483-1500.e9.

117. Gorges, T. M., Penkalla, N., Schalk, T., Joosse, S. A., Riethdorf, S., Tucholski, J., Lücke, K., Wikman, H., Jackson, S., Brychta, N., von Ahsen, O., Schumann, C., Krahn, T., & Pantel, K. (2016). Enumeration and Molecular Characterization of Tumor Cells in Lung Cancer Patients

Using a Novel In Vivo Device for Capturing Circulating Tumor Cells. *Clinical Cancer Research*, *22*(9), 2197–2206.

118. Gorgoulis, V. G., Vassiliou, L.-V. F., Karakaidos, P., Zacharatos, P., Kotsinas, A., Liloglou, T., Venere, M., DiTullio, R. A., Kastrinakis, N. G., Levy, B., Kletsas, D., Yoneta, A., Herlyn, M., Kittas, C., & Halazonetis, T. D. (2005). Activation of the DNA damage checkpoint and genomic instability in human precancerous lesions. *Nature*, *434*(7035), 907–913.
119. Graeser, M., McCarthy, A., Lord, C. J., Savage, K., Hills, M., Salter, J., Orr, N., Parton, M., Smith, I. E., Reis-Filho, J. S., Dowsett, M., Ashworth, A., & Turner, N. C. (2010). A Marker of Homologous Recombination Predicts Pathologic Complete Response to Neoadjuvant Chemotherapy in Primary Breast Cancer. *Clinical Cancer Research*, *16*(24), 6159–6168.
120. Gulbahce, N., Magbanua, M. J. M., Chin, R., Agarwal, M. R., Luo, X., Liu, J., Hayden, D. M., Mao, Q., Ciotlos, S., Li, Z., Chen, Y., Chen, X., Li, Y., Zhang, R. Y., Lee, K., Tearle, R., Park, E., Drmanac, S., Rugo, H. S., … Peters, B. A. (2017). Quantitative Whole Genome Sequencing of Circulating Tumor Cells Enables Personalized Combination Therapy of Metastatic Cancer. *Cancer Research*, *77*(16), 4530–4541.
121. Gupta, S., Li, J., Kemeny, G., Bitting, R. L., Beaver, J., Somarelli, J. A., Ware, K. E., Gregory, S., & Armstrong, A. J. (2017). Whole Genomic Copy Number Alterations in Circulating Tumor Cells from Men with Abiraterone or Enzalutamide-Resistant Metastatic Castration-Resistant Prostate Cancer. *Clinical Cancer Research*, *23*(5), 1346–1357.
122. Haemmerle, M., Stone, R. L., Menter, D. G., Afshar-Kharghan, V., & Sood, A. K. (2018). The Platelet Lifeline to Cancer: Challenges and Opportunities. *Cancer Cell*, *33*(6), 965–983.
123. Hanahan, D. (2022). Hallmarks of Cancer: New Dimensions. *Cancer Discovery*, *12*(1), 31–46.
124. Hanahan, D., & Weinberg, R. A. (2011). Hallmarks of Cancer: The Next Generation. *Cell*, *144*(5), 646–674.
125. Hart, I. R., & Fidler, I. J. (1980). *Role of Organ Selectivity in the Determination of Metastatic Patterns of B16 Melanoma*. *40*, 7.
126. Hayes, D. F., Cristofanilli, M., Budd, G. T., Ellis, M. J., Stopeck, A., Miller, M. C., Matera, J., Allard, W. J., Doyle, G. V., & Terstappen, L. W. W. M. (2006). Circulating Tumor Cells at Each Follow-up Time Point during Therapy of Metastatic Breast Cancer Patients Predict Progression-Free and Overall Survival. *Clinical Cancer Research*, *12*(14), 4218–4224.
127. Heeke, A. L., Pishvaian, M. J., Lynce, F., Xiu, J., Brody, J. R., Chen, W.-J., Baker, T. M., Marshall, J. L., & Isaacs, C. (2018). Prevalence of Homologous Recombination–Related Gene Mutations Across Multiple Cancer Types. *JCO Precision Oncology*, *2*, PO.17.00286.
128. Heitzer, E., Auer, M., Gasch, C., Pichler, M., Ulz, P., Hoffmann, E. M., Lax, S., Waldispuehl-Geigl, J., Mauermann, O., Lackner, C., Hofler, G., Eisner, F., Sill, H., Samonigg, H., Pantel, K., Riethdorf, S., Bauernhofer, T., Geigl, J. B., & Speicher, M. R. (2013). Complex Tumor Genomes Inferred from Single Circulating Tumor Cells by Array-CGH and Next-Generation Sequencing. *Cancer Research*, *73*(10), 2965–2975.
129. Hellmann, M. D., Paz-Ares, L., Bernabe Caro, R., Zurawski, B., Kim, S.-W., Carcereny Costa, E., Park, K., Alexandru, A., Lupinacci, L., de la Mora Jimenez, E., Sakai, H., Albert, I.,

Vergnenegre, A., Peters, S., Syrigos, K., Barlesi, F., Reck, M., Borghaei, H., Brahmer, J. R., … Ramalingam, S. S. (2019). Nivolumab plus Ipilimumab in Advanced Non–Small-Cell Lung Cancer. *New England Journal of Medicine*, *381*(21), 2020–2031.

130. Hewish, M., Lord, C. J., Martin, S. A., Cunningham, D., & Ashworth, A. (2010). Mismatch repair deficient colorectal cancer in the era of personalized treatment. *Nature Reviews Clinical Oncology*, *7*(4), 197–208.
131. Hidalgo, M., Amant, F., Biankin, A. V., Budinská, E., Byrne, A. T., Caldas, C., Clarke, R. B., de Jong, S., Jonkers, J., Mælandsmo, G. M., Roman-Roman, S., Seoane, J., Trusolino, L., & Villanueva, A. (2014). Patient Derived Xenograft Models: An Emerging Platform for Translational Cancer Research. *Cancer Discovery*, *4*(9), 998–1013.
132. Hiratsuka, S., Watanabe, A., Sakurai, Y., Akashi-Takamura, S., Ishibashi, S., Miyake, K., Shibuya, M., Akira, S., Aburatani, H., & Maru, Y. (2008). The S100A8–serum amyloid A3–TLR4 paracrine cascade establishes a pre-metastatic phase. *Nature Cell Biology*, *10*(11), 1349–1355.
133. Hoadley, K. A., Yau, C., Hinoue, T., Wolf, D. M., Lazar, A. J., Drill, E., Shen, R., Taylor, A. M., Cherniack, A. D., Thorsson, V., Akbani, R., Bowlby, R., Wong, C. K., Wiznerowicz, M., Sanchez-Vega, F., Robertson, A. G., Schneider, B. G., Lawrence, M. S., Noushmehr, H., … Mariamidze, A. (2018). Cell-of-Origin Patterns Dominate the Molecular Classification of 10,000 Tumors from 33 Types of Cancer. *Cell*, *173*(2), 291-304.e6.
134. Hodara, E., Morrison, G., Cunha, A., Zainfeld, D., Xu, T., Xu, Y., Dempsey, P. W., Pagano, P. C., Bischoff, F., Khurana, A., Koo, S., Ting, M., Cotter, P. D., Moore, M. W., Gunn, S., Usher, J., Rabizadeh, S., Danenberg, P., Danenberg, K., … Goldkorn, A. (2019). Multiparametric liquid biopsy analysis in metastatic prostate cancer. *JCI Insight*, *4*(5), Article 5.
135. Hodgkinson, C. L., Morrow, C. J., Li, Y., Metcalf, R. L., Rothwell, D. G., Trapani, F., Polanski, R., Burt, D. J., Simpson, K. L., Morris, K., Pepper, S. D., Nonaka, D., Greystoke, A., Kelly, P., Bola, B., Krebs, M. G., Antonello, J., Ayub, M., Faulkner, S., … Dive, C. (2014). Tumorigenicity and genetic profiling of circulating tumor cells in small-cell lung cancer. *Nature Medicine*, *20*(8), 897–903.
136. Hong, X., Roh, W., Sullivan, R. J., Wong, K. H. K., Wittner, B. S., Guo, H., Dubash, T. D., Sade-Feldman, M., Wesley, B., Horwitz, E., Boland, G. M., Marvin, D. L., Bonesteel, T., Lu, C., Aguet, F., Burr, R., Freeman, S. S., Parida, L., Calhoun, K., … Haber, D. A. (2021). The Lipogenic Regulator SREBP2 Induces Transferrin in Circulating Melanoma Cells and Suppresses Ferroptosis. *Cancer Discovery*, *11*(3), 678–695.
137. Horn, L., Wang, Z., Wu, G., Poddubskaya, E., Mok, T., Reck, M., Wakelee, H., Chiappori, A. A., Lee, D. H., Breder, V., Orlov, S., Cicin, I., Cheng, Y., Liu, Y., Fan, Y., Whisenant, J. G., Zhou, Y., Oertel, V., Harrow, K., … Wu, Y.-L. (2021). Ensartinib vs Crizotinib for Patients With Anaplastic Lymphoma Kinase−Positive Non–Small Cell Lung Cancer: A Randomized Clinical Trial. *JAMA Oncology*, *7*(11), 1617–1625.
138. Hoshino, A., Costa-Silva, B., Shen, T.-L., Rodrigues, G., Hashimoto, A., Mark, M. T., Molina, H., Kohsaka, S., Di Giannatale, A., Ceder, S., Singh, S., Williams, C., Soplop, N., Uryu, K.,

Pharmer, L., King, T., Bojmar, L., Davies, A. E., Ararso, Y., … Lyden, D. (2015). Tumour exosome integrins determine organotropic metastasis. *Nature*, *527*(7578), 329–335.

139. Hou, J.-M., Krebs, M. G., Lancashire, L., Sloane, R., Backen, A., Swain, R. K., Priest, L. J. C., Greystoke, A., Zhou, C., Morris, K., Ward, T., Blackhall, F. H., & Dive, C. (2012). Clinical Significance and Molecular Characteristics of Circulating Tumor Cells and Circulating Tumor Microemboli in Patients With Small-Cell Lung Cancer. *Journal of Clinical Oncology*, *30*(5), 525–532.
140. Hou, J.-M., Krebs, M., Ward, T., Sloane, R., Priest, L., Hughes, A., Clack, G., Ranson, M., Blackhall, F., & Dive, C. (2011). Circulating Tumor Cells as a Window on Metastasis Biology in Lung Cancer. *The American Journal of Pathology*, *178*(3), 989–996.
141. Huntly, B. J. P., & Gilliland, D. G. (2005). Leukaemia stem cells and the evolution of cancer-stem-cell research. *Nature Reviews Cancer*, *5*(4), 311–321.
142. Hurtado, P., Martínez-Pena, I., & Piñeiro, R. (2020). Dangerous Liaisons: Circulating Tumor Cells (CTCs) and Cancer-Associated Fibroblasts (CAFs). *Cancers*, *12*(10), 2861.
143. Hvichia, G. e., Parveen, Z., Wagner, C., Janning, M., Quidde, J., Stein, A., Müller, V., Loges, S., Neves, R. p. l., Stoecklein, N. h., Wikman, H., Riethdorf, S., Pantel, K., & Gorges, T. m. (2016). A novel microfluidic platform for size and deformability based separation and the subsequent molecular characterization of viable circulating tumor cells. *International Journal of Cancer*, *138*(12), 2894–2904.
144. Ignatiadis, M., Sledge, G. W., & Jeffrey, S. S. (2021). Liquid biopsy enters the clinic—Implementation issues and future challenges. *Nature Reviews Clinical Oncology*, *18*(5), 297–312.
145. Ilie, M., Long, E., Butori, C., Hofman, V., Coelle, C., Mauro, V., Zahaf, K., Marquette, C. H., Mouroux, J., Paterlini-Bréchot, P., & Hofman, P. (2012). ALK-gene rearrangement: A comparative analysis on circulating tumour cells and tumour tissue from patients with lung adenocarcinoma. *Annals of Oncology*, *23*(11), 2907–2913.
146. Illuzzi, G., Staniszewska, A. D., Gill, S. J., Pike, A., McWilliams, L., Critchlow, S. E., Cronin, A., Fawell, S., Hawthorne, G., Jamal, K., Johannes, J., Leonard, E., Macdonald, R., Maglennon, G., Nikkilä, J., O'Connor, M. J., Smith, A., Southgate, H., Wilson, J., … Leo, E. (2022). Preclinical characterization of AZD5305, a next generation, highly selective PARP1 inhibitor and trapper. *Clinical Cancer Research*, CCR-22-0301.
147. Izumi, H., Matsumoto, S., Liu, J., Tanaka, K., Mori, S., Hayashi, K., Kumagai, S., Shibata, Y., Hayashida, T., Watanabe, K., Fukuhara, T., Ikeda, T., Yoh, K., Kato, T., Nishino, K., Nakamura, A., Nakachi, I., Kuyama, S., Furuya, N., … Goto, K. (2021). The CLIP1–LTK fusion is an oncogenic driver in non-small-cell lung cancer. *Nature*, *600*(7888), 319–323.
148. Jamal-Hanjani, M., Wilson, G. A., McGranahan, N., Birkbak, N. J., Watkins, T. B. K., Veeriah, S., Shafi, S., Johnson, D. H., Mitter, R., Rosenthal, R., Salm, M., Horswell, S., Escudero, M., Matthews, N., Rowan, A., Chambers, T., Moore, D. A., Turajlic, S., Xu, H., … TRACERx Consortium. (2017). Tracking the Evolution of Non-Small-Cell Lung Cancer. *The New England Journal of Medicine*, *376*(22), 2109–2121.

149. Jänne, P. A., Riely, G. J., Gadgeel, S. M., Heist, R. S., Ou, S.-H. I., Pacheco, J. M., Johnson, M. L., Sabari, J. K., Leventakos, K., Yau, E., Bazhenova, L., Negrao, M. V., Pennell, N. A., Zhang, J., Anderes, K., Der-Torossian, H., Kheoh, T., Velastegui, K., Yan, X., … Spira, A. I. (2022). Adagrasib in Non–Small-Cell Lung Cancer Harboring a KRASG12C Mutation. *New England Journal of Medicine*, *387*(2), 120–131.

150. Jiang, R., Lu, Y.-T., Ho, H., Li, B., Chen, J.-F., Lin, M., Li, F., Wu, K., Wu, H., Lichterman, J., Wan, H., Lu, C.-L., OuYang, W., Ni, M., Wang, L., Li, G., Lee, T., Zhang, X., Yang, J., … Posadas, E. M. (2015). A comparison of isolated circulating tumor cells and tissue biopsies using whole-genome sequencing in prostate cancer. *Oncotarget*, *6*(42), 44781–44793.

151. Jordan, C. T., Guzman, M. L., & Noble, M. (2006). Cancer Stem Cells. *New England Journal of Medicine*, *355*(12), 1253–1261.

152. Kalemkerian, G. P., Narula, N., Kennedy, E. B., Biermann, W. A., Donington, J., Leighl, N. B., Lew, M., Pantelas, J., Ramalingam, S. S., Reck, M., Saqi, A., Simoff, M., Singh, N., & Sundaram, B. (2018). Molecular Testing Guideline for the Selection of Patients With Lung Cancer for Treatment With Targeted Tyrosine Kinase Inhibitors: American Society of Clinical Oncology Endorsement of the College of American Pathologists/International Association for the Study of Lung Cancer/Association for Molecular Pathology Clinical Practice Guideline Update. *Journal of Clinical Oncology: Official Journal of the American Society of Clinical Oncology*, *36*(9), 911–919.

153. Kallergi, G., Papadaki, M. A., Politaki, E., Mavroudis, D., Georgoulias, V., & Agelaki, S. (2011). Epithelial to mesenchymal transition markers expressed in circulating tumour cells of early and metastatic breast cancer patients. *Breast Cancer Research*, *13*(3), Article 3.

154. Kalluri, R., & Weinberg, R. A. (2009). The basics of epithelial-mesenchymal transition. *The Journal of Clinical Investigation*, *119*(6), 1420–1428.

155. Kaplan, R. N., Riba, R. D., Zacharoulis, S., Bramley, A. H., Vincent, L., Costa, C., MacDonald, D. D., Jin, D. K., Shido, K., Kerns, S. A., Zhu, Z., Hicklin, D., Wu, Y., Port, J. L., Altorki, N., Port, E. R., Ruggero, D., Shmelkov, S. V., Jensen, K. K., … Lyden, D. (2005). VEGFR1-positive haematopoietic bone marrow progenitors initiate the pre-metastatic niche. *Nature*, *438*(7069), 820–827.

156. Kasimir-Bauer, S., Bittner, A.-K., König, L., Reiter, K., Keller, T., Kimmig, R., & Hoffmann, O. (2016). Does primary neoadjuvant systemic therapy eradicate minimal residual disease? Analysis of disseminated and circulating tumor cells before and after therapy. *Breast Cancer Research*, *18*(1), 1–15.

157. Knijnenburg, T. A., Wang, L., Zimmermann, M. T., Chambwe, N., Gao, G. F., Cherniack, A. D., Fan, H., Shen, H., Way, G. P., Greene, C. S., Liu, Y., Akbani, R., Feng, B., Donehower, L. A., Miller, C., Shen, Y., Karimi, M., Chen, H., Kim, P., … Wang, C. (2018). Genomic and Molecular Landscape of DNA Damage Repair Deficiency across The Cancer Genome Atlas. *Cell Reports*, *23*(1), 239-254.e6.

158. Kobayashi, A., Okuda, H., Xing, F., Pandey, P. R., Watabe, M., Hirota, S., Pai, S. K., Liu, W., Fukuda, K., Chambers, C., Wilber, A., & Watabe, K. (2011). Bone morphogenetic protein 7 in

dormancy and metastasis of prostate cancer stem-like cells in bone. *The Journal of Experimental Medicine*, *208*(13), 2641–2655.

159. Koboldt, D. C., Fulton, R. S., McLellan, M. D., Schmidt, H., Kalicki-Veizer, J., McMichael, J. F., Fulton, L. L., Dooling, D. J., Ding, L., Mardis, E. R., Wilson, R. K., Ally, A., Balasundaram, M., Butterfield, Y. S. N., Carlsen, R., Carter, C., Chu, A., Chuah, E., Chun, H.-J. E., … MD Anderson Cancer Center. (2012). Comprehensive molecular portraits of human breast tumours. *Nature*, *490*(7418), 61–70.
160. Koch, C., Kuske, A., Joosse, S. A., Yigit, G., Sflomos, G., Thaler, S., Smit, D. J., Werner, S., Borgmann, K., Gärtner, S., Mossahebi Mohammadi, P., Battista, L., Cayrefourcq, L., Altmüller, J., Salinas-Riester, G., Raithatha, K., Zibat, A., Goy, Y., Ott, L., … Pantel, K. (2020). Characterization of circulating breast cancer cells with tumorigenic and metastatic capacity. *EMBO Molecular Medicine*, *12*(9), e11908.
161. Krämer, A., Maier, B., & Bartek, J. (2011). Centrosome clustering and chromosomal (in)stability: A matter of life and death. *Molecular Oncology*, *5*(4), 324–335.
162. Krebs, M. G., Hou, J.-M., Sloane, R., Lancashire, L., Priest, L., Nonaka, D., Ward, T. H., Backen, A., Clack, G., Hughes, A., Ranson, M., Blackhall, F. H., & Dive, C. (2012). Analysis of Circulating Tumor Cells in Patients with Non-small Cell Lung Cancer Using Epithelial Marker-Dependent and -Independent Approaches. *Journal of Thoracic Oncology*, *7*(2), 306–315.
163. Krebs, M. G., Metcalf, R. L., Carter, L., Brady, G., Blackhall, F. H., & Dive, C. (2014). Molecular analysis of circulating tumour cells-biology and biomarkers. *Nature Reviews. Clinical Oncology*, *11*(3), 129–144.
164. Krebs, M. G., Sloane, R., Priest, L., Lancashire, L., Hou, J.-M., Greystoke, A., Ward, T. H., Ferraldeschi, R., Hughes, A., Clack, G., Ranson, M., Dive, C., & Blackhall, F. H. (2011). Evaluation and Prognostic Significance of Circulating Tumor Cells in Patients With Non–Small-Cell Lung Cancer. *Journal of Clinical Oncology*, *29*(12), 1556–1563.
165. Kreso, A., & Dick, J. E. (2014). Evolution of the Cancer Stem Cell Model. *Cell Stem Cell*, *14*(3), 275–291.
166. Krivtsov, A. V., Twomey, D., Feng, Z., Stubbs, M. C., Wang, Y., Faber, J., Levine, J. E., Wang, J., Hahn, W. C., Gilliland, D. G., Golub, T. R., & Armstrong, S. A. (2006). Transformation from committed progenitor to leukaemia stem cell initiated by MLL–AF9. *Nature*, *442*(7104), 818–822.
167. Kuhlmann, J. D., Wimberger, P., Bankfalvi, A., Keller, T., Schöler, S., Aktas, B., Buderath, P., Hauch, S., Otterbach, F., Kimmig, R., & Kasimir-Bauer, S. (2014). ERCC1-positive circulating tumor cells in the blood of ovarian cancer patients as a predictive biomarker for platinum resistance. *Clinical Chemistry*, *60*(10), 1282–1289.
168. Kwon, J., & Bakhoum, S. F. (2020). The cytosolic DNA-sensing cGAS-STING pathway in cancer. *Cancer Discovery*, *10*(1), 26–39.
169. Labelle, M., Begum, S., & Hynes, R. O. (2011). Direct Signaling Between Platelets and Cancer Cells Induces an Epithelial-Mesenchymal-Like Transition and Promotes Metastasis. *Cancer Cell*, *20*(5), 576–590.

170. Labelle, M., & Hynes, R. O. (2012). The Initial Hours of Metastasis: The Importance of Cooperative Host–Tumor Cell Interactions during Hematogenous Dissemination. *Cancer Discovery*, *2*(12), 1091–1099.

171. Lallo, A., Frese, K. K., Morrow, C. J., Sloane, R., Gulati, S., Schenk, M. W., Trapani, F., Simms, N., Galvin, M., Brown, S., Hodgkinson, C. L., Priest, L., Hughes, A., Lai, Z., Cadogan, E., Khandelwal, G., Simpson, K. L., Miller, C., Blackhall, F., … Dive, C. (2018). The Combination of the PARP Inhibitor Olaparib and the WEE1 Inhibitor AZD1775 as a New Therapeutic Option for Small Cell Lung Cancer. *Clinical Cancer Research*, *24*(20), 5153–5164.

172. Lallo, A., Gulati, S., Schenk, M. W., Khandelwal, G., Berglund, U. W., Pateras, I. S., Chester, C. P. E., Pham, T. M., Kalderen, C., Frese, K. K., Gorgoulis, V. G., Miller, C., Blackhall, F., Helleday, T., & Dive, C. (2019). Ex vivo culture of cells derived from circulating tumour cell xenograft to support small cell lung cancer research and experimental therapeutics. *British Journal of Pharmacology*, *176*(3), 436–450.

173. Lallo, A., Schenk, M. W., Frese, K. K., Blackhall, F., & Dive, C. (2017). Circulating tumor cells and CDX models as a tool for preclinical drug development. *Translational Lung Cancer Research*, *6*(4), 397–408.

174. Lambert, A. W., Pattabiraman, D. R., & Weinberg, R. A. (2017). Emerging Biological Principles of Metastasis. *Cell*, *168*(4), 670–691.

175. Lamouille, S., Subramanyam, D., Blelloch, R., & Derynck, R. (2013). Regulation of epithelial–mesenchymal and mesenchymal–epithelial transitions by microRNAs. *Current Opinion in Cell Biology*, *25*(2), 200–207.

176. Langer, C. J., Besse, B., Gualberto, A., Brambilla, E., & Soria, J.-C. (2010). The Evolving Role of Histology in the Management of Advanced Non–Small-Cell Lung Cancer. *Journal of Clinical Oncology*, *28*(36), 5311–5320.

177. Lecharpentier, A., Vielh, P., Perez-Moreno, P., Planchard, D., Soria, J. C., & Farace, F. (2011). Detection of circulating tumour cells with a hybrid (epithelial/mesenchymal) phenotype in patients with metastatic non-small cell lung cancer. *British Journal of Cancer*, *105*(9), 1338–1341.

178. Lee, J., Ledermann, J. A., & Kohn, E. C. (2014). PARP Inhibitors for BRCA1/2 mutation-associated and BRCA-like malignancies. *Annals of Oncology*, *25*(1), 32–40.

179. Lee, J.-K., Lee, J., Kim, S., Kim, S., Youk, J., Park, S., An, Y., Keam, B., Kim, D.-W., Heo, D. S., Kim, Y. T., Kim, J.-S., Kim, S. H., Lee, J. S., Lee, S.-H., Park, K., Ku, J.-L., Jeon, Y. K., Chung, D. H., … Ju, Y. S. (2017). Clonal History and Genetic Predictors of Transformation Into Small-Cell Carcinomas From Lung Adenocarcinomas. *Journal of Clinical Oncology*, *35*(26), 3065–3074.

180. Lee, S. M., Falzon, M., Blackhall, F., Spicer, J., Nicolson, M., Chaudhuri, A., Middleton, G., Ahmed, S., Hicks, J., Crosse, B., Napier, M., Singer, J. M., Ferry, D., Lewanski, C., Forster, M., Rolls, S.-A., Capitanio, A., Rudd, R., Iles, N., … Hackshaw, A. (2017). Randomized Prospective Biomarker Trial of ERCC1 for Comparing Platinum and Nonplatinum Therapy in Advanced Non–Small-Cell Lung Cancer: ERCC1 Trial (ET). *Journal of Clinical Oncology*, *35*(4), 402–411.

181. Leonetti, A., Sharma, S., Minari, R., Perego, P., Giovannetti, E., & Tiseo, M. (2019). Resistance mechanisms to osimertinib in EGFR-mutated non-small cell lung cancer. *British Journal of Cancer*, *121*(9), 725–737.

182. Leversha, M. A., Han, J., Asgari, Z., Danila, D. C., Lin, O., Gonzalez-Espinoza, R., Anand, A., Lilja, H., Heller, G., Fleisher, M., & Scher, H. I. (2009). Fluorescence in situ Hybridization Analysis of Circulating Tumor Cells in Metastatic Prostate Cancer. *Clinical Cancer Research*, *15*(6), 2091–2097.

183. Li, X., & Heyer, W.-D. (2008). Homologous recombination in DNA repair and DNA damage tolerance. *Cell Research*, *18*(1), 99–113.

184. Lindsay, C. R., Blackhall, F. H., Carmel, A., Fernandez-Gutierrez, F., Gazzaniga, P., Groen, H. J. M., Hiltermann, T. J. N., Krebs, M. G., Loges, S., López-López, R., Muinelo-Romay, L., Pantel, K., Priest, L., Riethdorf, S., Rossi, E., Terstappen, L., Wikman, H., Soria, J.-C., Farace, F., … Michiels, S. (2019). EPAC-lung: Pooled analysis of circulating tumour cells in advanced non-small cell lung cancer. *European Journal of Cancer*, *117*, 60–68.

185. Lindsay, C. R., Faugeroux, V., Michiels, S., Pailler, E., Facchinetti, F., Ou, D., Bluthgen, M. V., Pannet, C., Ngo-Camus, M., Bescher, G., Caramella, C., Billiot, F., Remon, J., Planchard, D., Soria, J.-C., Besse, B., & Farace, F. (2017). A prospective examination of circulating tumor cell profiles in non-small-cell lung cancer molecular subgroups. *Annals of Oncology*, *28*(7), 1523–1531.

186. Lindsay, C. R., Le Moulec, S., Billiot, F., Loriot, Y., Ngo-Camus, M., Vielh, P., Fizazi, K., Massard, C., & Farace, F. (2016). Vimentin and Ki67 expression in circulating tumour cells derived from castrate-resistant prostate cancer. *BMC Cancer*, *16*(1), 1–11.

187. Liu, H., Patel, M. R., Prescher, J. A., Patsialou, A., Qian, D., Lin, J., Wen, S., Chang, Y.-F., Bachmann, M. H., Shimono, Y., Dalerba, P., Adorno, M., Lobo, N., Bueno, J., Dirbas, F. M., Goswami, S., Somlo, G., Condeelis, J., Contag, C. H., … Clarke, M. F. (2010). Cancer stem cells from human breast tumors are involved in spontaneous metastases in orthotopic mouse models. *Proceedings of the National Academy of Sciences*, *107*(42), 18115–18120.

188. Liu, Y., & Cao, X. (2016). Characteristics and Significance of the Pre-metastatic Niche. *Cancer Cell*, *30*(5), 668–681.

189. Lohr, J. G., Adalsteinsson, V. A., Cibulskis, K., Choudhury, A. D., Rosenberg, M., Cruz-Gordillo, P., Francis, J. M., Zhang, C.-Z., Shalek, A. K., Satija, R., Trombetta, J. J., Lu, D., Tallapragada, N., Tahirova, N., Kim, S., Blumenstiel, B., Sougnez, C., Lowe, A., Wong, B., … Love, J. C. (2014). Whole-exome sequencing of circulating tumor cells provides a window into metastatic prostate cancer. *Nature Biotechnology*, *32*(5), 479–484.

190. Lok, B. H., Gardner, E. E., Schneeberger, V. E., Ni, A., Desmeules, P., Rekhtman, N., de Stanchina, E., Teicher, B. A., Riaz, N., Powell, S. N., Poirier, J. T., & Rudin, C. M. (2017). PARP Inhibitor Activity Correlates with SLFN11 Expression and Demonstrates Synergy with Temozolomide in Small Cell Lung Cancer. *Clinical Cancer Research*, *23*(2), 523–535.

191. Lord, C. J., & Ashworth, A. (2012). The DNA damage response and cancer therapy. *Nature*, *481*(7381), 287–294.

192. Lord, C. J., & Ashworth, A. (2016). BRCAness revisited. *Nature Reviews Cancer*, *16*(2), 110–120.

193. Luzzi, K. J., MacDonald, I. C., Schmidt, E. E., Kerkvliet, N., Morris, V. L., Chambers, A. F., & Groom, A. C. (1998). Multistep Nature of Metastatic Inefficiency. *The American Journal of Pathology*, *153*(3), 865–873.

194. Lynch, T. J., Bell, D. W., Sordella, R., Gurubhagavatula, S., Okimoto, R. A., Brannigan, B. W., Harris, P. L., Haserlat, S. M., Supko, J. G., Haluska, F. G., Louis, D. N., Christiani, D. C., Settleman, J., & Haber, D. A. (2004). Activating Mutations in the Epidermal Growth Factor Receptor Underlying Responsiveness of Non–Small-Cell Lung Cancer to Gefitinib. *New England Journal of Medicine*, *350*(21), 2129–2139.

195. Mackenzie, K. J., Carroll, P., Martin, C.-A., Murina, O., Fluteau, A., Simpson, D. J., Olova, N., Sutcliffe, H., Rainger, J. K., Leitch, A., Osborn, R. T., Wheeler, A. P., Nowotny, M., Gilbert, N., Chandra, T., Reijns, M. A. M., & Jackson, A. P. (2017). CGAS surveillance of micronuclei links genome instability to innate immunity. *Nature*, *548*(7668), 461–465.

196. Maheswaran, S., Sequist, L. V., Nagrath, S., Ulkus, L., Brannigan, B., Collura, C. V., Inserra, E., Diederichs, S., Iafrate, A. J., Bell, D. W., Digumarthy, S., Muzikansky, A., Irimia, D., Settleman, J., Tompkins, R. G., Lynch, T. J., Toner, M., & Haber, D. A. (2008). Detection of Mutations in EGFR in Circulating Lung-Cancer Cells. *New England Journal of Medicine*, *359*(4), 366–377.

197. Malanchi, I., Santamaria-Martínez, A., Susanto, E., Peng, H., Lehr, H.-A., Delaloye, J.-F., & Huelsken, J. (2012). Interactions between cancer stem cells and their niche govern metastatic colonization. *Nature*, *481*(7379), 85–89.

198. Malihi, P. D., Graf, R. P., Rodriguez, A., Ramesh, N., Lee, J., Sutton, R., Jiles, R., Ruiz Velasco, C., Sei, E., Kolatkar, A., Logothetis, C., Navin, N. E., Corn, P., Aparicio, A. M., Dittamore, R., Hicks, J., Kuhn, P., & Zurita, A. J. (2020). Single-Cell Circulating Tumor Cell Analysis Reveals Genomic Instability as a Distinctive Feature of Aggressive Prostate Cancer. *Clinical Cancer Research*, *26*(15), 4143–4153.

199. Mani, S. A., Guo, W., Liao, M.-J., Eaton, E. Ng., Ayyanan, A., Zhou, A. Y., Brooks, M., Reinhard, F., Zhang, C. C., Shipitsin, M., Campbell, L. L., Polyak, K., Brisken, C., Yang, J., & Weinberg, R. A. (2008). The Epithelial-Mesenchymal Transition Generates Cells with Properties of Stem Cells. *Cell*, *133*(4), 704–715.

200. Maréchal, A., & Zou, L. (2013). DNA Damage Sensing by the ATM and ATR Kinases. *Cold Spring Harbor Perspectives in Biology*, *5*(9), a012716.

201. Martin, O. A., Anderson, R. L., Russell, P. A., Ashley Cox, R., Ivashkevich, A., Swierczak, A., Doherty, J. P., Jacobs, D. H. M., Smith, J., Siva, S., Daly, P. E., Ball, D. L., Martin, R. F., & MacManus, M. P. (2014). Mobilization of Viable Tumor Cells Into the Circulation During Radiation Therapy. *International Journal of Radiation Oncology*Biology*Physics*, *88*(2), 395–403.

202. Massagué, J., & Ganesh, K. (2021). Metastasis Initiating Cells and Ecosystems. *Cancer Discovery*, *11*(4), 971–994.

203. Massagué, J., & Obenauf, A. C. (2016). Metastatic colonization by circulating tumour cells. *Nature*, *529*(7586), 298–306.

204. Massard, C., Oulhen, M., Le Moulec, S., Auger, N., Foulon, S., Abou-Lovergne, A., Billiot, F., Valent, A., Marty, V., Loriot, Y., Fizazi, K., Vielh, P., & Farace, F. (2016). Phenotypic and genetic heterogeneity of tumor tissue and circulating tumor cells in patients with metastatic castrationresistant prostate cancer: A report from the PETRUS prospective study. *Oncotarget*, *7*(34), 55069–55082.

205. Mayer, J. A., Pham, T., Wong, K. L., Scoggin, J., Sales, E. V., Clarin, T., Pircher, T. J., Mikolajczyk, S. D., Cotter, P. D., & Bischoff, F. Z. (2011). FISH-based determination of HER2 status in circulating tumor cells isolated with the microfluidic CEE™ platform. *Cancer Genetics*, *204*(11), 589–595.

206. McCabe, N., Turner, N. C., Lord, C. J., Kluzek, K., Białkowska, A., Swift, S., Giavara, S., O'Connor, M. J., Tutt, A. N., Zdzienicka, M. Z., Smith, G. C. M., & Ashworth, A. (2006). Deficiency in the Repair of DNA Damage by Homologous Recombination and Sensitivity to Poly(ADP-Ribose) Polymerase Inhibition. *Cancer Research*, *66*(16), 8109–8115.

207. McGranahan, N., Burrell, R. A., Endesfelder, D., Novelli, M. R., & Swanton, C. (2012). Cancer chromosomal instability: Therapeutic and diagnostic challenges. *EMBO Reports*, *13*(6), 528–538.

208. McGranahan, N., & Swanton, C. (2017). Clonal Heterogeneity and Tumor Evolution: Past, Present, and the Future. *Cell*, *168*(4), 613–628.

209. Meng, S., Tripathy, D., Frenkel, E. P., Shete, S., Naftalis, E. Z., Huth, J. F., Beitsch, P. D., Leitch, M., Hoover, S., Euhus, D., Haley, B., Morrison, L., Fleming, T. P., Herlyn, D., Terstappen, L. W. M. M., Fehm, T., Tucker, T. F., Lane, N., Wang, J., & Uhr, J. W. (2004). Circulating Tumor Cells in Patients with Breast Cancer Dormancy. *Clinical Cancer Research*, *10*(24), 8152–8162.

210. Michels, J., Vitale, I., Saparbaev, M., Castedo, M., & Kroemer, G. (2014). Predictive biomarkers for cancer therapy with PARP inhibitors. *Oncogene*, *33*(30), 3894–3907.

211. Miller, R. E., Leary, A., Scott, C. L., Serra, V., Lord, C. J., Bowtell, D., Chang, D. K., Garsed, D. W., Jonkers, J., Ledermann, J. A., Nik-Zainal, S., Ray-Coquard, I., Shah, S. P., Matias-Guiu, X., Swisher, E. M., & Yates, L. R. (2020). ESMO recommendations on predictive biomarker testing for homologous recombination deficiency and PARP inhibitor benefit in ovarian cancer. *Annals of Oncology*, *31*(12), 1606–1622.

212. Miyamoto, D. T., Zheng, Y., Wittner, B. S., Lee, R. J., Zhu, H., Broderick, K. T., Desai, R., Fox, D. B., Brannigan, B. W., Trautwein, J., Arora, K. S., Desai, N., Dahl, D. M., Sequist, L. V., Smith, M. R., Kapur, R., Wu, C.-L., Shioda, T., Ramaswamy, S., … Haber, D. A. (2015). RNA-Seq of single prostate CTCs implicates noncanonical Wnt signaling in antiandrogen resistance. *Science*, *349*(6254), 1351–1356.

213. Mok, T. S., Wu, Y.-L., Ahn, M.-J., Garassino, M. C., Kim, H. R., Ramalingam, S. S., Shepherd, F. A., He, Y., Akamatsu, H., Theelen, W. S. M. E., Lee, C. K., Sebastian, M., Templeton, A., Mann, H., Marotti, M., Ghiorghiu, S., & Papadimitrakopoulou, V. A. (2017). Osimertinib or Platinum–Pemetrexed in *EGFR* T790M–Positive Lung Cancer. *New England Journal of Medicine*, *376*(7), 629–640.

214. Mok, T. S., Wu, Y.-L., Thongprasert, S., Yang, C.-H., Chu, D.-T., Saijo, N., Sunpaweravong, P., Han, B., Margono, B., Ichinose, Y., Nishiwaki, Y., Ohe, Y., Yang, J.-J., Chewaskulyong, B., Jiang, H., Duffield, E. L., Watkins, C. L., Armour, A. A., & Fukuoka, M. (2009). Gefitinib or Carboplatin–Paclitaxel in Pulmonary Adenocarcinoma. *New England Journal of Medicine*, *361*(10), 947–957.

215. Morel, A.-P., Hinkal, G. W., Thomas, C., Fauvet, F., Courtois-Cox, S., Wierinckx, A., Devouassoux-Shisheboran, M., Treilleux, I., Tissier, A., Gras, B., Pourchet, J., Puisieux, I., Browne, G. J., Spicer, D. B., Lachuer, J., Ansieau, S., & Puisieux, A. (2012). EMT Inducers Catalyze Malignant Transformation of Mammary Epithelial Cells and Drive Tumorigenesis towards Claudin-Low Tumors in Transgenic Mice. *PLOS Genetics*, *8*(5), e1002723.

216. Morel, A.-P., Lièvre, M., Thomas, C., Hinkal, G., Ansieau, S., & Puisieux, A. (2008). Generation of Breast Cancer Stem Cells through Epithelial-Mesenchymal Transition. *PLoS ONE*, *3*(8), e2888.

217. Morrow, C. J., Trapani, F., Metcalf, R. L., Bertolini, G., Hodgkinson, C. L., Khandelwal, G., Kelly, P., Galvin, M., Carter, L., Simpson, K. L., Williamson, S., Wirth, C., Simms, N., Frankliln, L., Frese, K. K., Rothwell, D. G., Nonaka, D., Miller, C. J., Brady, G., … Dive, C. (2016). Tumourigenic non-small-cell lung cancer mesenchymal circulating tumour cells: A clinical case study. *Annals of Oncology*, *27*(6), 1155–1160.

218. Mu, Y., Lou, J., Srivastava, M., Zhao, B., Feng, X., Liu, T., Chen, J., & Huang, J. (2016). SLFN11 inhibits checkpoint maintenance and homologous recombination repair. *EMBO Reports*, *17*(1), 94–109.

219. Munzone, E., Nolé, F., Goldhirsch, A., Botteri, E., Esposito, A., Zorzino, L., Curigliano, G., Minchella, I., Adamoli, L., Cassatella, M. C., Casadio, C., & Sandri, M. T. (2010). Changes of HER2 status in circulating tumor cells compared with the primary tumor during treatment for advanced breast cancer. *Clinical Breast Cancer*, *10*(5), 392–397.

220. Murai, J., Feng, Y., Yu, G. K., Ru, Y., Tang, S.-W., Shen, Y., & Pommier, Y. (2016). Resistance to PARP inhibitors by SLFN11 inactivation can be overcome by ATR inhibition. *Oncotarget*, *7*(47), 76534–76550.

221. Murai, J., Huang, S. N., Das, B. B., Renaud, A., Zhang, Y., Doroshow, J. H., Ji, J., Takeda, S., & Pommier, Y. (2012). Differential trapping of PARP1 and PARP2 by clinical PARP inhibitors. *Cancer Research*, *72*(21), 5588–5599.

222. Murai, J., Tang, S.-W., Leo, E., Baechler, S. A., Redon, C. E., Zhang, H., Al Abo, M., Rajapakse, V. N., Nakamura, E., Jenkins, L. M. M., Aladjem, M. I., & Pommier, Y. (2018). SLFN11 Blocks Stressed Replication Forks Independently of ATR. *Molecular Cell*, *69*(3), 371-384.e6.

223. Murai, J., Thomas, A., Miettinen, M., & Pommier, Y. (2019). Schlafen 11 (SLFN11), a restriction factor for replicative stress induced by DNA-targeting anti-cancer therapies. *Pharmacology & Therapeutics*, *201*, 94–102.

224. Muzny, D. M., Bainbridge, M. N., Chang, K., Dinh, H. H., Drummond, J. A., Fowler, G., Kovar, C. L., Lewis, L. R., Morgan, M. B., Newsham, I. F., Reid, J. G., Santibanez, J., Shinbrot, E., Trevino, L. R., Wu, Y.-Q., Wang, M., Gunaratne, P., Donehower, L. A., Creighton, C. J., …

Tissue source sites and disease working group. (2012). Comprehensive molecular characterization of human colon and rectal cancer. *Nature*, *487*(7407), 330–337.

225. Nagrath, S., Sequist, L. V., Maheswaran, S., Bell, D. W., Irimia, D., Ulkus, L., Smith, M. R., Kwak, E. L., Digumarthy, S., Muzikansky, A., Ryan, P., Balis, U. J., Tompkins, R. G., Haber, D. A., & Toner, M. (2007). Isolation of rare circulating tumour cells in cancer patients by microchip technology. *Nature*, *450*(7173), 1235–1239.
226. Neumann, M. H. D., Schneck, H., Decker, Y., Schömer, S., Franken, A., Endris, V., Pfarr, N., Weichert, W., Niederacher, D., Fehm, T., & Neubauer, H. (2017). Isolation and characterization of circulating tumor cells using a novel workflow combining the CellSearch® system and the CellCelector™. *Biotechnology Progress*, *33*(1), 125–132.
227. Ni, X., Zhuo, M., Su, Z., Duan, J., Gao, Y., Wang, Z., Zong, C., Bai, H., Chapman, A. R., Zhao, J., Xu, L., An, T., Ma, Q., Wang, Y., Wu, M., Sun, Y., Wang, S., Li, Z., Yang, X., … Wang, J. (2013). Reproducible copy number variation patterns among single circulating tumor cells of lung cancer patients. *Proceedings of the National Academy of Sciences of the United States of America*, *110*(52), 21083–21088.
228. Nieto, M. A., Huang, R. Y.-J., Jackson, R. A., & Thiery, J. P. (2016). EMT: 2016. *Cell*, *166*(1), 21–45.
229. Nik-Zainal, S., Alexandrov, L. B., Wedge, D. C., Van Loo, P., Greenman, C. D., Raine, K., Jones, D., Hinton, J., Marshall, J., Stebbings, L. A., Menzies, A., Martin, S., Leung, K., Chen, L., Leroy, C., Ramakrishna, M., Rance, R., Lau, K. W., Mudie, L. J., … Stratton, M. R. (2012). Mutational Processes Molding the Genomes of 21 Breast Cancers. *Cell*, *149*(5–10), 979–993.
230. Nogales, V., Reinhold, W. C., Varma, S., Martinez-Cardus, A., Moutinho, C., Moran, S., Heyn, H., Sebio, A., Barnadas, A., Pommier, Y., & Esteller, M. (2015). Epigenetic inactivation of the putative DNA/RNA helicase SLFN11 in human cancer confers resistance to platinum drugs. *Oncotarget*, *7*(3), 3084–3097.
231. Noordermeer, S. M., Adam, S., Setiaputra, D., Barazas, M., Pettitt, S. J., Ling, A. K., Olivieri, M., Álvarez-Quilón, A., Moatti, N., Zimmermann, M., Annunziato, S., Krastev, D. B., Song, F., Brandsma, I., Frankum, J., Brough, R., Sherker, A., Landry, S., Szilard, R. K., … Durocher, D. (2018). The shieldin complex mediates 53BP1-dependent DNA repair. *Nature*, *560*(7716), 117–121.
232. Novello, S., Barlesi, F., Califano, R., Cufer, T., Ekman, S., Levra, M. G., Kerr, K., Popat, S., Reck, M., Senan, S., Simo, G. V., Vansteenkiste, J., & Peters, S. (2016). Metastatic non-small-cell lung cancer: ESMO Clinical Practice Guidelines for diagnosis, treatment and follow-up. *Annals of Oncology*, *27*, v1–v27.
233. O'Connor, M. J. (2015). Targeting the DNA Damage Response in Cancer. *Molecular Cell*, *60*(4), 547–560.
234. Ohashi, S., Natsuizaka, M., Wong, G. S., Michaylira, C. Z., Grugan, K. D., Stairs, D. B., Kalabis, J., Vega, M. E., Kalman, R. A., Nakagawa, M., Klein-Szanto, A. J., Herlyn, M., Diehl, J. A., Rustgi, A. K., & Nakagawa, H. (2010). Epidermal Growth Factor Receptor and Mutant p53 Expand an Esophageal Cellular Subpopulation Capable of Epithelial-to-Mesenchymal Transition through ZEB Transcription Factors. *Cancer Research*, *70*(10), 4174–4184.

235. Öhlund, D., Elyada, E., & Tuveson, D. (2014). Fibroblast heterogeneity in the cancer wound. *The Journal of Experimental Medicine*, *211*(8), 1503–1523.

236. Olaussen, K. A., Dunant, A., Fouret, P., Brambilla, E., André, F., Haddad, V., Taranchon, E., Filipits, M., Pirker, R., Popper, H. H., Stahel, R., Sabatier, L., Pignon, J.-P., Tursz, T., Le Chevalier, T., & Soria, J.-C. (2006). DNA Repair by ERCC1 in Non–Small-Cell Lung Cancer and Cisplatin-Based Adjuvant Chemotherapy. *New England Journal of Medicine*, *355*(10), 983–991.

237. Olmos, D., Arkenau, H.-T., Ang, J. E., Ledaki, I., Attard, G., Carden, C. P., Reid, A. H. M., A'Hern, R., Fong, P. C., Oomen, N. B., Molife, R., Dearnaley, D., Parker, C., Terstappen, L. W. M. M., & de Bono, J. S. (2009). Circulating tumour cell (CTC) counts as intermediate end points in castration-resistant prostate cancer (CRPC): A single-centre experience. *Annals of Oncology*, *20*(1), 27–33.

238. Oskarsson, T., Acharyya, S., Zhang, X. H.-F., Vanharanta, S., Tavazoie, S. F., Morris, P. G., Downey, R. J., Manova-Todorova, K., Brogi, E., & Massagué, J. (2011). Breast cancer cells produce tenascin C as a metastatic niche component to colonize the lungs. *Nature Medicine*, *17*(7), 867–874.

239. Oskarsson, T., Batlle, E., & Massagué, J. (2014). Metastatic Stem Cells: Sources, Niches, and Vital Pathways. *Cell Stem Cell*, *14*(3), 306–321.

240. Oulhen, M., Pawlikowska, P., Tayoun, T., Garonzi, M., Buson, G., Forcato, C., Manaresi, N., Aberlenc, A., Mezquita, L., Lecluse, Y., Lavaud, P., Naltet, C., Planchard, D., Besse, B., & Farace, F. (2021). Circulating tumor cell copy-number heterogeneity in ALK-rearranged non-small-cell lung cancer resistant to ALK inhibitors. *Npj Precision Oncology*, *5*(1), 1–11.

241. Owonikoko, T. K., Redman, M. W., Byers, L. A., Hirsch, F. R., Mack, P. C., Schwartz, L. H., Bradley, J. D., Stinchcombe, T., Leighl, N. B., Al Baghdadi, T., Lara, P., Miao, J., Kelly, K., Ramalingam, S. S., Herbst, R. S., Papadimitrakopoulou, V., & Gandara, D. R. (2019). A phase II study of talazoparib (BMN 673) in patients with homologous recombination repair deficiency (HRRD) positive stage IV squamous cell lung cancer (Lung-MAP Sub-Study, S1400G). *Journal of Clinical Oncology*, *37*(15_suppl), 9022–9022.

242. Paget, S. (1889). THE DISTRIBUTION OF SECONDARY GROWTHS IN CANCER OF THE BREAST. *The Lancet*, *133*(3421), 571–573.

243. Pailler, E., Adam, J., Barthélémy, A., Oulhen, M., Auger, N., Valent, A., Borget, I., Planchard, D., Taylor, M., André, F., Soria, J. C., Vielh, P., Besse, B., & Farace, F. (2013). Detection of Circulating Tumor Cells Harboring a Unique *ALK* Rearrangement in *ALK* -Positive Non–Small-Cell Lung Cancer. *Journal of Clinical Oncology*, *31*(18), 2273–2281.

244. Pailler, E., Auger, N., Lindsay, C. R., Vielh, P., Islas-Morris-Hernandez, A., Borget, I., Ngo-Camus, M., Planchard, D., Soria, J.-C., Besse, B., & Farace, F. (2015). High level of chromosomal instability in circulating tumor cells of ROS1-rearranged non-small-cell lung cancer. *Annals of Oncology*, *26*(7), 1408–1415.

245. Pailler, E., Faugeroux, V., Oulhen, M., Mezquita, L., Laporte, M., Honoré, A., Lecluse, Y., Queffelec, P., NgoCamus, M., Nicotra, C., Remon, J., Lacroix, L., Planchard, D., Friboulet, L., Besse, B., & Farace, F. (2019). Acquired Resistance Mutations to ALK Inhibitors Identified by

Single Circulating Tumor Cell Sequencing in ALK-Rearranged Non–Small-Cell Lung Cancer. *Clinical Cancer Research*, *25*(22), 6671–6682.

246. Pailler, E., Oulhen, M., Billiot, F., Galland, A., Auger, N., Faugeroux, V., Laplace-Builhé, C., Besse, B., Loriot, Y., Ngo-Camus, M., Hemanda, M., Lindsay, C. R., Soria, J.-C., Vielh, P., & Farace, F. (2016). Method for semi-automated microscopy of filtration-enriched circulating tumor cells. *BMC Cancer*, *16*.

247. Pailler, E., Oulhen, M., Borget, I., Remon, J., Ross, K., Auger, N., Billiot, F., Ngo Camus, M., Commo, F., Lindsay, C. R., Planchard, D., Soria, J.-C., Besse, B., & Farace, F. (2017). Circulating Tumor Cells with Aberrant *ALK* Copy Number Predict Progression-Free Survival during Crizotinib Treatment in *ALK* -Rearranged Non–Small Cell Lung Cancer Patients. *Cancer Research*, *77*(9), 2222–2230.

248. Palumbo, J. S., Talmage, K. E., Massari, J. V., La Jeunesse, C. M., Flick, M. J., Kombrinck, K. W., Jirousková, M., & Degen, J. L. (2005). Platelets and fibrin(ogen) increase metastatic potential by impeding natural killer cell–mediated elimination of tumor cells. *Blood*, *105*(1), 178–185.

249. Pan, H., Gray, R., Braybrooke, J., Davies, C., Taylor, C., McGale, P., Peto, R., Pritchard, K. I., Bergh, J., Dowsett, M., & Hayes, D. F. (2017). 20-Year Risks of Breast-Cancer Recurrence after Stopping Endocrine Therapy at 5 Years. *New England Journal of Medicine*, *377*(19), 1836–1846.

250. Pantel, K., & Alix-Panabières, C. (2015). Functional Studies on Viable Circulating Tumor Cells. *Clinical Chemistry*, *62*.

251. Pantel, K., & Alix-Panabières, C. (2019). Liquid biopsy and minimal residual disease—Latest advances and implications for cure. *Nature Reviews Clinical Oncology*, *16*(7), 409–424.

252. Pantelidou, C., Sonzogni, O., De Oliveria Taveira, M., Mehta, A. K., Kothari, A., Wang, D., Visal, T., Li, M. K., Pinto, J., Castrillon, J. A., Cheney, E. M., Bouwman, P., Jonkers, J., Rottenberg, S., Guerriero, J. L., Wulf, G. M., & Shapiro, G. I. (2019). PARP Inhibitor Efficacy Depends on CD8+ T-cell Recruitment via Intratumoral STING Pathway Activation in BRCA-Deficient Models of Triple-Negative Breast Cancer. *Cancer Discovery*, *9*(6), 722–737.

253. Papadaki, M. A., Stoupis, G., Theodoropoulos, P. A., Mavroudis, D., Georgoulias, V., & Agelaki, S. (2019). Circulating Tumor Cells with Stemness and Epithelial-to-Mesenchymal Transition Features Are Chemoresistant and Predictive of Poor Outcome in Metastatic Breast Cancer. *Molecular Cancer Therapeutics*, *18*(2), 437–447.

254. Parkes, E. E., Walker, S. M., Taggart, L. E., McCabe, N., Knight, L. A., Wilkinson, R., McCloskey, K. D., Buckley, N. E., Savage, K. I., Salto-Tellez, M., McQuaid, S., Harte, M. T., Mullan, P. B., Harkin, D. P., & Kennedy, R. D. (2016). Activation of STING-Dependent Innate Immune Signaling By S-Phase-Specific DNA Damage in Breast Cancer. *JNCI Journal of the National Cancer Institute*, *109*(1), djw199.

255. Pascual, J., Attard, G., Bidard, F.-C., Curigliano, G., Mattos-Arruda, L. D., Diehn, M., Italiano, A., Lindberg, J., Merker, J. D., Montagut, C., Normanno, N., Pantel, K., Pentheroudakis, G., Popat, S., Reis-Filho, J. S., Tie, J., Seoane, J., Tarazona, N., Yoshino, T., &

Turner, N. C. (2022). ESMO recommendations on the use of circulating tumour DNA assays for patients with cancer: A report from the ESMO Precision Medicine Working Group. *Annals of Oncology*, *33*(8), 750–768.

256. Passiglia, F., Reale, M. L., Cetoretta, V., Parlagreco, E., Jacobs, F., Listì, A., Righi, L., Bironzo, P., Novello, S., & Scagliotti, G. V. (2021). Repositioning PARP inhibitors in the treatment of thoracic malignancies. *Cancer Treatment Reviews*, *99*, 102256.
257. Patterson-Fortin, J., Bose, A., Tsai, W.-C., Grochala, C. J., Nguyen, H., Zhou, J., Parmar, K., Lazaro, J.-B., Liu, J. F., McQueen, K., Shapiro, G. I., Kozono, D., & D'Andrea, A. D. (2022). Targeting DNA repair with combined inhibition of NHEJ and MMEJ induces synthetic lethality in TP53-mutant cancers. *Cancer Research*, CAN-22-1124.
258. Pawlikowska, P., Tayoun, T., Oulhen, M., Faugeroux, V., Rouffiac, V., Aberlenc, A., Pommier, A. L., Honore, A., Marty, V., Bawa, O., Lacroix, L., Scoazec, J. Y., Chauchereau, A., Laplace-Builhe, C., & Farace, F. (2020). Exploitation of the chick embryo chorioallantoic membrane (CAM) as a platform for anti-metastatic drug testing. *Scientific Reports*, *10*(1), 16876.
259. Paz-Ares, L., Ciuleanu, T.-E., Cobo, M., Schenker, M., Zurawski, B., Menezes, J., Richardet, E., Bennouna, J., Felip, E., Juan-Vidal, O., Alexandru, A., Sakai, H., Lingua, A., Salman, P., Souquet, P.-J., De Marchi, P., Martin, C., Pérol, M., Scherpereel, A., … Reck, M. (2021). First-line nivolumab plus ipilimumab combined with two cycles of chemotherapy in patients with non-small-cell lung cancer (CheckMate 9LA): An international, randomised, open-label, phase 3 trial. *The Lancet Oncology*, *22*(2), 198–211.
260. Paz-Ares, L. G., Ramalingam, S. S., Ciuleanu, T.-E., Lee, J.-S., Urban, L., Caro, R. B., Park, K., Sakai, H., Ohe, Y., Nishio, M., Audigier-Valette, C., Burgers, J. A., Pluzanski, A., Sangha, R., Gallardo, C., Takeda, M., Linardou, H., Lupinacci, L., Lee, K. H., … Reck, M. (2022). First-Line Nivolumab Plus Ipilimumab in Advanced NSCLC: 4-Year Outcomes From the Randomized, Open-Label, Phase 3 CheckMate 227 Part 1 Trial. *Journal of Thoracic Oncology*, *17*(2), 289–308.
261. Paz-Ares, L., Luft, A., Vicente, D., Tafreshi, A., Gümüş, M., Mazières, J., Hermes, B., Çay Şenler, F., Csőszi, T., Fülöp, A., Rodríguez-Cid, J., Wilson, J., Sugawara, S., Kato, T., Lee, K. H., Cheng, Y., Novello, S., Halmos, B., Li, X., … Kowalski, D. M. (2018). Pembrolizumab plus Chemotherapy for Squamous Non–Small-Cell Lung Cancer. *New England Journal of Medicine*, *379*(21), 2040–2051.
262. Paz-Ares, L., Vicente, D., Tafreshi, A., Robinson, A., Soto Parra, H., Mazières, J., Hermes, B., Cicin, I., Medgyasszay, B., Rodríguez-Cid, J., Okamoto, I., Lee, S., Ramlau, R., Vladimirov, V., Cheng, Y., Deng, X., Zhang, Y., Bas, T., Piperdi, B., & Halmos, B. (2020). A Randomized, Placebo-Controlled Trial of Pembrolizumab Plus Chemotherapy in Patients With Metastatic Squamous NSCLC: Protocol-Specified Final Analysis of KEYNOTE-407. *Journal of Thoracic Oncology*, *15*(10), 1657–1669.
263. Pearl, L. H., Schierz, A. C., Ward, S. E., Al-Lazikani, B., & Pearl, F. M. G. (2015). Therapeutic opportunities within the DNA damage response. *Nature Reviews Cancer*, *15*(3), 166–180.

264. Peinado, H., Zhang, H., Matei, I. R., Costa-Silva, B., Hoshino, A., Rodrigues, G., Psaila, B., Kaplan, R. N., Bromberg, J. F., Kang, Y., Bissell, M. J., Cox, T. R., Giaccia, A. J., Erler, J. T., Hiratsuka, S., Ghajar, C. M., & Lyden, D. (2017). Pre-metastatic niches: Organ-specific homes for metastases. *Nature Reviews Cancer*, *17*(5), 302–317.

265. Pereira-Veiga, T., Abreu, M., Robledo, D., Matias-Guiu, X., Santacana, M., Sánchez, L., Cueva, J., Palacios, P., Abdulkader, I., López-López, R., Muinelo-Romay, L., & Costa, C. (2019). CTCs-derived xenograft development in a triple negative breast cancer case. *International Journal of Cancer*, *144*(9), 2254–2265.

266. Peters, S., Camidge, D. R., Shaw, A. T., Gadgeel, S., Ahn, J. S., Kim, D.-W., Ou, S.-H. I., Pérol, M., Dziadziuszko, R., Rosell, R., Zeaiter, A., Mitry, E., Golding, S., Balas, B., Noe, J., Morcos, P. N., Mok, T., & ALEX Trial Investigators. (2017). Alectinib versus Crizotinib in Untreated ALK-Positive Non-Small-Cell Lung Cancer. *The New England Journal of Medicine*, *377*(9), 829–838.

267. Pierga, J.-Y., Bidard, F.-C., Mathiot, C., Brain, E., Delaloge, S., Giachetti, S., de Cremoux, P., Salmon, R., Vincent-Salomon, A., & Marty, M. (2008). Circulating Tumor Cell Detection Predicts Early Metastatic Relapse After Neoadjuvant Chemotherapy in Large Operable and Locally Advanced Breast Cancer in a Phase II Randomized Trial. *Clinical Cancer Research*, *14*(21), 7004–7010.

268. Pietanza, M. C., Waqar, S. N., Krug, L. M., Dowlati, A., Hann, C. L., Chiappori, A., Owonikoko, T. K., Woo, K. M., Cardnell, R. J., Fujimoto, J., Long, L., Diao, L., Wang, J., Bensman, Y., Hurtado, B., de Groot, P., Sulman, E. P., Wistuba, I. I., Chen, A., … Byers, L. A. (2018). Randomized, Double-Blind, Phase II Study of Temozolomide in Combination With Either Veliparib or Placebo in Patients With Relapsed-Sensitive or Refractory Small-Cell Lung Cancer. *Journal of Clinical Oncology*, *36*(23), 2386–2394.

269. Pilié, P. G., Gay, C. M., Byers, L. A., O'Connor, M. J., & Yap, T. A. (2019). PARP Inhibitors: Extending Benefit Beyond BRCA-Mutant Cancers. *Clinical Cancer Research*, *25*(13), 3759–3771.

270. Pilié, P. G., Tang, C., Mills, G. B., & Yap, T. A. (2019). State-of-the-art strategies for targeting the DNA damage response in cancer. *Nature Reviews Clinical Oncology*, *16*(2), 81–104.

271. Planchard, D., Besse, B., Groen, H. J. M., Hashemi, S. M. S., Mazieres, J., Kim, T. M., Quoix, E., Souquet, P.-J., Barlesi, F., Baik, C., Villaruz, L. C., Kelly, R. J., Zhang, S., Tan, M., Gasal, E., Santarpia, L., & Johnson, B. E. (2021). Phase 2 Study of Dabrafenib Plus Trametinib in Patients With BRAF V600E-Mutant Metastatic NSCLC: Updated 5-Year Survival Rates and Genomic Analysis. *Journal of Thoracic Oncology*, *17*(1), 103–115.

272. Planchard, D., Besse, B., Groen, H. J. M., Souquet, P.-J., Quoix, E., Baik, C. S., Barlesi, F., Kim, T. M., Mazieres, J., Novello, S., Rigas, J. R., Upalawanna, A., D'Amelio, A. M., Zhang, P., Mookerjee, B., & Johnson, B. E. (2016). An open-label phase 2 trial of dabrafenib plus trametinib in patients with previously treated BRAF V600E–mutant metastatic non-small cell lung cancer. *The Lancet. Oncology*, *17*(7), 984–993.

273. Planchard, D., Kim, T. M., Mazieres, J., Quoix, E., Riely, G., Barlesi, F., Souquet, P.-J., Smit, E. F., Groen, H. J. M., Kelly, R. J., Cho, B. C., Socinski, M. A., Pandite, L., Nase, C., Ma, B., D'Amelio, A., Mookerjee, B., Curtis, C. M., & Johnson, B. E. (2016). Dabrafenib in patients with BRAFV600E-positive advanced non-small-cell lung cancer: A single-arm, multicentre, open-label, phase 2 trial. *The Lancet Oncology*, *17*(5), 642–650.

274. Pommier, Y., O'Connor, M. J., & de Bono, J. (2016). Laying a trap to kill cancer cells: PARP inhibitors and their mechanisms of action. *Science Translational Medicine*, *8*(362), 362ps17-362ps17.

275. Postel-Vinay, S., Planchard, D., Antigny, M., Sarto, J. C., Gomez, M. D., Bataller, R. de las P., Gonzalez, M. A. S., Viteri, S., Pérez, J. P., Texier, M., Granados, A. L. O., Bueno, M. T. M., Camps, C. J., Lopez-Martin, A., Provencio, M., Gazzah, A., Soria, J.-C., Besse, B., Sureda, B. M., & Rosell, R. (2021). 100MO Olaparib maintenance vs placebo in platinum-sensitive non-small cell lung cancer: The phase II randomized PIPSeN trial. *Journal of Thoracic Oncology*, *16*(4), S752.

276. Postel-Vinay, S., Vanhecke, E., Olaussen, K. A., Lord, C. J., Ashworth, A., & Soria, J.-C. (2012). The potential of exploiting DNA-repair defects for optimizing lung cancer treatment. *Nature Reviews Clinical Oncology*, *9*(3), 144–155.

277. Psaila, B., & Lyden, D. (2009). The Metastatic Niche: Adapting the Foreign Soil. *Nature Reviews. Cancer*, *9*(4), 285–293.

278. Puisieux, A., Brabletz, T., & Caramel, J. (2014). Oncogenic roles of EMT-inducing transcription factors. *Nature Cell Biology*, *16*(6), 488–494.

279. Punnoose, E. A., Atwal, S., Liu, W., Raja, R., Fine, B. M., Hughes, B. G. M., Hicks, R. J., Hampton, G. M., Amler, L. C., Pirzkall, A., & Lackner, M. R. (2012). Evaluation of Circulating Tumor Cells and Circulating Tumor DNA in Non–Small Cell Lung Cancer: Association with Clinical Endpoints in a Phase II Clinical Trial of Pertuzumab and Erlotinib. *Clinical Cancer Research*, *18*(8), 2391–2401.

280. Purnell, M. R., & Whish, W. J. (1980). Novel inhibitors of poly(ADP-ribose) synthetase. *Biochemical Journal*, *185*(3), 775–777.

281. Qian, B.-Z., Li, J., Zhang, H., Kitamura, T., Zhang, J., Campion, L. R., Kaiser, E. A., Snyder, L. A., & Pollard, J. W. (2011). CCL2 recruits inflammatory monocytes to facilitate breast tumor metastasis. *Nature*, *475*(7355), 222–225.

282. Quail, D., & Joyce, J. (2013). Microenvironmental regulation of tumor progression and metastasis. *Nature Medicine*, *19*(11), 1423–1437.

283. Quanz, M., Berthault, N., Roulin, C., Roy, M., Herbette, A., Agrario, C., Alberti, C., Josserand, V., Coll, J.-L., Sastre-Garau, X., Cosset, J.-M., Larue, L., Sun, J.-S., & Dutreix, M. (2009). Small-Molecule Drugs Mimicking DNA Damage: A New Strategy for Sensitizing Tumors to Radiotherapy. *Clinical Cancer Research*, *15*(4), 1308–1316.

284. Rahman, N., Seal, S., Thompson, D., Kelly, P., Renwick, A., Elliott, A., Reid, S., Spanova, K., Barfoot, R., Chagtai, T., Jayatilake, H., McGuffog, L., Hanks, S., Evans, D. G., Eccles, D., Easton, D. F., & Stratton, M. R. (2007). PALB2, which encodes a BRCA2-interacting protein, is a breast cancer susceptibility gene. *Nature Genetics*, *39*(2), 165–167.

285. Ramalingam, S. S., Cheng, Y., Zhou, C., Ohe, Y., Imamura, F., Cho, B. C., Lin, M.-C., Majem, M., Shah, R., Rukazenkov, Y., Todd, A., Markovets, A., Barrett, J. C., Chmielecki, J., & Gray, J. (2018). Mechanisms of acquired resistance to first-line osimertinib: Preliminary data from the phase III FLAURA study. *Annals of Oncology*, *29*, viii740.

286. Ramalingam, S. S., Novello, S., Guclu, S. Z., Bentsion, D., Zvirbule, Z., Szilasi, M., Bernabe, R., Syrigos, K., Byers, L. A., Clingan, P., Bar, J., Vokes, E. E., Govindan, R., Dunbar, M., Ansell, P., He, L., Huang, X., Sehgal, V., Glasgow, J., … Mazieres, J. (2021). Veliparib in Combination With Platinum-Based Chemotherapy for First-Line Treatment of Advanced Squamous Cell Lung Cancer: A Randomized, Multicenter Phase III Study. *Journal of Clinical Oncology*, JCO.20.03318.

287. Ramalingam, S. S., Vansteenkiste, J., Planchard, D., Cho, B. C., Gray, J. E., Ohe, Y., Zhou, C., Reungwetwattana, T., Cheng, Y., Chewaskulyong, B., Shah, R., Cobo, M., Lee, K. H., Cheema, P., Tiseo, M., John, T., Lin, M.-C., Imamura, F., Kurata, T., … Soria, J.-C. (2020). Overall Survival with Osimertinib in Untreated, *EGFR* -Mutated Advanced NSCLC. *New England Journal of Medicine*, *382*(1), 41–50.

288. Ramsköld, D., Luo, S., Wang, Y.-C., Li, R., Deng, Q., Faridani, O. R., Daniels, G. A., Khrebtukova, I., Loring, J. F., Laurent, L. C., Schroth, G. P., & Sandberg, R. (2012). Full-length mRNA-Seq from single-cell levels of RNA and individual circulating tumor cells. *Nature Biotechnology*, *30*(8), 777–782.

289. Ray Chaudhuri, A., & Nussenzweig, A. (2017). The multifaceted roles of PARP1 in DNA repair and chromatin remodelling. *Nature Reviews Molecular Cell Biology*, *18*(10), 610–621.

290. Reck, M., Rodríguez-Abreu, D., Robinson, A. G., Hui, R., Csőszi, T., Fülöp, A., Gottfried, M., Peled, N., Tafreshi, A., Cuffe, S., O'Brien, M., Rao, S., Hotta, K., Leiby, M. A., Lubiniecki, G. M., Shentu, Y., Rangwala, R., & Brahmer, J. R. (2016). Pembrolizumab versus Chemotherapy for PD-L1–Positive Non–Small-Cell Lung Cancer. *New England Journal of Medicine*, *375*(19), 1823–1833.

291. Recondo, G., Mezquita, L., Facchinetti, F., Planchard, D., Gazzah, A., Bigot, L., Rizvi, A. Z., Frias, R. L., Thiery, J. P., Scoazec, J.-Y., Sourisseau, T., Howarth, K., Deas, O., Samofalova, D., Galissant, J., Tesson, P., Braye, F., Naltet, C., Lavaud, P., … Friboulet, L. (2020). Diverse Resistance Mechanisms to the Third-Generation ALK Inhibitor Lorlatinib in ALK-Rearranged Lung Cancer. *Clinical Cancer Research*, *26*(1), 242–255.

292. Reiss, K. A., Herman, J. M., Zahurak, M., Brade, A., Dawson, L. A., Scardina, A., Joffe, C., Petito, E., Hacker-Prietz, A., Kinders, R. J., Wang, L., Chen, A., Temkin, S., Horiba, N., Siu, L. L., & Azad, N. S. (2015). A Phase I study of veliparib (ABT-888) in combination with low-dose fractionated whole abdominal radiation therapy in patients with advanced solid malignancies and peritoneal carcinomatosis. *Clinical Cancer Research*, *21*(1), 68–76.

293. Remon, J., Besse, B., Leary, A., Bièche, I., Job, B., Lacroix, L., Auguste, A., Mauduit, M., Audigier-Valette, C., Raimbourg, J., Madroszyk, A., Michels, S., Bayar, M. A., Jimenez, M., Soria, J.-C., Rouleau, E., & Barlesi, F. (2020). Somatic and Germline BRCA 1 and 2 Mutations in Advanced NSCLC From the SAFIR02-Lung Trial. *JTO Clinical and Research Reports*, *1*(3), 100068.

294. Reya, T., Morrison, S. J., Clarke, M. F., & Weissman, I. L. (2001). Stem cells, cancer, and cancer stem cells. *Nature*, *414*(6859), 105–111.

295. Reymond, N., d'Água, B. B., & Ridley, A. J. (2013). Crossing the endothelial barrier during metastasis. *Nature Reviews Cancer*, *13*(12), 858–870.

296. Ribatti, D. (2016). The chick embryo chorioallantoic membrane (CAM). A multifaceted experimental model. *Mechanisms of Development*, *141*, 70–77.

297. Ricciuti, B., Recondo, G., Spurr, L. F., Li, Y. Y., Lamberti, G., Venkatraman, D., Umeton, R., Cherniack, A. D., Nishino, M., Sholl, L. M., Shapiro, G. I., Awad, M. M., & Cheng, M. L. (2020). Impact of DNA Damage Response and Repair (DDR) Gene Mutations on Efficacy of PD-(L)1 Immune Checkpoint Inhibition in Non–Small Cell Lung Cancer. *Clinical Cancer Research*, *26*(15), 4135–4142.

298. Ricci-Vitiani, L., Lombardi, D. G., Pilozzi, E., Biffoni, M., Todaro, M., Peschle, C., & De Maria, R. (2007). Identification and expansion of human colon-cancer-initiating cells. *Nature*, *445*(7123), 111–115.

299. Risson, E., Nobre, A. R., Maguer-Satta, V., & Aguirre-Ghiso, J. A. (2020). The current paradigm and challenges ahead for the dormancy of disseminated tumor cells. *Nature Cancer*, *1*(7), 672–680.

300. Rosell, R., Carcereny, E., Gervais, R., Vergnenegre, A., Massuti, B., Felip, E., Palmero, R., Garcia-Gomez, R., Pallares, C., Sanchez, J. M., Porta, R., Cobo, M., Garrido, P., Longo, F., Moran, T., Insa, A., De Marinis, F., Corre, R., Bover, I., … Paz-Ares, L. (2012). Erlotinib versus standard chemotherapy as first-line treatment for European patients with advanced EGFR mutation-positive non-small-cell lung cancer (EURTAC): A multicentre, open-label, randomised phase 3 trial. *The Lancet Oncology*, *13*(3), 239–246.

301. Ross, K., Pailler, E., Faugeroux, V., Taylor, M., Oulhen, M., Auger, N., Planchard, D., Soria, J.-C., Lindsay, C. R., Besse, B., Vielh, P., & Farace, F. (2015). The potential diagnostic power of circulating tumor cell analysis for non-small-cell lung cancer. *Expert Review of Molecular Diagnostics*, *15*(12), 1605–1629.

302. Roulston, A., Zimmermann, M., Papp, R., Skeldon, A., Pellerin, C., Dumas-Bérube, É., Dumais, V., Dorich, S., Fader, L. D., Fournier, S., Li, L., Leclaire, M.-E., Yin, S. Y., Chefson, A., Alam, H., Yang, W., Fugère-Desjardins, C., Vignini-Hammond, S., Skorey, K., … Black, W. C. (2022). RP-3500: A Novel, Potent, and Selective ATR Inhibitor that is Effective in Preclinical Models as a Monotherapy and in Combination with PARP Inhibitors. *Molecular Cancer Therapeutics*, *21*(2), 245–256.

303. Sansregret, L., Vanhaesebroeck, B., & Swanton, C. (2018). Determinants and clinical implications of chromosomal instability in cancer. *Nature Reviews. Clinical Oncology*, *15*(3), 139–150.

304. Satoh, M. S., & Lindahl, T. (1992). Role of poly(ADP-ribose) formation in DNA repair. *Nature*, *356*(6367), 356–358.

305. Scher, H. I., Graf, R. P., Schreiber, N. A., McLaughlin, B., Jendrisak, A., Wang, Y., Lee, J., Greene, S., Krupa, R., Lu, D., Bamford, P., Louw, J. E., Dugan, L., Vargas, H. A., Fleisher, M., Landers, M., Heller, G., & Dittamore, R. (2017). Phenotypic Heterogeneity of Circulating

Tumor Cells Informs Clinical Decisions between AR Signaling Inhibitors and Taxanes in Metastatic Prostate Cancer. *Cancer Research*, *77*(20), 5687–5698.

306. Schram, A. M., Goto, K., Kim, D.-W., Martin-Romano, P., Ou, S.-H. I., O'Kane, G. M., O'Reilly, E. M., Umemoto, K., Duruisseaux, M., Neuzillet, C., Opdam, F., Rodon Ahnert, J., Nagasaka, M., Weinberg, B. A., Macarulla, T., Joe, A. K., Ford, J., Stalbovskaya, V., Wasserman, E., & Drilon, A. E. (2022). Efficacy and safety of zenocutuzumab, a HER2 x HER3 bispecific antibody, across advanced NRG1 fusion (NRG1+) cancers. *Journal of Clinical Oncology*, *40*(16_suppl), 105–105.
307. Scully, R., Panday, A., Elango, R., & Willis, N. A. (2019). DNA double-strand break repair-pathway choice in somatic mammalian cells. *Nature Reviews Molecular Cell Biology*, *20*(11), 698–714.
308. Sen, T., Rodriguez, B. L., Chen, L., Corte, C. M. D., Morikawa, N., Fujimoto, J., Cristea, S., Nguyen, T., Diao, L., Li, L., Fan, Y., Yang, Y., Wang, J., Glisson, B. S., Wistuba, I. I., Sage, J., Heymach, J. V., Gibbons, D. L., & Byers, L. A. (2019). Targeting DNA Damage Response Promotes Antitumor Immunity through STING-Mediated T-cell Activation in Small Cell Lung Cancer. *Cancer Discovery*, *9*(5), 646–661.
309. Sequist, L. V., Waltman, B. A., Dias-Santagata, D., Digumarthy, S., Turke, A. B., Fidias, P., Bergethon, K., Shaw, A. T., Gettinger, S., Cosper, A. K., Akhavanfard, S., Heist, R. S., Temel, J., Christensen, J. G., Wain, J. C., Lynch, T. J., Vernovsky, K., Mark, E. J., Lanuti, M., … Engelman, J. A. (2011). Genotypic and Histological Evolution of Lung Cancers Acquiring Resistance to EGFR Inhibitors. *Science Translational Medicine*, *3*(75), 75ra26.
310. Sequist, L. V., Yang, J. C.-H., Yamamoto, N., O'Byrne, K., Hirsh, V., Mok, T., Geater, S. L., Orlov, S., Tsai, C.-M., Boyer, M., Su, W.-C., Bennouna, J., Kato, T., Gorbunova, V., Lee, K. H., Shah, R., Massey, D., Zazulina, V., Shahidi, M., & Schuler, M. (2013). Phase III Study of Afatinib or Cisplatin Plus Pemetrexed in Patients With Metastatic Lung Adenocarcinoma With EGFR Mutations. *Journal of Clinical Oncology*, *31*(27), 3327–3334.
311. Serra, V., Wang, A. T., Castroviejo-Bermejo, M., Polanska, U. M., Palafox, M., Herencia-Ropero, A., Jones, G. N., Lai, Z., Armenia, J., Michopoulos, F., Llop-Guevara, A., Brough, R., Gulati, A., Pettitt, S. J., Bulusu, K. C., Nikkilä, J., Wilson, Z., Hughes, A. M., Wijnhoven, P. W. G., … O'Connor, M. J. (2022). Identification of a molecularly-defined subset of breast and ovarian cancer models that respond to WEE1 or ATR inhibition, overcoming PARP inhibitor resistance. *Clinical Cancer Research*, CCR-22-0568.
312. Shaw, A. T., Bauer, T. M., de Marinis, F., Felip, E., Goto, Y., Liu, G., Mazieres, J., Kim, D.-W., Mok, T., Polli, A., Thurm, H., Calella, A. M., Peltz, G., & Solomon, B. J. (2020). First-Line Lorlatinib or Crizotinib in Advanced ALK-Positive Lung Cancer. *New England Journal of Medicine*, *383*(21), 2018–2029.
313. Shaw, A. T., Kim, D.-W., Mehra, R., Tan, D. S. W., Felip, E., Chow, L. Q. M., Camidge, D. R., Vansteenkiste, J., Sharma, S., De Pas, T., Riely, G. J., Solomon, B. J., Wolf, J., Thomas, M., Schuler, M., Liu, G., Santoro, A., Lau, Y. Y., Goldwasser, M., … Engelman, J. A. (2014). Ceritinib in *ALK* -Rearranged Non–Small-Cell Lung Cancer. *New England Journal of Medicine*, *370*(13), 1189–1197.

314. Shaw, A. T., Kim, D.-W., Nakagawa, K., Seto, T., Crinó, L., Ahn, M.-J., De Pas, T., Besse, B., Solomon, B. J., Blackhall, F., Wu, Y.-L., Thomas, M., O'Byrne, K. J., Moro-Sibilot, D., Camidge, D. R., Mok, T., Hirsh, V., Riely, G. J., Iyer, S., … Jänne, P. A. (2013). Crizotinib versus Chemotherapy in Advanced *ALK* -Positive Lung Cancer. *New England Journal of Medicine*, *368*(25), 2385–2394.

315. Shaw, A. T., Ou, S.-H. I., Bang, Y.-J., Camidge, D. R., Solomon, B. J., Salgia, R., Riely, G. J., Varella-Garcia, M., Shapiro, G. I., Costa, D. B., Doebele, R. C., Le, L. P., Zheng, Z., Tan, W., Stephenson, P., Shreeve, S. M., Tye, L. M., Christensen, J. G., Wilner, K. D., … Iafrate, A. J. (2014, November 19). *Crizotinib in ROS1-Rearranged Non–Small-Cell Lung Cancer* (world) [Research-article]. Http://Dx.Doi.Org/10.1056/NEJMoa1406766; Massachusetts Medical Society.

316. Shibue, T., & Weinberg, R. A. (2017). EMT, CSCs, and drug resistance: The mechanistic link and clinical implications. *Nature Reviews. Clinical Oncology*, *14*(10), 611–629.

317. Shree, T., Olson, O. C., Elie, B. T., Kester, J. C., Garfall, A. L., Simpson, K., Bell-McGuinn, K. M., Zabor, E. C., Brogi, E., & Joyce, J. A. (2011). Macrophages and cathepsin proteases blunt chemotherapeutic response in breast cancer. *Genes & Development*, *25*(23), 2465–2479.

318. Shuck, S. C., Short, E. A., & Turchi, J. J. (2008). Eukaryotic nucleotide excision repair: From understanding mechanisms to influencing biology. *Cell Research*, *18*(1), 64–72.

319. Siegel, R. L., Miller, K. D., Fuchs, H. E., & Jemal, A. (2022). Cancer statistics, 2022. *CA: A Cancer Journal for Clinicians*, *72*(1), 7–33.

320. Simpson, K. L., Stoney, R., Frese, K. K., Simms, N., Rowe, W., Pearce, S. P., Humphrey, S., Booth, L., Morgan, D., Dynowski, M., Trapani, F., Catozzi, A., Revill, M., Helps, T., Galvin, M., Girard, L., Nonaka, D., Carter, L., Krebs, M. G., … Dive, C. (2020). A biobank of small cell lung cancer CDX models elucidates inter- and intratumoral phenotypic heterogeneity. *Nature Cancer*, *1*(4), 437–451.

321. Singal, G., Miller, P. G., Agarwala, V., Li, G., Kaushik, G., Backenroth, D., Gossai, A., Frampton, G. M., Torres, A. Z., Lehnert, E. M., Bourque, D., O'Connell, C., Bowser, B., Caron, T., Baydur, E., Seidl-Rathkopf, K., Ivanov, I., Alpha-Cobb, G., Guria, A., … Miller, V. A. (2019). Association of Patient Characteristics and Tumor Genomics With Clinical Outcomes Among Patients With Non–Small Cell Lung Cancer Using a Clinicogenomic Database. *JAMA*, *321*(14), 1391–1399.

322. Skoulidis, F., Li, B. T., Dy, G. K., Price, T. J., Falchook, G. S., Wolf, J., Italiano, A., Schuler, M., Borghaei, H., Barlesi, F., Kato, T., Curioni-Fontecedro, A., Sacher, A., Spira, A., Ramalingam, S. S., Takahashi, T., Besse, B., Anderson, A., Ang, A., … Govindan, R. (2021). Sotorasib for Lung Cancers with KRAS p.G12C Mutation. *New England Journal of Medicine*.

323. Soda, M., Choi, Y. L., Enomoto, M., Takada, S., Yamashita, Y., Ishikawa, S., Fujiwara, S., Watanabe, H., Kurashina, K., Hatanaka, H., Bando, M., Ohno, S., Ishikawa, Y., Aburatani, H., Niki, T., Sohara, Y., Sugiyama, Y., & Mano, H. (2007). Identification of the transforming EML4–ALK fusion gene in non-small-cell lung cancer. *Nature*, *448*(7153), 561–566.

324. Soler, A., Cayrefourcq, L., Mazard, T., Babayan, A., Lamy, P.-J., Assou, S., Assenat, E., Pantel, K., & Alix-Panabières, C. (2018). Autologous cell lines from circulating colon cancer

cells captured from sequential liquid biopsies as model to study therapy-driven tumor changes. *Scientific Reports*, *8*(1), 15931.

325. Solomon, B. J., Bauer, T. M., Ignatius Ou, S.-H., Liu, G., Hayashi, H., Bearz, A., Penkov, K., Wu, Y.-L., Arrieta, O., Jassem, J., Calella, A. M., Peltz, G., Polli, A., Thurm, H., & Mok, T. (2022). Post Hoc Analysis of Lorlatinib Intracranial Efficacy and Safety in Patients With ALK-Positive Advanced Non–Small-Cell Lung Cancer From the Phase III CROWN Study. *Journal of Clinical Oncology*, JCO.21.02278.
326. Solomon, B. J., Besse, B., Bauer, T. M., Felip, E., Soo, R. A., Camidge, D. R., Chiari, R., Bearz, A., Lin, C.-C., Gadgeel, S. M., Riely, G. J., Tan, E. H., Seto, T., James, L. P., Clancy, J. S., Abbattista, A., Martini, J.-F., Chen, J., Peltz, G., … Shaw, A. T. (2018). Lorlatinib in patients with ALK-positive non-small-cell lung cancer: Results from a global phase 2 study. *The Lancet Oncology*, *19*(12), 1654–1667.
327. Solomon, B. J., Mok, T., Kim, D.-W., Wu, Y.-L., Nakagawa, K., Mekhail, T., Felip, E., Cappuzzo, F., Paolini, J., Usari, T., Iyer, S., Reisman, A., Wilner, K. D., Tursi, J., & Blackhall, F. (2014). First-Line Crizotinib versus Chemotherapy in *ALK* -Positive Lung Cancer. *New England Journal of Medicine*, *371*(23), 2167–2177.
328. Sonnenblick, A., de Azambuja, E., Azim, H. A., & Piccart, M. (2015). An update on PARP inhibitors—Moving to the adjuvant setting. *Nature Reviews Clinical Oncology*, *12*(1), 27–41.
329. Soria, J.-C., Ohe, Y., Vansteenkiste, J., Reungwetwattana, T., Chewaskulyong, B., Lee, K. H., Dechaphunkul, A., Imamura, F., Nogami, N., Kurata, T., Okamoto, I., Zhou, C., Cho, B. C., Cheng, Y., Cho, E. K., Voon, P. J., Planchard, D., Su, W.-C., Gray, J. E., … Ramalingam, S. S. (2018). Osimertinib in Untreated EGFR-Mutated Advanced Non–Small-Cell Lung Cancer. *New England Journal of Medicine*, *378*(2), 113–125.
330. Sperger, J. M., Emamekhoo, H., McKay, R. R., Stahlfeld, C. N., Singh, A., Chen, X. E., Kwak, L., Gilsdorf, C. S., Wolfe, S. K., Wei, X. X., Silver, R., Zhang, Z., Morris, M. J., Bubley, G., Feng, F. Y., Scher, H. I., Rathkopf, D., Dehm, S. M., Choueiri, T. K., … Lang, J. M. (2021). Prospective Evaluation of Clinical Outcomes Using a Multiplex Liquid Biopsy Targeting Diverse Resistance Mechanisms in Metastatic Prostate Cancer. *Journal of Clinical Oncology*, *39*(26), 2926–2937.
331. Spiegel, A., Brooks, M. W., Houshyar, S., Reinhardt, F., Ardolino, M., Fessler, E., Chen, M. B., Krall, J. A., DeCock, J., Zervantonakis, I. K., Iannello, A., Iwamoto, Y., Cortez-Retamozo, V., Kamm, R. D., Pittet, M. J., Raulet, D. H., & Weinberg, R. A. (2016). Neutrophils Suppress Intraluminal NK Cell–Mediated Tumor Cell Clearance and Enhance Extravasation of Disseminated Carcinoma Cells. *Cancer Discovery*, *6*(6), 630–649.
332. Stewart, C. A., Gay, C. M., Xi, Y., Sivajothi, S., Sivakamasundari, V., Fujimoto, J., Bolisetty, M., Hartsfield, P. M., Balasubramaniyan, V., Chalishazar, M. D., Moran, C., Kalhor, N., Stewart, J., Tran, H., Swisher, S. G., Roth, J. A., Zhang, J., de Groot, J., Glisson, B., … Byers, L. A. (2020). Single-cell analyses reveal increased intratumoral heterogeneity after the onset of therapy resistance in small-cell lung cancer. *Nature Cancer*, *1*(4), 423–436.
333. Stewart, C. A., Tong, P., Cardnell, R. J., Sen, T., Li, L., Gay, C. M., Masrorpour, F., Fan, Y., Bara, R. O., Feng, Y., Ru, Y., Fujimoto, J., Kundu, S. T., Post, L. E., Yu, G. K., Shen, Y., Glisson, B.

S., Wistuba, I., Heymach, J. V., … Byers, L. A. (2017). Dynamic variations in epithelial-to-mesenchymal transition (EMT), ATM, and SLFN11 govern response to PARP inhibitors and cisplatin in small cell lung cancer. *Oncotarget*, *8*(17), 28575–28587.

334. Stott, S. L., Hsu, C.-H., Tsukrov, D. I., Yu, M., Miyamoto, D. T., Waltman, B. A., Rothenberg, S. M., Shah, A. M., Smas, M. E., Korir, G. K., Floyd, F. P., Gilman, A. J., Lord, J. B., Winokur, D., Springer, S., Irimia, D., Nagrath, S., Sequist, L. V., Lee, R. J., … Toner, M. (2010). Isolation of circulating tumor cells using a microvortex-generating herringbone-chip. *Proceedings of the National Academy of Sciences*, *107*(43), 18392–18397.
335. Stott, S. L., Lee, R. J., Nagrath, S., Yu, M., Miyamoto, D. T., Ulkus, L., Inserra, E. J., Ulman, M., Springer, S., Nakamura, Z., Moore, A. L., Tsukrov, D. I., Kempner, M. E., Dahl, D. M., Wu, C.-L., Iafrate, A. J., Smith, M. R., Tompkins, R. G., Sequist, L. V., … Maheswaran, S. (2010). Isolation and Characterization of Circulating Tumor Cells from Patients with Localized and Metastatic Prostate Cancer. *Science Translational Medicine*, *2*(25), 25ra23-25ra23.
336. Su, Z., Wang, Z., Ni, X., Duan, J., Gao, Y., Zhuo, M., Li, R., Zhao, J., Ma, Q., Bai, H., Chen, H., Wang, S., Chen, X., An, T., Wang, Y., Tian, Y., Yu, J., Wang, D., Xie, X. S., … Wang, J. (2019). Inferring the Evolution and Progression of Small-Cell Lung Cancer by Single-Cell Sequencing of Circulating Tumor Cells. *Clinical Cancer Research*, *25*(16), 5049–5060.
337. Sun, Y.-F., Wu, L., Liu, S.-P., Jiang, M.-M., Hu, B., Zhou, K.-Q., Guo, W., Xu, Y., Zhong, Y., Zhou, X.-R., Zhang, Z.-F., Liu, G., Liu, S., Shi, Y.-H., Ji, Y., Du, M., Li, N.-N., Li, G.-B., Zhao, Z.-K., … Yang, X.-R. (2021). Dissecting spatial heterogeneity and the immune-evasion mechanism of CTCs by single-cell RNA-seq in hepatocellular carcinoma. *Nature Communications*, *12*(1), 4091.
338. Sung, H., Ferlay, J., Siegel, R. L., Laversanne, M., Soerjomataram, I., Jemal, A., & Bray, F. (2021). Global Cancer Statistics 2020: GLOBOCAN Estimates of Incidence and Mortality Worldwide for 36 Cancers in 185 Countries. *CA: A Cancer Journal for Clinicians*, *71*(3), 209–249.
339. Symington, L. S., & Gautier, J. (2011). Double-Strand Break End Resection and Repair Pathway Choice. *Annual Review of Genetics*, *45*(1), 247–271.
340. Szczerba, B. M., Castro-Giner, F., Vetter, M., Krol, I., Gkountela, S., Landin, J., Scheidmann, M. C., Donato, C., Scherrer, R., Singer, J., Beisel, C., Kurzeder, C., Heinzelmann-Schwarz, V., Rochlitz, C., Weber, W. P., Beerenwinkel, N., & Aceto, N. (2019). Neutrophils escort circulating tumour cells to enable cell cycle progression. *Nature*, *566*(7745), 553–557.
341. Talasaz, A. H., Powell, A. A., Huber, D. E., Berbee, J. G., Roh, K.-H., Yu, W., Xiao, W., Davis, M. M., Pease, R. F., Mindrinos, M. N., Jeffrey, S. S., & Davis, R. W. (2009). Isolating highly enriched populations of circulating epithelial cells and other rare cells from blood using a magnetic sweeper device. *Proceedings of the National Academy of Sciences of the United States of America*, *106*(10), 3970–3975.
342. Tan, C. L., Lim, T. H., Lim, T. K., Tan, D. S.-W., Chua, Y. W., Ang, M. K., Pang, B., Lim, C. T., Takano, A., Lim, A. S.-T., Leong, M. C., & Lim, W.-T. (2016). Concordance of anaplastic lymphoma kinase (ALK) gene rearrangements between circulating tumor cells and tumor in non-small cell lung cancer. *Oncotarget*, *7*(17), 23251–23262.

343. Tayoun, T., Faugeroux, V., Oulhen, M., Aberlenc, A., Pawlikowska, P., & Farace, F. (2019). CTC-Derived Models: A Window into the Seeding Capacity of Circulating Tumor Cells (CTCs). *Cells*, *8*(10), 1145.

344. Tayoun, T., Faugeroux, V., Oulhen, M., Déas, O., Michels, J., Brulle-Soumare, L., Cairo, S., Scoazec, J.-Y., Marty, V., Aberlenc, A., Planchard, D., Remon, J., Ponce, S., Besse, B., Kannouche, P. L., Judde, J.-G., Pawlikowska, P., & Farace, F. (2022). Targeting genome integrity dysfunctions impedes metastatic potency in non–small cell lung cancer circulating tumor cell–derived explants. *JCI Insight*, *7*(11), Article 11.

345. Tayoun, T., Oulhen, M., Aberlenc, A., Farace, F., & Pawlikowska, P. (2021). Tumor Evolution and Therapeutic Choice Seen through a Prism of Circulating Tumor Cell Genomic Instability. *Cells*, *10*(2), 337.

346. Tellez-Gabriel, M., Cochonneau, D., Cadé, M., Jubelin, C., Heymann, M.-F., & Heymann, D. (2018). Circulating Tumor Cell-Derived Pre-Clinical Models for Personalized Medicine. *Cancers*, *11*(1), 19.

347. Thai, A. A., Solomon, B. J., Sequist, L. V., Gainor, J. F., & Heist, R. S. (2021). Lung cancer. *The Lancet*, *398*(10299), 535–554.

348. The Cancer Genome Atlas Research Network. (2011). Integrated Genomic Analyses of Ovarian Carcinoma. *Nature*, *474*(7353), 609–615.

349. Thiery, J. P., Acloque, H., Huang, R. Y. J., & Nieto, M. A. (2009). Epithelial-Mesenchymal Transitions in Development and Disease. *Cell*, *139*(5), 871–890.

350. Tie, J., Cohen, J. D., Lahouel, K., Lo, S. N., Wang, Y., Kosmider, S., Wong, R., Shapiro, J., Lee, M., Harris, S., Khattak, A., Burge, M., Harris, M., Lynam, J., Nott, L., Day, F., Hayes, T., McLachlan, S.-A., Lee, B., … Gibbs, P. (2022). Circulating Tumor DNA Analysis Guiding Adjuvant Therapy in Stage II Colon Cancer. *New England Journal of Medicine*, *386*(24), 2261–2272.

351. Trenner, A., & Sartori, A. A. (2019). Harnessing DNA Double-Strand Break Repair for Cancer Treatment. *Frontiers in Oncology*, *9*, 1388.

352. Tutt, A., Tovey, H., Cheang, M. C. U., Kernaghan, S., Kilburn, L., Gazinska, P., Owen, J., Abraham, J., Barrett, S., Barrett-Lee, P., Brown, R., Chan, S., Dowsett, M., Flanagan, J. M., Fox, L., Grigoriadis, A., Gutin, A., Harper-Wynne, C., Hatton, M. Q., … Bliss, J. M. (2018). Carboplatin in BRCA1/2-mutated and triple-negative breast cancer BRCAness subgroups: The TNT Trial. *Nature Medicine*, *24*(5), 628–637.

353. van de Stolpe, A., Pantel, K., Sleijfer, S., Terstappen, L. W., & den Toonder, J. M. J. (2011). Circulating Tumor Cell Isolation and Diagnostics: Toward Routine Clinical Use. *Cancer Research*, *71*(18), 5955–5960.

354. Vishnoi, M., Liu, N. H., Yin, W., Boral, D., Scamardo, A., Hong, D., & Marchetti, D. (2019). The identification of a TNBC liver metastasis gene signature by sequential CTC-xenograft modeling. *Molecular Oncology*, *13*(9), 1913–1926.

355. Vona, G., Sabile, A., Louha, M., Sitruk, V., Romana, S., Schütze, K., Capron, F., Franco, D., Pazzagli, M., Vekemans, M., Lacour, B., Bréchot, C., & Paterlini-Bréchot, P. (2000). Isolation by Size of Epithelial Tumor Cells. *The American Journal of Pathology*, *156*(1), 57–63.

356. Walsh, T., Casadei, S., Lee, M. K., Pennil, C. C., Nord, A. S., Thornton, A. M., Roeb, W., Agnew, K. J., Stray, S. M., Wickramanayake, A., Norquist, B., Pennington, K. P., Garcia, R. L., King, M.-C., & Swisher, E. M. (2011). Mutations in 12 genes for inherited ovarian, fallopian tube, and peritoneal carcinoma identified by massively parallel sequencing. *Proceedings of the National Academy of Sciences*, *108*(44), 18032–18037.

357. Wanderley, C. W. S., Correa, T. S., Scaranti, M., Cunha, F. Q., & Barroso-Sousa, R. (2022). Targeting PARP1 to Enhance Anticancer Checkpoint Immunotherapy Response: Rationale and Clinical Implications. *Frontiers in Immunology*, *13*. https://www.frontiersin.org/articles/10.3389/fimmu.2022.816642

358. Wang, L. H., Pfister, T. D., Parchment, R. E., Kummar, S., Rubinstein, L., Evrard, Y. A., Gutierrez, M. E., Murgo, A. J., Tomaszewski, J. E., Doroshow, J. H., & Kinders, R. J. (2010). Monitoring Drug-Induced γH2AX as a Pharmacodynamic Biomarker in Individual Circulating Tumor Cells. *Clinical Cancer Research*, *16*(3), 1073–1084.

359. Wang, Y., McKay, J. D., Rafnar, T., Wang, Z., Timofeeva, M. N., Broderick, P., Zong, X., Laplana, M., Wei, Y., Han, Y., Lloyd, A., Delahaye-Sourdeix, M., Chubb, D., Gaborieau, V., Wheeler, W., Chatterjee, N., Thorleifsson, G., Sulem, P., Liu, G., … Amos, C. I. (2014). Rare variants of large effect in BRCA2 and CHEK2 affect risk of lung cancer. *Nature Genetics*, *46*(7), 736–741.

360. Werner, S. L., Graf, R. P., Landers, M., Valenta, D. T., Schroeder, M., Greene, S. B., Bales, N., Dittamore, R., & Marrinucci, D. (2015). Analytical Validation and Capabilities of the Epic CTC Platform: Enrichment-Free Circulating Tumour Cell Detection and Characterization. *Journal of Circulating Biomarkers*, *4*, 3.

361. Winkler, C., Armenia, J., Jones, G. N., Tobalina, L., Sale, M. J., Petreus, T., Baird, T., Serra, V., Wang, A. T., Lau, A., Garnett, M. J., Jaaks, P., Coker, E. A., Pierce, A. J., O'Connor, M. J., & Leo, E. (2021). SLFN11 informs on standard of care and novel treatments in a wide range of cancer models. *British Journal of Cancer*, *124*(5), 951–962.

362. Wit, S. de, Dalum, G. van, Lenferink, A. T. M., Tibbe, A. G. J., Hiltermann, T. J. N., Groen, H. J. M., van Rijn, C. J. M., & Terstappen, L. W. M. M. (2015). The detection of EpCAM+ and EpCAM– circulating tumor cells. *Scientific Reports*, *5*(1), 12270.

363. Wolf, M. J., Hoos, A., Bauer, J., Boettcher, S., Knust, M., Weber, A., Simonavicius, N., Schneider, C., Lang, M., Stürzl, M., Croner, R. S., Konrad, A., Manz, M. G., Moch, H., Aguzzi, A., van Loo, G., Pasparakis, M., Prinz, M., Borsig, L., & Heikenwalder, M. (2012). Endothelial CCR2 Signaling Induced by Colon Carcinoma Cells Enables Extravasation via the JAK2-Stat5 and p38MAPK Pathway. *Cancer Cell*, *22*(1), 91–105.

364. Wong, C. W., Lee, A., Shientag, L., Yu, J., Dong, Y., Kao, G., Al-Mehdi, A. B., Bernhard, E. J., & Muschel, R. J. (2001). Apoptosis: An early event in metastatic inefficiency. *Cancer Research*, *61*(1), 333–338.

365. Wu, Y.-H., Hung, Y.-P., Chiu, N.-C., Lee, R.-C., Li, C.-P., Chao, Y., Shyr, Y.-M., Wang, S.-E., Chen, S.-C., Lin, S.-H., Chen, Y.-H., Kang, Y.-M., Hsu, S.-M., Yen, S.-H., Wu, J.-Y., Lee, K.-D., Tseng, H.-E., Tsai, J.-R., Tang, J.-H., … Lu, L.-S. (2022). Correlation between drug sensitivity

profiles of circulating tumour cell-derived organoids and clinical treatment response in patients with pancreatic ductal adenocarcinoma. *European Journal of Cancer*, *166*, 208–218.

366. Wu, Y.-L., Cheng, Y., Zhou, X., Lee, K. H., Nakagawa, K., Niho, S., Tsuji, F., Linke, R., Rosell, R., Corral, J., Migliorino, M. R., Pluzanski, A., Sbar, E. I., Wang, T., White, J. L., Nadanaciva, S., Sandin, R., & Mok, T. S. (2017). Dacomitinib versus gefitinib as first-line treatment for patients with EGFR-mutation-positive non-small-cell lung cancer (ARCHER 1050): A randomised, open-label, phase 3 trial. *The Lancet Oncology*, *18*(11), 1454–1466.
367. Xu, G., Chapman, J. R., Brandsma, I., Yuan, J., Mistrik, M., Bouwman, P., Bartkova, J., Gogola, E., Warmerdam, D., Barazas, M., Jaspers, J. E., Watanabe, K., Pieterse, M., Kersbergen, A., Sol, W., Celie, P. H. N., Schouten, P. C., van den Broek, B., Salman, A., … Rottenberg, S. (2015). REV7 counteracts DNA double-strand break resection and affects PARP inhibition. *Nature*, *521*(7553), 541–544.
368. Yap, T. A., Im, S.-A., Schram, A. M., Sharp, A., Balmana, J., Baird, R. D., Brown, J. S., Schwaederle, M., Pilling, E. A., Moorthy, G., Linardopoulos, S., Dowson, A., Pound, C., Lukacs, E., Cosulich, S., & Luen, S. J. (2022). Abstract CT007: PETRA: First in class, first in human trial of the next generation PARP1-selective inhibitor AZD5305 in patients (pts) with BRCA1/2, PALB2 or RAD51C/D mutations. *Cancer Research*, *82*(12_Supplement), CT007.
369. Yap, T. A., O'Carrigan, B., Penney, M. S., Lim, J. S., Brown, J. S., de Miguel Luken, M. J., Tunariu, N., Perez-Lopez, R., Rodrigues, D. N., Riisnaes, R., Figueiredo, I., Carreira, S., Hare, B., McDermott, K., Khalique, S., Williamson, C. T., Natrajan, R., Pettitt, S. J., Lord, C. J., … de Bono, J. S. (2020). Phase I Trial of First-in-Class ATR Inhibitor M6620 (VX-970) as Monotherapy or in Combination With Carboplatin in Patients With Advanced Solid Tumors. *Journal of Clinical Oncology*, *38*(27), 3195–3204.
370. Yap, T. A., Tan, D. S. P., Terbuch, A., Caldwell, R., Guo, C., Goh, B. C., Heong, V., Haris, N. R. Md., Bashir, S., Drew, Y., Hong, D. S., Meric-Bernstam, F., Wilkinson, G., Hreiki, J., Wengner, A. M., Bladt, F., Schlicker, A., Ludwig, M., Zhou, Y., … de Bono, J. S. (2021). First-in-Human Trial of the Oral Ataxia Telangiectasia and RAD3-Related (ATR) Inhibitor BAY 1895344 in Patients with Advanced Solid Tumors. *Cancer Discovery*, *11*(1), 80–91.
371. Yu, H. A., Arcila, M. E., Rekhtman, N., Sima, C. S., Zakowski, M. F., Pao, W., Kris, M. G., Miller, V. A., Ladanyi, M., & Riely, G. J. (2013). Analysis of Tumor Specimens at the Time of Acquired Resistance to EGFR-TKI Therapy in 155 Patients with EGFR-Mutant Lung Cancers. *Clinical Cancer Research*, *19*(8), 2240–2247.
372. Yu, M., Bardia, A., Aceto, N., Bersani, F., Madden, M. W., Donaldson, M. C., Desai, R., Zhu, H., Comaills, V., Zheng, Z., Wittner, B. S., Stojanov, P., Brachtel, E., Sgroi, D., Kapur, R., Shioda, T., Ting, D. T., Ramaswamy, S., Getz, G., … Haber, D. A. (2014). Ex vivo culture of circulating breast tumor cells for individualized testing of drug susceptibility. *Science*, *345*(6193), 216–220.
373. Zaremba, T., & Curtin, N. J. (2007). PARP Inhibitor Development for Systemic Cancer Targeting. *Anti-Cancer Agents in Medicinal Chemistry*, *7*(5), 515–523.
374. Zhang, B., Stewart, C. A., Wang, Q., Cardnell, R. J., Rocha, P., Fujimoto, J., Solis Soto, L. M., Wang, R., Novegil, V., Ansell, P., He, L., Fernandez, L., Jendrisak, A., Gilbertson, C.,

Schonhoft, J. D., Byun, J., Jones, J., Anderson, A. K. L., Aparicio, A., … Gay, C. M. (2022). Dynamic expression of Schlafen 11 (SLFN11) in circulating tumour cells as a liquid biomarker in small cell lung cancer. *British Journal of Cancer*, *127*(3), 569–576.

375. Zhang, J., Shi, H., Jiang, T., Liu, Z., Lin, P. P., & Chen, N. (2018). Circulating tumor cells with karyotyping as a novel biomarker for diagnosis and treatment of nasopharyngeal carcinoma. *BMC Cancer*, *18*(1), 1133.
376. Zhang, L., Ridgway, L. D., Wetzel, M. D., Ngo, J., Yin, W., Kumar, D., Goodman, J. C., Groves, M. D., & Marchetti, D. (2013). The Identification and Characterization of Breast Cancer CTCs Competent for Brain Metastasis. *Science Translational Medicine*, *5*(180), 180ra48-180ra48.
377. Zhang, W., Zhai, L., Wang, Y., Boohaker, R. J., Lu, W., Gupta, V. V., Padmalayam, I., Bostwick, R. J., White, E. L., Ross, L. J., Maddry, J., Ananthan, S., Augelli-Szafran, C. E., Suto, M. J., Xu, B., Li, R., & Li, Y. (2016). Discovery of a novel inhibitor of kinesin-like protein KIFC1*. *The Biochemical Journal*, *473*(8), 1027–1035.
378. Zhang, Z., Shiratsuchi, H., Lin, J., Chen, G., Reddy, R. M., Azizi, E., Fouladdel, S., Chang, A. C., Lin, L., Jiang, H., Waghray, M., Luker, G., Simeone, D. M., Wicha, M. S., Beer, D. G., Ramnath, N., & Nagrath, S. (2014). Expansion of CTCs from early stage lung cancer patients using a microfluidic co-culture model. *Oncotarget*, *5*(23), 12383–12397.
379. Zheng, G. X. Y., Terry, J. M., Belgrader, P., Ryvkin, P., Bent, Z. W., Wilson, R., Ziraldo, S. B., Wheeler, T. D., McDermott, G. P., Zhu, J., Gregory, M. T., Shuga, J., Montesclaros, L., Underwood, J. G., Masquelier, D. A., Nishimura, S. Y., Schnall-Levin, M., Wyatt, P. W., Hindson, C. M., … Bielas, J. H. (2017). Massively parallel digital transcriptional profiling of single cells. *Nature Communications*, *8*(1), 14049.
380. Zheng, X., Carstens, J. L., Kim, J., Scheible, M., Kaye, J., Sugimoto, H., Wu, C.-C., LeBleu, V. S., & Kalluri, R. (2015). Epithelial-to-mesenchymal transition is dispensable for metastasis but induces chemoresistance in pancreatic cancer. *Nature*, *527*(7579), 525–530.
381. Zhou, J., Gelot, C., Pantelidou, C., Li, A., Yücel, H., Davis, R. E., Färkkilä, A., Kochupurakkal, B., Syed, A., Shapiro, G. I., Tainer, J. A., Blagg, B. S. J., Ceccaldi, R., & D'Andrea, A. D. (2021). A first-in-class polymerase theta inhibitor selectively targets homologous-recombination-deficient tumors. *Nature Cancer*, *2*(6), 598–610.
382. Zoppoli, G., Regairaz, M., Leo, E., Reinhold, W. C., Varma, S., Ballestrero, A., Doroshow, J. H., & Pommier, Y. (2012). Putative DNA/RNA helicase Schlafen-11 (SLFN11) sensitizes cancer cells to DNA-damaging agents. *Proceedings of the National Academy of Sciences*, *109*(37), 15030–15035.
383. Zou, H. Y., Friboulet, L., Kodack, D. P., Engstrom, L. D., Li, Q., West, M., Tang, R. W., Wang, H., Tsaparikos, K., Wang, J., Timofeevski, S., Katayama, R., Dinh, D. M., Lam, H., Lam, J. L., Yamazaki, S., Hu, W., Patel, B., Bezwada, D., … Smeal, T. (2015). PF-06463922, an ALK/ROS1 Inhibitor, Overcomes Resistance to First and Second Generation ALK Inhibitors in Preclinical Models. *Cancer Cell*, *28*(1), 70–81.

Synthèse en français

Introduction

Le cancer du poumon est la première cause de décès par cancer dans le monde. La majorité des cancers bronchiques sont diagnostiqués à des stades avancés et non-opérables et le décès est généralement dû au développement de métastases. Il existe deux formes histologiques : le cancer bronchique non à petites cellules (CBNPC) et le cancer bronchique à petites cellules (CBPC), qui représentent respectivement environ 85% et 15% des cas. Ce manuscrit est consacré exclusivement au CBNPC.

Les défauts de la réponse aux dommages à l'ADN (DDR) génèrent des altérations (mutations, altérations du nombre de copies de gènes (CNA), anomalies chromosomiques) et une instabilité du génome qui favorise la progression tumorale. De nouvelles stratégies thérapeutiques ciblant la DDR comme les inhibiteurs de PARP (PARPi) ont montré une efficacité dans plusieurs cancers, notamment les cancers de l'ovaire et du sein. Cependant, ces molécules se sont révélées peu efficaces dans le CBNPC. Les cellules tumorales circulantes (CTC) sont très rares dans la circulation sanguine. Issues de tumeurs primaires ou de métastases, elles possèdent des propriétés biologiques particulières leur permettant de transiter dans le sang et de former une nouvelle tumeur. Initiatrices de la progression métastatique, ces cellules constituent une cible thérapeutique particulièrement intéressante. Cependant, leur caractérisation moléculaire et fonctionnelle est limitée par leur rareté, ainsi que leur grande hétérogénéité phénotypique et génomique. Notre laboratoire a établi quatre modèles de xénogreffes de CTC (*CTC-derived xenografts* – CDX) GR-CDXL1, GR-CDXL2, GR-CDXL3 et GR-CDXL4 à partir d'une cohorte de 55 patients atteints de CBNPC avancé, ainsi que trois lignées cellulaires dérivées de ces CDX. À ce jour, un seul modèle CDX dans le CBNPC a été rapporté dans la littérature. Des travaux préliminaires ont montré que ces CDX présentent un phénotype épithélial concordant avec l'histologie des biopsies tumorales correspondantes et reproduisent la réponse des patients aux

chimiothérapies. Ces premières données ont montré la pertinence clinique de nos modèles.

Objectifs

Nous avons émis l'hypothèse que des déficiences des voies de réparation et des mécanismes de la DDR ont un rôle clé dans le potentiel métastatique des CTC de CBNPC et pourraient constituer des vulnérabilités et potentiellement des cibles thérapeutiques. Notre objectif principal a été de mener une analyse moléculaire et fonctionnelle approfondie de nos modèles et d'explorer les mécanismes qui sous-tendent le potentiel métastatique des CTC. Notre étude a reposé sur quatre axes principaux : (i) réaliser un séquençage total de l'exome (*whole-exome sequencing* – WES) des CDX, des lignées dérivées, des biopsies correspondantes et des CTC de patients collectées chez les patients au moment de la xénogreffe, et identifier les anomalies moléculaires présentes dans ces différents échantillons afin de reconstruire leur organisation phylogénétique, (ii) réaliser une étude mécanistique de l'activité de la DDR et de l'instabilité chromosomique (CIN) dans nos trois lignées cellulaires, (iii) réaliser des tests pharmacologiques *in vitro* ciblant les déficiences de la DDR et de la CIN identifiées dans notre étude génomique et fonctionnelle, (iv) évaluer l'activité métastatique des lignées dérivées de CDX chez la souris immunodéficiente (NSG) et dans le modèle de membrane chorioallantoique du poulet (CAM) et finalement valider les cibles thérapeutiques précedemment sélectionnées *in vitro*, *in ovo* et *in vivo*.

Résultats

Caractérisation génomique et analyse phylogénétique

L'analyse génomique comparative des données de WES a révélé une similarité de 52-76% entre les profils mutationnels des CDX, les lignées, les biopsies correspondantes et les CTC isolées en cellules uniques. Les arbres phylogénétiques ont montré la présence de mutations clonales dans plusieurs gènes « *drivers* » de la DDR et de l'intégrité du génome, notamment *TP53*, *BRCA1*, *BRCA2*, *PARP1*, *CHK2*, *ARID1A* et

ARID1B, ainsi que des CNA sous-clonales, tels que des pertes de *FANCA* et *WWOX* et des gains du nombre de copies des gènes de la DDR *MDM2* et *MDM4* et du gène *AKT1*. Ces résultats montrent un dysfonctionnement des mécanismes de la DDR, ce qui nous a orienté vers l'étude fonctionnelle de la DDR dans nos modèles.

Étude de la DDR dans les lignées dérivées de CDX

Afin d'estimer le taux de cassures double-brin (*double-strand breaks* – DSB) présents dans nos trois lignées, nous avons réalisé des co-marquages par immunofluorescence (IF) des protéines cycline A (marqueur de phase S/G2 du cycle cellulaire) et 53BP1. 53BP1 est spécifique des DSB et se présente en forme de foci dans les cellules en S/G2 et en foyers nucléaires (*nuclear body* – NB) dans les cellules en phase G1. Les trois modèles présentent des taux élevés de DSB en phase S (plus de cinq foci 53BP1) en comparaison de ceux observés dans la lignée de CBNPC A549. Plus de 50% des cellules GR-CDXL1 présentent plus de trois NB, ce qui témoigne de la persistance de dommages non-réparés en post-mitose dans ces cellules. Ceci a été confirmé par des taux élevés de cellules mitotiques GR-CDXL1 γH2AX^{+}, conférant une activation constitutive du point de contrôle du cycle cellulaire CHK1. Afin d'évaluer l'activité de réparation des DSB par la voie de *homologous recombination* (HR) de nos lignées, nous avons étudié le recrutement de la protéine clé RAD51 en phase S (double-marquage anti-RAD51/anti-géminine) après irradiation des cellules. Les cellules GR-CDXL1 et GR-CDXL4 montrent un défaut de formation de foci nucléaires RAD51 en comparaison du modèle GR-CDXL3 et de la lignée contrôle A549, indiquant une déficience HR (HRD) dans GR-CDXL1 et GR-CDXL4. La voie *non-homologous end joining* (NHEJ), quant à elle, est normalement activée dans les trois lignées.

Évaluation de la CIN et des défauts mitotiques dans les lignées dérivées de CDX

L'étalement des chromosomes métaphasiques a mis en évidence une aneuploidie dans les lignées GR-CDXL1, GR-CDXL3 et GR-CDXL4 avec respectivement 54, 110 et 59 chromosomes. Des défauts mitotiques ont été détectés par IF dans les trois lignées dérivées de CDX. Nous mettons aussi en évidence un « regroupement de

centrosomes » (*centrosome clustering*), notamment dans les cellules GR-CDXL3, qui constitue un mécanisme d'adaptation des cellules tumorales comportant des centrosomes surnuméraires, leur permettant de former un fuseau mitotique bipolaire et ainsi de survivre. Ce mécanisme génère une CIN et constitue une cible thérapeutique potentielle. La CIN est aussi alimentée dans GR-CDXL3 par une duplication du génome.

Évaluation du potentiel métastatique des lignées dérivées de CDX et tests pharmacologiques *in vitro*, *in ovo* et *in vivo*

Cet axe consiste tout d'abord à évaluer l'activité métastatique de nos lignées dérivées de CDX dans le modèle de la CAM et chez la souris NSG. Dans les expériences *in ovo*, les cellules ont été infectées par des particules rétrovirales exprimant mCherry et celles-ci ont ensuite été implantées sur la CAM. D'autre part, les cellules ont été infectées avec un lentivirus porteur du gène GFP-luciférase, avant leur injection par voie intracardiaque dans des souris NSG. Les trois lignées sont tumorigéniques dans les deux modèles : GR-CDXL1 a formé des tumeurs locales, tandis que les cellules GR-CDXL3 et GR-CDXL4 ont formé plusieurs métastases, concordant avec leur profil de CIN.

Les profils mutationnels générés par WES et l'étude fonctionnelle ont fourni un rationnel biologique pour identifier de potentielles cibles thérapeutiques de la DDR et des mécanismes de réparation des dommages à l'ADN. Les cellules GR-CDXL1, présentant une HRD résultant d'une mutation biallélique *BRCA2* et de la perte du promoteur de *FANCA*, sont sensibles au PARPi olaparib *in vitro*, *in ovo* et *in vivo*, malgré leur résistance à la chimiothérapie. Les cellules GR-CDXL4 présentent aussi un profil HRD engendrant une sensibilité à l'olaparib *in vitro*, *in ovo* et *in vivo*, mais ne présentent pas de mutation *BRCAness*. Afin de comprendre la sensibilité des cellules GR-CDXL4, nous avons étudié le gène *SLFN11*, dont l'expression a été associée à une réponse à la chimiothérapie ainsi qu'aux PARPi et inhibiteurs de topoisomérase dans certains cancers, et notamment le CBPC. Nous avons observé une surexpression de la protéine SLFN11 dans les cellules GR-CDXL4 exclusivement. Puis, par immunohistochimie, nous avons montré que les cellules tumorales des biopsies du patient L4 (au diagnostic et à

progression de la maladie), de la lignée cellulaire et la tumeur du CDX expriment aussi fortement SLFN11. Ce résultat suggère donc que SLFN11 pourrait être un biomarqueur prédictif de sensibilité à l'olaparib dans le CBNPC, indépendamment d'une mutation *BRCA1/2*, et nécessite des investigations plus approfondies. De plus, la surexpression de SLFN11 coïncide avec l'expression de marqueurs neuroendocrines dans la biopsie du patient à progression sous crizotinib (inhibiteur de tyrosine kinase – TKI), ce qui pourrait témoigner d'une transformation du CBNPC en CBPC. En effet, cette transformation a été décrite comme mécanisme de résistance aux TKI dans le CBNPC porteur de la mutation *EGFR* ou du réarrangement *ALK*. Ces résultats suggèrent un rôle de SLFN11 dans la prédiction de la transformation histologique CBNPC en CBPC. Enfin, nous avons obtenu un effet synergique de la combinaison de l'inhibiteur de PI3Kα (ciblant le gain d'*AKT*) et AZ82 (inhibiteur de *centrosome clustering*) dans le traitement de tumeurs GR-CDXL3 *in ovo* et *in vivo*, ciblant ainsi deux mécanismes d'adaptation tumorale du modèle.

Conclusion

Nous rapportons pour la première fois une caractérisation approfondie moléculaire et fonctionnelle de quatre modèles de CDX et de trois lignées dérivées de CDX dans le CBNPC. Ce travail met en évidence des déficiences de la DDR, dont le ciblage par différents agents pharmacologiques inhibe l'activité métastatique de nos CDX. Il montre donc que les déficiences de la DDR et des mécanismes de CIN ont un rôle important dans le potentiel métastatique des CTC de CBNPC et constituent un rationnel biologique pour des approches thérapeutiques prometteuses dans cette maladie. De plus, l'identification de biomarqueurs prédictifs de réponse à des thérapies ciblant la DDR, tels que le gène *SLFN11*, permettra, si nos résultats sont confirmés par de plus vastes études, d'élargir leur intérêt clinique à de nouvelles catégories de patients.

université PARIS-SACLAY | ÉCOLE DOCTORALE Cancérologie : biologie - médecine - santé (CBMS)

Title : Genomic instability of non-small cell lung cancer circulating tumor cells as a driving force for their metastatic potential.

Keywords : circulating tumor cells, circulating tumor cell-derived xenografts, non-small cell lung cancer, DNA damage response, genomic instability, therapeutic targets

Abstract : Lung cancer is the leading cause of cancer-related death worldwide. The majority of patients are diagnosed at advanced and currently incurable stages. Non-small cell lung cancer (NSCLC) represents around 85% of cases. Alterations in the DNA damage response (DDR) and resulting genomic instability (GI) contribute to NSCLC etiology and progression. However, their therapeutic exploitation is disappointing. Circulating tumor cells (CTCs) that dissociate from the primary tumor or its metastases harbor distinct biological properties that allow them to travel through circulation and colonize distant organs. Further insight into CTC biology and identification of their vulnerabilities would provide a rationale for the targeting of the most aggressive tumor clones that fuel metastatic progression.

We hypothesized that the DDR and genome integrity maintenance dysfunctions are critical processes in CTC metastatic potency and NSCLC progression. The main aim of my PhD project was to perform a molecular and functional characterization of NSCLC CTCs to elucidate the mechanistic basis of their tumorigenic potential and identify novel therapeutic targets. Using CTCs from 55 patients with advanced-stage NSCLC, our laboratory has established four CTC-derived xenografts (CDX) (GR-CDXL1, GR-CDXL2, GR-CDXL3 and GR-CDXL4) and three CDX-derived cell lines. Preliminary analyses have shown that the four CDX recapitulated patient tumor histology and response to platinum-based chemotherapy, which validated the clinical relevance of our models. To determine the extent to which the CDX was representative of the corresponding patient tumor biopsy, whole-exome sequencing (WES) was performed on the CDX (GR-CDXL1, GR-CDXL2, GR-CDXL3, GR-CDXL4), CDX-derived cell lines, corresponding patient tumor biopsy and single CTCs.

The four major goals of my thesis were as follows: (i) identification of genomic alterations and in-depth comparative genomic analysis of the CDX, CDX-derived cell lines, corresponding patient tumor biopsy and CTCs using WES analysis data, (ii) functional characterization of DDR activity and chromosomal instability (CIN) events in the CDX-derived cell lines, (iii) *in vitro* drug assays targeting DDR defects, (iv) 3D modeling of the metastatic potency of our CDX-derived cell lines *in ovo* in the chick embryo chorioallantoic membrane (CAM) and *in vivo* in immunodeficient mice and pharmacological targeting of metastasis.

Genomic analysis by WES has shown considerable mutational landscape similarity between the CDX, the cell lines, the patient biopsies and single CTCs. WES and reconstruction of phylogenetic trees of the CDX and the CDX-derived cell lines revealed truncal alterations in key DDR and genome integrity-related genes prevalent across models and assessed as therapeutic targets *in vitro*, *in ovo* and *in vivo*. GR-CDXL1 presented homologous recombination deficiency linked to bi-allelic *BRCA2* mutation and *FANCA* deletion and unrepaired DNA lesions post-mitosis. GR-CDXL1 cells were sensitive to PARP inhibitor (PARPi) olaparib, despite chemoresistance, which challenges the current clinical rationale claiming that chemosensitive NSCLC patients should respond to PARPi. Targeting CIN through centrosome clustering inhibition in GR-CDXL3 impeded tumor growth *in ovo* and *in vivo*. In GR-CDXL4, olaparib sensitivity was dictated by SLFN11 overexpression, which also corresponded with increased neuroendocrine marker expression at patient disease progression, suggesting a predictive value of SLFN11 in histological transformation of NSCLC into SCLC.

This study unravels distinct DDR profiles as a central mechanism underpinning CTC metastatic potency. It also suggests SLFN11 overexpression as a potential biomarker of sensitivity to PARPi in NSCLC independently of BRCAness. Overall, our models provide a robust platform for drug testing of DDR-targeted strategies to expand patient categories that may benefit from precision medicine in metastatic NSCLC.

université PARIS-SACLAY | ÉCOLE DOCTORALE Cancérologie : biologie - médecine - santé (CBMS)

Titre : Rôle de l'instabilité génomique dans le potentiel métastatique des cellules tumorales circulantes dans le cancer bronchique non à petites cellules.

Mots clés : cellules tumorales circulantes, xénogreffes de cellules tumorales circulantes, cancer bronchique non à petites cellules, réponse des dommages à l'ADN, instabilité génomique, cibles thérapeutiques

Résumé : Le cancer du poumon est la 1ère cause de décès par cancer dans le monde. La majorité des patients sont diagnostiqués à un stade avancé pour lequel il n'existe actuellement pas de traitement curatif. Le cancer bronchique non à petites cellules (CBNPC) représente 85% des cas. Les altérations de la réponse aux dommages à l'ADN (DDR) et l'instabilité génomique (GI) sont impliqués dans l'étiologie et la progression du CBNPC. Cependant, leur ciblage thérapeutique est peu exploité. Les cellules tumorales circulantes (CTC) issues de tumeurs primitives ou métastatiques ont des caractéristiques biologiques très particulières leur permettant de transiter dans le sang et de former des métastases dans des organes secondaires. Une meilleure connaissance de la biologie des CTC pourrait permettre d'identifier des « vulnérabilités » dans ces cellules et de cibler les clones tumoraux les plus agressifs, moteurs de la progression métastatique.

Nous avons émis l'hypothèse que des déficiences de la DDR et les mécanismes de GI ont un rôle clé dans le potentiel métastatique des CTC. L'objectif de ma thèse a été de réaliser une étude moléculaire et fonctionnelle des CTC de CBNPC afin de caractériser les mécanismes qui sous-tendent leur potentiel tumorigénique et d'identifier de nouvelles cibles thérapeutiques. À partir des CTC de 55 patients atteints de CBNPC avancé, nous avons développé 4 modèles de xénogreffes (*CTC-derived xenografts* - CDX) GR-CDXL1, GR-CDXL2, GR-CDXL3, GR-CDXL4 et établi 3 lignées *in vitro* issues des CDX GR-CDXL1, GR-CDXL3 et GR-CDXL4. Des analyses préliminaires ont montré que les CDX présentent un phénotype concordant avec l'histologie des tumeurs des patients et reflètent leur réponse à la chimiothérapie, validant la pertinence clinique de nos modèles. Un séquençage de l'exome a été réalisé sur les CDX, les lignées dérivées, les biopsies et les CTC collectées au moment de la xénogreffe.

Mon projet de thèse s'articule en 4 axes majeurs : (i) identifier les altérations génétiques dans nos différents échantillons séquencés et réaliser une analyse comparative des données, (ii) réaliser une étude fonctionnelle de la DDR et des mécanismes d'instabilité chromosomique de nos lignées, (iii) réaliser des tests pharmacologiques *in vitro* ciblant les déficiences de la DDR, (iv) étudier et cibler le potentiel métastatique *in ovo* dans le modèle de membrane chorioallantoique du poulet et *in vivo* chez la souris immunodéficiente.

Notre analyse génomique a révélé des profils mutationnels similaires entre les CDX, les lignées dérivées, les biopsies correspondantes et les CTC. La reconstruction des arbres phylogénétiques a montré la présence d'altérations du nombre de copies de plusieurs gènes « *drivers* » impliqués dans la GI et la DDR. GR-CDXL1 présente une déficience de la réparation par recombinaison homologue du fait d'une mutation du gène *BRCA2*, une délétion du promoteur de *FANCA*, ainsi qu'un taux élevé de cellules post-mitotiques non-réparées. Les cellules GR-CDXL1 sont sensibles à l'inhibiteur de PARP-1 (PARPi) olaparib, malgré une résistance à la chimiothérapie. Dans GR-CDXL3, un « clustering » des centrosomes ciblable *in ovo* et *in vivo* a été détecté. GR-CDXL4 présente une sensibilité à l'olaparib qui résulte de la surexpression de SLFN11. Celle-ci coïncide avec l'expression de marqueurs neuroendocrines par la tumeur du patient à progression, suggérant une valeur prédictive de SLFN11 dans la transformation histologique d'un CBNPC en CBPC.

Notre travail met en évidence des altérations de la DDR impliquées dans le potentiel métastatique des CTC de CBNPC. Il suggère la surexpression de SLFN11 comme potentiel biomarqueur prédictif de sensibilité aux PARPi dans les CBNPC indépendant du profil *BRCAness*. Nos modèles sont des outils pour tester de nouvelles thérapies ciblant la DDR dans la progression métastatique du CBNPC, qui pourraient élargir la catégorie des patients bénéficiant de la médecine personnalisée.